การพัฒนาโมโนเอซิลกลีเซอรอลในรูปแบบอนุภาคนาโนต่อเซลล์มะเร็งปากมดลูก

DEVELOPMENT OF MONOACYLGLYCEROL-ENCAPSULATED NANOPARTICLES (NPS) AGAINST CERVICAL CANCER CELL LINES

SIRIRAT BOONDIREKE

Graduate School Srinakharinwirot University

2018

การพัฒนาโมโนเอซิลกลีเซอรอลในรูปแบบอนุภาคนาโนต่อเซลล์มะเร็งปากมดลูก

สิริรัตน์ บุญดิเรก

ปริญญานิพนธ์นี้เป็นส่วนหนึ่งของการศึกษาตามหลักสูตร
ปรัชญาดุษฎีบัณฑิต สาขาวิชาชีวภาพการแพทย์
คณะแพทยศาสตร์ มหาวิทยาลัยศรีนครินทรวิโรฒ
ปีการศึกษา 2561

DEVELOPMENT OF MONOACYLGLYCEROL-ENCAPSULATED NANOPARTICLES (NPs) AGAINST CERVICAL CANCER CELL LINES

SIRIRAT BOONDIREKE

A Dissertation Submitted in partial Fulfillment of Requirements

for DOCTOR OF PHILOSOPHY (Biomedical Sciences)

Faculty of Medicine Srinakharinwirot University

2018

THE DISSERTATION TITLED

DEVELOPMENT OF MONOACYLGLYCEROL-ENCAPSULATED NANOPARTICLES (NPS) AGAINST CERVICAL CANCER CELL LINES

BY

SIRIRAT BOONDIREKE

HAS BEEN APPROVED BY THE GRADUATE SCHOOL IN PARTIAL FULFILLMENT OF THE REQUIREMENTS FOR THE DOCTOR OF PHILOSOPHY IN BIOMEDICAL SCIENCES AT SRINAKHARINWIROT UNIVERSITY

..... Dean of Graduate School

(Asst. Prof. Dr. Chatchai Ekpanyaskul, MD.)

.....

ORAL DEFENSE COMMITTEE

..... Major-advisor
(Assoc. Prof. Dr.Benjamas Wongsatayanon)

..... Co-advisor
(Prof. Dr.Alain Durand)

..... Chair
(Asst. Prof. Dr.Wanlaya Tanechpongtamb)

..... Committee
(SRISOMBAT PUTTIKAMONKUL, Ph.D.)

..... Committee
(Dr.Nattika Saengkrit)

Title	DEVELOPMENT OF MONOACYLGLYCEROL-ENCAPSULATED NANOPARTICLES (NPs) AGAINST CERVICAL CANCER CELL LINES
Author	SIRIRAT BOONDIREKE
Degree	DOCTOR OF PHILOSOPHY
Academic Year	2018
Thesis Advisor	Associate Professor Benjamas Wongsatayanon

At present, chemotherapy is still effective against cancer, but it is hindered by limitations in drug absorption, drug accumulation, drug loss in blood circulation, and drug targeting. Therefore, the normal rapid-proliferating cells are helplessly destroyed and eventually lead to the death of the patient. Drug delivery systems have the power to bring the effective anticancer agents towards cancerous tissues. Accordingly, this study aimed to develop polymeric nanoparticles (NPs) to encapsulate monomyristin (MM), a monoacylglycerol with antiproliferative activity against HeLa cervical cancer cells but poor water-solubility. The dextran structure was modified by phenoxy attachment to obtain different degrees of hydrophobically-modified dextran (dextran-phenoxy, DexP), i.e., $DexP_{15.5}$, $DexP_{21}$, and $DexP_{26}$, which were used to synthesize the poly(lactic acid) (PLA)-based nanoparticle (PLA NP). The size distribution results showed that PLA NP grafted with $DexP_{26}$ and demonstrated very low aggregation. Therefore, MM-encapsulated NPs were newly prepared with PLA and $DexP_{26}$, with or without the conjugated transferrin (Tf) ligand for targeting. A cytotoxicity assay of MM solution showed that MM significantly inhibited HeLa cell growth in a dose-dependent manner, but had a low inhibitory effect against Vero and uterine epithelial cells. The study of HeLa cell death induced by MM showed the increments of apoptotic dead cells by activating intrinsic mitochondrial pathways. In comparison, MM solution at low dose (<15.63 μg/mL) had no effect in terms of cytotoxicity enhancement and were found in HeLa cells treated with MM in NP forms. Furthermore, Tf-conjugated MM-NP (Tf-MM-NP) had a higher cytotoxic effect than MM-loaded NP (MM-NP). These results indicated the improvement of the cytotoxic efficiency of MM against HeLa cells by MM encapsulation and Tf targeting. The overall results demonstrated that the newly developed MM-NPs and Tf-MM-NP could serve as promising carriers for MM delivery towards HeLa cervical cancer cells.

Keyword : Monoacylglycerol-Encapsulated Nanoparticles, Cervical Cancer, Cell Lines, Cytotoxicity, Apoptosis, Transferrin

ACKNOWLEDGEMENTS

For the success of my dissertation, I would like to express my deeply sincere gratitude and appreciation to my supervisor, Assoc. Prof. Dr. Benjamas Wongsatayanon, for her endless kindness, support, encouragement, and intensive supervision throughout the period of this dissertation.

I am also deeply grateful to my co-advisor, Prof. Dr. Alain Durand for his kindness, expert guidance and encouragement for the completeness of this dissertation.

I am grateful to Dr. Michèle Léonard at LCPM laboratory, University of Lorraine, Nancy, France for guiding my research and her helpful suggestions throughout the laboratory works at LCPM.

I would like to thank the oral defense committee, Asst. Prof. Dr. Wanlaya Tanechpongtamb, Dr. Srisombat Puttikamonkuland Dr. Nattika Saengkrit for their valuable time with great advice, comments and feedback to improve my dissertation.

I am deeply thankful to the Royal Golden Jubilee Program, Thailand Research Fund for the financial support of the Ph.D. study (Grant No. PHD/0066/2554).

I also thank Faculty of Medicine, Srinakharinwirot University (Grant No. 620/2558, 245/2558, 250/2559), Office of the Higher Education Commission (Grant No. 429/2557) and Graduate School of Srinakharinwirot University for parts of financial support to conduct this research.

I would like to thank Department of Microbiology and Faculty of Medicine of Srinakharinwirot University for supporting chemicals, equipment, instruments and facilities during my research study in Thailand. I am also thankful LCPM laboratory, University of Lorraine for supporting all chemicals, equipment, instruments and facilities during my research study in France.

Special thanks are given to friends, colleagues, staffs, and all members of LCPM laboratory, University of Lorraine and Faculty of Medicine, Srinakharinwirot University for their friendship, helpfulness, advise and encouragements.

Most of all, I give all my heart to my dear family for their unconditional love, caring, support, encouragement, contribution and understanding in every aspect throughout my whole life. Without them, my success would have never been come true. Thank you.

SIRIRAT BOONDIREKE

TABLE OF CONTENTS

Page

LIST OF TABLES

Page

LIST OF FIGURES

Page

CHAPTER I
INTRODUCTION

Background

Cancer is a general term that refers to a group of over 100 distinct diseases affecting many different cell types and tissues. The diseases can be classified into 5 major types including of sarcoma, carcinoma, melanoma, lymphoma, and leukemia [42], but all of them share one hallmark characteristic of the unchecked growth that progresses towards limitless expansion within the body which eventually results in loss of organ functions, illnesses and finally leads to death. It is fundamentally a disease at the molecular level and characterized by abnormal cell proliferation. At present, cancer appears to be a leading cause of morbidity and mortality throughout the world. There were 18.1 million new cancer cases and 9.6 million cancer deaths in 2018 worldwide [1, 2], with an incidence of various cancers including lung, breast, colorectum, prostate, stomach, liver, oesophagus, cervix uteri and other cancers [1]. In males, lung, prostate and colorectal cancer are the most frequent cancers while in females, breast, colorectal, lung and cervical cancer are the most commonly diagnosed cancers. In addition, cancer of the cervix is ranked the fourth most common as well as cancer mortality in women worldwide, with the estimated 569, 847 new cases and 311, 365 deaths in 2018 [1, 2].

Currently, in spite of intensive research and advances in cancer treatment, over half patients with cancer eventually die of their diseases, and thus treatment of cancer seems difficult. Possible treatments for the first stage of cervical cancer patients include surgery, radiotherapy, and chemotherapy. However, the latest method of choice by using anticancer drugs appears to be effective for the first stage as well as in the spread out cases [3], and is thus a major treatment which can prolong patient's life. Available drugs frequently used as anticancer agents are directed against all rapid proliferating cells such as doxorubicin, paclitaxel, etoposide, and cisplatin [3-6].

Consequently, available drug used not only kill cancer cells, but also some normal cells particularly the rapidly dividing cells that line intestine, forming scalp, bone marrow which produce blood cells are affected. Therefore, the use of traditional chemotherapeutic agents that typically target rapidly dividing cancer cells is frequently associated with extremely destructive side-effects and mortality caused by the inattentive drug-induced damages to healthy cells and tissues [7-9]. For this reason, research and development for a new class of anticancer agents particularly from natural extracts, which show antiproliferative activity only to cancerous cells, has been considerably interested. Several researchers have reported the cytotoxic activity of monoacylglycerols on cancer cell lines, but not normal cells [10-12]. Moreover, there have been several groups of researcher that attempt to develop macromolecule-based nanoparticles (NPs) for the encapsulation of anticancer drugs, as to develop the drug delivery system which is capable of controlled release and yet for preventing drug loss while traveling to target tissues. Drug delivery system also improves drug absorption due to tiny size carriers which can pass through blood fenestra towards cancerous tissues or sites, thus lead to the improved drug accumulation and treatment efficiency.

Recently, there have been efforts to develop drug carriers for the particular cell types as for “targeted therapy”. This advancement in nanomedicine is consequently directing to ease patients with side effects since the established NPs along with its conjugated peptides or ligands can thus bind only to those cells which present the certain types of receptor that specific to the conjugated peptides or ligands. Therefore, patients who receive the targeted therapy are more secure in relieving side effects. In targeted cancer therapy, the affinity of conjugated peptides or ligands is to specifically bind to cancer cell surface receptors that usually relate to cell growth, proliferation, movement, and response. In cervical cancer cell surface, it has been found that transferrin receptor is overexpressed more than normal cells. Hence transferrin has been used as a conjugated ligand on NPs in targeting on HeLa cell surface [13, 14]. Accordingly, transferrin has been considered as an advertent candidate for the effective targeted cervical cancer therapy.

In this research studies, monomyristin (MM), a previously tested monoacylglycerol was used as anticancer drug and be encapsulated in transferrin receptor (TfR)-targeted polymeric NPs and test the cytotoxicity against HeLa cell lines compared with the non-targeted NPs *in vitro*, in order to develop the targeted drug delivery system.

Objectives

1. To develop the PLA/dextran-based NPs for the encapsulation of monomyristin (MM) and fluorescein isothiocyanate (FITC) by using emulsion-solvent evaporation process, in order to prepare a drug delivery model towards human cervical cancer cell lines.
2. To develop the transferrin (Tf)-conjugated MM-loaded NPs which are specifically recognized by the overexpressed transferrin receptors (TfRs) on HeLa cells surface, in order to enhance the targeted drug delivery and improve the NPs internalization in HeLa cells.
3. To perform the cytotoxicity assay in order to evaluate the antiproliferative efficiency of the developed MM-loaded NPs and Tf-conjugated MM-loaded NPs on human cervical cancer cells and normal cells (Vero and endometrial cells), comparing to MM solution.
4. To investigate the apoptotic cell death in HeLa cells induced by MM solution by using imaging flow cytometry technique.
5. To determine the specificity of Tf ligand attached onto NPs by performing the inhibition assay using free Tf.
6. To study the percentage of HeLa cells with the internalization of FITC-loaded NPs by using imaging flow cytometry technique.

CHAPTER II
REVIEW OF THE LITERATURE

2.1 Cancer

"Cancer" is a term commonly used to refer to a group of more than 200 distinct diseases affecting different types of cell and tissue in nearly every parts of the body. Another terms used to refer to cancer are "malignant tumors" and "neoplasms". The diseases can be classified into 5 major types including of carcinoma, sarcoma, lymphoma and myeloma, melanoma, and leukemia [15]. One defining feature of cancer is rapid creation of the abnormal cells within specific tissues (Figure 1). These cells are no longer responsive to the regulatory signals of cellular differentiation, proliferation and death, resulting in the rapid and uncontrolled growth of cells which can develop to form a tumor mass. In a benign or noncancerous tumor, though pressing of the bulky mass on the surrounding organs can cause the problem but no spreading of tumor cells to other parts of the body. However, if tumor cells grow beyond their usual boundaries and invade the adjoining body parts or spread to other organs/tissues, thereby "cancer metastasis" occurs (Figure 1). Accordingly, the original site of tumor becomes invasive malignant cancer, of which the malignant cells travel via the blood or lymphatic vessels and form a new tumor (a secondary cancer). This occurrence is thus potentially life-threatening since cancer is aggressive and eventually lead to death.

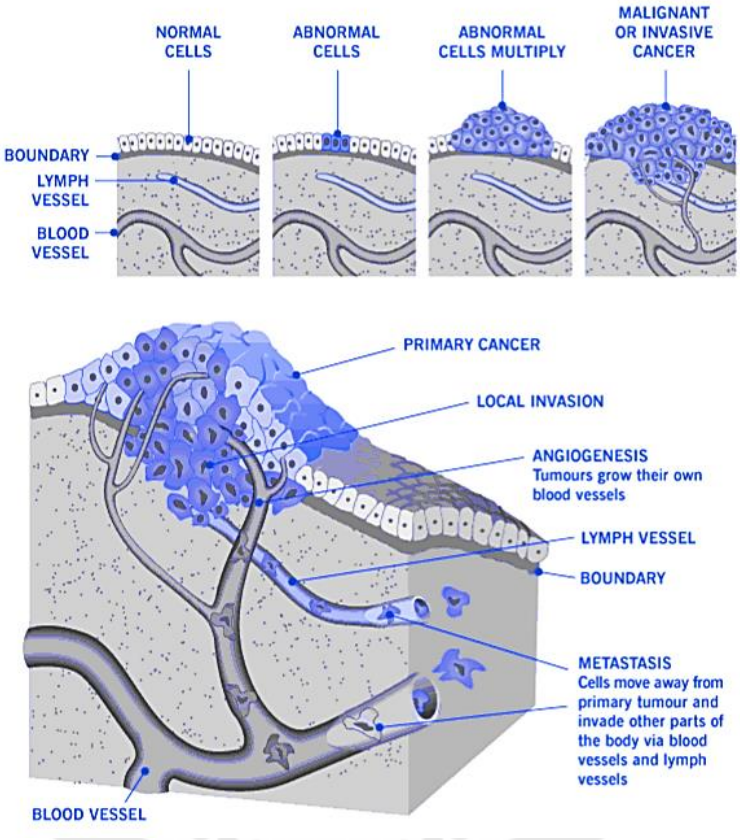

Figure 1 The development of primary cancer, malignant tumor and metastasis

The rapid dividing cells progress towards limitless expansion, invasion and metastasis via blood stream and lymphatic system in order to form the secondary cancer [16].

2.1.1 Epidemiology of cancer

2.1.1.1 Epidemiology of cancer worldwide

According to World Health Organization (WHO), the noncommunicable diseases (NCDs) is the major cause of global mortality in 2016, [17] of which cancer is the leading cause of death and the most critical obstruction to life expectancy in the 21st century [1]. The International Agency for Research on Cancer (IARC), the specialized cancer agency of the WHO, has released the reports on global cancer burden by focusing on cancer incidence and mortality in 2002, [18] 2008, [19] 2012, [20] and recently, 2018 [21] which inform the magnitude and distributions of all cancers across the world regions.

Figure 2 and Figure 3 showed the worldwide cancer incidences in 2018 for males and females respectively, provided by GLOBOCAN 2018. Moreover, the global cancer statistics 2018 by IARC provides a status report on the contemporary estimates of cancer incidence and mortality of 36 cancers in 185 countries [1]. The global cancer burden accounts that there will be 18.1 million new cancer cases and 9.6 million cancer deaths in both sexes in all regions [1]. Mortifyingly, nearly half of all cancer cases (48.4%) and over half of the cancer deaths (57.3%) occur in Asia, follow by Europe (23.4% cases and 20.3% deaths), America (21% cases and 14.4% deaths) and Africa (5.8% cases and 7.3% deaths), [1] as shown in Figure 4. In addition, the cancer burden is mostly pointed in Asia, with the highest number (39.7%) of 5-year prevalence in all population [2]. In both sexes, the four most common diagnosed cancers worldwide in 2018 are the lung (11.6%) and closely followed by breast (11.6%), colorectum (10.2%), and prostate (7.1%) while the four most common cancers death were caused by the lung (18.4%), colorectum (9.2%), stomach (8.2%) and liver (8.2%), as shown in Figure 5. In addition, lung, prostate, colorectum, liver and stomach cancer are mostly frequent and the leading cause of death among males. In female, breast, colorectum and lung cancer are the most diagnosed cancers and the leading causes of mortality. In addition, cervical cancer is ranked the fourth commonly diagnosed cancer as well as the forth commonly cause of death [1]. Overall global cancer burden pointed that the most

frequently diagnosed cancers and the leading cause of cancer deaths are varied across all regions depending on the degree economic development [1].

Beyond the estimations in the rising of new cancer cases from 12.7 million (2008) [19] to 14.1 million (2012) [20] and 18.1 million (2018) [21], the GLOBOCAN predicted the global new cancer cases to be 19.3 million per year by 2025 [22] and 22.2 million per year by 2030 [23] due to growth and ageing of the world population.

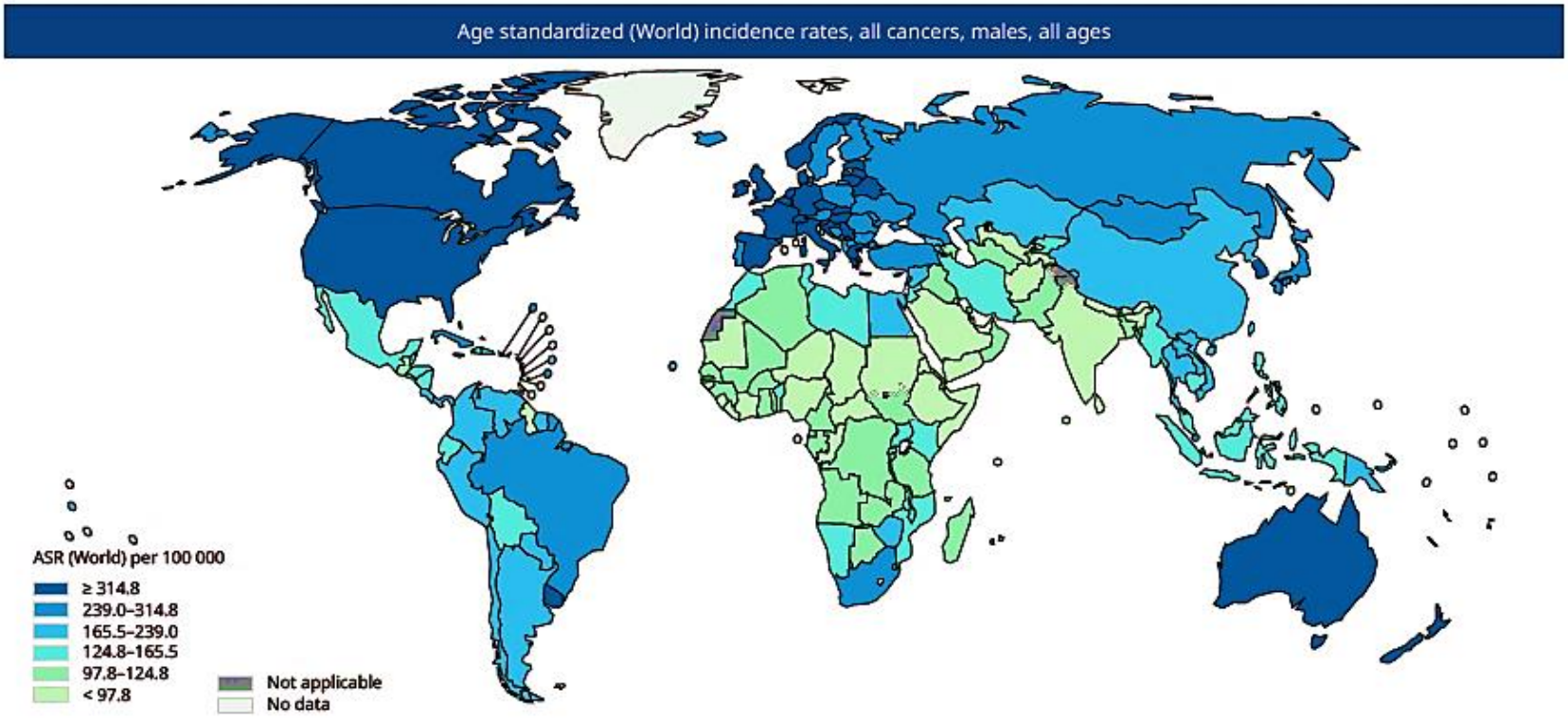

Figure 2 The overall aged-standardized cancer incidence in 2018, males

ASR refers to age-standardized rate per 100,000 person-years [2].

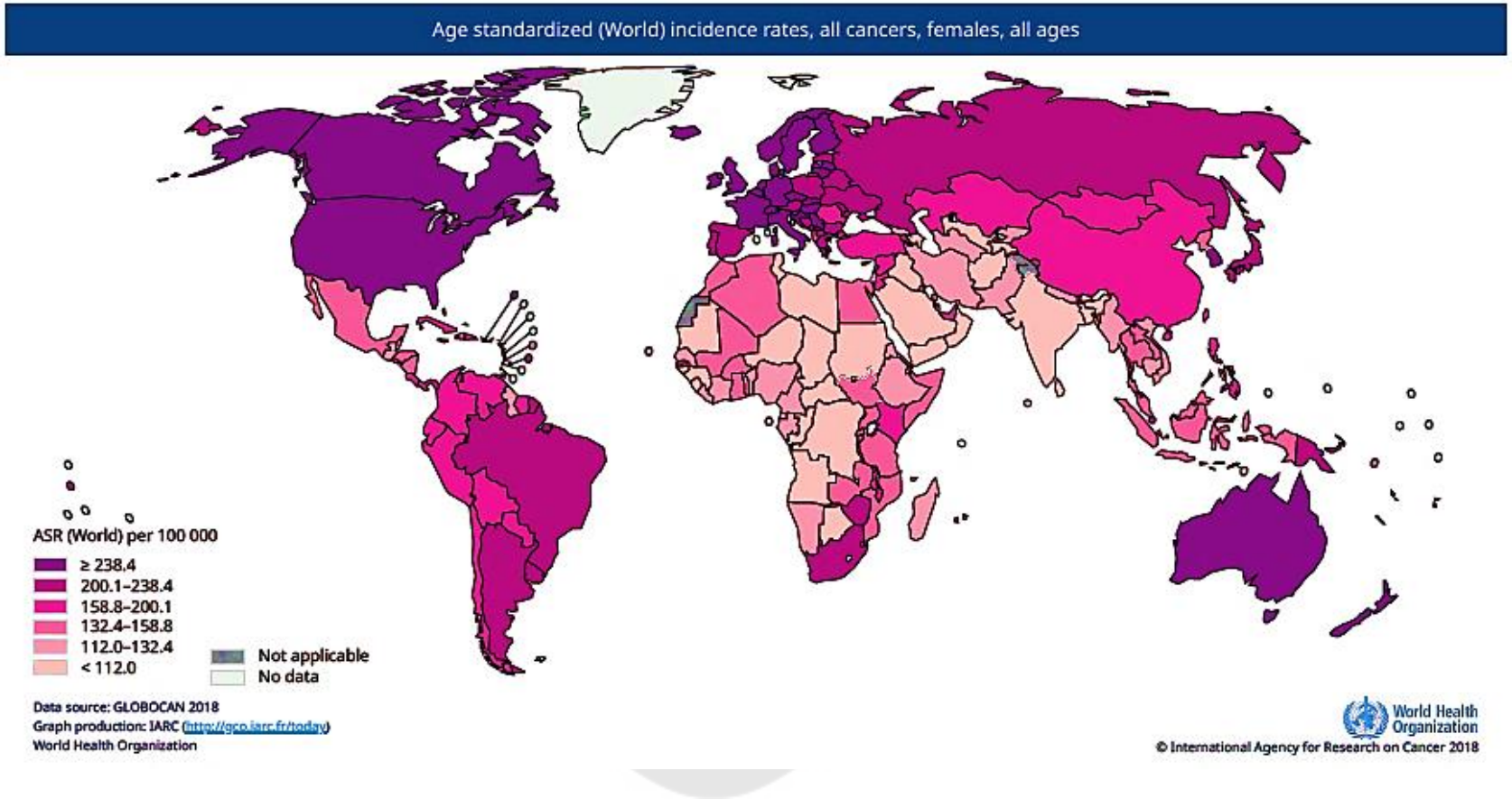

Figure 3 The overall aged-standardized cancer incidence in 2018, females

ASR refers to age-standardized rate per 100,000 person-years [2].

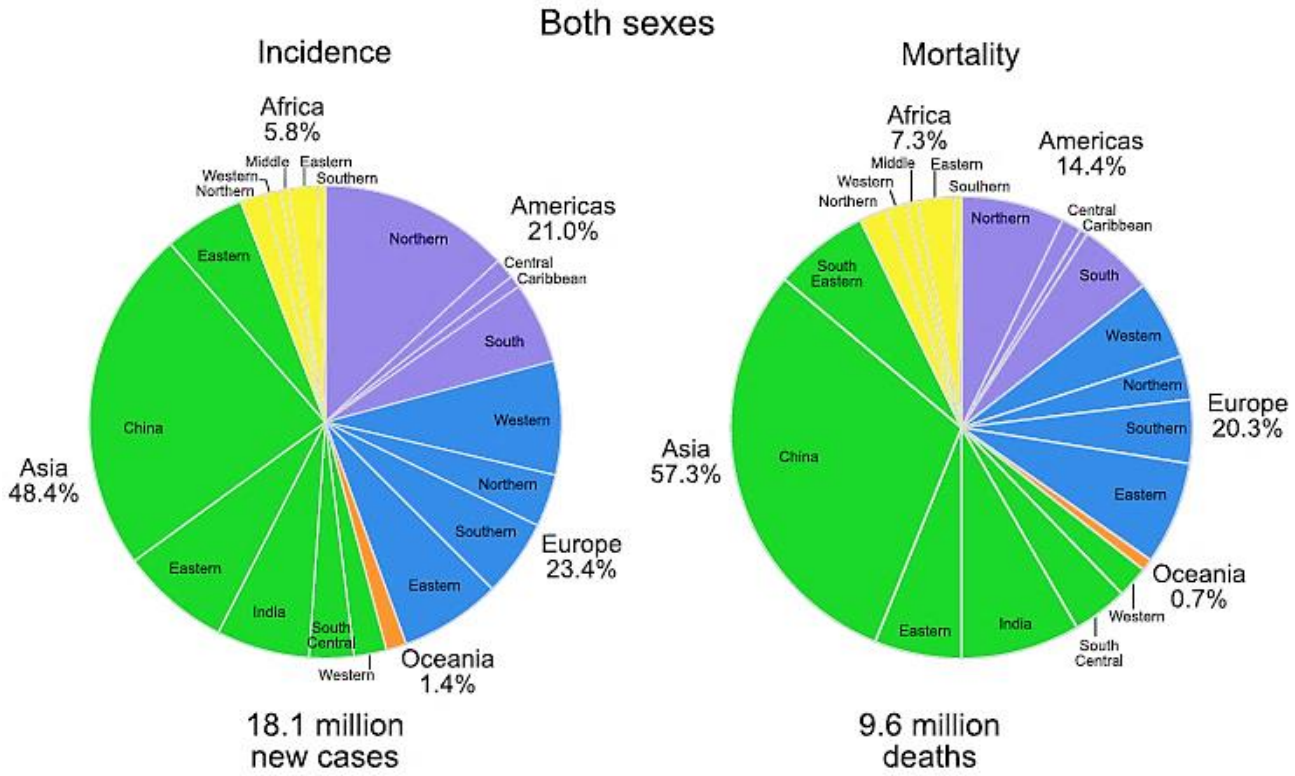

Figure 4 The global cancer incidence and mortality in 2018, both sexes

Almost one-half of all cancer cases (48.4%) and over one-half of all cancer deaths (57.3%) is occurring in Asia, follow by Europe (23.4% incidence and 20.3% mortality), America (21% incidence and 14.4% mortality) and Africa (5.8% incidence and 7.3% mortality) [(1)]

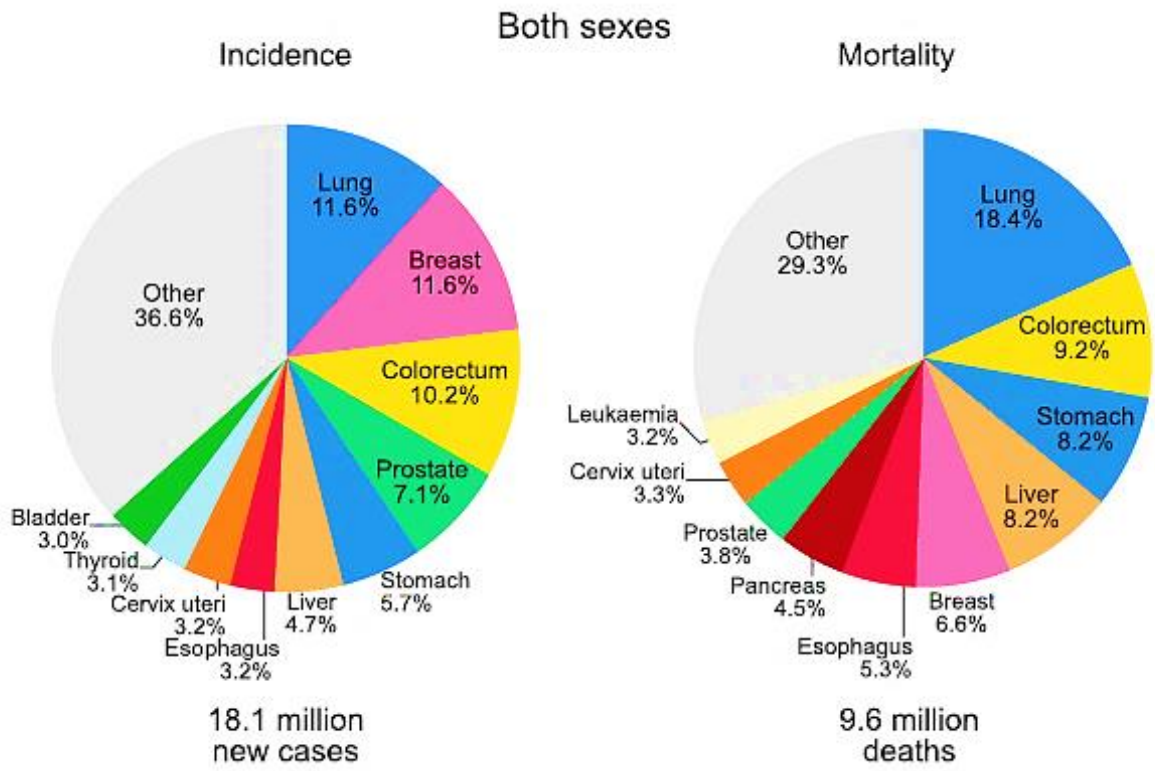

Figure 5 The most diagnosed cancers and cancer deaths in 2018, both sexes

The four most diagnosed cancers are the lung, breast, colorectum and prostate cancer while the four most cause of cancers deaths are the lung, colorectum, stomach and liver [1].

2.1.1.2 Epidemiology of cancer in Thailand

Thailand is located in South-east Asia and is bordered to the north by Laos and Myanmar, to the east and the northeast by Cambodia and Laos, to the west by the Andaman Sea and Myanmar, and to the south by the Gulf of Thailand and Malaysia. Southwestern coast of Thailand stretches along the Andaman Sea, whereas the southern and southeastern coastlines border the Gulf of Thailand [24, 25]. In each region, there is a representative population-based cancer registry which refers to a cancer registration finding in that geographical area. The first start was in Chiang Mai (1986), as for the Northern, followed by Khon Kaen (1988), Songkhla (1990) and Bangkok (1990) for Northeastern, Southern and Central [24-26] region, respectively. Afterwards, the following registry was in Lampang, a representative for the Northern in 1993 [25]. Each registry reveals different cancer sites as most prevalent, for examples, liver cancer especially cholangiocarcinoma is first in Khon Kaen, lung cancer predominates in Chiang Mai; cancer of cervix is high in all registry, i.e., Khon Kaen, Chiang Mai, Songkhla, Bangkok [27]. Moreover, with co-operation of the registries of Chiang Mai, Khon Kaen, Songkhla, the National Cancer Institute (Bangkok), and the International Agency for Research on Cancer (IARC), the volume of "Cancer in Thailand" was first published in 1993 [27, 28]. Afterwards, the second, third, fourth, fifth, sixth and seventh volumes of "Cancer in Thailand" have been published in series in 1999, 2003, 2007, 2010, 2012 and 2013 [24, 27-32].

According to volumes of Cancer in Thailand, the estimated numbers of the incidence rate for 1990-2008 have been revealed, as shown in Table 1. In 1990, the estimated numbers of new cancer cases in males was 29,195 and the estimated number in females was 28,773. These number of cases correlate to age-standardized rates (ASR) of 149.6 and 125.2 per 100 000 in males and in females, respectively [27]. The estimated numbers of new cancer have increased in the year 1993, 1996 and 1999—with 32,801, 35,539 and 31,582 cases for males and 30,940, 38,467 and 33,678 cases for females [28, 31, 32]. Nevertheless, with subsequent addition of cancer registries in Thailand, the estimated numbers of new cancer cases have even more increased in the

year 2001-2006—with 121,986 and 145,788 cases for males and 119,065 and 150,768 cases for females [29, 30]. The estimated numbers of new cancer cases in 2008 was 50,966 and 51,825 cases for males and for females, respectively [24].

Table 1 Estimated cancer incidence in Thailand, 1990-2008

Estimated year	Male		Female		Reference
	Number of cases	ASR/ 100,000	Number of cases	ASR/ 100,000	
1990	29,195	149.6	28,773	125.2	Cancer in Thailand: vol. I, 1993 [27]
1993	32,801	151.3	30,940	123.8	Cancer in Thailand: vol. II, 1999 [28]
1996	35,539	149.2	38,467	125.0	Cancer in Thailand: vol. III, 2003 [32]
1999	31,582	127.7	33,678	125.5	Cancer in Thailand: vol. IV, 2007 [31]
2001-2003	121,986	143.3	119,065	118.6	Cancer in Thailand: vol. V, 2010 [30]
2004-2006	145,788	158.8	150,768	138.3	Cancer in Thailand: vol. VI, 2012 [29]
2008	50,966	156.7	51,825	138.2	Cancer in Thailand: vol. VII, 2013 [24]

Taken together according to Cancer in Thailand vol. III to VII [24, 29-32], the high incidence of liver and bile duct cancer, preferably in northeastern region, and of bronchus and lung cancer denote to be significant in affecting male populations of the whole country since 1996. Nevertheless, cancer incidence was more concerned in Thai female populations. From 1996 to 2008, breast cancer and cancer of the cervix (cervical cancer) have been the 2 most leading cancers in Thai females. Moreover, liver cancer has been the leading cancer in both sexes, while the incidence of colorectal cancer has also been increasing. Accordingly, liver, lung, breast, cervix and colorectal cancer have been the 5 significant cancers of Thailand from 1996 to 2008.

With reasons of rapid socioeconomic development and the handling performance of noncommunicable disease in Thailand resulted in the emergence of cancer as the third most common cause of death in 1996 [25], with the rate of 48.9/100,000 per year (1996) [25], and then turned out to be the second most common

cause of death—60.5/100,000 per year in 1999 and finally the most common cause of death—65.4/100,000 per year in 2002 [25]. According to Centers for Disease Control and Prevention (CDC), Thailand (July 2014), cancer (19%) has been ranked as the most common cause of death by disease in Thailand, followed by ischemic heart disease (12%) and stroke (10%) [33]. Obviously, with significant cancers as the leading causes of death in Thai and yet global populations, should also guide the development and execution of screening, diagnostic, and therapeutic intervention.

2.1.2 Types of cancer

Cancer can be classified into 5 major types according to their tissue of origin (location or to their normal cell types).

2.1.2.1 Carcinoma

Carcinoma is the most commonly diagnosed cancer type that originates in the cells that make up skin or in the epithelium tissues that line or cover internal organs such as liver or kidneys, lungs, breasts, colon, pancreas, ovarian, and other organs and glands, for examples, adenocarcinoma, ductal carcinoma, and basal cell carcinoma.

2.1.2.2 Sarcoma

Sarcoma is a malignant tumor derived or originated from the connective or supportive tissues of the body such as bone, cartilage, fat, muscle, blood vessels, nerves, tendons, e. g., osteosarcoma, synovial sarcoma, liposarcoma, angiosarcoma, rhabdosarcoma and fibrosarcoma.

2.1.2.3 Lymphoma and myeloma

These refer to a group of cancers in lymph nodes which are found in clusters throughout the body including underarms, groin, neck, chest, abdomen, stomach, intestines and skin, which play important role in taking parts of the body's defense mechanism. Therefore, this type of cancer is derived from hematopoietic stem cells developed in lymph nodes and immune tissues, e.g., T-cell lymphoma, B-cell lymphoma, Hodgkin lymphoma, non-Hodgkin lymphoma, and lymphoproliferative lymphoma.

2.1.2.4 Melanoma

Melanoma is a cancer that predominantly originates in melanocytes, the melanin-producing cells in the skin. The vast majority of melanoma begins with skin melanoma, but can also be found in pigmented tissues elsewhere such as in the eye or in the intestines.

2.1.2.5 Leukemia

Leukemia is a cancer that starts in blood-forming tissues of the body, such as bone marrow, and involves white blood cells. The disease causes a large number production of abnormal white blood cells that enter the blood circulation, e.g., lymphoblastic leukemia, myelogenous leukemia, T-cell leukemia, and hairy-cell leukemia.

2.1.3 Cancer risk factors

Transformation of cells in cancer derived from genetic factors with exposing external factors, agents or carcinogens including physical carcinogens, chemical carcinogens and biological carcinogens. These factors are described below.

2.1.3.1 Age and sex

Ageing is a fundamental risk factor in cancer development. Cancer incidence rises with age due to an accumulating of risks along age and due to less effective cellular repair mechanisms as a person grows older. For example, less than 1% of cancers are diagnosed in children with age 0-14 years, leukemia and lymphoma are frequent in children, while cancer of lung, colon and rectum prevalently appear in the older. Additionally, many cancers certainly occur in women such as cancer of cervix, breast and ovary, while lung cancer has more risk in men due to smoking habit.

2.1.3.2 Diet and lifestyle

These include smoking, heavy alcohol consumption, prolonged UV exposure and unhealthy diet. Smoking habit is a major cause of lung cancer and a risk factor of larynx, oesophagus, oral cavity and pharynx, bladder, pancreas, kidney, liver, stomach, bowel, cervix, leukemia, and ovarian cancers. People who prolonged UV exposure can

develop melanoma. The unhealthy diet such as high animal fats can influence development of breast, bowel and prostate cancers while the obesity has often led to breast or kidney cancer. In addition, a low diet in vegetables and fresh fruit may associate with some cancer development.

2.1.3.3 Environmental and occupational workplace

The person's exposure of certain harmful substances or carcinogens in the environmental or occupational workplace can influence to cause cancer. For example, mesothelioma developed in 9 out of 10 people who contacts with asbestos in ship-building and construction. Development of bladder cancer has all been associated with certain chemicals in dye factories, rubber production, gas working and other chemical.

2.1.3.4 Virus and bacterial infections

Chronic infections by microorganisms can contribute to cancers development. For example, sexually acquired infection by human papilloma virus (HPV) is known to associate with cervical carcinoma. Other viral infections include: Hepatitis B virus (HBV)—associates with liver cancer; Hepatitis C virus (HCV)—associates with cervical cancer; human immunodeficiency virus (HIV)—associates with cervical cancer; Epstein-Barr virus—associates with lymphoma. Moreover, bacterial infection with *Helicobacter pylori* is also known to associate with a rare type of stomach cancer.

2.1.3.5 Genetics

About 5-10% of cancers are thought to be caused by accumulated inherited genes mutation. Genes which involve in carcinogenesis consist of oncogenes, tumor suppressor genes and DNA repair genes. Multiple mutations of DNA repair genes are the cause of cells to fail in repairing several other genes from error. Multiple mutations of oncogenes, tumor suppressor genes or other growth-related genes cause the cell to proliferate excessively, which eventually produce a highly malignant tumor.

2.1.4 Molecular causes of cancer

Cancer is an incredibly complicated disease. In 2000, Hanahan and Weinberg described that every single cancer cells exhibit six common traits known as "Six

Hallmarks of Cancer" [15] (Figure 6) which facilitate the transformation of a normal cell to become a cancer cell and enable growth and metastasis to distant organs. The emergence of traits is from a multistage [34, 35] alteration in genes expression that modulate the growth/apoptosis [36], angiogenesis [37], or metastasis [38] pathways, in cancer. Moreover, in 2011, Weinberg and Hanahan identified 2 more hallmark features and 2 additional enabling characteristics which facilitate in carcinogenic process [39].

Overall features that distinguish tumor cells apart from normal cells include six original hallmarks (Figure 6)—1) sustained proliferative signaling, 2) evasion from growth suppressors, 3) resisting cell death, 4) enabling replicative immortality, 5) angiogenesis induction, 6) invasion and metastasis activation; [15] and four recent hallmarks: 1) reregulation of cellular energetics, 2) immune avoidance, 3) genomic instability, 4) tumor promoting inflammation [39]. The original "Six Hallmarks of Cancer" is described in detail below. In addition, the basis in the formation of such features is concerned with genome instability. By considering a single tumor specimen, over a hundred gene mutations could be found. Moreover, if two cancer specimens are compared, the set of mutated genes are far from identical, indicating that every tumor is unique.

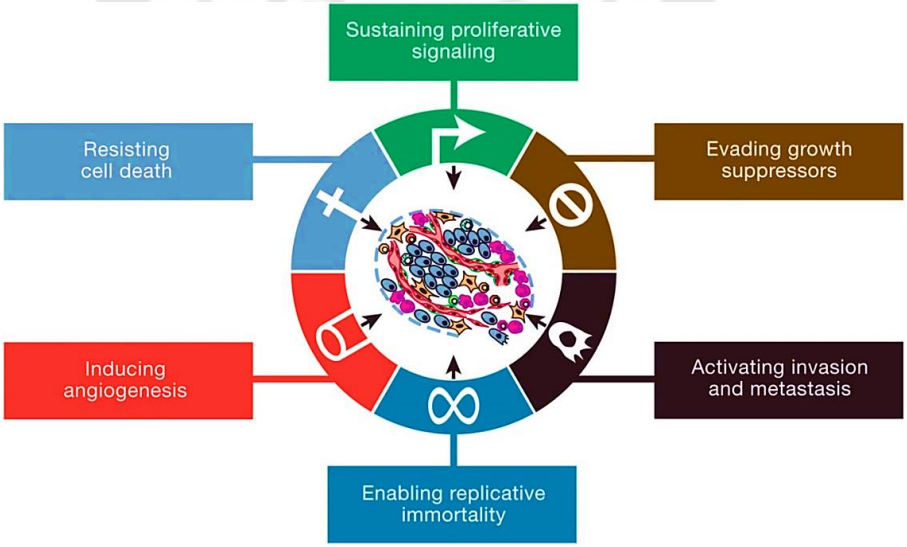

Figure 6 Six Hallmarks of cancer

Available from: https://www.cell.com/fulltext/S0092-8674(11)00127-9

2.1.4.1 Sustained proliferative signaling (Self-sufficiency in growth signals)

Normal tissues carefully control the production and release of growth-stimulatory signals which order towards progression of cell growth-and-division cycle. Signaling in normal cell growth and proliferation is highly regulated as activation only occurs in a necessity. The highly regulation in normal cells thus ensures a homeostasis of the number of cell, as well as maintaining normal tissue architecture and function. Strangely, cancer cells themselves have the capability of inducing and sustaining positively acting growth-stimulatory signals. This impairment in growth signaling regulation eventually results in the sustaining of ongoing proliferation. Capability of cancer cells to proliferate without signaling input achieved in a number of ways [39] including of increasing growth factor production, stimulating normal cells in the microenvironment to provide growth factors for cancer cells, increasing the number of cell surface receptors, activating the downstream signaling proteins and finally resulting in cell proliferation.

2.1.4.2 Evading growth suppressors (Insensitivity to growth inhibition signal)

In normal cells, cell proliferation is a tightly controlled process wherein the signals of proliferation and antiproliferation concurrently work at the cell cycle level wherein the antigrowth signals exert against proliferation [40]. At the level of G1 phase, there is an essential checkpoint wherein the antigrowth signals can block proliferation by the induction of the G0 phase and a postmitotic state, which usually associate with cell cycle arrest, senescence, terminal differentiation or apoptosis of the cell [40, 41]. These negative regulations to prevent excessive cells proliferation are achieved by activation of tumor suppressor genes and proteins which operate as central nodes to control decisions of the cells to proliferate or activate senescence and apoptotic programs [39].

However, cancer cells have ability to circumvent these growth suppressors which results in continuity of cell proliferation [39]. The two most tumor suppressors involved in the controls of cell cycle in normal tissues but be deregulated in cancer cells are the retinoblastoma and p53 (TP53) proteins [39, 40]. The Rb protein energetically inhibits cell passage at G1 cell cycle phase while mutated Rb defects in RB pathway as

that eliminate critical gatekeeper of cell-cycle progression, and thereby permits for ongoing cell proliferation. The p53 protein functions as a central regulator by triggering in apoptotic pathway in order to provide cell cycle arrests in the presence of DNA damage while the loss of functional p53 protein certainly allows for the ongoing cell cycle progression in spite of occurrence in genomic damage and/or cellular stress [39].

2.1.4.3 Resisting cell death (Evasion of apoptosis)

Apoptosis is a type of programmed cell death which serves as a natural barrier against the development of cancer. The apoptotic pathway can be triggered or switched on in response to stress-inducing events that cells experience such as irreparable DNA damage. However, cancer cells with the experience of various physiologic stresses, such as during anticancer therapy, can avoid ordering a response in apoptosis [42].

Apoptotic machinery in normal cells is composed of upstream regulators and downstream effectors [43]. The regulators are divided into 2 significant circuits of the "extrinsic pathway"—receiving and processing extracellular apoptosis-inducing signals triggering by binding of pro-apoptotic ligands to pro-apoptotic cell surface receptors (Fas ligand/Fas receptor) and the "intrinsic pathway"—sensing as well as integrating various signals of intracellular origin triggering as a safety mechanism in response to severe cell stress, e.g., DNA damage. Both intrinsic and extrinsic programs are responsible in proceeding to the activation of 2 latent functional proteases in apoptosis pathway, i.e., caspases 8 and caspases 9, which serve to initiate a downstream cascade of proteolysis-involving effector caspases which are responsible in the execution phase of apoptotic pathway, wherein cell is progressively break up and finally consumed by either neighboring or phagocytic cells [39].

Triggering in apoptosis is controlled by counterbalancing between pro-apoptotic and anti-apoptotic members in the Bcl-2 family of regulatory proteins [43]. The anti-apoptotic proteins (Bcl-2, Bcl-xL, Bcl-w, Mcl-1 and A1) act by binding and suppressing two pro-apoptotic triggering proteins, Bax and Bak, embedded in the mitochondrial outer membrane, and inhibit cytochrome c release. Whenever relieving of Bax and Bak disrupt the mitochondrial outer membrane integrity, resulting in pro-

apoptotic signaling proteins release and release of cytochrome c into cytosol. The subsequent event is the activation of a caspases signaling cascade which possesses proteolytic activities to induce numerous cellular changes in apoptosis [43, 44].

Dreadfully, cancer cells are capable to evolve in order to circumvent with death sensing. Basically, they accumulate genetic alterations machinery which thereafter provide them to disable the vital apoptotic-signaling program [42, 44, 45], particularly, the intrinsic apoptosis pathway which usually serves as a barrier to cancer pathogenesis. Nearly all cancer cells can deregulate this pathway by downregulating or silencing the pro-apoptotic proteins, e.g., Bax, Bak, Bim, Puma, and overexpressing the anti-apoptotic proteins, i.e., Bcl-2 proteins family [39, 42, 44, 45].

Apart from alteration in apoptosis, cancer cells have ability in resisting cell death through the alteration of typical cellular autophagy—cell regulation process for breaking down organelles in energy metabolism [39, 46], and necrosis—a type of cell death to explode and release cellular contents which serve as pro-inflammatory signals into surrounding tissue microenvironment that may actively supports tumor growth [39].

2.1.4.4 Enabling replicative immortality

Normal cell lineages are capable to pass through only a finite number of cell growth-and-division cycles. This intrinsic cellular mechanism associates with two distinct barriers: 1) senescence—a typically irreversible entrance into a viable nonproliferative state, and 2) crisis—a state which involves with apoptosis [39]. Mechanism is involved with functioning of telomerase, a DNA polymerase that normally serves to maintain telomere length. However, the capability in proliferating without either senescence or crisis evidence that lead to unlimited replicative potential—i.e. termed “immortalization”, is a trait possessed by most established cell lines and cancer cells [39]. These cells have ability to overexpress the functional telomerase that correlated with the senescence and crisis/apoptosis resistance.

2.1.4.5 Angiogenesis induction (Sustained angiogenesis)

In normal state during embryogenesis and adult transient physiologic conditions, e.g., wound healing and female reproductive cycling, the development of blood vessel (vasculature) termed “angiogenesis” is switched on and becomes mainly quiescent thereafter. This process involves with a growth stimulation of new blood vessels from the existing ones (neo-angiogenesis) and a birth origin of new endothelial cells as well as their assembly into tubes (vasculogenesis). In contrast, during tumor progression angiogenesis is required for the enlargement beyond 1–2 mm of solid tumor. Thus the process is always switched and remains on, in order to continually receive nutrients and oxygen as well as to remove carbon dioxide and metabolic wastes.

The angiogenic switch is controlled by inducing or opposing factors [47, 48] known as pro- and anti-angiogenesis proteins that bind to stimulatory and inhibitory receptors, respectively, on vascular endothelial cells surface [39]. Two well-known pro- and anti-angiogenesis proteins are vascular endothelial growth factor-A (VEGF-A) and thrombospondin-1 (TSP-1), respectively. Nevertheless, to promote the process of tumor angiogenesis, multistep signaling is activated by various pro-angiogenic growth factors [48, 49]. Angiogenic switch in cellular stress such as hypoxia can lead to overexpression and release of pro-angiogenesis proteins such as VEGF (vascular endothelial growth factor) or FGF (fibroblast growth factor), into extracellular matrix (ECM) [39] which may simply effect in stimulation of tumors to produce new vessels. In addition, the anti-angiogenic p53 protein is often disabled in tumors, while recruitment of pericytes and bone marrow–derived cells (e.g. macrophages and neutrophils), also play a role in forming new blood vessels [39] and may assist angiogenesis initiation [39]. Eventually stable angiogenesis allows tumor expansion, local invasion, and enable tumor cells to enter blood circulation which lead to cancer metastasis [49].

2.1.4.6 Invasion and metastasis activation

Tissue invasion and metastasis indicate how tumor cells evade far from primary site and disseminate to distant organs or tissues. The process is a complex series of cell-biological events termed the “invasion-metastasis cascade” [50] that associates with

multistep in changing the way in cell-cell and cell-ECM attachments [51, 52]. In such process, the invasive cancer cells have ability to break through the basal lamina by the secretion of matrix metalloproteinases (MMPs), the enzymes which degrade ECM and environment, providing the cancer cells to exit their primary sites of growth to enter the bloodstream and circulate until they exit the bloodstream at distant organs or tissues. During the process, the cancer cells have ability to develop alterations in shape and attachment by the increased expression of adhesion molecules, e.g., N-cadherin and E-cadherin [39]. Cancer metastasis is also involved with molecular cross-talk between tumor cells and neoplastic stroma [39] by the aid of tumor-associated macrophages (TAMs) that supply epidermal growth factor (EGF) and colony-stimulating factor 1 (CSF-1) to cancer cells during intravasation.

2.1.5 Multistep process of cancer metastasis

The cancerous cells can break away from the primary cancer and spread to other parts/organs within the body through the bloodstream or lymphatic system. When the cancer cells reach a new part of the body, they may carry on dividing and form a new tumor called “secondary cancer” while such progress is known as “metastasis” (Figure 1). Only malignant tumors are capable in metastasizing by the multistep invasion-metastasis cascade (Figure 7), as described below:

Step 1: Local invasion

In this step, cancer cells invade only nearby normal tissue. Therefore, the step involves progressive tumor growth with supplied nutrients and extensive vascularization when a tumor mass is to exceed 1–2 mm in diameter. Therefore, such tumor requires the synthesis and secretion of angiogenic factors in order to establish a capillary network from the surrounding tissue to support the growing tumor.

Step 2: Intravasation

Cancer cells start to invade by destroying surrounding tissues. The cancer cells relieve adhesion to neighboring cells and clear a path for their migration into the vasculature-rich stroma. The cells can eventually penetrate through the walls of the

nearby blood or lymph vessels by causing endothelial cell retraction. Particularly, the thin-walled venules (small vein) provide the most common route for cancer cells to enter the bloodstream. This is enhanced by VEGF, MMPs as well as reactive oxygen species (cause endothelial cell death), released by metastasizing cells. In the bloodstream, most tumor cells are rapidly destroyed while the survivors translocate systemically or arrest at a secondary distant organ by being trapped in the capillary bed or adhering to the capillary endothelial cells or subendothelial basement membrane. Cancer cells can also bind to platelets which protect them from shear forces and shield them to evade immune detection [53, 54].

Step 3: Extravasation:

At the secondary organ, cancer cells can exit the bloodstream by inducing endothelial cell retraction or death. In order to survive and proliferate at the secondary organ, a cancer cell must be able to tolerate with different local microenvironments [55] by releasing pro-inflammatory compounds and proteinases that stimulate neighboring cells to release growth factors to support tumor growth. The progress is referred to “micrometastasis” and “colonization”. Moreover, the secondary cancer needs to develop a vascular network that allows cells to reinvade by entering the blood circulation and producing more metastases throughout the body thus becomes “macrometastasis” [55]. The successful cancer metastasizing also depends on the ability of the immune cells at a primary site, within the bloodstream and lymphatic system and at distant organ sites. Furthermore, cancer cells may lie dormant at a distant organ for many years before they begin to grow.

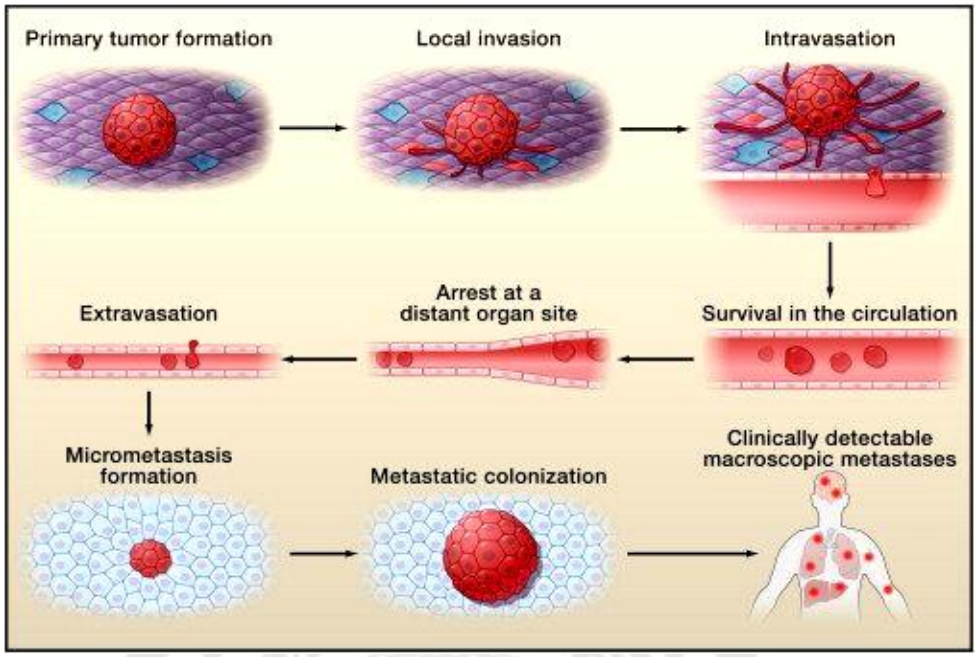

Figure 7 Tumor metastasis showing the invasion-metastasis cascade

Tumor cells exit primary sites of growth via local invasion and intravasation to enter nearby blood circulation, translocate systemically (survive in blood and lymphatic circulation, then arrest at a distant organ site) and exit the circulation via extravasation at a distant organ tissue. They adapt to survive as the small cancer nodules in the new microenvironment known as “micrometastasis”. After colonization at several sites, cancer lesions become macroscopic tumors known as “macrometastasis” [30, 34, 56].

Available from: https://www.researchgate.net/figure/The-invasion-metastasis-cascade-Tumor-cells-exit-their-primary-sites-of-growth-local_fig1_229072893

2.1.6 Stages of cancer

Cancer staging is the process of determining or diagnosing the extent of a cancer locally or developed spreading to another part of the body. The process is also used to describe the cancer severity by determining cancer size and how far it has grown (invade to adjacent organs, spread to regional lymph nodes or distant locations). Same stage of cancers tends to have similar prognosis and are often treated in a similar way. The TNM classification is one of the most common system used in staging based

upon values of tumor formation (T), lymph node involvement (N) and presence of metastasis (M). These values are combined together to determine the overall stage grouping, as followings:

Stage 0

This stage is used to describe cancer *in situ*, i.e., cancer is in the original site and there is no invasion to nearby tissues. Stage 0 cancer is often highly curable, normally by removing the entire tumor by surgery.

Stage I

This stage is often called the “early-stage cancer”. It is the small size cancer of which abnormal cells clump together and start to penetrate beneath the top layer of the original organ. Cancer has not grown deeply into nearby tissues and no spreading to lymph nodes or other parts of the body. Stage I cancer is typically highly treatable by surgery.

Stage II

Cancers are locally advanced as cancerous cells begin to grow into a small tumor within the organ of origin as well as spread into the local lymph nodes. Stage II cancer can be treated by chemotherapy, radiation, or surgery.

Stage III

Cancers are also locally advanced as the cancerous cells have grown into a larger tumor, more deeply into nearby tissue and have spread into lymph nodes and surrounding tissues but not to other parts of the body. Stage III cancer can be treated by chemotherapy, radiation, or surgery (similar to stage II).

Stage IV

This stage of cancer is also called “advanced”, “secondary”, or “metastatic” cancer, since the cancers have frequent metastasized or spread to other organs or parts of the body. Usually, stage IV cancer is the most often difficult to treat by chemotherapy, radiation, or surgery.

2.1.7 Cancer signs and symptoms

Cancer patients can present a variety of signs and symptoms depending on cancer size and location, such as, being adjacent to nearby organs/tissues and whether spreading to distant parts. In early stages of cancer, patients may have no symptoms. Once cancer becomes grower, it begins to press the nearby organs, blood vessels and nerves, thus causing pain and bleeding symptoms. With the large or malignant tumors, such areas are eventually compromised since the function of organs and body's systems are interfered. Moreover, even small tumor size can cause symptoms if it locates in a critical area such as certain parts of the brain. Cancer patients can also have nonspecific signs and symptoms due to the responsive immune system or the substances released by cancer cells that cause changing in metabolism. The followings are the most common signs and symptoms occurring in cancer patients.

2.1.7.1 Local symptoms

Local symptoms include unusual clumps or swelling, pain, hemorrhage, and ulceration. With compression of larger tumor mass within surrounding tissues may also cause symptoms such as jaundice. Moreover, suspicious skin changes can be seen in malignant melanoma.

2.1.7.2 Symptoms of metastasis

Metastasis is an advanced stage of cancer. Therefore, the symptoms found in cancer patients are enlarged lymph nodes, coughing and hemoptysis (coughing up blood), hepatomegaly, bone pain and fracture, and neurological symptoms.

2.1.7.3 Systemic symptoms

When cancer metastasize and invade throughout the body, the symptoms are systemic. These consist of fever, unexplained weight loss, poor appetite, fatigue (extreme tiredness) and cachexia (body weakness), excessive or night sweating and anemia. Moreover, the specific symptom referred to "paraneoplastic phenomena" can be found in patients. For example, some pancreas cancers can cause thrombosis (blood clot) in veins, whereas some lung cancers make the hormonal changes that raise

the blood calcium levels, thereby affecting nerves and muscles and thus make the patients weakness and dizzy.

2.1.8 Cancer treatment and therapy

Cancer therapy depends on the specific tumor type, location, grade and stage of the disease. After patient being diagnosed with cancer, patient is usually treated with a combination treatment or therapy. Since all cancers are not identical thus individual type of cancer would have its own treatment strategy and becomes more specific. In addition, a number of experimental studies and clinical trials for cancer treatment and therapy are under development with a goal to eliminate cancers without damaging the rest of the body. For example, the development of targeted therapy is to utilize drugs for acting specifically on the defined molecular abnormalities of certain tumors, and thus minimize damaging to the normal cells.

2.1.8.1 Surgery

Surgery is an operation to remove the tumor mass situated only in one area of the body (no spreading to other body parts) as well as the affected lymph nodes. However, after operation the treatment's limit might come from cancer cell invasion to the adjacent tissues or spreading to the distant sites by microscopic metastasis.

2.1.8.2 Radiotherapy

The radiotherapy is the use of high energy X-rays to destroy cancer cells at the affected area of the body. However, radiation treatment also causes a damage to normal cells. Moreover, it can commonly cause the tiredness and side effects depending on the treated part of the body.

2.1.8.3 Hormonal therapy

Hormone therapy is the use of anti-hormone drugs, for examples, anti-estrogen and anti-androgen, to alter the levels of particular hormones related to cancer cells growth and division, or to block the growth hormones from binding to cancer cells.

2.1.8.4 Biological therapy

Biological therapy is the use of body's substances for destroying cancer cells. The examples of biological agents are cancer growth inhibitors, monoclonal antibodies,

immunotoxins, antibody-toxin fusion proteins and tumor vaccines that trigger immune responses to specific tumor antigens, and therapeutic genes.

2.1.8.5 Chemotherapy

Chemotherapy is the use of anti-cancer or cytotoxic drugs or agents for destroying cancer cells. The forms of drugs, a single drug or drugs in combination, given to the cancer patients include tablets, capsules and injections into vein. Anti-cancer drugs in the bloodstream can travel throughout the body to destroy cancer cells of the affected tissues though frequently also effect to normal cells and cause side effects.

Most chemotherapeutics agents target the rapid proliferating tumor cells. These agents include: DNA damaging drugs, e.g., carboplatin and melphalan; DNA repair inhibitors, e.g., nitrosoureas; microtubule modifiers that target the mitotic spindle in M-phase cells, e.g., paclitaxel, vinblastine, and vincristine [57]; antimetabolites that interfere DNA or RNA replication, e.g., doxorubicin, gemcitabine, and 5-fluorouracil [58]; steroids that inhibit hematopoietic cells growth in hematological malignancies, e.g., dexamethasone [59]. The agents also include anti-hormone drugs to slow growth of hormone-responsive cancers such as anti-estrogens (tamoxifen and fulvestrant) for breast cancer [60] and anti-androgens (bicalutamide and flutamide) for prostate cancer [61]. Recently, therapies are likely to direct at specific signaling molecules in order to inhibit the signaling of: tumor growth, e.g., trastuzumab and gefitinib [62]; angiogenesis, e.g., 2-methoxyestradiol and anti-VEGF [63]; invasion, e.g., MMP inhibitors [64]. Furthermore, the targeted therapy offers the effectiveness in specificity and selectivity that rely on the elevated expression of the target molecules in tumor cells—e.g. Herceptin that targets the overexpressed Her2/neu in breast cancer, thereby reducing toxicity to normal cells. [65, 66]

Despite most patients initially respond to these therapies, the chemoresistance frequently occurs and thus the outcome is incomplete elimination of cancerous cells. [67, 68] Such resistant is caused by decreased drug uptake and increased effusion due to tumor modifications in ways such as the modified tumor

microenvironments and the absence of the targeted molecules [69-72]. Thus, two approaches have been developed in order to overcome drug resistance. The first approach is to search for new anticancer drugs or agents for replacing several current chemotherapeutics that frequently lose their effectiveness, while the second is to develop new strategies for cancer treatment.

2.2 Cervical cancer

Cervical cancer or cancer of the cervix is caused by sexually acquired infection with the certain types of Human papilomavirus (HPV), a small, non-enveloped circular-DNA virus of papillomavirus family that infects genital skin or mucosal cells [47, 48]. Mostly, HPV infections do not cause symptoms and can be resolved spontaneously. However, the persistent infection of HPV especially types 16 and 18 can lead to the precancerous cervical lesions that may progress to cervical cancer if left untreated [73].

2.2.1 Epidemiology of cervical cancer

Cervical cancer is the second most common cancer among women worldwide. It has been the leading cause of mortality among women especially in the developing countries. In 2012, WHO estimated 530,000 new cervical cancer cases with approximately 270,000 deaths, [74-80] of which more than 85% occurred in low- and middle-income countries [73]. Currently, cervical cancer has been ranked as the second most common disease occurring in Thai women. Moreover, GLOBOCAN estimated the marked increase patterns of cervical cancer in women. Accordingly, the priority should be given to the cervical cancer prevention and control globally.

2.2.2 Risk factors of cervical cancer

Though most HPV infections can be cleared up and precancerous lesions can be resolved spontaneously, the women with HPV infection at the cervix still have the most frequent risk since chronic infection and precancerous lesions might progress to invasive cervical cancer. Other possible risk factors of developing cervical cancer include: [81, 82]

1) Giving birth to many children
2) Having several sexual partners or having sex with person who has had multiple sexual partners
3) Having first sexual intercourse at a young age
4) Using oral contraceptives longer than 5 years
5) Immunosuppression
6) Infection with human immunodeficiency virus, type 1 (HIV-1)
7) Chlamydia infection
8) Family history of cervical cancer
9) Age (30 -60 years)
10) Cigarette smoking
11) Diet with low fruits and vegetables

2.2.3 Anatomical structure of cervix and cervical cancer

Cervix is an area in connection between the body of uterus and vagina [81] (Figure 8). The cervix can be divided into 2 parts: endocervix—a part of cervix adjoining to the uterus and ectocervix (exocervix)—a part of cervix adjoining to the vagina. Two cell types lining the surface of the cervix can become cancerous, i.e., glandular cells (column shape) of the endocervix and squamous cells (thin and flat shape) of the ectocervix (Figure 9). The boundary between these 2 cell types, called the squamocolumnar junction zone, is where cervical cancer most often occurs [83].

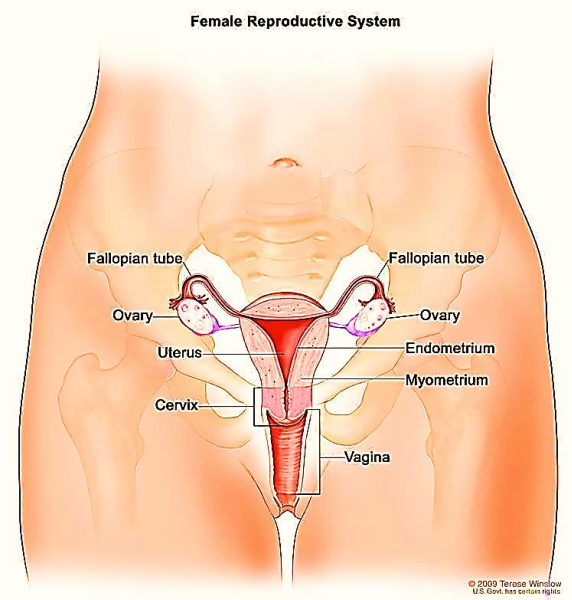

Figure 8 The anatomy of female reproductive system

Available from: https://www.cancer.gov/types/cervical/patient/cervical-treatment-pdq#section/all?redirect=true

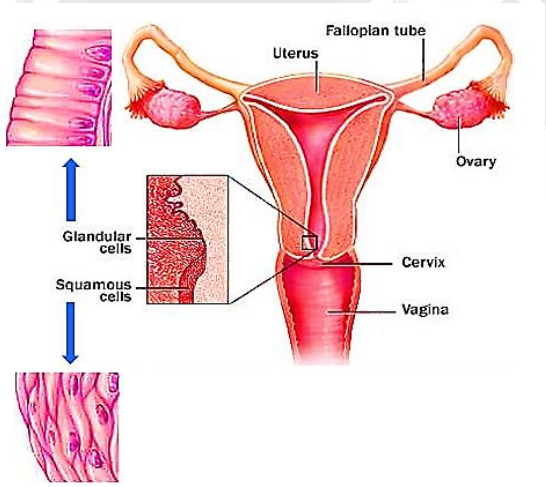

Figure 9 The cervix structure is between the body of uterus and vagina

Two cell types of the cervix, i.e., glandular cells and squamous cells, are shown.

Modified from: https://www.mayoclinic.org/diseases-conditions/cervical-cancer/multimedia/where-cervical-cancer-begins/img-20007066; https://pathologyproject.files.wordpress.com/2012/02/cervical-cancer7.jpg

2.2.4 HPV infection and cervical cancer

Mostly, cervical cancer patients previously has HPV infection by sexual contact [73] and leads to the mutation of genes involving in cell growth and proliferation. The 13 types of high-risk HPV, called oncogenic or carcinogenic HPVs, include types 16, 18, 31, 33, 35, 39, 45, 51, 52, 56, 58, 59 and 68, of which types 16 and 18 are the most critical for ~70 % of cervical cancers [73]. While the 12 types of low-risk HPV include types 6, 11, 40, 42, 43, 44, 53, 54, 61, 72, 73 and 81, which cannot cause cervical cancer but can cause genital warts or little changes in the cervix tissue.

Spreading of HPVs occurs by direct skin-to-skin contact during vaginal, anal and/or oral sex with the individual who has HPV infection. After HPV infection in the cervix tissue, it leads the normal cervix cells to change into the abnormal cervix cell called dysplasia (Figure 10) which can cause genital cancers including cervical, vulvar, and anal cancers [80, 84]. However, the progression into cervical cancer is usually slow. It takes about 5-10 years in women with the weakened immune systems or about 15-20 years in the healthy women to develop cervical cancer [73].

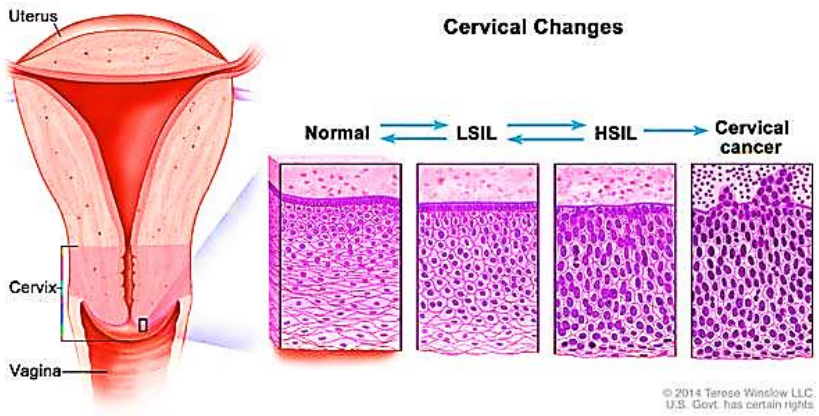

Figure 10 The change of cervix cells over time after HPV infection

Abnormal cells might return to normal cells without treatment especially in younger women. LSIL (Low-grade squamous intraepithelial lesion) and HSIL (High-grade squamous intraepithelial lesion) are two types of abnormal changes to cervical squamous cells. Available from: https://www.cancer.gov/types/cervical/understanding-cervical-changes

2.2.5 Types of cervical cancer

Cervical cancers are classified into 2 major types—squamous cell carcinoma and adenocarcinoma. About 80-90 % of cervical cancers are squamous cell carcinomas which occur at the surface of the ectocervix, while the less common adenocarcinoma occurs at the endocervix, which is more difficult to diagnose due to its site [83, 85-87]. In addition, the cervical cancers of mixed carcinomas called adenosquamous carcinomas are rarely found. Cervical cancer can metastasize to other parts of the body via the lymphatic system. Microinvasive cervical cancer means that cancer cells break through the boundary between epithelium and stroma and cells do not spread into the cervix tissues over 5 mm. While invasive cervical cancer means that cancer cells spread into the underlying stroma over 5 mm and is capable to spread to the vagina, lymph nodes, surrounding tissues, or nearby organs such as bladder or rectum [82].

2.2.6 Grades, stages and metastasis of cervical cancer

For premalignant transformation of cervix cells into dysplasia, cervical intraepithelial neoplasia (CIN) grading is used to grade the abnormal cells growth on the surface of cervix. CIN refers to the potentially premalignant precancerous condition in which abnormal cells can lead to cervical cancer. Figure 11 shows the differences amongst normal cervix, low- and high-grade CIN of the precancerous stage, and the cancer stage. The CIN are divided into 3 stages: [88]

CIN 1: mild dysplasia, affecting 1/3 of the epithelium
(graded as LSIL);
CIN 2: moderate dysplasia, affecting 1/3 to 2/3 of the epithelium
(graded as HSIL);
CIN 3: severe dysplasia, affecting more than 2/3 of the epithelium
(graded as HSIL).

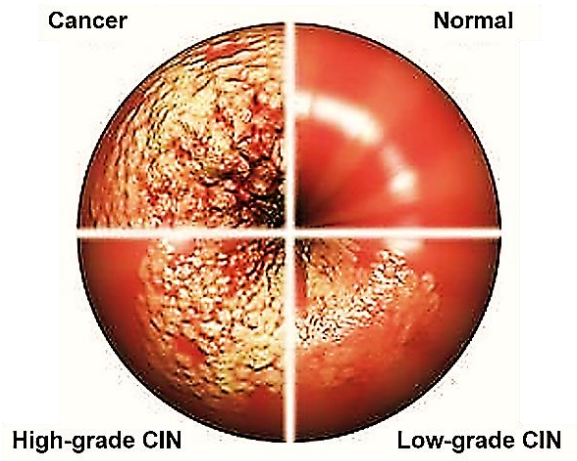

Figure 11 The normal cervix, CIN of precancerous cervix and cervical cancer
Available from: http://globedia.com/cancer-cuello-utero-estadisticas-afeccion

Cervical cancer is staged by two systems, the International Federation of Gynecology and Obstetrics (FIGO) staging system and the American Joint Committee on Cancer (AJCC) TNM staging system. These staging systems classify cervical cancer according to tumor size, depth of invasion and width of spreading, in which serve as a guideline for clinical treatment. It begins with Stage 0, the least advanced, to Stage IVB, the most advanced progression [89, 90]. Table 2 informs the clinical staging of cervical cancer and figure 12 shows the progression of cervical cancer staging.

Table 2 Clinical cancerous staging of cervical cancer

Stage			Characteristics of cervical cancer
0			Full-thickness involvement of the epithelium without invasion into the stroma; carcinoma *in situ*; CIN grades 1, 2, or 3 are assigned
I			Invade the cervix without spreading further
	IA		No visible lesion; can be diagnosed by microscopy
		IA1	Area of invasion: <3 mm (1/8-inch) deep and <7 mm (1/4-inch) wide
		IA2	Area of invasion: 3-5 mm (≂1/5-inch) with horizontal spread of ≦7 mm
	IB		Visible lesion or diagnosed by microscopy; >5 mm in depth or horizontal spread of >7 mm; spread to connective tissue of the cervix
		IB1	Visible lesion: ≦4 cm
		IB2	Visible lesion: >4 cm
II			Invade over the cervix to the 1/3 upper vagina only
	IIA		Without parametrial invasion (invade to nearby tissue of the cervix)
	IIB		Parametrial invasion
III			Invade and extend to the pelvic wall or to the 1/3 lower vagina
	IIIA		Invade to the 1/3 lower vagina without to the pelvic wall
	IIIB		Extend to the pelvic wall and/or block urine to flow to the bladder; may spread to the pelvic lymph nodes
IV			Extend over the true pelvis
	IVA		Invade bladder or rectum mucosa and/or extend over the true pelvis
	IVB		Distant organ metastasis, e.g., lung

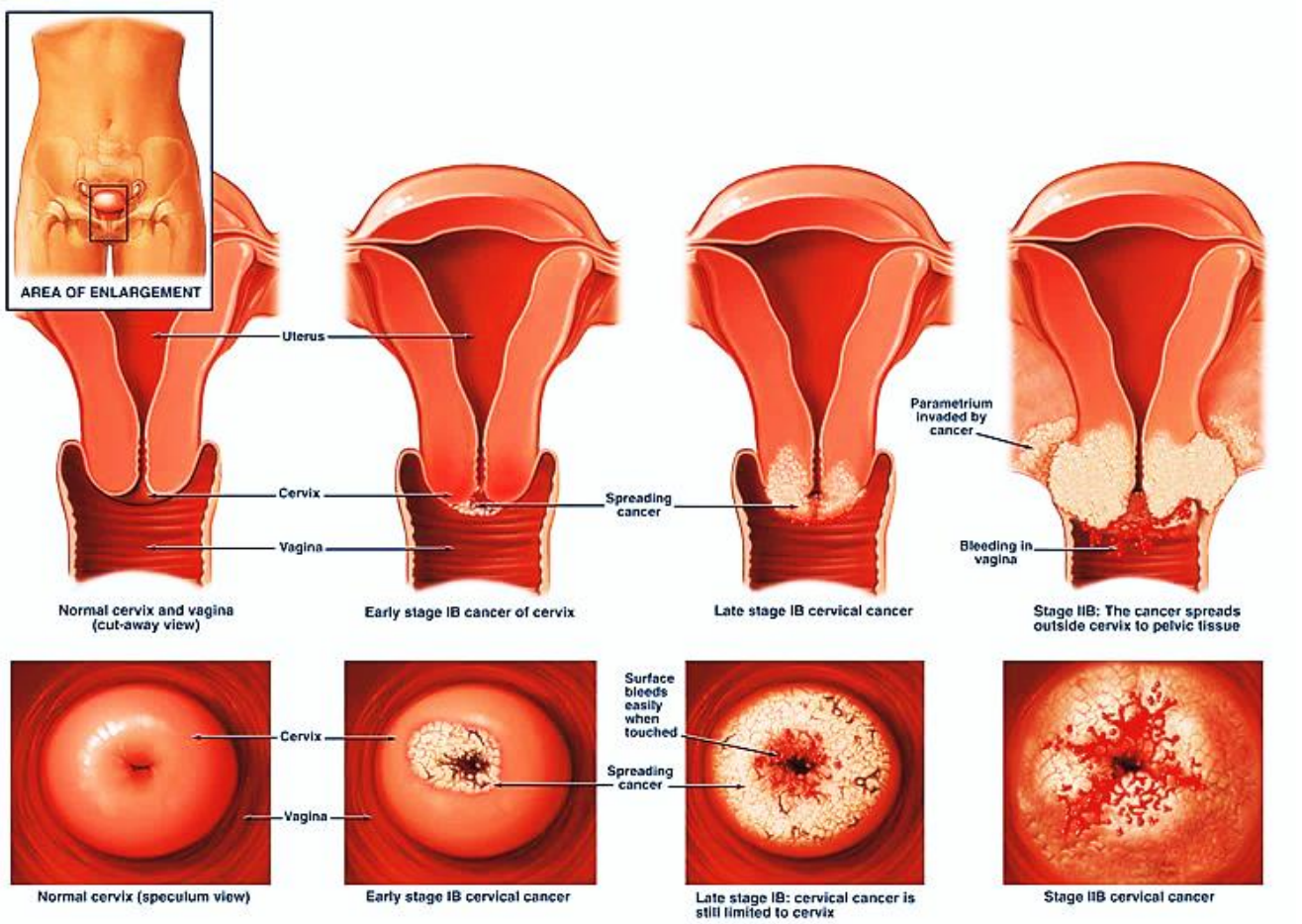

Figure 12 Cervical cancer staging

Available from: https://www.physio-pedia.com/Cervical_Cancer

2.2.7 Signs, symptoms, diagnosis and prevention of cervical cancer

The precancerous and early stage of cervical cancer usually do not present signs and symptoms but it can be early detected with regular cervix check-ups. Thus symptoms are often appeared when cancer becomes invasive which grows into nearby tissue or an advanced stage [73]. Followings are the symptoms of cervical cancer commonly found [73, 83, 85, 91], with more severity at the advanced stages.

1) irregular intermenstrual (between periods)
2) vaginal bleeding after sexual intercourse
3) lower back/leg/pelvic pain or swelling
4) fatigue, weight loss, loss of appetite
5) vaginal pain, discomfort or odorous discharge
6) excessive tiredness
7) abnormal appearance of the cervix (suspicion of malignancy)

Screening test for cervical cancer diagnosis is Pap test or Pap smear to examine the collected cells of the cervix and vagina under microscope, in order to detect precancerous or abnormal cells. Apart from Pap test, HPV DNA test can be performed for cervical cancer screening [81] to detect high-risk HPVs, e.g., types 16 and 18. The prognosis is better when cancer is found early. Regular screening for HPV DNAs or abnormal cells in the cervix, especially in women with the age of $\geqslant$30 or in a suspicious group, should be performed at least once a year. Moreover, an approach to prevent HPV infection is to obtain the vaccine that prevent high-risk HPV (types 16 and 18) and low-risk HPV (types 6 and 11). This vaccine is Cervarix™ and Gardasil® [92].

2.2.8 Cervical cancer treatment

The treatment of cervical cancer depends on cancer type, stage, size and shape of the tumor, the age and general health of the woman. Cervical cancer can be treated by three main methods including surgery, radiation and chemotherapy [93-95]. Radiation and chemotherapy are generally used before or after surgery to treat the spreading cancer beyond the pelvis. Moreover, cryotherapy is another treatment using

freezing technique (extremely cold temperature of liquid nitrogen) for destroying the precancerous abnormal cells.

In the earliest stages, cervical cancer is curable by removing the precancerous or cancerous tissue without damaging the uterus or the cervix so that a woman is still capable of having children. The precancerous cervical cancer can be treated by cryotherapy while cervical cancers that spread to the cervix can be treated by surgery or radiation, followed by chemotherapy. In advanced stages, a radical hysterectomy may be used to remove the uterus, the surrounding tissues and internal lymph nodes. Treatment of other cases is done by removing the uterus with/without ovaries removal. For fully success of treatment, follow-up Pap test and following treatments are essential to be performed [85].

2.3 Trends in drug discovery

Currently, trends in drug discovery is to discover the compounds involving in promoting or inhibition mechanisms of various signaling pathways involved in human diseases. Calcium (Ca^{2+}) signaling is one of the significant pathways in eukaryotic organisms that plays key regulatory roles in various biological processes including to controlling of hormones action, growth factors, cytokines as well as release of neurotransmitters. Several molecules are associated in Ca^{2+} signaling and cell cycle, e.g., calcineurin, protein kinase C, the components of MAP kinase cascade and its downstream component Mck1. It is advantageous to discover the new therapeutic drugs that act or regulate on these molecules. For examples, the anti-inflammatory drugs and the anticancer drugs have effective chemical structures on the Ca^{2+} signaling pathway and thereby can inhibit the cancer cells.

2.4 Biosurfactant

Biosurfactants are amphipathic compounds which contains both hydrophobic and hydrophilic moieties [96]. They are surface active compounds which are produced and secreted or as part of the cell membrane of mostly microorganisms including of yeast, bacteria and fungi [97]. Biosurfactants are many substances include proteins, lipids

and sugars. Their amphipathic molecules facilitate the formation of surface tension either via the association between the molecules themselves as to form the micelle, or via the action of molecules to the interface (surfaces between phases) of different polarities, e.g., air/water, oil/water, water/solid interfaces [98]. The consequence of this action is to lower the surface tension of liquid [99] and thus biosurfactants have been recognized to show the advantages over the chemically synthesized compounds due to their provided applicable properties including of structure diversity, biodegradability, specificity, stability and absence of toxicity. These provide the attraction as well as large-scale production for the industrial applications and environmental conservations, for examples, in food industry, pharmaceutics, cosmetics, medicine, textiles, oil recovery, pollution control and bioremediation [99].

Several surfactants are employed as therapeutic agents including of: antimicrobial activity, e.g., amino acid-based surfactants, saccharide-fatty acid esters, and glycolipid biosurfactants [100, 101]; anticancer activity, e.g., glycolipid biosurfactants and polyunsaturated fatty acid monoacylglycerol (MAGs) [102]; immunomodulatory, e.g., sophorolipid and biosurfactants [103].

2.4.1 Monoacylglycerols (MAGs)

Monoacylglycerols (MAGs), monoglycerides or glycerol ethers are a single saturated or unsaturated fatty acid (monoesters) attaching on a glycerol backbone which existed in two isomeric forms. MAGs are the most polar components of simple lipids found in a very low amount from cells extract. They are biosurfactant which possess only a hydrocarbon chain and 2 alcohol groups (Figure 13), thereby they need the protection from their loss in the hydrophilic solutions. Moreover, they have the detergent-like property and thus can form micelles easily. MAG intermediates are from the degradation of triacylglycerols and diacylglycerols via lipolysis by the lingual and pancreatic lipases, by which diacylglycerols are hydrolyzed to form sn-2-monoacylglycerols. However, MAGs are mostly isomerized to form sn-1 and sn-3-monoacylglycerols in the duodenum which can be hydrolyzed further. This

characteristic can be observed during the purification process and in an acidic medium. Therefore, it is challenging to produce high yield of MAGs from various reaction systems by either chemical or enzyme catalysts [98].

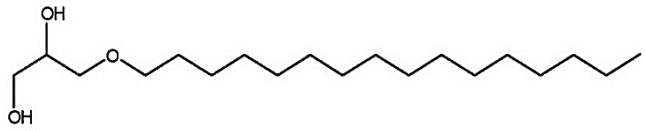

Figure 13 Chemical structure of glycerol ether (3-Hexadecyloxy-propane-1,2-diol) It contains one hydrocarbon chain and two alcohol groups.

Advantages of MAGs include utilities as: surfactants in food industry to increase shelf life of food products; raw materials for making lipophilic or hydrophilic molecules in cosmetics and food industry. It has been long known that MAGs possess antimicrobial activity [104-106], for examples, monolaurin is the antimicrobial supplement mostly added in food and cosmetic industries to protect the product against several *Bacillus* spp. and *Staphylococcus* spp., monocaprin has also been tried as monolaurin, monocaprylin has been used for antimicrobial textiles and footwear [104]. MAGs also show antifungal and antiviral activity [107-109]. Moreover, MAGs possess other biological activities including of anti-inflammation, anti-tumor, and anti-metastasis, which associate with the capability in cell signaling pathway such as Ca^{2+}-signaling pathway and apoptosis induction [110]. MAGs have been reported to their cytotoxic effect and apoptotic induction in leukemia and cancerous cells but not on normal cells [110, 111].

The mechanism of lipid derivatives including of MAGs have received an attention in their ability to induce cell death. Noticeably, MAGs's ability in apoptosis induction in cancer cells is varied and correlated with their chemical structure [110]. In addition, it has been thought that MAGs-induced apoptosis does not occur because of their surfactant property, of which normally leads to cell disruption [110]. One proposed mechanism includes a non-specific effect after MAGs binding and intercalation to cell

membrane non-specifically due to their amphipathic nature [110]. MAGs then alter cytoplasmic membrane fluidity and permeability which lead to cellular apoptosis [110]. Alternatively, interaction of MAGs to cell membrane can induce apoptosis through G protein-coupled receptors [112]. In particular mechanism, MAGs have shown the involvement in caspases activations since they can rapidly trigger cascade events including the production of mitochondrial transmembrane potential and reactive oxygen species (ROS), activation of protein caspases, which result in DNA degradation. These cascade events can eventually culminate in apoptosis while enhancing in Bcl-2 overexpression could inhibit such cascade mechanism [110]. Moreover, MAGs have shown the ability to induce a prolonged elevation of intracellular Ca^{2+} via the flux of extracellular Ca^{2+} and translocation of intracellular Ca^{2+} [110]. This phenomenon has been known as an apoptotic stimulus [113]. However, the MAGs-induce Ca^{2+} flux is not essential for apoptotic cell death [110].

2.4.2 Monomyristin (MM)

Monomyristin (MM, $C_{17}H_{34}O_4$, MW 302.44946 g/mol) is a MAG with saturated fatty acid (Figure 14). It can be referred as 1-monomyristin, 1-monoglyceride, glycerol monomyristate, rac-glycerol 1-myristate or myristic acid. The melting point of MM is 68-70 °C and boiling point is 424.8 °C at 760 mmHg. This compound is soluble in chloroform and ethyl acetate. MM can be obtained by fruits extracts of saw-palmetto (an extract of the fruit of *Serenoa repens*) that showed antibacterial activity [114] MM, being as a food additive, can inactivate spores and vegetative cells by cell lysis due to alteration of metabolic activity of cell membrane, cell growth and cell wall synthesis [115, 116]. Since MAGs have ability to form micelles in the medium which could intercalate or penetrate the lipid cell membrane and alter membrane permeability [116, 117], thus this could be one possible mechanism that cause cell lysis by MM. A study has showed the morphological changes, altering in vacuolization and inhibition to the cell metabolic activity which effect the fungal membrane integrity caused by acylglycerides comprising of MM [118]. Furthermore, MM from fruits of saw-palmetto has been revealed to prevent

prostatic hyperplasias and decrease the symptoms of an enlarged prostate [119]. MM has shown cytotoxicity against renal (A-498), pancreatic (PACA-2) and prostatic (PC-3) tumor cells [119]. Recently, MM has shown to have the antiproliferative activity against HeLa cervical cancer cells [120]. Further investigation of MM-treated HeLa cells showed that MM induced cell death by the elevations of caspase-3 expression and chromosomal DNA fragmentation, the hallmarks of apoptosis.

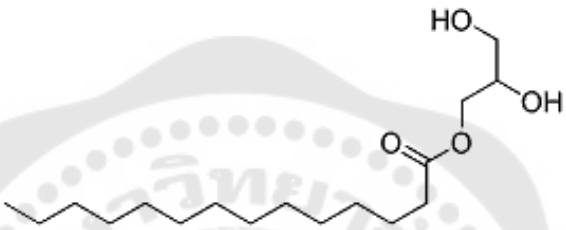

Figure 14 Chemical structure of monomyristin ($C_{17}H_{34}O_4$)

2.5 Nanoparticles (NPs) and drug delivery system

Nanoparticles (NPs) are defined to the particulate dispersions or solid particles with a size in the range of 10-1000 nm [121, 122]. These objects ensure the novel properties for drug delivery system i.e. small size, modified surface, improved solubility and multi-functionality [123]. NPs are developed to control the particle size-surface property and to optimize rate of drug release in order to achieve the site-specific action [124]. For the past few decades, NPs have been tried to improve pharmacokinetics and pharmacodynamics properties of different types of drugs. Moreover, NPs have shown the capability in the systemic circulation *in vivo*, by restricting drug towards the selective sites as well as delivery at a controlled or sustained rate to their sites of action. Therefore, drug delivery system has offered the following advantages:

1) High drug encapsulation, efficient drug protection against chemical or enzymatic degradation, internalization capability and reversion of multidrug resistance are improved.

2) The particle size and surface characteristics of NPs can be conveniently modified in order to achieve drug targeting.
3) Site-specific targeting can be achieved by targeting ligands attachment to NPs surface.
4) Distinctive drug-controlled/sustained release in circulation can be modified. Avoidance of drug distribution by organs and subsequent clearance by the body system can be achieved. Therefore, NPs offer the increase of drug therapeutic efficacy and significant reduction in side effects.
5) Controlled release and particle degradation at localization site can be easily modified by the choice of matrix constituents.
6) The system is applicable for various route of administration such as oral, nasal, parenteral, intra-ocular, etc.

Nanoparticles can be prepared from the materials such as proteins, polysaccharides and synthetic polymers. The utility of such materials depends on the products—include 1) particle size, 2) fundamental properties e.g. aqueous solubility and stability, 3) surface characteristics e.g. charge and permeability, 4) degree of biodegradability, biocompatibility and toxicity, 5) drug release profile, 6) antigenicity of the final product [124]. The selective methods for NPs preparation and NPs characteristics on drug delivery system are described below.

2.5.1 The most frequent methods for NPs preparation

2.5.1.1 Dispersion of preformed polymers

This method is commonly used to prepare biodegradable nanoparticles by utilization of degradable materials including poly (lactic acid) (PLA), poly(D,L-glycolide) (PLG), poly(D,L-lactide-co-glycolide) (PLGA) and poly (cyanoacrylate) (PCA) [125-128]

I. Solvent evaporation method

In this method, the polymer is dissolved in an organic solvent, such as dichloromethane, chloroform, ethyl acetate, for dissolving the hydrophobic drug. The mixture of polymer and drug solution is further emulsified in an aqueous solution containing a surfactant or emulsifying agent to form an oil in water (o/w) emulsion. After the formation of stable emulsion, organic solvent is then evaporated either by reducing the pressure or by continuous stirring. Particle size is depended on the type and concentration of a stabilizer, speed of homogenization as well as polymer concentration. In order to develop small size particle, a high speed homogenization or ultrasonication is often employed [124].

II. Spontaneous emulsification or solvent diffusion method

This method is modified from solvent evaporation method [129]. The water miscible solvent and a small amount of water immiscible organic solvent are used together to serve as an oil phase. An interfacial turbulence between the two phases is then created, and small particles are formed due to the spontaneous diffusion of solvents. The increasing concentration of water miscible solvent can lead to a decreasing of particles size [124]. Both solvent evaporation and spontaneous emulsification techniques can be used to encapsulate hydrophobic and hydrophilic drugs, of which a multiple w/o/w emulsion is formed by drug dissolving in the internal aqueous phase [124].

2.5.1.2 Polymerisation method

This method is achieved from polymerization of monomers in order to produce NPs in an aqueous solution. Drug can be incorporated into the particles either by dissolution in the medium or by adsorption onto the nanoparticle after polymerization process. The NPs suspension is then purified to remove residual stabilizers and surfactants by ultracentrifugation and resuspending the particles in an isotonic medium [124].

2.5.1.3 Coacervation or ionic gelation method

This method has been used in the preparation of NPs from biodegradable hydrophilic polymers, e.g., chitosan, gelatin and sodium alginate. For chitosan NPs, a

mixture of two aqueous phases are involved, of which one is a hydrophilic polymer chitosan and the other is a polyanion sodium tripolyphosphate [130, 131]. The positively-charged chitosan amino group and the negatively-charged tripolyphosphate interacts to form “coacervates”, a result of electrostatic interaction between two aqueous phases.

2.5.1.4 Supercritical fluid technology

This is the use of supercritical fluid to prepare biodegradable micro- and nanoparticles due to its environmentally reservation [132]. The supercritical fluids are referred to solvents at a temperature above its critical temperature, at which the fluid remains a single phase [124].

2.5.1.5 Sol-Gel method

The sol-gel process is known as chemical solution deposition, widely used in the fields of materials science and ceramic engineering [124].

2.5.2 Effect of NPs characteristics on drug delivery

2.5.2.1 Particle size

This includes two most significant characteristics of NPs including of particle size and size distribution, since they can influence the *in vivo* distribution, biological fate, toxicity and the targeting ability of nanoparticle systems [124].

Particle size and size distribution also have an influence in drug loading, drug release and stability of NPs. Conversely, smaller particles possess larger surface area, thus resulting in drug positioning at or near the particle surface that lead to rapid drug release. Whereas larger particles possess larger cores which benefit more amount of encapsulated drug with slow rate in drug diffusing out. Nevertheless, smaller particles may have a risk of aggregation during storage and transportation of nanoparticle dispersion. Thus, it is challenging to establish the smallest size NPs with maximum stability [124].

2.5.2.2 Surface properties

Concerning the administration of NPs intravenously, they are easily recognized by the immune system and are eventually destroyed by phagocytes within the

circulation [133]. The surface hydrophobicity of conventional NPs can be adsorbed with the blood components, mainly opsonins [124]. This changes the fate in application of NPs *in vivo* as the binding of opsonins onto nanoparticle surface (opsonization) acts as a linkage between NPs and the phagocytes such as macrophages in the mononuclear phagocytes system [71] including liver, spleen, lungs and bone marrow [124]. Therefore, after administration of conventional drug-loaded NPs into the blood stream, they are mainly delivered to MPS, which are repeatedly opsonized and massively cleared by macrophages, leading to altered drug biodistribution. In order to increase drug targeting, minimization in opsonization and prolonged circulation of NPs must be modified. There are several method including of NPs surface coating with hydrophilic polymers/surfactants and nanoparticles formulation with biodegradable co-polymers as well as hydrophilic segments such as polyethylene glycol (PEG) [124].

A commonly used to characterize the surface charge property of NPs is zeta potential [134], which reflects the electrical potential of particles that is influenced by the composition and the medium in which NPs is depressed. NPs with electrical zeta potential above 30 mV have shown to be stable in suspension due to the low aggregation of NPs provided by the surface charge. Moreover, zeta potential can be used to determine the position of encapsulated drug, such as drug is within the center or is adsorbed onto the surface of NPs [124].

2.5.2.3 Drug loading

A successful nanoparticle system should present a high drug-loading capacity to reduce the matrix materials for administration. Drug loading can be done by either incorporating drug during preparation process of NPs or absorbing drug after NPs production. Entrapment efficiency is highly depended on the stability of solid-state drug in the matrix material or polymer. This refers to, 1) solid dissolution or dispersion which associated with matrix/polymer composition, 2) drug and polymer molecular weight, 3) drug-polymer interaction, 4) the presence of end functional groups, e.g., ester or carboxyl. The ionic interaction between drug and matrix materials can be highly effective to increase drug loading. Using macromolecule or protein provide a greatest

loading efficiency by offering minimum solubility but maximum adsorption for small molecules [124].

2.5.2.4 Drug Release

In order to develop a successful nanoparticle system, both drug release and polymer biodegradation are considerable. Rate of drug release is influenced by: 1) solubility of drug, 2) desorption of the surface bound or adsorbed, 3) drug diffusion through the matrix, 4) matrix biodegradation, 5) combination between degradation and diffusion process [124].

2.5.3 Application of NPs in cancer treatment

With administration of anticancer drugs intravenously, they are basically distributed throughout the body due to the physicochemical properties of the molecules. Such this evidence, an accumulation of drug and pharmacologically active concentration at the tumor tissue is poorly reached. This also leads to toxicity to normal cells which is a serious obstacle to effective therapy. However, using colloidal drug carriers such as NPs could offer a more rational approach to specific cancer therapy. Moreover, the possibility in circumventing the multidrug resistance might be successful.

2.6 Advancement in nanomedicine

2.6.1 EPR effect and passive targeting

Establishment of solid tumor relies on the enhanced permeability and retention (EPR) effect that associated with anatomical and pathophysiological difference of tumor tissue to normal tissue. In this regard, angiogenesis in tumor provides high vascular density in tumor mass, high leakiness of vascular endothelial cells in blood vessels by means of VEGF stimulation to create hyperpermeability of vasculature, allowing particles or macromolecules of 10–500 nm to extravasate and accumulate inside the interstitium of tumor, the impaired lymphatic drainage system with diminished renal clearance renders particles entrapping with delayed clearance, and this allows the retention of such macromolecules [135-139]. Accordingly, large particles including polymeric NPs are fundamentally transported and accumulated into the solid tumor via the EPR effect

(Figure 15) that offers the passive targeting/accumulation and retention of the minute size particles within the tumor tissue by hyperpermeability of neovasculature and the impaired lymphatic drainage [135, 139].

However, EPR effect is heterogeneous from tumor to tumor and also within each individual tumor due to the complexity and vascular permeability differences. [137, 140]. This extensive heterogeneity is the barriers to macromolecular transport into tumor microenvironment, referring to the obstruction from abnormal tumor vasculature, interstitial fluid pressure (IFP) elevation, and ECM hyperdensity (Figure 15). This can result in the heterogeneous treatment outcomes and therefore treatments should be individualized. Furthermore, researchers try to improve EPR effect or relieve anti-EPR effect for nanomedicine via these ways: using anti-angiogenic treatments to normalize the tumor vasculature, modulating the ECM such as modifying collagenases and hyaluronidase levels, and diminishing IFP in the tumor microenvironment to enhance transvascular filtration and transport of particles [141]. Presently, EPR effect has become the mainstream in passive targeting for macromolecular anticancer therapy [142].

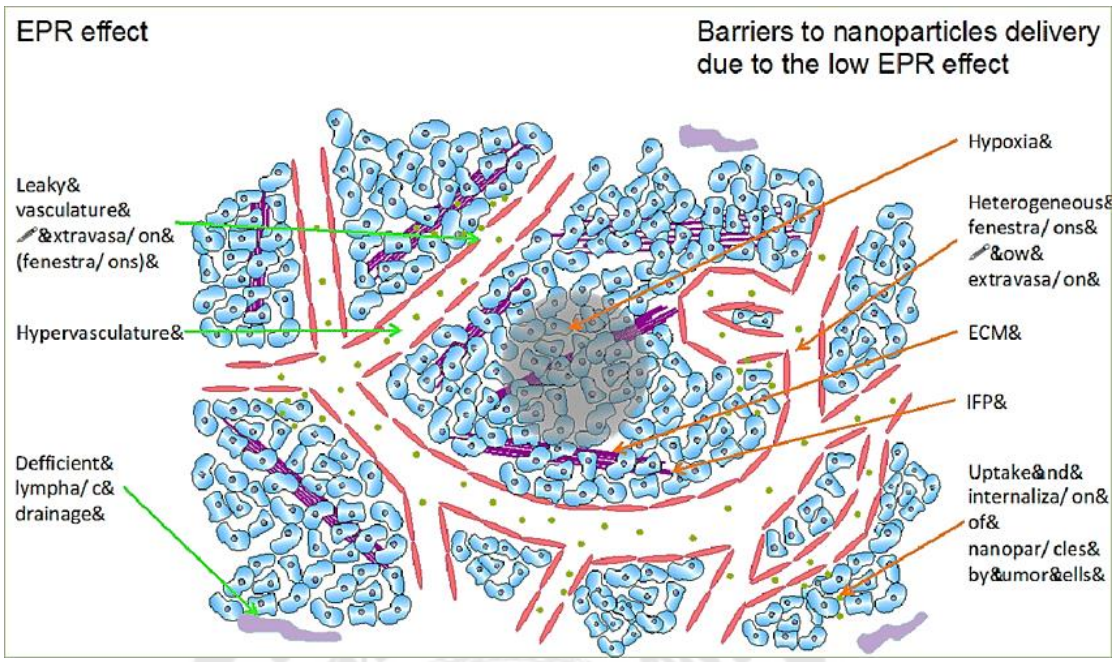

Figure 15 The EPR effect and barriers to nanomedicine due to poor EPR effect

High EPR effect shows leaky vasculature, extravasation, hypervasculature, and diminish lymphatic drainage. Low EPR effect in tumor tissue cause the obstructions due to low fenestrations, heterogeneous distribution, and high ECM density in tumor microenvironment, providing inaccessibility for nanomedicines.

Available from: https://www.researchgate.net/publication/277204398_Strategies_to_improve_the_EPR_effect_for_the_delivery_of_anti-cancer_nanomedicines

2.6.2 Active targeting nanomedicine

As known, typical cancer treatment by chemotherapy still has the limitations from multi-drug resistance and systemic toxicity due to lack of tumor-specific property of the circulating drug. Though biodistribution can be improved by the EPR effect, the direction of therapeutic is attentive at the reticuloendothelial system [143] which offers the clearance by phagocytes [144]. Accordingly, nanomedicine-based therapy via active tumor targeting is being pronounced to increase localization and landing of drug carriers or NPs to the specific target cells or tissues whilst off-target to the normal tissue

[139]. This approach is known as “targeted drug delivery”, a reliable strategy for reducing systemic toxicity or possible side effects and improving therapeutic benefit by mean of specific intracellular uptake.

In addition, the targeted cancer therapy encompasses an extensive variety of direct or indirect approaches (Figure 16) which include the targeted drug delivery. The direct interference can be proceeded via targeting tumor proteins/antigens to alter cellular signaling pathway while indirect interference relies on tumor antigens expressed on the cellular surface which serve as target molecules for targeting moieties. Examples of targeting molecules for both approaches are monoclonal antibodies (MoAbs), antibody fragments, peptides, growth factors, carbohydrates, glycoproteins, and receptor ligands specific to overexpressed or selectively expressed on cancer cells [145-149]. Thus targeted drug delivery can induce the uptake of drugs towards the tumor-associated molecules and sufficient active compounds to tumor mass can be brought. Such this evidence, cancer cells can be exposed to abundant cytotoxic drugs and thus be killed. This will improve the therapeutic efficacy of cancer treatment as well as can avoid the toxicity to normal tissues since the suboptimal doses of drug administration can be reduced. Moreover, the incomplete tumor response, early disease relapse, and the development of drug resistance could be overcome [145].

One of the overexpressed receptors found in cancerous cells is the transferrin receptor (TfR), of which its specific transferrin (Tf) ligand has received a major attention since Tf is capable to achieve site-specific targeting due to high abundance of TfR on cell surface [13]. Moreover, with their biodegradable, nontoxic, and nonimmunogenic properties [13], the Tf was conjugated with NPs and served as the first targeted NPs towards cancer cells before internalizing via receptor-mediated endocytosis [139]. The pathway of Tf uptake has shown to be potential in the delivery of anticancer agents, proteins, as well as therapeutic genes into proliferating malignant cells that show their overexpression of transferrin receptors (TfRs) [150-153]. Furthermore, there has been utilization of TfR-targeting peptide for targeting cancer cells recently [154-157].

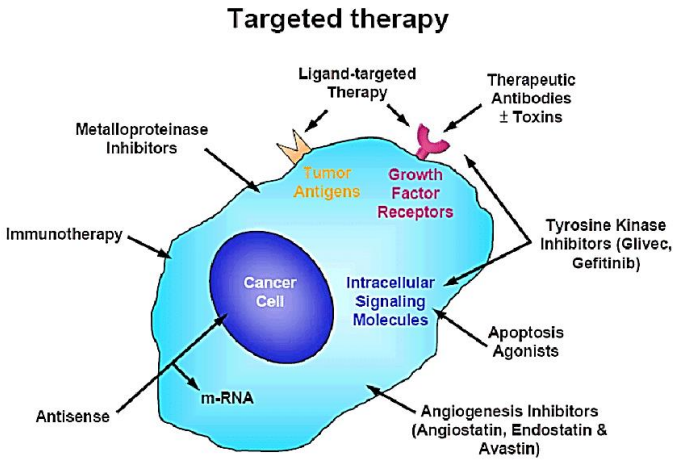

Figure 16 Targeting molecules involved in targeted cancer therapy

Available from: https://www.researchgate.net/figure/Targeted-therapy-refers-to-a-new_fig3_270273793

2.6.3 Transferrin (Tf) and its receptor

Transferrin (Tf), discovered over half a century ago, has attracted a great interest as a targeting ligand towards cancer cells. This functional molecule plays a significant role in the major pathway of cellular iron uptake through the internalization of iron-bound transferrin (Tf)-transferrin receptor (TfR) complex [158] via clathrin-mediated endocytosis [108, 109, 111]. Due to acidic pH in the endosome, iron is released out from Tf into the cytosol by iron transporter protein DMT1 (divalent metal transporter) [158]. Thereafter, the iron is utilized as a cofactor by heme and ribonucleotide reductase or kept inside ferritin, [158] whereas TfR translocate back to the cell membrane for the forwarding iron transport [158]. Beside the iron, several other metal ions of therapeutic or diagnostic utilizations can also bind to Tf at the iron sites. Therefore, Tf has been used in the delivery system of many beneficial or harmful metal ions to the cells [158].

2.6.3.1 Occurrence and biological function of Tf

The Tfs are a family of large iron-binding glycoproteins, with a single polypeptide chain of 670–700 amino acids and a molecular weight of 80 kDa. Three major types of Tf have been characterized including of: 1) serum Tf, mostly known and found in blood and other mammalian fluids including bile, amniotic fluid, cerebrospinal

fluid, lymph, colostrom, and milk [158, 159]; 2) Ovotransferrin (oTf), found in avian egg white [158]; 3) lactoferrin [62], found in milk, tear, saliva, and other secretions [158, 160, 161]. Later, melanotransferrin, an integral membrane protein, was found to anchor to the membrane surface of melanocytes in human malignant melanoma cells and in some fetal tissues. The Tfs are mainly synthesized by hepatocytes. However, they can also be expressed in the culture of liver and intestinal cells [13, 162]. The Tf are acidic proteins. In human serum, the Tf concentration is aproximately 2.5 mg/ml (35 mM) with 30% occupied with iron [163].

The fundamental role of serum Tf is to maintain the distribution of free Fe^{3+} iron levels and availability in body fluids by binding, sequestering, and transporting ions, thus preventing the insoluble ferric hydroxide aggregates deposition. The role of Tf is for iron transport amongst the sites of absorption, storage, as well as utilization via carrying iron from the sites of intake into the systemic circulation towards cells and tissues for biological processes including DNA synthesis, cellular metabolism and proliferation. The Tf also function for regulation of iron homeostasis and protection against the toxicity of free iron—cells may be damaged by the formation of free radicals. In addition, it is involved in transportation of several other metal ions, such as therapeutic, radio diagnostic, and some toxic metal ions [158, 164].

2.6.3.2 Functional structure of Tf

Transferrin (Tf) is single-chain glycoprotein consisting of 700 amino acids with a molecular mass of 80 kDa [158]. From X-ray crystallography, structures of over 10 Tf, have been determined and summarized in a recent review [164] as well as elucidated in various protein databases with high degree of similarity—70% identity amongst lactoferrins, 50–60% amongst lactoferrins and 40% amongst melanotransferrin and human Tf or lactoferrin.

The crystal structures show high levels of conservation amongst all proteins of Tf family as that their polypeptide folding into three-dimensional structures is very similar. Briefly, a single polypeptide chain is folded into 2 structurally identical but functionally different lobes, N- and C-lobe, connected by a short peptide (Figure 17A). An individual lobe can be further divided into 2 similar domains with alternating α-helical

and β-sheet segments, enclosing a deep hydrophilic cleft at which an iron binding site is revealed, i.e., a Fe^{3+} binding site is situated in the deep cleft between the two domains. Therefore, Tf possesses 2 iron-binding sites which are extremely similar. The amino acid residues of N-lobe and the Fe^{3+} binding site of Tf are shown (Figure 17B).

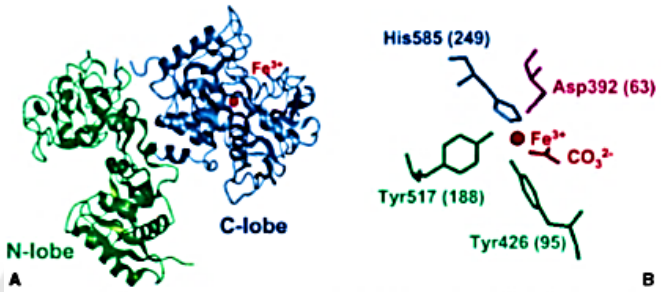

Figure 17 Diagram of X-ray crystal structure of human serum Tf

The C-lobe containing bound Fe^{3+} in a closed form (blue) and the apo N-lobe in an open form [85] (A); The N-lobe and the Fe^{3+} binding site of human serum Tf with amino acid residue numbers in the brackets (B) [158].

Fe^{3+} associated with distorted octahedral geometry to the 2 oxygens from 2 tyrosines (Tyr), 1 nitrogen from a histidine (His), 1 oxygen from an aspartate [105], and 2 oxygens from a bidentate carbonate (synergistic anion) (Figure 17B). The ligands are from two domains: domain 1 (Asp63) and domain 2 (Tyr188), and two polypeptide strands (Try95) and (His249) which cross over between the two domains at the back of Fe^{3+} site. This arrangement is critical as that domains are capable to move apart to form an open conformation, hinged by the backbone strands, thus leading to iron release. Bicarbonate functions as for the strong binding of Fe^{3+} to the specific site of Tf and might play role in iron release. Apart from Fe(III), several divalent and trivalent metal ions have also been revealed to bind to the specific Fe^{3+} sites [158]. During Fe^{3+} uptake or release, Tf undergoes conformational changes for lope opening and closing. This has been thought to be critical in the recognition of cell surface receptor and may involve

with the pH-sensitive interdomain interaction with lower pH may be a trigger for cleft opening and facilitate iron release.

Uptake of Fe^{3+}-Tf complex into an acidic endosome (pH 5.5) results in the protonation of both residues Lys209 and Lys301 located on the opposite domains (dilysine trigger), which provide the driving force for pushing two domains apart and thus expose Fe^{3+} for its release [165]. The Asp63 an iron binding ligand, may also trigger for the closing of two domains during Fe^{3+} uptake, since this trigger is completely eliminated by Asp63 mutation to Ser or Cys, i.e., the lobe remains in an open conformation [166]. Tf is capable to reversibly bind 2 atoms of ferric iron, i.e., Fe^{3+}, with high affinity (1,022 M^{-1} at pH 7.4) [167, 168]. Free transferrin peptide (apotransferrin) shows a conformational change after iron binding (diferric Tf or holotransferrin) which is significant for transferrin receptor (TfR) recognition. It was proved that holotransferrin has a 10 to 100-fold higher affinity for TfR as compared to apotransferrin [167-169].

2.6.3.3 Functional structure of TfR

The transmembrane glycoprotein of transferrin receptors (TfRs) have been identified in 1982 [167, 170-172]. Generally, TfR have a higher affinity (10- to 100-fold higher) to holotransferrin than apotransferrin [167, 169]. The TfR1 is involved in iron uptake and cell growth regulation [167, 173]. Its primary structure consists of 2 identical glycosylated subunits with 95 kDa each linked by two disulphide bonds to form a dimer [167, 174]. Each polypeptide subunit, compost of 760 amino acids, consists of a short N-terminal cytoplasmic domain, a hydrophobic transmembrane domain and a large, globular extracellular C-terminal domain that possesses the binding site of Tf [167, 175, 176]. Due to that each subunit may bind a Tf peptide, the TfR is capable for internalization of 4 ferric ions (Fe^{3+}) at maximum during 1 cycle.

Recently in 2010, a TfR2 has been discovered [167, 177]. It is a homologue of TfR1 with 45–66 % identity for the extracellular domain. The differentiation between TfR1 and TfR2 depends on tissue distribution [167, 178, 179]. While TfR2 is mainly expressed within the tissues responsible for regulation of iron metabolism, e.g., liver and small intestine, TfR1 is ubiquitously expressed on the most active proliferating cell types [120, 167, 179, 180].

Interestingly, TfR2 tends to have a significantly lower affinity for Tf (25-fold decrease) when compared to TfR1 [167, 179].

The 3D structure of TfR monomer shows 3 distinct domains: 1) the protease-like domain that possesses amino acid residues 122–188 and residues 384–606 of a central seven-stranded mixed β-sheet with flanking a helices [158]; 2) the apical domain that possesses residues 189–383 with a β-sandwich in which the 2 sheets are outspread with a helix along the open edge [158]; 3) the helical domain that contains residues 607–760 of a four-helix bundle formed by a pair of parallel α-hairpins (Figure 18). The TfR has conformational changes concerned with pH, similar to Tf. The motion of the apical domain will transduce pH changes into the changes of Tf binding cleft which will certainly affect the relative affinity of TfR for apo- or holo-Tf as well as the affinity of Tf for Fe^{3+}. From other studies, it has been suggested that the TfR helical domain are essential for Tf binding [158, 181].

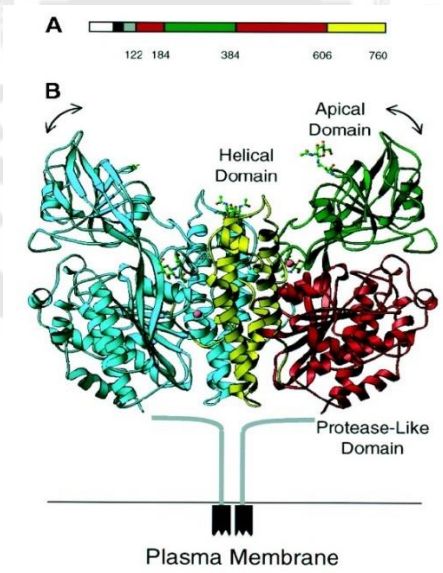

Figure 18 X-ray crystal structure of the dimeric ectodomain of the human TfR

It consists of three distinct domains: 1) protease-like (red), 2) apical (dark green), and 3) helical (light green), which are organized in a butterfly-like shape. The transmembrane segment is shown in black and the stalk in blue, connected to the membrane-spanning helices [158].

Available from: http://science.sciencemag.org/content/286/5440/779.full

2.6.4 Tf ligand as a drug carrier

It has been found that the transferrin receptors (TfRs) are overexpressed on many malignant cells and brain capillary endothelial cells, due to their high rate of proliferation [157, 182-186]. Relevant studies have shown the elevated levels of the expression of TfR on cancer cells, which is distinct from the normal cells, and its expression is also concerned with tumor grade, stage and prognosis [187-193], attributed to the requirement of high level of iron for their growth. Furthermore, it has been revealed of upregulation of TfR expression on metastatic and drug resistant tumors when compared to the normal organ tissues of the pancreas, colon, lung and bladder [167, 182, 189, 194-196]. Due to its expression pattern, thus TfR highlight its selectivity to cancer and therefore TfR have been an attractive target in the delivery of therapeutic drugs of cancer and central nervous system diseases.

In active targeting of cancer, Tf ligand has been potentially used for the specific delivery of anticancer agents, proteins, and genes, primarily to the proliferating malignant cells which show the TfR overexpression [13, 150-153, 167, 183]. Furthermore, the significance in the development of cancer specific therapies can be successful by direct conjugation of Tf or anti-transferrin receptor antibodies such as OX26 monoclonal antibody, with drugs, proteins or as hybrid systems that can enhance cellular uptake via transferrin-mediated mechanisms and increase selective cytotoxicity [158, 167]. The utilization of Tf and its successes in cancer therapies include the achievement in coupling of Tf with DNA via a polycation or cationic liposomes that targets the proliferating cells via TfR-mediated endocytosis [158], a successful reversal in drug resistance through the incubation of drug-insensitive cancer cells with Tf-targeted conjugates *in vitro* [167], the successful delivery of anticancer drugs across blood brain barrier to target the tumor cells that showed the TfR overexpression in brain glioma, thus revealing an important discovery, and the promising result of Tf-immunotoxins (Tf-CRM107) utilization which has been currently proven in clinical trials for the treatment of glioblastoma [167].

In nanoparticles (NPs)-based drug delivery system, Tf has been utilized in the system of liposome or polymer and received major attention in a few years ago due to its potential of both non-immunogenic and site-specific targeting. Concerning with cellular uptake, Tf-conjugated NPs should be internalized into cells through the clathrin-mediated endocytosis [183]—it has been generally considered that the small particles of <100 nm in diameter are preferred due to their steric characteristics [252-253], however, larger particles possess more advantages such as higher capacity and slower drug release, [183, 197]. The Tf conjugation with the NPs-based system to deliver doxorubicin, a potent anticancer drug, showed the significantly elevated cytotoxic levels in various cancer cell lines including HeLa [158]. Moreover, the potent lipoplexes and pH-sensitive fusogenic liposomes with the Tf conjugation for gene delivery to cancer cell lines revealed that these hybrid complexes with Tf showed higher transfection efficiency towards cancer cells than the complexes without Tf [14]. However, the extent of the Tf-induced enhancement was dependent on cell types. Gene delivery towards HeLa and KB cells was found to have a higher transfection activity since they were rapidly internalized, whereas only slightly enhanced transfection was found for HT1080, HepG2, and K562 since these cells were internalized slowly.

3.1 Materials and apparatus

3.1.1 Cell lines and primary cells

Cell lines used in this study were the Human cervical cancer [198] [198] cell line and African green monkey kidney (Vero) cell line, originated from American Type Culture Collection (ATCC, USA) and previously kept as stocks in the liquid N_2 at Department of Microbiology, Faculty of medicine, Srinakarinwirot University. The uterine endometrial epithelial cells were the primary cells isolated as previously described [199] from the porcine uterine tissue from slaughterhouse in Bangkok. The primary cells were kindly provided by Dr. Chatsri Daechapunya, Faculty of Medicine, Srinakharinwirot University, Thailand.

3.1.2 Chemicals, reagents, and biochemical assay kits

All chemicals, reagents, and assay kits used in this study were of analytical reagent or tissue culture grade and be listed in Table 3.

Table 3 List of chemicals, reagents, and biochemical assay kits

Chemicals, reagents, assay kits	Suppliers
Dulbecco's Modified Eagle Medium (DMEM)	Gibco-Invitrogen (USA)
Medium 199 (M199)	Gibco-Invitrogen (USA)
Fetal Bovine Serum (FBS)	Gibco-Invitrogen (USA)
0.25% Trypsin-EDTA	Gibco-Invitrogen (USA)
Penicillin-streptomycin	Gibco-Invitrogen (USA)
Dimethyl sulfoxide (DMSO)	Sigma-Aldrich (Germany)
3-(4,5-dimethylthiazol-2-yl) 2,5 diphenyltetrazolium bromide (MTT	

Table 3 (continued)

Chemicals, reagents, assay kits	Suppliers
3-(4,5-dimethylthiazol-2-yl) 2,5 diphenyltetrazolium bromide (MTT)	Sigma-Aldrich (Germany)
Trypan blue	Merck (Darmstadt, Germany)
Sodium bicarbonate (NaHCO3)	Merck (Darmstadt, Germany)
Monomyristin ($C_{17}H_{34}O_4$)	TCI (Shanghai, China)
Fluorescein isothiocyanate (FITC),	Sigma–Aldrich (St. Louis, MO, USA)
Human holo-transferrin (Tf)	Calbiochem®, Millipore (USA)
Dextran T40	Amersham Pharmacia Biotech AB (Sweden)
Poly(D,L-lactide) (PLA)	Sigma–Aldrich (St. Louis, MO, USA)
Dichloromethane (CH_2Cl_2)	Carlo Erba Reagents (Val de Reuil, France)
Ethanol (C_2H_5OH)	Sigma–Aldrich (St. Louis, MO, USA)
1,2-epoxy-3-phenoxypropane	Sigma–Aldrich (St. Louis, MO, USA)
N-(3-Dimethylaminopropyl)-N'-ethylcarbodiimide (EDC)	Sigma–Aldrich (St. Louis, MO, USA)
N-hydroxysuccinimide (NHS)	Sigma–Aldrich (St. Louis, MO, USA)
succinic anhydride	Sigma–Aldrich (St. Louis, MO, USA)
anhydrous pyridine	Sigma–Aldrich (St. Louis, MO, USA)
Dimethyl sulfoxide–d_6 (DMSO-d_6) (>99.8%)	Amresco (OH, USA)
Sodium hydroxide (NaOH)	Carlo Erba (Milano, Italy)
Sodium chloride (NaCl)	Carlo Erba (Milano, Italy)
Phenol	Sigma–Aldrich (St. Louis, MO, USA)
Butanol-2	Sigma–Aldrich (St. Louis, MO, USA)
FlowCellect Annexin Red Kit	Merck KGaA (Darmstadt, Germany)
FlowCellect MitoPotential Red Kit	Merck KGaA (Darmstadt, Germany)

3.1.3 Instruments for cell culture and manipulation

All instruments used for cell culture and manipulation were listed in Table 4.

Table 4 List of instruments used in tissue culture and manipulation

Instruments	Suppliers
Inverted microscope	Nikon TMS (Japan)
Fluorescent Microscope	Olympus (Tokyo, Japan)
Holten Laminar Air HVR 2448 Laminar Flow Hood, biosafety class II	Thermofisher (USA)
Amnis FlowSight®, Imaging Flow Cytometer	Merck KGaA (Darmstadt, Germany)
CO_2 incubator and supplied tank	Shel-lab (USA)
-86°C upright freezer	Thermo Fisher Scientific (USA)
Liquid N_2 and supplied tank	Taylor-wharton (USA)
Benchtop centrifuge, Centra CL2	Thermo Fisher Scientific (USA)
Ultrasonic cleaner set, WUC-D03H	Daihan Scientific Co., Ltd.
V-32 Multi Vortex Mixer	Thomas Scientific (USA)
Microplate reader	Synergy™ HT, Bio-tek Instruments, Inc.

3.1.4 Instruments for nanoparticles syntheses and characterizations

The instruments and materials used for nanoparticles syntheses and characterizations were listed in Table 5.

Table 5 List of instruments and materials used in nanoparticles syntheses and characterizations

Instruments/materials	Suppliers
Ultrasonic Vibra Cell Meter, Scientific-600W	Sonics & Materials Inc. (Danbury, CT, USA)
BRUKER spectrometer Avance-300	Bruker AG (Fällanden, Switzerland)
Thermoshake incubator-shaker	C. Gerhardt GmbH & Co. (Königswinter, Germany)
Scanning Spectrophotometer Uvikon XL	Bio-Tek Instruments (USA)
Particle size analyzer, Mastersizer 2000	Malvern-instruments Ltd. (Worcestershire, UK)
Benchtop Freeze Dry System	LabCongo (Kansas, USA)
Ultracentrifuge, Optima™ L-80 XP	Beckman Coulter Inc. (CA, USA)

3.2 Cell lines and primary cells cultivation and subculture

All reagents, solutions, and equipment used in cell culture technique were sterile. The culture and manipulation of cell lines were handled with appropriate biosafety and aseptic technique. The sterile cell culture medium—i.e., DMEM for HeLa and endometrial cells or M199 for Vero cells, was pre-warmed to 37ºC using water bath. Then culture medium as well as sterile culture flasks, pipettes, and other supplied equipment were transferred into the laminar flow hood.

3.2.1 Thawing frozen cells and cultivation of cell lines and primary cells

Typically, only a cryovial containing frozen HeLa cells or Vero cells from the liquid N_2 was thawed at a time to avoid cross-contamination of the cells. For the best cell recovery and viability, cryopreserved frozen cells in DMSO were thawed as quickly as possible in order to protect cells from DMSO damaging and cells lysis from ice crystals,

in order that recover viable cells at high density. Thawing cryopreserved or frozen cells was done as following procedure.

Before thawing, 5 ml of freshly warm (37ºC) complete culture medium—i.e., Dulbecco's Modified Eagle's Medium (DMEM) for HeLa cells or Medium 199 (M199) for Vero cells, with pre-adjusted pH 7.4, and supplemented with 20% (v/v) fetal bovine serum (FBS) and 1% (v/v) (100 U/ml) of penicillin-streptomycin—was added into a 15-ml conical tube. Then, a cryovial was removed from the liquid N_2 freezer and immediately transferred to a 37° C water bath, in which the vial was gently swirled continuously until the frozen cells become almost completely thawed, i.e., a small bit of ice left in the vial—in other words, approximately 3/4 was being melted and usually done in less than 60 sec [99]. After ensuring that vial cap remained tight—to prevent leakage and contamination, the vial was transferred to the laminar flow hood before wiping it with 70% ethanol or submerging it in 70% ethanol, and air-drying. After opening up vial cap, the cells suspension was pipetted up carefully by avoiding to touch any part of vial edge and exterior that might be a chance of contamination, then placed it into a sterile 15-ml conical tube containing pre-warmed (37ºC) complete medium. The cell suspension was centrifuged for 2 min at ~1000 rpm at room temperature to concentrate cells and collect the completely packed pellet by discarding the supernatant. The pellet was gently resuspended in a small volume of complete growth medium and transferred the suspended cells into a fresh 25-cm^2 plastic tissue culture flask containing appropriate amount (5 or 7 ml) of the warm complete culture medium DMEM (for HeLa) or M199 (for Vero).

Cell maintenance of each primary culture, i.e., HeLa and endometrial cells in DMEM and Vero cells in M199, was carried out in a CO_2 incubator, wherein the culture condition was controlled at 37°C, 5% CO_2, and 95% humidified atmosphere [99]. Cells were grown in a medium supplemented with 10% FBS and 1% (v/v) (100 U/ml) of penicillin-streptomycin (for HeLa cells and Vero cells) and with 1% kanamycin (for endometrial cells). The culture was often microscopically examined in order to observe the morphology and the growth of cells that normally proceeds from the "lag" or "latent"

phase to the “log” or “exponential” phase, wherein cells proliferated rapidly and exponentially [200, 201] . The old medium was changed to a fresh growth medium in an appropriate day or whenever the color of medium, with pH indicator, shifted. Until reaching the confluence, HeLa and Vero cells growing in a monolayer inside a 25-cm^2 plastic tissue culture flask was individually brought into subpassaging before their progressions into the stationary phase, in which the rapid cell growth gradually decreases [200].

3.2.2 Subculturing of a monolayer cell culture

Typically, whenever logarithmic growth phase of cultured cells was reached and they become nearly confluent—i.e., cells grew to nearly reach whole area of the flask, then the subculture (or subpassaging) of the primary culture was needed to refresh nutrients in order to support growing continuously and stimulating further proliferation to produce secondary cultures.

In detail, after cells of primary culture were microscopically observed to be healthy in a logarithmic phase, the culture medium was removed with a sterile Pasteur pipet or a graduated pipette. A monolayer of cells was washed once or twice with a small volume of 37°C PBS to remove any residual proteins secreted by cells and FBS that might inhibit trypsin activity. Furthermore, cells were trypsinized from the surface of primary tissue culture flask by using a convenient and effective chemical method [99, 202], by adding 0.5-1.0 ml of 37°C, 0.25% trypsin-EDTA reagent into a 25-cm^2 tissue culture flask (alternatively, by adding 1-2 ml of 37°C, 0.25% trypsin-EDTA into a 75-cm^2 tissue culture flask) to cover the adhering cell layer [99, 198] The culture flask was placed into a humidified 37°C incubator with 5% CO_2 for a few minutes, then checked with an inverted microscope that cells rounded up as well as detached from the surface into suspension, otherwise gently tapped the flask to detach and unpack cells to become well trypsinized [198] in order to avoid the clonal selection of these cells from partial trypsinization. The cells were thereafter flooded with 5-10 ml of 37°C FBS-containing medium to inhibit trypsin-EDTA activity that might damage cells and further suspended by pipetting and rinsing cell layer a few times in order to dissociate any remaining adherent or packed

cells as well as to create a single cell suspension [198]. Cells were transferred into a 15-ml conical tube with further centrifugation at ~1500 rpm for 5 min at room temperature, in order to concentrate viable cells in the suspension.

After discard the supernatant, cell pellet was resuspended by gently mixing with 5 ml of 37°C complete growth medium DMEM or M199 (pH 7.4)—i.e., 10% FBS (v/v) and 1% (v/v) (100 U/ml) penicillin-streptomycin supplemented—using graduated pipette. Then, the 0.5 ml of cell suspension was transferred to a 25-cm^2 fresh tissue culture flask containing 5-7 ml of complete growth medium DMEM or M199 (or the 1-2 ml of cell suspension was transferred to a fresh a 75-cm^2 fresh tissue culture flask containing 15-20 ml of complete growth medium). Alternatively, the resuspended cells were counted to determine viable cell number by cell staining with trypan blue and then counting cells using a hemacytometer (method described in section 3.3, before diluted to a specific number of cells to be passaged into a fresh culture vessel [198]. In addition, for primary cultures and early subcultures, 25-cm^2 flasks were used, while 75-cm^2 flasks were used for later subculturing [198]. Finally, subculturing cells were incubated in a CO_2 incubator at 37°C, 5% CO_2, and in a 95% humidified atmospheric condition [99]. As well, the passaged cells were often microscopically examined to observe cell growth and morphology. Subconfluent cultures were periodically fed after 2 or 3 days by removal of previous medium prior to addition of 37°C fresh complete culture medium in order that maintained the cell growth. Whenever confluence of cells was nearly reached, the secondary culture was then passaged to produce tertiary cultures and so forth, by repeating steps above.

3.2.3 Cryopreservation of monolayer cells (HeLa and Vero)

For long-term storage of HeLa and Vero cells and in order to obtain the most cell recovery, it is best to preserve cells in logarithmic phase of growth from a nearly confluent culture flask [198] and cells should be frozen slowly in the cryoprotective agent. Without using a cryoprotective agent, cells in most cases would be lethal [198]. DMSO, a cryoprotective agent, has been generally used in cell preservation at -70°C or lower [198].

It acts to reduce the freezing point of the cryopreserved cells. Thus a slower cooling rate into frozen cells decreases the formation of ice crystal that may damage cells [198]. By typical procedure of cryopreservation of monolayer cells, the cells from more than one culture flask can be pooled together if they are from the same subculture of the same original source [198]. Cells preservation was performed through the trypsinizion of the actively growing cells in the tissue culture flasks and by harvesting them in a normal way (see 3.2.2).

In brief, cells were trypsinized from the surface of from 25-cm^2 tissue culture flask. Consequently, cell suspension was transferred into a sterile 15 ml conical tube that was further subjected to centrifugation at ~1500 rpm for 5 minutes, at room temperature. After removal of the supernatant, the pellet from 25-cm^2 tissue culture flask was resuspended by thoroughly mixing with 2 or 3 ml of 4°C sterile complete growth medium—i.e., DMEM for HeLa or M199 for Vero cells, by using graduated pipette. Alternatively, cells in the suspension were counted using a hemacytometer (see 3.3) before addition of the medium as necessary to dilute cells into a final concentration of $1x10^6$ or $1x10^7$ cells/ml. Aseptically, aliquot a volume of 0.5 ml of cell suspension into each labeled 2-ml cryovial, following with addition of 0.4 ml FBS and 0.1 ml DMSO, before tightened each vial cap. The cells-containing cryovials were placed into a styrofoam container and immediately froze them in a –80°C freezer for 1 h to overnight, and then transferred to the liquid N_2 tank within the next 2-5 days for long-term storage [99].

3.3 Determination of cell viability using hemacytometer and trypan blue staining

Determination of viable cells in the culture is significant in culture standardization and to perform experiments in an accurate quantitation. Figure 19 showed a diagram of hemacytometer, a thick glass slide with a counting platform at the central portion of which is separated into two counting chambers, which can be individually used to perform cell counting. Each side of counting chamber has a 3 × 3-mm grid of which is separated into 9 secondary squares, 1 × 1 mm each. The four

corner squares (1, 2, 4, and 5) and a central square (3) were used in cell counting. Each four corner square is splitted into 16 squares and one central square is splitted into 25 squares.

Prior to utilization, surface of a hemacytometer as well as a coverslip was cleaned using 70% ethanol. Then coverslip was evenly placed onto a hemacytometer. Before counting, the cell suspension was prepared from a monolayer of the cultured HeLa or Vero cells by detaching them from the surface of the flask through trypsinization protocol (see 3.2.2). After centrifugation, cells were resuspended and diluted with medium and mix thoroughly to obtain a uniform suspension. Next step, a 1:1 ratio of trypan blue per cell suspension was prepared, e.g., 0.5 ml of trypan blue: 0.5 ml cell suspension in a microcentrifuge tube, then let stand before loading into hemacytometer. By using a sterile micropipette, one drop or ~20 µl of trypan blue-cell suspension was transferred to the edge of counting chamber by holding the pipette tip under the coverslip and dispensing. The suspension was naturally drawn to under the coverslip via capillary action. After filling the second counting chamber, cells were allowed to settle for a few minutes. After tissue blot off an excess liquid, observed slide on a microscope with 100× magnification, i.e., 10× ocular and 10× objective lens. In case of that cells were not evenly distributed, then washed hemacytometer and reload cell suspension. Otherwise, cells counting was started by counting in four corner and one central squares (Figure 19) using a hand-held counter. As recommendation [198], cells at the middle line on the top and left must be counted, but do not count cells lining at the middle line on the bottom and right. If a total number of counted cells was less than 100 then count more squares. Count another chamber, then determine the number of cells per milliliter and total viable cells in culture as the following calculations. The dilution factor was derived from the ratio of total volume of cell and trypan blue dye per volume of taken cell, i.e., 2/1 in this case. The 10^4 is the volume correction factor of the hemacytometer derived from 1-mm^2 square x 0.1 mm depth—i.e., 1 mm × 1 mm x 0.1 mm, and thus representing a total volume of 0.1 mm^3 or 10^{-4} ml. After the cell count,

hemacytometer and coverslip were rinsed with 70% ethanol and deionized water for decontamination for future use.

Cells per milliliter = average cell count in a 1-mm^2 square × dilution factor × 10^4

Total cells = cells per milliliter × total original volume of cell suspension of which sample was taken

$$\% \text{ viable cells} = \frac{\text{Number of unstained cells}}{\text{Total number of (stained + unstained) cells}} \times 100$$

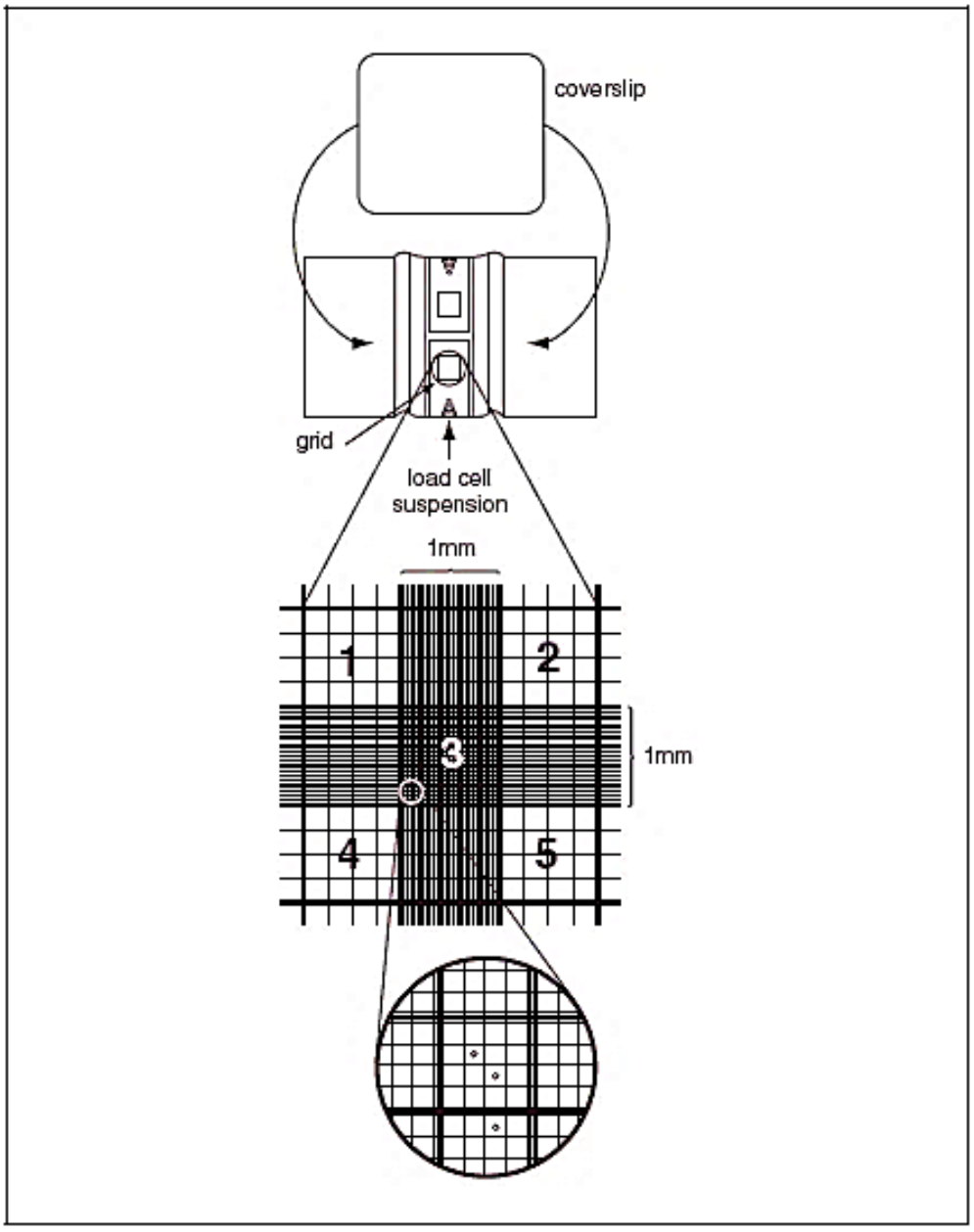

Figure 19 Diagram of a Hemacytometer slide (Improved Neubauer) and coverslip Available from: https://bme.ucdavis.edu/georgelab/files/2017/07/Basic-Technique-for-Tissue-Culture.pdf

3.4 Measurement of cell standard

A monolayer of HeLa or Vero cells was detached through trypsinization as normal (see 3.2.2) to make a single cell suspension and cells were counted using a hemacytometer (see 3.3). After cells were diluted with complete growth medium (DMEM or M199) to give an appropriate density of cells for seeding, 100 µl of suspension containing cells numbers of 1 x 10^4, 2 x 10^4, 3 x 10^4, 4 x 10^4, and 5 x 10^4 were seeded into each well of the sterile 96-well microtiterplate by using a multichannel pipette. The cells were allowed for adherence at the plate bottom by incubating for 24 hours in a CO_2 incubator at 37°C, 5% CO_2, and a 95% humidified atmospheric condition. Then cells were subjected into the cytotoxic assay using MTT method (see 3.5).

3.5 Cell culture treatment of MM and cytotoxicity assay

Cytotoxic effects of MM in solution on cell growth of HeLa, Vero and uterine endometrial cells were evaluated using MTT assay. Growth medium, i.e., DMEM for HeLa and endometrial cells, and M199 for Vero cells, were referred as the experimental controls, while a medium containing 0.5% ethanol were referred as the negative control of MM. The evaluation of cell viability via MTT assay was done according to Mosmann, 1983, with modification [(203)].

In detail, a monolayer of each cell line was detached from the cultured flask by trypsinization as previously described (see 3.2.2). Cells was counted with a hemacytometer and diluted with the complete growth medium DMEM or M199. The 100 µl of individually cell suspension was seeded into the sterile 96-well microtiter plates at an optimal density of 1 x 10^4 cells/well (HeLa cells) and 2 x 10^4 cells/well (Vero and endometrial cells), then allowed cell to attach and proliferate by incubating at 37°C, 5% CO_2, 95% humidified atmospheric condition for 24 h. On next day, MM solution (pre-dissolved in Milli-Q water) were diluted with the complete growth media to a concentration of 1 mg/ml, then sonicated for 10 min before diluted with growth media to give the final concentrations in wells (100 µl/well) at 1.953, 3.906, 7.812, 15.625, 31.25, 62.5, 125, 250, 500, and 1,000 µg/ml. Cells were then added with 100 µl of MM solutions prepared above after removing the old medium in wells. Cell culture treatment was

maintained in a CO_2 incubator at 37 °C with 5% CO_2 for 24 h. The growth medium, either DMEM or M199, was used as an experimental control. Triplicate wells of each MM concentration as well as growth media (DMEM and M199) were maintained throughout the experiments.

At the end of treatment, cells were visualized under the light inverted microscope. To evaluate cell viability, old medium in wells was carefully removed by flicking off prior to 100-µl addition of the 0.5 mg/ml MTT (diluted with growth medium) into the wells. The plate was further incubated at 37°C for 4 h to allow the formazan crystal formation on the plate bottom. Thereafter, the medium was carefully removed prior to addition of 100 µl DMSO and shaking by hands to completely dissolve the dark blue formazan crystals in the wells. Next, cell viability was examined by color intensity measurement (absorbance) at 570 nm using the microplate reader (Synergy™ HT, Bio-tek Instruments, Inc.). The obtained raw data from measurement was recorded as optical density (OD) per well and further used to calculate the percentage of cell viability in respect to the experimental control. The study was done in three independent experiments. All of the OD were transferred to the software Microsoft Excel to calculate the % cell viability, compared with the untreated controls, as shown below:

$$\text{Viability (\%)} = [A_{\text{treated}} / A_{\text{control}}] \times 100$$

From the above formulations, A_{control} is the mean OD of the untreated control cells while A_{treated} is the mean OD of the treated cells at each MM concentration. The dose-response curves of MM solution were plotted by using GraphPad Prism 5 software (GraphPad, San Diego, CA). By using the nonlinear regression analysis, the drug **inhibitory** concentration for 50% cell growth (IC_{50}) after MM treatment was estimated. The results were expressed into mean±SEM (mean±standard error of the mean) (N=3).

3.6 Investigation of cell death in HeLa cells after MM treatment

3.6.1 Analysis of phosphatidylserine externalization

Cell death assay was studied by detection of phosphatidylserine externalization of HeLa cell surface. In brief, HeLa cells were seeded onto 6-well plates (0.6 x10^6 cells/well) and maintained growth at 37 °C in a CO_2 incubator for 24 h. After removal of old medium DMEM, 2 ml of freshly prepared MM solution (70, 100 or 150 µg/ml) were added into the wells and cells were incubated at 37°C for 16 h. Thereafter, cells were trypsinized and PBS washed by centrifugation. Cells pellet was resuspended in the assay buffer HSC (1X), transferred to a microcentrifuge tube, before staining with Annexin V and 7-AAD according to the manufacturer's protocol of FlowCellect Annexin Red Kit (FCCH100108) (Merck KGaA, Darmstadt, Germany). In brief, Annexin V working solution was added into each microcentrifuge tube containing cell suspension and incubated at 37°C for 15 min. The cells were washed once with the assay buffer HSC (1X) by centrifugation to collect the pellet. Then cell pellet was resuspended with buffer HSC (1X) before addition of 7-AAD (5 µl). Cells with staining dye were incubated at RT in the dark for 5 min prior to washing with buffer HSC. Approximately, 10,000 cells were analyzed by using the Amnis FlowSight® Imaging Flow Cytometer (Merck KGaA, Darmstadt, Germany) with excitation blue laser (488 nm) for 7-AAD and red laser (642 nm) for Annexin V. Untreated HeLa cells grown in DMEM were served as the control group of the experiments.

The study was done in three independent experiments. The obtained results were subjected to cell death analyses by cell image visualization and quadrant gating using the IDEAS® 6.2 Image Analysis Software in order to distinguish four different cell populations. Dose response of MM-induced apoptosis were determined by using GraphPad Prism 5 software (GraphPad, San Diego, CA, USA).

3.6.2 Analysis of mitochondrial membrane potential depolarization

HeLa cells were seeded onto 6-well plates (0.6 x10^6 cells/well). Cell growth in DMEM was maintained at 37 °C in a CO_2 incubator for 24 h. After that, the medium was removed from the wells before addition of 2 ml of freshly prepared MM solution (70, 100,

150 µg/ml), with further incubation at 37°C for 16 h. With similar protocol done in section 3.6.1, cells were trypsinized, collected, and resuspended with the assay buffer HSC (1X). To study the mitochondrial membrane potential depolarization, the resuspended cells were stained with dyes of the FlowCellect MitoPotential Red Kit (FCCH100105) (Merck KGaA, Darmstadt, Germany) in the microcentrifuge tube. Briefly, cells were added with MitoSense Red working solution, incubated at 37°C, 15 min, and washed twice with buffer HSC (1X). The resuspended cells in HSC (1X) were added with 7-AAD (5 µl), mixed well, and washed with buffer HSC (1X). Approximately, 10,000 cells were immediately measured on the Amnis FlowSight® Imaging Flow Cytometer (Merck KGaA, Darmstadt, Germany) using excitation blue laser (488 nm) and red laser (642 nm) for 7-AAD and Annexin V, respectively. Untreated HeLa cells grown in DMEM served as the control group. The study was done in three independent experiments. The obtained results were analyzed and dose response of MM-induced apoptosis were determined with similar method as section 3.6.1.

3.7 Optimization of the synthesis of phenoxy-grafted dextran (DexP$_\tau$)

In order to develop the stable PLA-Dextran nanoparticles (PLA-dex NPs) by using PLA and dextran as degradable materials, therefore the structure of polysaccharide dextran was modified to be less hydrophilic. The process was done by the attachment of aromatic groups on dextran backbone by using the previous protocol with modification form Chiewpattanakul et al., 2010 [143].

The 10 g of dextran T40 was dissolved in 100 ml of aqueous NaOH (1M) for 1-2 h, before the addition of 7 ml of 1, 2-epoxy-3-phenoxypropane (700 µl/g dextran) and covering with aluminium foil. The heterogeneous medium was stirred magnetically for 48 h at 37°C. Then, obtained milky crude solution was precipitated with 1 L of cold absolute ethanol under stirring vigorously on ice. The obtained polymer was filtered through a fritté using vacuum filtration to separate DexP, rewashed 2-3 times with cold absolute ethanol (total 1 L) to eliminate excess residual reagent, and dried overnight in the vacuum oven at 40°C. In order to eliminate the free epoxy and to purify the product

by ultrafiltration, each polymer DexP was redissolved in 200 ml deionized water prior to membrane dialysis against deionized water (10 L) for 24 h using a membrane tube with the molecular weight cut off 6-8 kDa (Spectra/Por® 1 Dialysis Membrane Tubing, MWCO: 6,000 – 8,000 Daltons), by changing water several (3-5) times. Thereafter, the recovered polymer Dextran-phenoxy, DexP, was freeze-dried before subjected to ^{1}H nuclear magnetic resonance (^{1}H NMR) analysis, using DMSO-d_6 (>99.8%) and deuterated water (D_2O) as solvents. ^{1}H NMR spectra were used to determine the molar ratios of the attached phenoxy rings to sugar repeat unit.

The reaction in the attachment of epoxy groups on dextran backbone were tried with some modifications to obtain different degrees of low hydrophobic modified dextran. The analyzed NMR results revealed three dextran derivatives, of which shown the degree of modification 15.5%, 21%, and 26%. These phenoxy-grafted dextran, i.e., $DexP_{15.5}$, $DexP_{21}$, $DexP_{26,}$ designated as $DexP_{\tau}$, were further utilized for the nanoparticles development.

3.8 Preparation of dextran-phenoxy ($DexP_{\tau}$)-grafted PLA NPs

3.8.1 Optimization of the synthesis of $DexP_{\tau}$-grafted PLA NPs

The previously synthesized polymers $DexP_{\tau}$ were utilized in the synthesis of PLA-DexP NPs through emulsion-solvent evaporation method, modified from Chiewpattanakul et al., 2010 [143].

PLA in a solvent (50 g/l) was prepared by dissolving 50 mg of PLA in 1 ml of CH_2Cl_2 (dichloromethane) by shaking overnight or until dissolution. An aqueous solution containing $DexP_{\tau}$ (5 g/l), i.e., $DexP_{1\,5.5}$ or $DexP_{21}$ or $DexP_{2\,6}$ (obtained from 3.2) were prepared by dissolving 50 mg of $DexP_{\tau}$ in 10 ml ultrapure water (Milli-Q) by shaking until dissolution. On next day, mixtures of PLA/$DexP_{\tau}$ (1:10) were prepared by adding 1 ml of predissoved PLA in CH_2Cl_2 into 10 mL of an aqueous solution containing $DexP_{\tau}$ before mixing vigorously. The mixture was subjected to sonication for 120 sec on ice by using varying sonication power 5 to 8 (45W to 90W), 50% active cycles, using Ultrasonic Vibra Cell Meter, Bioblock Scientific-600W (Sonics& Materials Inc., USA). Thereafter, the

organic solvent (CH_2Cl_2) was eliminated from the emulsion by evaporation at 37°C for 4 h in Thermoshake Incubator Shaker (C. Gerhardt GmbH & Co. KG, Germany). The suspensions of nanoparticles were washed thrice with ultrapure water (Mill-Q) by centrifugation at 18,000 rpm, 20°C, for 45 min, using Ultracentrifuge, Optima™ L-80 XP (Beckman Coulter Inc., USA) in order to remove the excess chemicals and to purify the product. Finally, the synthesized PLA-DexP NPs were freeze-dried using FreeZone® 4.5 Liter Benchtop Freeze Dry System Model 77500 (LabCongo, USA).

3.8.2 Characterizations of DexP$_\tau$-grafted PLA NPs

In order to examine particle size, components, and colloidal stability, the PLA-DexP NPs: DexP$_{15.5}$-grafted NPs, DexP$_{21}$-grafted NPs, and DexP$_{26}$-grafted NPs, were characterized as follows:

3.8.2.1 Size measurement

To examine nanoparticles size and aggregations, aliquots of nanoparticle suspensions before and after wash (see 3.8.1) were measured by using the granulometry technique, using the particle size analyzer, Mastersizer 2000 (Malvern-instruments Ltd., UK).

3.8.2.2 ^{1}H NMR analysis

The nanoparticles after freeze-dried (see 3.8.1) were dissolved in DMSO-d_6 (>99.8%) and deuterated water (D_2O) and subjected to ^{1}H NMR spectroscopy using 300 MHz, BRUKER spectrometer Avance 300 (Bruker AG, Switzerland) to determine the molar ratios of NPs components, i.e., PLA and DexP, incorporated into nanoparticles. NMR peaks were used to calculate specific surface area, A_p in mg of DexP$_\tau$/g PLA) and surface coverage in mg of DexP$_\tau$/m^2 PLA, of the NPs grafted with different DexP$_\tau$.

3.8.2.3 Colloidal stability in the presence of NaCl

Since the synthesized NPs could be further used in the biomedical study and applications, therefore, colloidal stability of NPs in a similar condition as the body fluid environment was ensured.

PLA NPs were freshly prepared with $DexP_{\tau}$, i.e., $DexP_{15.5}$, $DexP_{21,}$ $DexP_{26}$, by using an emulsion-solvent evaporation process as performed in section 3.8.1 but only with sonication power 5. Before freeze-drying, aliquots of nanoparticle suspensions were subjected to stability determination by preparing NPs suspension in varying concentrations of NaCl (10^{-4}, 10^{-3}, 10^{-2}, 10^{-1}, 1, 2, and 4 M): 0.3 ml of NPs suspension was added to 2.7 ml NaCl and let stand for 1 h, before the absorbance (OD) measurement at wavelengths (λ) 450, 500, 550, 600 and 650 nm using Uvikon XL UV-Visible, Scanning Spectrophotometer (Bio-Tek Instruments, USA). Nanoparticle suspension (0.3 ml) diluted with Milli-Q water (2.7 ml) was used to serve as a blank. The recorded OD (optical density) of each NaCl concentration were further used to create a linear graph of log OD vs. log λ, of which taken n values from the linear log (OD) = n(log λ) + c, to plot a graph of $|n|$ vs. NaCl concentrations. To evaluate particle colloidal stability in a Na^+ condition as the normal blood, the nanoparticles must be stable in a range of 0.136-0.145 M (136-145 mM) of sodium (Na^+) [204].

3.9 Preparation of drug-loaded $DexP_{26}$-grafted NPs

3.9.1 Chemical properties of MM and FITC

Monomyristin (MM) was tested to inhibit HeLa cells growth and thus will be loaded into nanoparticles. Moreover, the encapsulated FITC will be used as a model drug to study the nanoparticles internalization. Therefore, chemical properties of MM and FITC were examined as follows:

3.9.1.1 Stability of MM and FITC after ultrasonication

In the synthesis of nanoparticles for MM and FITC encapsulation, P5 sonication is required in the process which might cause the loss of or damage to MM or FITC. Therefore, stability of MM as well as FITC after sonication was studied. Briefly, 10 mg of MM and FITC was dissolved in 1 ml CH_2Cl_2 (dichloromethane) by allowing the complete dissolution on a shaker for overnight. On next day, 10 ml of ultrapure water (Milli-Q) was added before applied on a sonication on ice using P5 at 50% active cycle for 120 sec. After solvent (CH_2Cl_2) evaporation at 37 ° C for 4 h using an incubator shaker, the

resultant was subjected to a freezer dryer and ^{1}H NMR analysis, using DMSO and D_2O as solvents, to examine the MM and FITC composition after sonication.

3.9.1.2 Solubility of MM and FITC in D_2O

In the synthesis of MM- or FITC-encapsulated NPs, the agents might be lost into the water used in the process. Therefore, MM and FITC solubility in water was tested to ensure if it can be dissolved in water. The excess amount of MM or FITC was added into a vial containing 6 ml of heavy water, D_2O (deuterium oxide) until no more dissolution by shaking for 24 h. Then MM or FITC in D_2O was subjected to centrifugation at 13,000-18,000 rpm, 45 min, 2-3 rounds and/or by filtering the undissolved amount of MM and FITC to separate the sediment from an aqueous phase of D_2O. Next, 2 ml of solution was mixed with phenol and butanol-2, as a reference of MM and FITC respectively, and let to dissolve overnight on a shaker. One milliliter of each solution was then analyzed by ^{1}H NMR analysis to determine the compositions in D_2O.

3.9.1.3 Miscibility of MM and FITC with PLA

Prior to preparation of NPs for the encapsulation of MM and FITC, the miscibility between PLA and the additional agent, i.e., MM or FITC, was examined using (differential scanning calorimetry) DSC technique, in order to determine at which ratios that MM and FITC is miscible with PLA and form a homogeneous phase which thus will be used in the encapsulation synthesis.

In detail, 50 mg of PLA/MM and PLA/FITC mixtures (Table 7) were prepared in the glass vials by dissolving in 2 ml of acetone. These mixtures were shaken for 2 h to ensure the complete dissolution. Then solvent was evaporated in an ambient temperature overnight before complete drying using a dryer to eliminate the residual acetone and subsequently placing in an oven at 90°C overnight. Next, the dried samples were scratched from the vials using a sterile spatula and cut into small pieces using sterile forceps and scissors before transferred to DSC measurement. The results were analyzed to determine the miscibility ratios of PLA/MM and PLA/FITC.

Table 6 The ratios of PLA/MM and PLA/FITC for miscibility evaluation

Vial	Nanoparticle components (mg)			Ratios	
no.	PLA	MM	FITC	PLA: MM	PLA: FITC
1	50	-	-	10: 0	-
2	-	50	-	0: 10	-
3	25	25	-	5: 5	-
4	35	15	-	7: 3	-
5	40	10	-	8: 2	-
6	45	5	-	9: 1	-
7	47.5	2.5	-	9.5: 0.5	-
9	45	-	5	-	9: 1

3.9.2 Syntheses and characterizations of MM-NPs and FITC-NPs

3.9.2.1 Synthesis of MM-NPs and FITC-NPs

Characterization results from size and turbidity measurements of the synthesized $DexP_{26}$-grafted PLA NPs indicated the stability of nanoparticles (section 4.4). Thus, $DexP_{26}$ was considered as a good stabilizer for drug-encapsulated NPs and the syntheses of drug-loaded NPs were done through the emulsion-solvent evaporation process by using sonication P5, similar to section 3.8.1. The core materials—i.e. PLA/MM (9:1) and PLA/FITC (9:1) mixtures—were used to synthesize MM-loaded NPs (MM-NPs) and FITC-loaded NPs (FITC-NPs) as explained below:

The PLA/MM and PLA/FITC mixtures in CH_2Cl_2 (50 g/L) and $DexP_{26}$ in ultrapure water (Milli-Q) (5 g/L) were prepared. On next day, the volume ratio 1:10 of core materials / $DexP_{26}$ was used by adding 1 ml of PLA or PLA/MM or PLA/FITC in CH_2Cl_2 10 ml of $DexP_{26}$ solution, before mixing vigorously and sonicating for 120 sec on ice with the pulse mode P5 (45W) and 50% active cycles using Ultrasonic Vibra Cell Meter (Sonics& Materials Inc., USA), to form an emulsion of nanoparticles. After organic solvent (CH_2Cl_2) evaporation at 37°C for 4 h, the nanoparticle suspensions were washed thrice with ultrapure water (Milli-Q) by centrifugation at 18,000 rpm, 20°C, 45 min using

the Ultracentrifuge Optima™ L-80 XP (Beckman Coulter Inc., USA) to remove the excess chemicals.

Aliquots of nanoparticle suspensions both before and after wash were collected for size measurements using granulometry technique similar to section 3.8.2.1. In addition, aliquots of suspension only after wash were collected to study the colloidal stability in NaCl similar to section 3.8.2.3. The synthesized MM-NPs and FITC-NPs were freeze-dried and subjected to ^{1}H NMR analysis (see 3.8.3) using 300 MHz, BRUKER spectrometer Avance 300 (Bruker AG, Switzerland) to determine the molar ratios of DexP per gram PLA and per m^2 PLA and amount of MM and FITC per gram nanoparticles.

3.9.2.2 Calculation of components and drug loaded into nanoparticles

In order to determine the amount of drug encapsulated within NPs, areas under peaks from ^{1}H NMR spectra were used to estimate the molar ratios of $DexP_{26}$/PLA, MM/PLA, FITC/PLA and gram encapsulated drug (MM and FITC) per gram NPs.

3.9.2.3 Drug release study

In the synthesis of $DexP_{26}$-grafted MM-NPs and $DexP_{26}$-grafted FITC-NPs by emulsion-solvent evaporation, nanoparticle suspensions after centrifugation were subjected to the study of MM and FITC release in water. The 6 aliquots of each synthesized NPs suspension were added into dialysis membrane tubes—with the molecular weight cut off 12-14 kDa (Spectra/Por® 2 Dialysis Membrane Tubing, MWCO: 12,000 – 14,000 Daltons), then dialyzed against Milli-Q water (10 L) for 5, 16, 24, 48 and 72 h, by changing water at the appropriate times. When each dialysis time was ended, the dialysis membrane tube was removed to take the nanoparticle suspension and subjected to freeze dry and ^{1}H NMR analysis in order to determine the amount of encapsulated MM and FITC remaining inside the NPs at each time point, comparing to the beginning time (T_0) of dialysis. Then the released MM and FITC amounts were further used to create the releasing curves.

3.10 Preparation of Transferrin (Tf)-conjugated drug-loaded NPs

3.10.1 Synthesis of carboxylated dextran-phenoxy$_{26}$ (DexP$_{26}$-COOH)

The development of transferrin (Tf)-conjugated NPs (Tf-NPs) for specific Tf binding to the Tf receptor requires a linker on nanoparticles for Tf attachment. Therefore, DexP$_{26}$ was modified further by addition of carboxyl (-COOH) group, to form a functional linker for Tf attachment to obtain carboxylated dextran-phenoxy$_{26}$ (DexP$_{26}$-COOH).

In detail, DexP$_{26}$ was subjected to freeze dry in order to achieve a constant weight. Next, the dry DexP$_{26}$ was dissolved in DMSO containing succinic anhydride and anhydrous pyridine and allowed the reaction to occur on a magnetic stirrer for 48 h. The product from reaction, i.e., DexP$_{26}$-COOH was purified with membrane dialysis in ethanol/d.H_2O (50/50, v/v) medium for 48 h by replacing media 3 times daily, followed by dialysis in d.H_2O for 96 h by changing water 3 times daily. Next, the DexP$_{26}$-COOH was freeze-dried and subjected to titration to determine the amount of COOH grafted on DexP$_{26}$.

3.10.1.1 Determination the amount of COOH grafting on DexP$_{26}$

The synthesized DexP$_{26}$-COOH was determined the amount of COOH grafting on DexP$_{26}$ by titration with NaOH. Briefly, DexP$_{26}$-COOH after freeze-dry was resuspended and reacted with 5% HCl in ethanol for 1 h before being filtered and washed with ethanol/d.H_2O (95/5, v/v) and d.H_2O before freeze-drying. Then the DexP$_{26}$-COOH/DexP$_{26}$-COO^- was resuspended with ultrapure water (Milli-Q) followed by pH measurement and titration with 0.01 M NaOH—by adding 50 µl NaOH dropwise to a swirling aqueous containing DexP$_{26}$-COOH and measuring the pH value after a drop addition of HaOH, until pH was higher than pKa. The obtained data were plotted as the relationship between the volume of NaOH added versus the pH increase. Next, the % of COOH grafted on 1 g of dextran was calculated.

3.10.2 Synthesis and characterizations of drug-loaded NPs

For development of the Tf-conjugated NPs, PLA NPs (empty NPs), MM-NPs, and FITC-NPs were firstly synthesized with similar method as section 3.9.2, by using the pulse mode at P5 (45W) for sonication. The components used in this encapsulation

synthesis were the $DexP_{26}$-COOH (carboxylated dextran-phenoxy$_{26}$) for grafting (instead of $DexP_{26}$) and core materials, i.e., PLA, PLA/MM and PLA/FITC at %wt 9:1. The synthesized $DexP_{26}$-COOH-grafted NPs were characterized similarly as section 3.8.2 and 3.9.2: i) size measurements; ii) ^{1}H NMR analysis; iii) colloidal stability in NaCl.

3.10.2.1 Calculation of Tf moles absorbed on $DexP_{26}$-COOH-grafted NPs

In order to calculate the number of moles and Tf molecules fully absorbed on 1 g of $DexP_{26}$-COOH-grafted NPs, the specific surface area of $DexP_{26}$ /gPLA from size distribution was used.

3.10.2.2 Calculation of components loaded in nanoparticles

In order to estimate the molar ratio of NPs components and to estimate the amount of drug encapsulated within NPs, the areas under peaks from ^{1}H NMR spectra were used, with similar calculation to section 3.9.2.2.

3.10.3 Conjugation of human holo-transferrin (Tf) with drug-loaded NPs

After synthesizing drug-loaded NPs (section 3.10.2.), the $DexP_{26}$-COOH-grafted NPs were then conjugated to human holo-transferrin (Tf) using a two-step procedure modified from Tsuji et al., 2013 [271]: firstly, carboxyl activation of $DexP_{26}$-COOH by using EDC/NHS to prepare the amine-reactive esters from COOH; secondly, chemical bonding between Tf and the activated $DexP_{26}$-COOH on NPs surface.

In brief, 50 mg of each $DexP_{26}$-COOH-grafted NPs—i.e. PLA NPs, MM-NPs, FITC-NPs, were reconstituted in 25 ml ultrapure water (Milli-Q) by applying sonication in an ultrasonic bath (Branson® 2510 Ultrasonic Cleaner) for 30 min. Each suspension of $DexP_{26}$-COOH-grafted NPs was adjusted pH to 6.8 before gradually adding N-(3-Dimethylaminopropyl)-N'-ethylcarbodiimide (EDC) (20 mg/mL, pH 6.8), with continuous stirring at 37°C. Thereafter 10 min, N-hydroxysuccinimide (NHS) (20 mg/mL, pH 6.8) was added before the addition of Tf (5 mg/mL, pH 6.8). Carboxyl activation and surface grafting was allowed to complete by stirring magnetically for 1 h before subjected to ultracentrifugation (Beckman Coulter Optima™ L-80 XP Ultracentrifuge) at 18,000 rpm, 20°C, 45 min to eliminate the excess Tf and freeze-dry (FreeZone® 4.5 Liter Benchtop

Freeze Dry System Model 77500, LabCongo). The sizes of NPs before and after Tf conjugation were examined using a particle size analyzer (Mastersizer 2000-Malvern instruments).

3.11 Cell culture treatment of MM-loaded NPs and cytotoxicity assay

Cytotoxic effects of MM in NPs forms (MM-NPs and Tf-MM-NPs) on the growth of HeLa, Vero, and uterine endometrial cells were evaluated using MTT assay, similar as section 3.5. Table 8 displayed all NPs forms for cytotoxicity assay. Nanoparticles without MM encapsulation, i.e., PLA NPs and Tf-PLA NPs, served as the negative vehicle controls of NPs. Growth medium alone, i.e., DMEM for HeLa and endometrial cells and M199 for Vero cells, were referred as the experimental control for MM and NPs. The evaluation of cell viability via MTT assay was done according to Mosmann, 1983, with modification [(203)].

Table 7 NPs used in the cytotoxicity test against HeLa, Vero and endometrial cells

NPs forms	Plain NPs	MM-loaded NP
Unconjugated NPs	PLA NPs	MM-NPs
Tf-conjugated NPs	Tf-PLA NPs	Tf-MM-NPs

In cell culture treatment, a monolayer of each cell line was detached from the cultured flask by trypsinization as previously described (see 3.2.2). Cells was counted with a hemacytometer and diluted with the complete growth medium DMEM or M199. The 100 µl of cell suspension was individually seeded into the sterile 96-well microtiter plates at an optimal density of 1 x 10^4 cells/well and of 2 x 10^4 cells/well, then allowed for cell attachment and growth by incubating at 37°C, 5% CO_2, 95% humidified atmospheric condition for 24 h. On next day, all NPs forms pre-dissolved with Milli-Q water were diluted with the complete growth media DMEM and M199 to a concentration of 1 mg/ml. The NPs suspensions were sonicated for 10 min and then diluted with growth media to give the final concentrations in well (100 µl/well) at 1.953, 3.906, 7.812,

15.625, 31.25, 62.5, 125, 250, 500, and 1,000 µg/ml. Cells were then treated with different NPs forms prepared above by removing the old medium in wells by flicking off the 96-well plate prior to addition of 100 µl of the pre-diluted NPs suspensions. Cell culture treatment was maintained in a CO_2 incubator at 37 °C with 5% CO_2 for 24 h.

At the end of treatment, cells were visualized and evaluated for the viability. The old medium in wells was carefully removed by flicking off prior to 100-µl addition of 0.5 mg/ml MTT (diluted with growth medium). The plate was then incubated at 37°C for 4 h to allow the formazan crystal formation on the plate bottom. Thereafter, the medium was carefully removed and 100 µl DMSO was added into wells. The plate was shaken by hands to completely dissolve the dark blue formazan crystals in the wells. Next, cell viability was examined by color intensity measurement (absorbance) at 570 nm using the microplate reader (Synergy™ HT, Bio-tek Instruments, Inc.) to record the optical density (OD) of each well. Triplicate wells of each NP concentration as well as growth media (DMEM and M199) were maintained throughout the experiments. The study was done in three independent times. The dose-response curves of each treatment were plotted by using GraphPad Prism 5 software (GraphPad, San Diego, CA) then % cell viability was evaluated, compared with the untreated controls. By using the nonlinear regression analysis, the IC_{50} of treated NPs and MM amount loaded in an individual NP form was calculated. The results were expressed into mean±SEM (mean±standard error of the mean) (N=3).

3.12 Competitive co-cultivation assay of Tf-MM-NPs with Tf for specificity evaluation

In order to evaluate the specificity of Tf-MM-NP which binds to a cell surface transferrin receptor (TfR) expressed by HeLa cells, human holo-transferrin (Tf) was used as a competitive binding molecule and HeLa cells viability was evaluated. In brief, a monolayer of HeLa cells was trypsinized and seeded into sterile 96-well plates (1×10^4 cells/well). After 24 h of incubation, HeLa cells were treated with Tf-MM-NPs similar to section 3.11. Firstly, the previous growth medium DMEM was removed and then free Tf (100 µg/ml and 500 µg/ml) in the complete DMEM (20 µl/well) was added into wells. The

plates were incubated at 37°C for 1 h before the addition of Tf-MM-NPs (1.95-1,000 µg/ml, 80 µl/well). Cell culture treatment was further maintained in a CO_2 incubator at 37 °C with 5% CO_2 for 24 h. The assessment of HeLa cell viability in respect to the control was done using MTT assay and OD measurement (570 nm) similar to section 3.11.

The study was done in triplicate wells and in independent triplicate experiments. The dose-response curves of Tf-MM-NPs with Tf treatment were plotted by using GraphPad Prism 5 software (GraphPad, San Diego, CA, USA). The IC_{50} was calculated with the nonlinear regression analysis. The results were expressed as mean±SEM (N=3).

3.13 Internalization assay of FITC-loaded NPs in HeLa cells

To examine the internalization of FITC-loaded NPs, HeLa cells were seeded into 6-well plates (0.6 x10^6 cells/well) and incubated at 37°C with 5% CO_2 for 24 h. On next day, 2 ml of freshly prepared FITC-loaded NPs, i.e., FITC-NPs and Tf-FITC-NPs, in complete growth medium DMEM (~1.29 µg/mL FITC), were added into wells. The plates were incubated at 37°C for 0.5, 1, 4, and 16 h. After each ending of incubation time, cells were trypsinized as normal, washed with PBS via centrifugation, collected the pellet, and resuspended in a buffer (1% FBS in PBS). Approximately, 10,000 cells of each sample were measured with Amnis FlowSight® Imaging Flow Cytometer (Merck KGaA, Darmstadt, Germany) by using the excitation blue laser at wavelength 488 nm for FITC.

The study was done in three independent experiments. The obtained results were analyzed with IDEAS® 6.2 Image Analysis Software. Count of single cells which showed fluorescence intensity of FITC were analyzed to determine the count of cells with internalized FITC-loaded NPs. Data were expressed as % cell internalization of FITC-loaded NPs. Time-response internalization of FITC-loaded NPs by HeLa cells were plotted by using GraphPad Prism 5 software (GraphPad, San Diego, CA).

3.14 Statistical analysis

All the biological experiments were performed in three independent replicate experiments. The results were expressed as mean±SEM (N=3). The differences of variable treatment groups were done by performing the statistical analysis of variance and *p*-values of < 0.05 were considered as statistically significant.

CHAPTER IV
RESULTS

4.1 Cytotoxicity of MM against HeLa and Vero cells

Cytotoxic effects of MM solution, MM-NPs, and Tf-MM-NPs against HeLa and Vero cells growth were evaluated with MTT assay, a conventional method to estimate the number of viable cells growing in a microtiter plate. This assay has been widely used based on changes of colorimetric formation in wells that can be measured by automatic microplate reader, as described by Mosmann, 1983 [203]. The principle of MTT assay is to examine the activity of intracellular mitochondrial dehydrogenase since this enzyme is able to cleave the tetrazolium rings of the yellow MTT (3-(4,5-dimethylthiazol-2-yl)-2,5-diphenyltetrazolium bromide) in viable cells [205] and form the insoluble dark blue formazan crystals which are impermeable to cell membranes. The amount of formazan crystals accumulated within healthy viable cells is therefore directly proportional to the number of viable cells [203].

After cells were exposed to various concentrations of samples for 24 h, the % cell viability at each treated concentration were determined. Figure 20 showed the % cell viability of HeLa (A), Vero (B), and endometrial cells after 24-h incubation with MM (1.95-1,000 µg/ml). From the results, MM showed the cytotoxicity against HeLa cells in dose-dependent manner (Figure 20A), while cytotoxicity of MM against Vero cells and endometrial cells was low (Figure 20B and 20C).

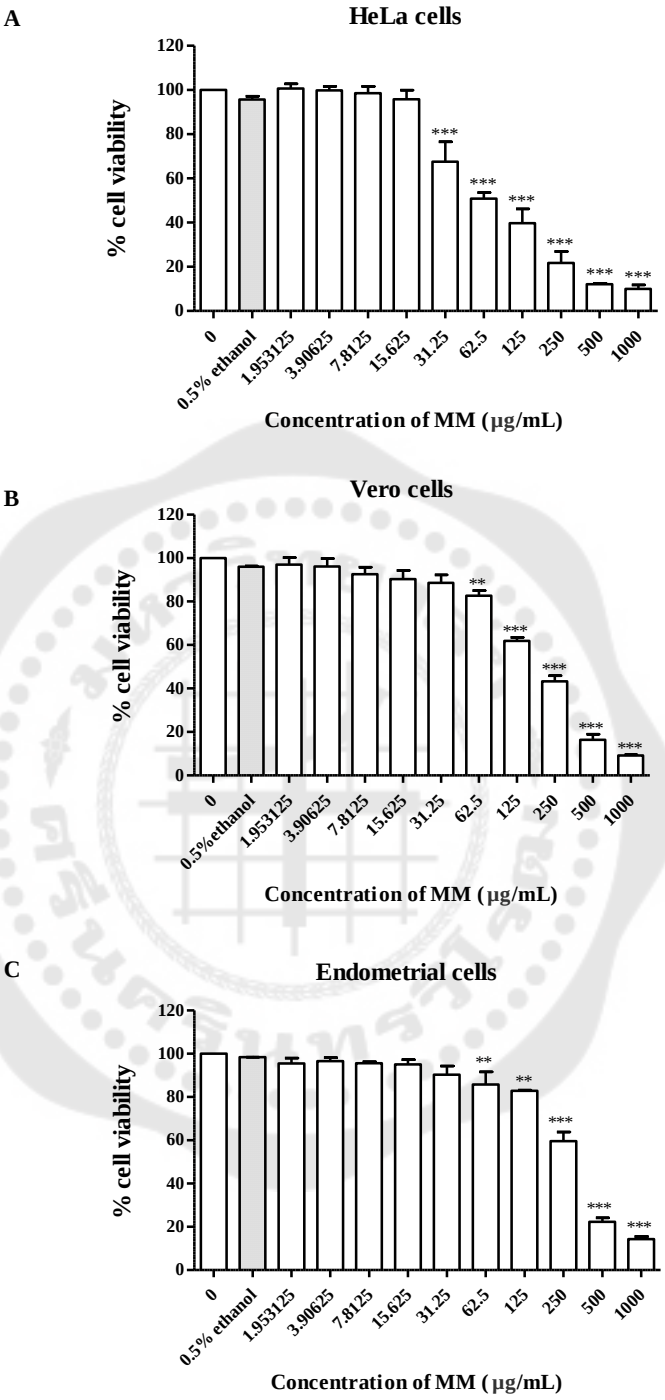

Figure 20 The % viability of HeLa (A), Vero (B), and endometrial (C) cells after 24-h incubation with MM (1.95-1,000 µg/ml)

The results are shown as mean ± SEM. ** and *** means statistically significant difference compared to the control group at $p<0.01$ and 0.001, respectively.

4.2 Effect of MM on apoptosis induction in HeLa cells

4.2.1 Dose response of phosphatidylserine (PS) externalization in HeLa cells

Phosphatidylserine (PS) externalization on cell surface is considered as a characteristic of the apoptotic cells. With double staining of Annexin V-CF647, a dye accumulated at the externalizing PS, and 7-AAD, a cell membrane impermeant dead cell dye, allowed the simultaneous detection of early and late apoptotic cells. In this study, Hela cells treated with MM (70, 100, 150 µg/ml) for 16 h were double stained with Annexin V-CF647/7-AAD and examined for the % cell apoptosis using the imaging flow cytometry.

Figure 21A showed four distinct characteristics of the representative HeLa cells identified by using the imaging flow cytometry. Figure 21B showed four different HeLa cell populations (Q1-Q4) gated as viable (lower left quadrant, Annexin V^- 7-AAD^-), early apoptotic (lower right quadrant, Annexin V^+ 7-AAD^-), late apoptotic/necrotic (upper right quadrant, Annexin V^+ 7-AAD^+), and dead cells (upper left quadrant, Annexin V^- 7-AAD^+). Figure 21C showed the % of apoptotic HeLa cell approximately 16.04%, 24.3%, 30.1%, and 33.42% of the control group and groups treated with MM at 70, 100, and 150 µg/ml, respectively. As the dot plots shown in Figure 21B and the bar graphs shown in Figure 21C, MM gradually induced the % of apoptotic HeLa cell when MM concentration increased. However, the % of apoptotic cell after treated at 100 and 150 µg/ml were significantly higher from the control group (* $p<0.05$, ** $p<0.01$). Moreover, it was found that late apoptotic HeLa cells were increased when treated with higher dose of MM, as shown in Figure 21D at 100 and 150 µg/ml, with significant difference from the control group (** $p<0.01$, *** $p<0.001$).

These results indicated that HeLa cell growth inhibition by MM was due to the apoptotic induction. Moreover, MM could induce more notable apoptosis in dose-dependent manner.

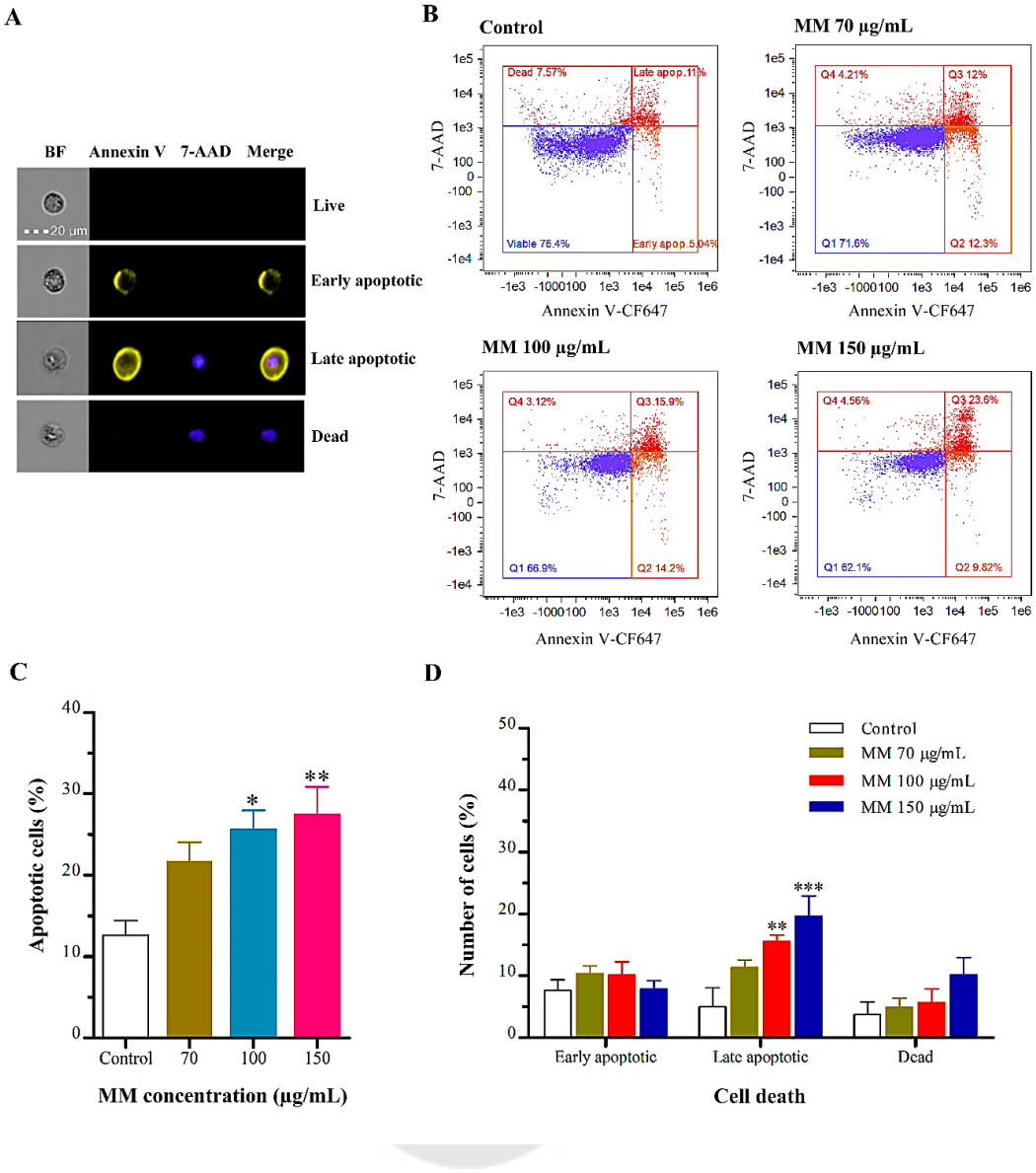

Figure 21 Effect of MM on apoptosis induction in HeLa cells: PS externalization

HeLa cells were treated with different concentrations (70, 100, 150 µg/ml) of MM for 16 h. (A) Image analysis of viable (row1), early apoptotic (row 2), late apoptotic (row 3), dead (row 4) cells; (B) Four different cell populations gated as viable, Q1 quadrant; early apoptotic cells, Q2 quadrant; late apoptotic/necrotic cells, Q3 quadrant; dead cells, Q4 quadrant; (C) % apoptotic cells via the PS externalization; (D) % of cell deaths, are demonstrated. The results are shown as mean ± SEM. *, **, *** means statistically significant difference compared to the control group at $p<0.05$, 0.01, 0.001, respectively. Abbreviations: BF, bright field; MM, monomyristin

4.2.2 Mitochondrial membrane potential changes in HeLa cells

Collapse of inner mitochondrial membrane potential is considered as an early hallmark of apoptosis. Accordingly, detection of the mitochondrial membrane potential changes is a crucial indicator to indicate mitochondrial dysfunction. By simultaneous labeling MitoSense Red dye that only accumulates in healthy mitochondria and 7-AAD, an impermeant dead cell dye, could identify live and apoptotic dead cells population. Therefore, after treated Hela cells with MM (70, 100, 150 µg/mL) for 16 h, the cells were double stained with MitoSense Red/7-AAD and examined for the % cell apoptosis using the imaging flow cytometry.

Figure 22A showed four distinct characteristics of the representative HeLa cells identified by using the imaging flow cytometry. The cell populations (Q1-Q4) were gated as viable (upper left quadrant, MitoSense Red^{+} 7-AAD^{-}), early apoptotic (lower left quadrant, MitoSense Red^{-} 7-AAD^{-}), late apoptotic/necrotic (lower right quadrant, MitoSense Red^{-} 7-AAD^{+}), and dead cells (upper right quadrant, MitoSense Red^{+} 7-AAD^{+}), as shown in Figure 22B. Figure 22C showed the % of apoptotic HeLa cell approximately 13.5%, 23.71%, 36.7%, 55.6% of the control group and the groups treated with MM at 70, 100, and 150 µg/ml, respectively. The results indicated that MM sharply induced the % of apoptotic HeLa cell when MM concentration increased, as the dot plots shown in Figure 22B and the bar graphs shown in Figure 22C. The % apoptotic cell after treated with 70, 100 and 150 µg/ml MM was significantly increased (* $p<0.05$, *** $p<0.001$, *** $p<0.001$), as compared to the control.

Figure 22D showed that the % of early apoptotic HeLa cells treated with 70, 100, and 150 µg/ml MM significantly increased as compared to the control (** $p<0.01$, *** $p<0.001$, *** $p<0.001$). Moreover, the % late apoptotic HeLa cells after treated with 100 and 150 µg/ml MM significantly increased from control (* $p<0.05$, *** $p<0.001$). These results indicated that both numbers of early and late apoptotic HeLa cells were significantly increased when treated with higher dose of MM (100 and 150 µg/ml). Therefore, upon treatment of Hela cells with MM (70, 100, 150 µg/mL), the MM-treated cells showed the progressive loss of MitoSense Red dye in a dose-dependent

manner, suggesting that MM-induced apoptosis could be involved with the intrinsic mitochondrial pathway.

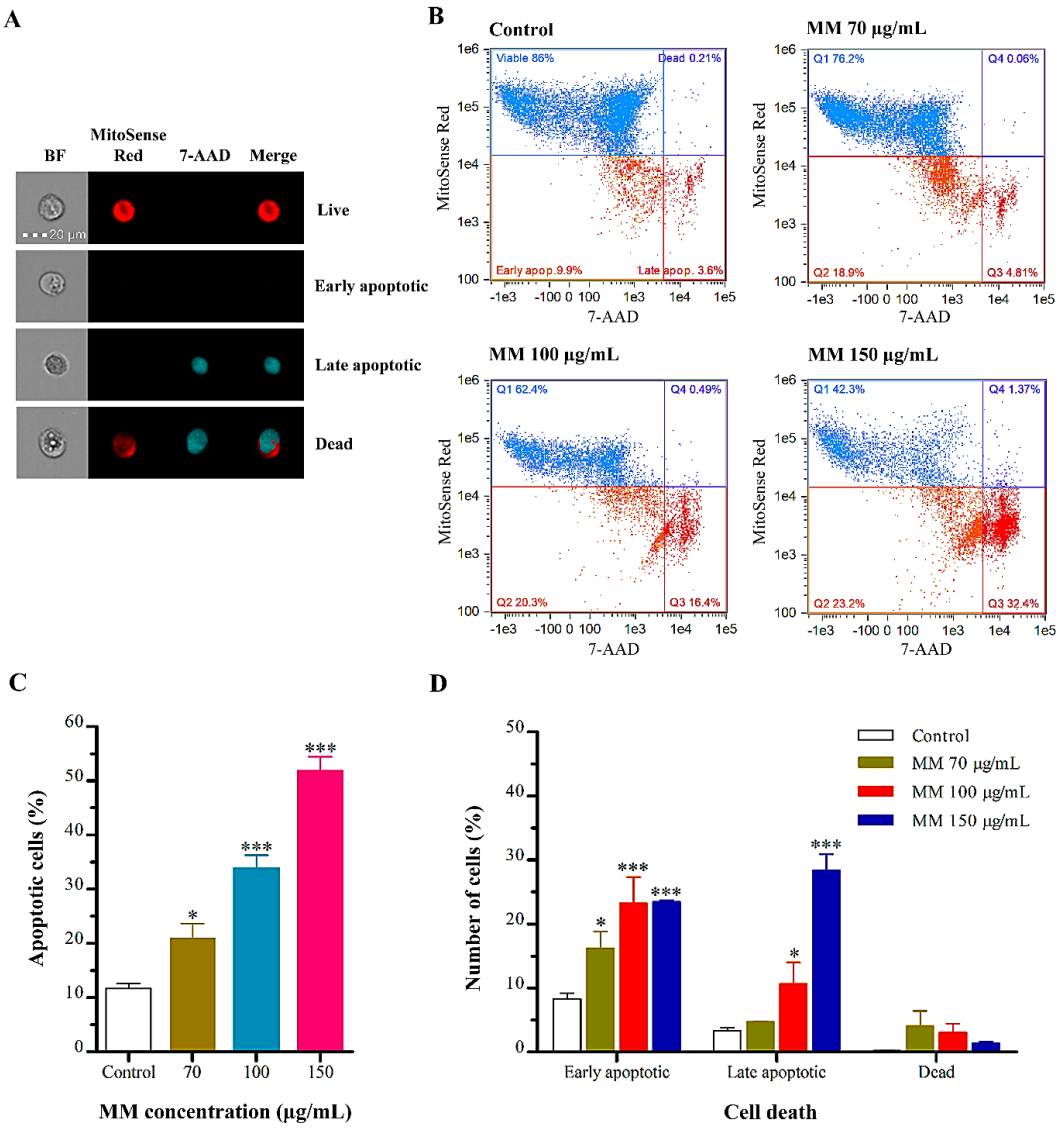

Figure 22 Effect of MM on apoptosis induction in HeLa cells: mitochondrial changes

HeLa cells were treated with different concentrations (70, 100, 150 µg/ml) of MM for 16 h. (A) Image analysis of viable (row1), early apoptotic (row 2), late apoptotic (row 3), dead (row 4) cells; (B) Four different cell populations gated as viable, Q1 quadrant; early apoptotic cells, Q2 quadrant; late apoptotic/necrotic cells, Q3 quadrant;

dead cells, Q4 quadrant; (C) % apoptotic cells via the mitochondrial membrane potential depolarization; (D) % of cell deaths, are demonstrated. The results are shown as mean ± SEM. *, *** means statistically significant difference compared to control at $p<0.05$, 0.001, respectively. Abbreviations: BF, bright field; MM, monomyristin

4.3 Synthesis of hydrophobic derivatives of dextran (DexPτ)

The structure of polysaccharide dextran (Dextran T40; MW = 37, 500 g/mol) was modified by attachment of the phenoxy groups to glucose units and obtained different hydrophobic derivatives of dextran.

Figure 23 to Figure 25 showed ^{1}H NMR spectra of three modified dextran, DexPτ, of which the chemical structure was presented in Figure 63, Appendix C. The percentage of the modified molecule compared to non-modified molecule (% substitution) was designated as τ, calculated by the areas under peaks of $H_{phenoxy}$ (phenoxy protons) and $H_{anomeric}$ (dextran anomeric proton) from NMR spectra and equation [206].

$$\tau = \frac{\text{Number of attached phenoxy groups}}{\text{Number of glucose units in the chains}} \times 100$$

$$\tau = \frac{H_{phenoxy}}{H_{anomeric}} \times 100$$

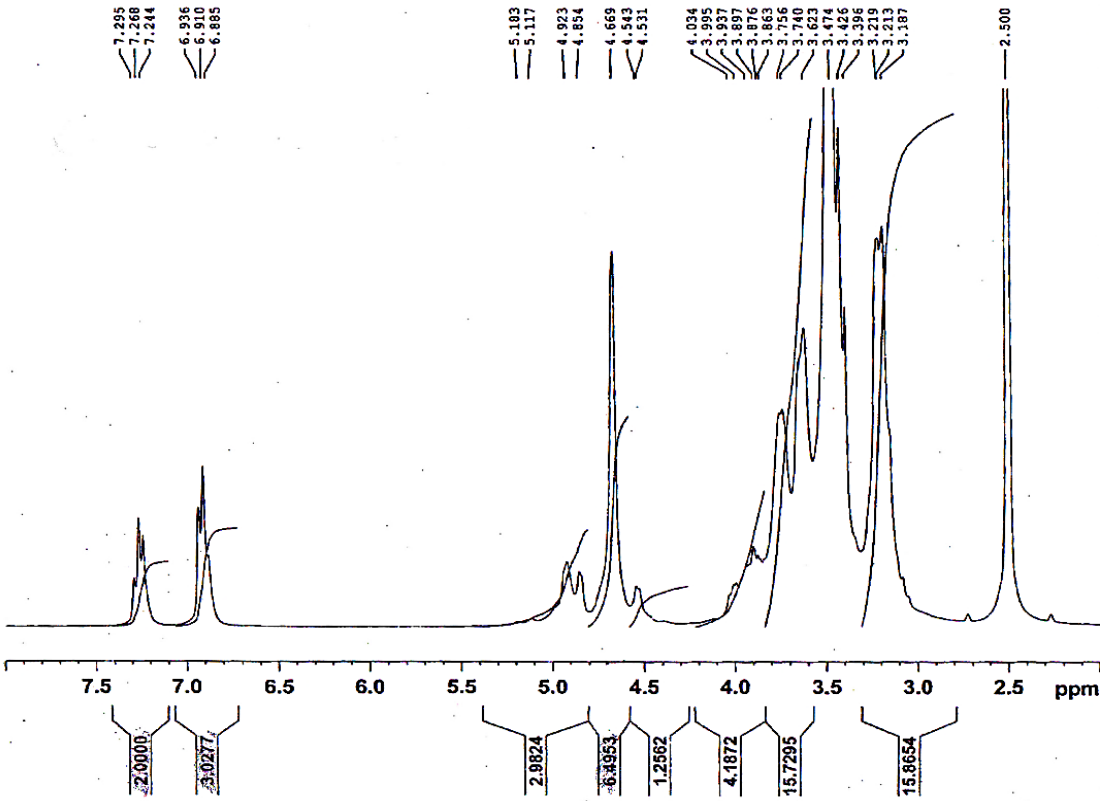

Figure 23 ^{1}H NMR spectrum of $DexP_{15.5}$ in DMSO D_6 and D_2O

Figure 23 showed ^{1}H NMR spectrum of $DexP_{15.5}$ in DMSO D_6 and D_2O. The peaks at 6.91-7.268 ppm and 4.669 ppm attributed to $H_{phenoxy}$ and $H_{anomeric}$, respectively. The degree of substitution of phenoxy groups on dextran units were determined as follows,

$$\tau = \frac{(2+3.0277)/5}{6.4953} \times 100$$

$$\tau = 15.48\%$$

Therefore, the percentage of above modified dextran was approximately 15.5%.

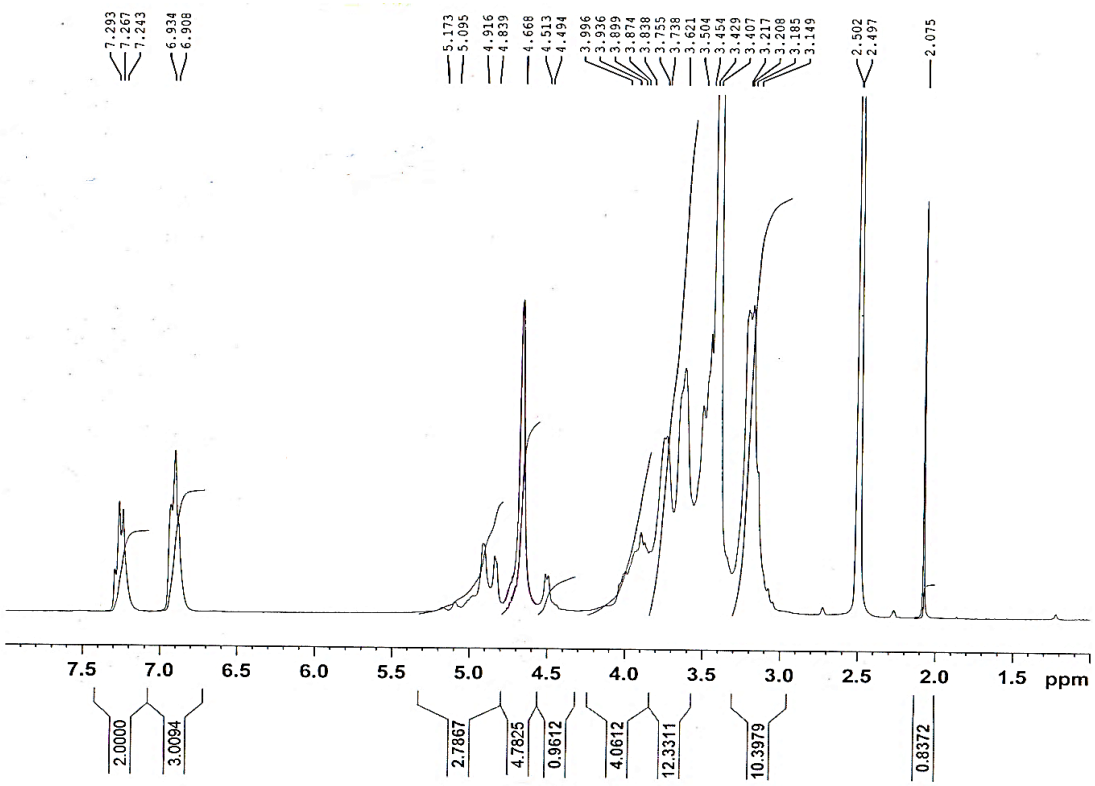

Figure 24 ^{1}H NMR spectrum of $DexP_{21}$ in DMSO D_6 and D_2O

Figure 24 showed ^{1}H NMR spectrum of $DexP_{21}$ in DMSO D_6 and D_2O. The peaks at 6 . 908-7 . 267 ppm and 4 . 668 ppm attributed to $H_{phenoxy}$ and $H_{anomeric}$, respectively. The degree of substitution of phenoxy groups on dextran units were determined as follows,

$$\tau = \frac{(2+3.0094)/5}{4.7825} \times 100$$

$$\tau = 20.95\%$$

Therefore, the percentage of above modified dextran was approximately 21%.

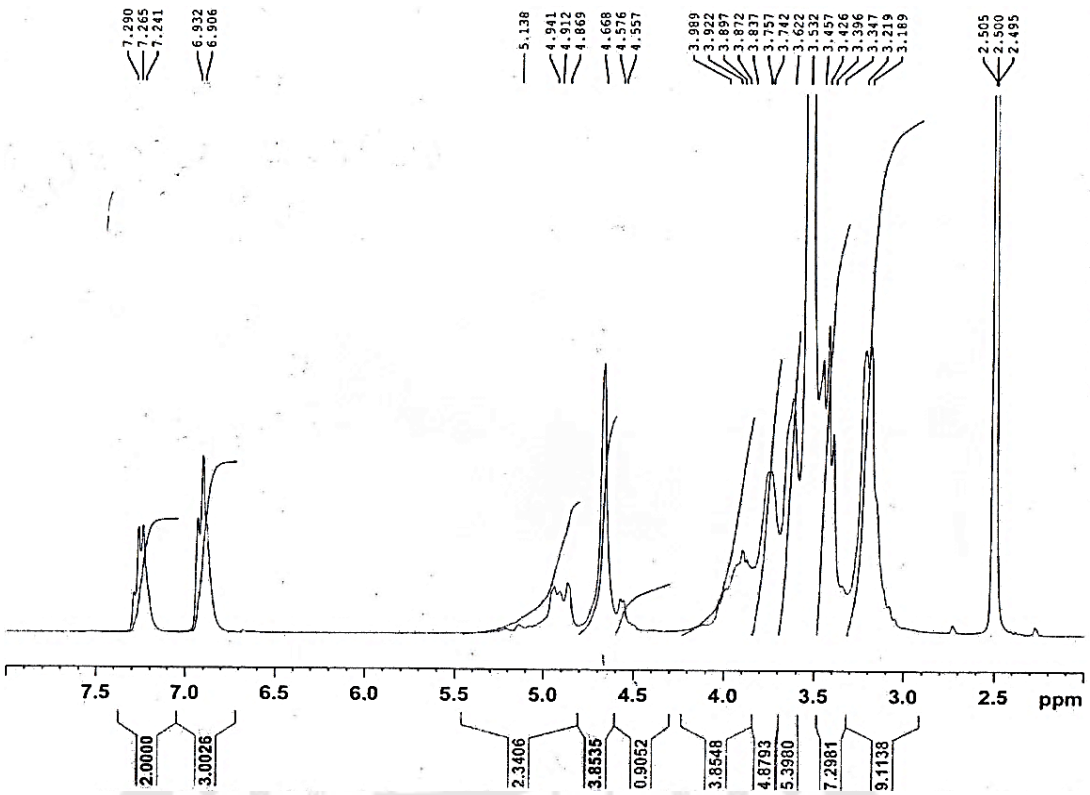

Figure 25 ^{1}H NMR spectrum of $DexP_{26}$ in DMSO D_6 and D_2O

Figure 25 showed ^{1}H NMR spectrum of $DexP_{26}$ in DMSO D_6 and D_2O. The peaks at 6 . 906-7 . 265 ppm and 4 . 668 ppm attributed to $H_{phenoxy}$ and $H_{anomeric}$, respectively. The degree of substitution of phenoxy groups on dextran units were determined as follows,

$$\tau = \frac{(2+3.0026)/5}{3.8535} \times 100$$

$$\tau = 25.96\%$$

The percentage of above modified dextran was approximately 21%.

Accordingly, molar ratios of the attached phenoxy rings to sugar repeat unit of the recovered polymer were 0.155, 0.21 and 0.26 and thus three obtained

dextran derivatives were $DexP_{15.5}$, $DexP_{21}$, and $DexP_{26.}$ These polymers were further utilized for the development of nanoparticles.

4.4 Preparation and characterizations of DexPτ-grafted PLA NPs

4.4.1 Size measurements

In the synthesis of $DexP_{15.5}$-, $DexP_{21}$- and $DexP_{26}$-grafted PLA NPs by using different sonication powers, P5, P6, P7, P8, the particles before and after wash were subjected to size measurements by granulometry technique. The results from size distribution both before and after wash were shown in Appendix D (Figure 70 to Figure 72). It was found that PLA NPs grafted with $DexP_{15.5}$ and $DexP_{21}$ after wash tended to increase in aggregation after the increasing of sonication power (Figure 70 and Figure 71), while $DexP_{26}$-grafted PLA NPs showed no aggregation both before and after wash (Figure 72).

Average diameter of synthesized PLA NPs was summarized in Table 9 and depicted in Figure 26 to Figure 29. By using three modified dextran derivatives as stabilizers grafted on PLA NPs, the increase in average size after wash was more clearly seen in $DexP_{21}$-grafted NPs than in $DexP_{15.5}$- and $DexP_{26}$-grafted NPs (Figure 27 to Figure 29). Obviously, PLA NPs grafted with $DexP_{26}$, synthesized by using P5, P6, P7, P8, showed the average particle sizes of lower than 130 nm (Table 9 and Figure 29). These implied that $DexP_{26}$ served as a good stabilizer for the synthesis of PLA NPs. In addition, the aggregation of PLA NPs after freeze-dry was seen in $DexP_{15.5}$ and $DexP_{21}$ grafting, while $DexP_{26}$-grafted NPs showed few aggregations.

Table 8 Average diameter of with $DexP_{15.5}$-, $DexP_{21}$-, and $DexP_{26}$-grafted PLA NPs

Condition		Average particle diameter, D[3,2] (nm)	
$DexP_{\tau}$	Sonication	Before centrifugation	After centrifugation
$DexP_{15.5}$	P5	125	129
	P6	131	160
	P7	130	137
	P8	144	144
$DexP_{21}$	P5	108	132
	P6	118	170
	P7	117	155
	P8	128	152
$DexP_{26}$	P5	105	126
	P6	107	122
	P7	116	106
	P8	116	118

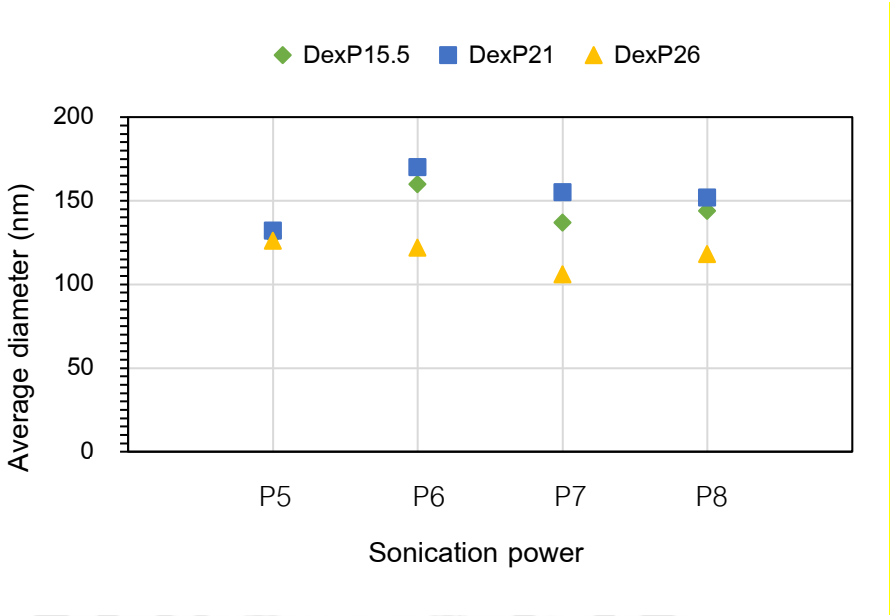

Figure 26 The comparison of average diameter of $DexP_{15.5}$-, $DexP_{21}$- and $DexP_{26}$-grafted PLA NPs after wash

The NPs were synthesized by emulsion-solvent evaporation process and the pulse mode from P5 to P8 were used.

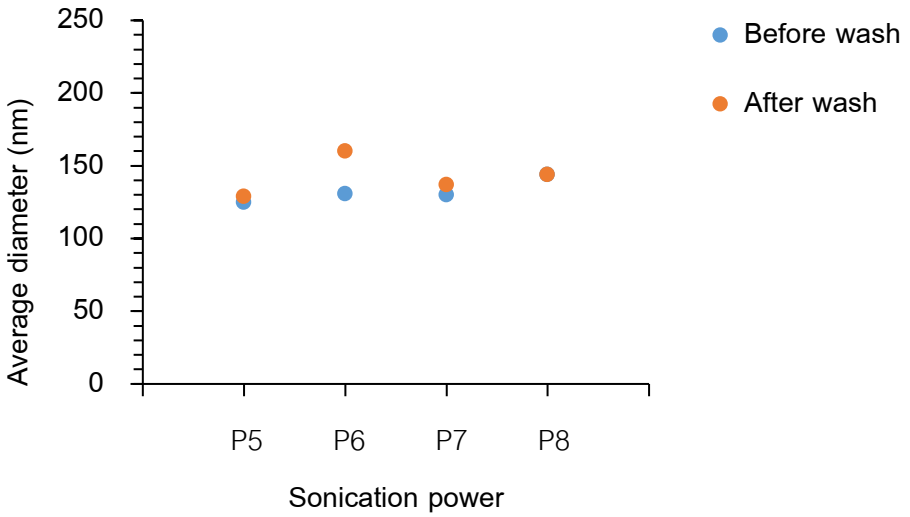

Figure 27 Average diameter of $DexP_{15.5}$-grafted PLA NPs before and after wash

The NPs were synthesized using the pulse mode from P5 to P8.

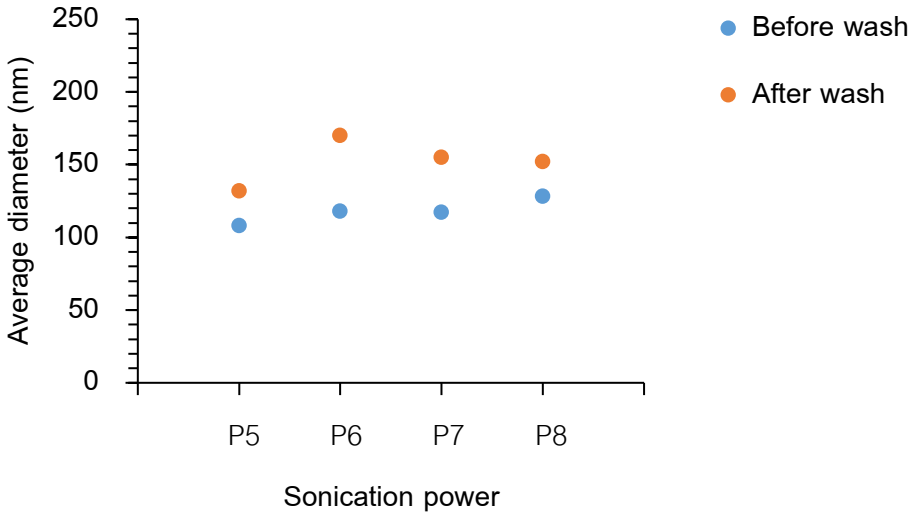

Figure 28 Average diameter of $DexP_{21}$-grafted PLA NPs before and after wash

The NPs were synthesized using the pulse mode from P5 to P8.

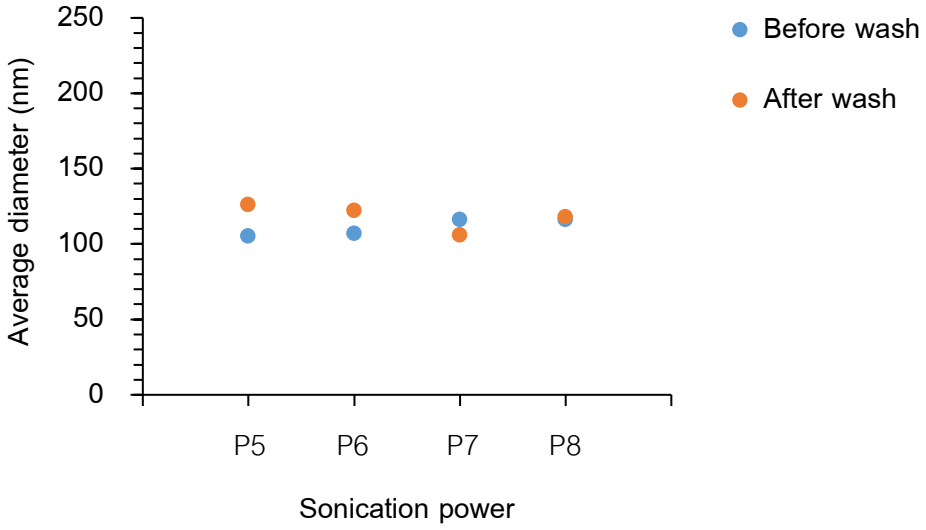

Figure 29 Average diameter of $DexP_{26}$-grafted PLA NPs before and after wash

The NPs were synthesized using the pulse mode from P5 to P8.

4.4.2 ^{1}H NMR analyses

Figure 89 to figure 91 (Appenxix D) showed ^{1}H NMR spectrum of $DexP_{15.5}$-, $DexP_{21}$-, and $DexP_{26}$-grafted PLA NPs synthesized by sonication with pulse mode from P5 to P8.

The obtained data from size distributions, i.e. average particle sizes from D[3,2] and specific surface areas (A_p) of $DexP_{\tau}$ /g PLA ($m^2.g^{-1}$) after wash, as well as from ^{1}H NMR spectra were summarized in Table 10. The peaks at 4.67 and 6.9-7.3 ppm were the areas of $H_{anomeric}$ (dextran anomeric protons) and $5H_{phenoxy}$ (phenoxy protons) respectively, corresponding to dextran-phenoxy, while at 5.1-5.2 ppm were the areas of H_{PLA} (PLA methine proton). The areas under these peaks were used to calculate mg $DexP_{\tau}$/g PLA and mg $DexP_{\tau}$/m^2 PLA of NPs grafted with $DexP_{15.5}$, $DexP_{21}$, and $DexP_{26}$, as equation (2).

$$DexP_{\tau}/PLA = A_{Hanomeric} \times MW_{DexP\tau} / A_{CHPLA} \times MW_{PLA} \quad (2)$$

The results from calculation were summarized in Table 10. The difference of calculated surface coverage among these synthesized PLA NPs was low. Nevertheless, $DexP_{26}$-grafted PLA NPs synthesized by using sonication P5 showed the surface coverage at 7.1 mg /m^2 PLA which might be caused by technical error during purification step from centrifugation.

Table 9 Summary and calculated results obtained from size distributions and ^{1}H NMR spectra of DexP_{τ}-grafted PLA NPs

NPs preparation		Granulometry after wash		Area from ^{1}H NMR			mg DexP_{τ}/	
Stabilizer	Mode	D[3,2] (nm)	A_p ($m^2.g^{-1}$)	$5H_{phenoxy}$	$H_{anomeric}$	H_{PLA}	g PLA	m^2 PLA
$DexP_{15.5}$	P5	129	37.5	0.0442	0.0436	1.0000	112.18	3.0
	P6	160	30.2	0.0370	0.0373	1.0000	95.97	3.2
	P7	137	35.3	0.0369	0.0383	1.0000	98.54	2.8
	P8	144	33.6	0.0372	0.0363	1.0000	93.40	2.8
$DexP_{21}$	P5	132	36.7	0.0634	0.0500	1.0000	133.33	3.6
	P6	170	28.5	0.0634	0.0474	1.0000	126.40	4.4
	P7	155	31.2	0.0571	0.0442	1.0000	117.87	3.8
	P8	152	31.8	0.0559	0.0393	1.0000	104.80	3.3
$DexP_{26}$	P5	126	38.4	0.1652	0.0978	1.0000	273.03	7.1
	P6	122	39.7	0.0883	0.0520	1.0000	145.17	3.7
	P7	106	45.6	0.0824	0.0467	1.0000	130.37	2.9
	P8	118	41.0	0.0835	0.0473	1.0000	132.05	3.2

4.4.3 Colloidal stability in presence of NaCl

The colloidal stability of PLA NPs—newly prepared with P5 and grafted with $DexP_{15.5}$, $DexP_{21}$, and $DexP_{26}$—in the presence of NaCl was studied by absorbance (OD) measurements of particle suspensions. The recorded OD of each NaCl concentration were used to create a linear graph of log OD vs. log λ. Then n values from the slope of linear equation log (OD) = n(log λ) + c were taken to plot a graph of $|n|$ vs. NaCl concentrations. This graph indicated the fluctuation of particle size, determining the particle variation and aggregation.

Figure 30 to figure 32 showed the graphs of $|n|$ vs. concentration of NaCl (M) of $DexP_{1\ 5.5}$-, $DexP_{21}$-, and $DexP_{26}$-grafted PLA NPs, synthesized in 3.8.1. These results indicated that the $DexP_{\tau}$-grafted PLA NPs was stable in the salt condition to 1 M. However, aggregation of NPs might form in the higher concentrations of NaCl. Nevertheless, normal concentration of sodium (Na^{+}) in blood is approximately 0.136-0.145 mM (136-145 mmol/l), while in the culture media is approximately 137-164 mM [204]. Accordingly, the PLA NPs with $DexP_{15.5}$ or $DexP_{21}$ or $DexP_{26}$ grafting could be stable in conditions of normal blood and cell culture media.

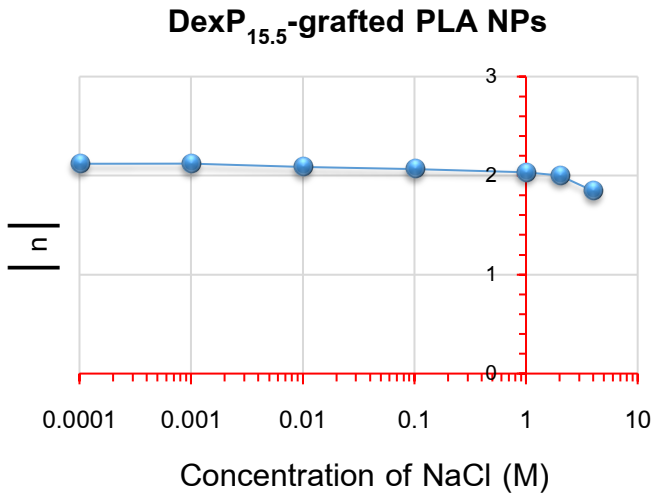

Figure 30 The determination of colloidal stability of $DexP_{15.5}$-grafted PLA NPs in NaCl

The graph is represented by mean of $|n|$ versus concentration of NaCl (M). The NPs were newly prepared with pulse mode P5.

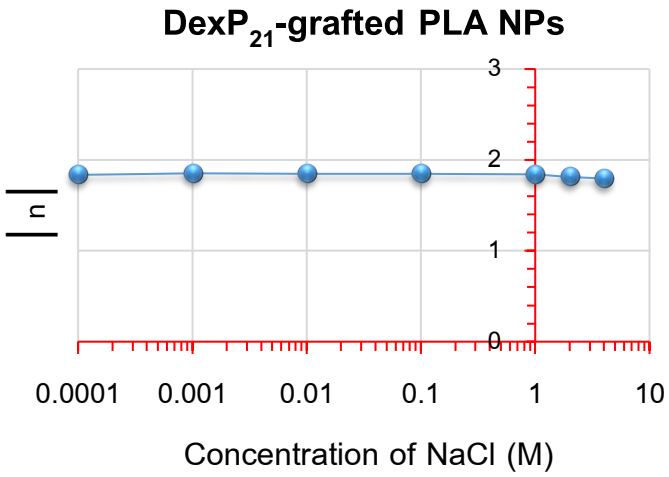

Figure 31 The determination of colloidal stability of $DexP_{21}$-grafted PLA NPs in NaCl The graph is represented by mean of $|n|$ versus concentration of NaCl (M). The NPs were newly prepared with pulse mode P5.

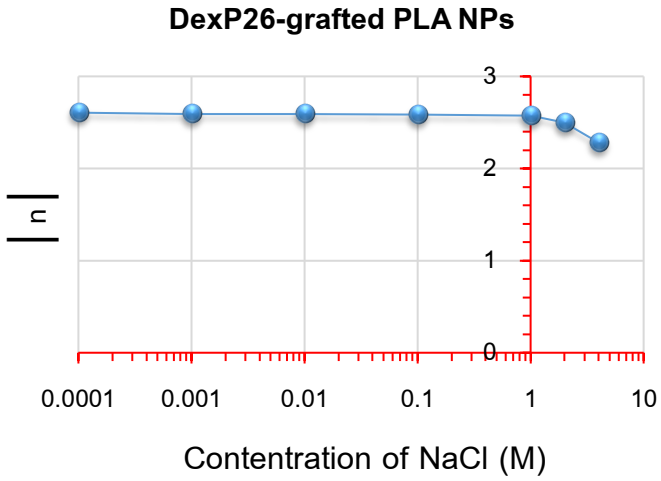

Figure 32 The determination of colloidal stability of $DexP_{26}$-grafted PLA NPs in NaCl The graph is represented by mean of $|n|$ versus concentration of NaCl (M). The NPs were newly prepared with pulse mode P5.

Overall characterizations indicated that PLA NPs, synthesized with P5 and grafted with $DexP_{26}$ showed the stability in the measurements of suspensions both in size and turbidity in salt (NaCl) condition. Thus using $DexP_{26}$ for grafting on NPs could serve an appropriate stabilizer for further development of drug-encapsulated NPs.

4.5 Preparation and characterizations of drug-loaded $DexP_{26}$-grafted NPs

4.5.1 Chemical properties of MM and FITC

In order to confirm that MM and FITC could be encapsulated by using the process of nanoparticle synthesis, thus MM and FITC were examined for its structure and chemical properties using ^1H NMR analysis.

4.5.1.1 Stability of MM and FITC after ultrasonication

In the study of MM and FITC stability using sonication P5 , ^1H NMR spectrum showed the results of chemical components of MM and FITC (Figure 33 to figure 36).

I. Stability of MM after ultrasonication

Figure 33 to figure 34 showed ^1H NMR spectra of MM before and after sonication P5. NMR spectrum of MM after sonication (Figure 34) showed the appearance of structural components of MM at 0.85 (CH_3), 1.235 (CH_2), 1.509 (2H), 2.75 (2H), and 3.582 to 4.056 (5H) ppm, which were not different from prior sonication—peaks at 0.84 (CH_3), 1.224 (CH_2), 1.499 (2H), 2.269 (2H), and 3.27-4.9 (5H) ppm (Figure 33). It appeared that MM was stable when using sonication at P5. Notice that peaks at 2.5 and 3.4 corresponded to DMSO and D_2O, respectively. The peak of 2H of MM at about 3.3 ppm might be combined into a peak of D_2O after sonication. Therefore, the results indicated that MM can be used in the synthesize process of MM-loaded nanoparticles

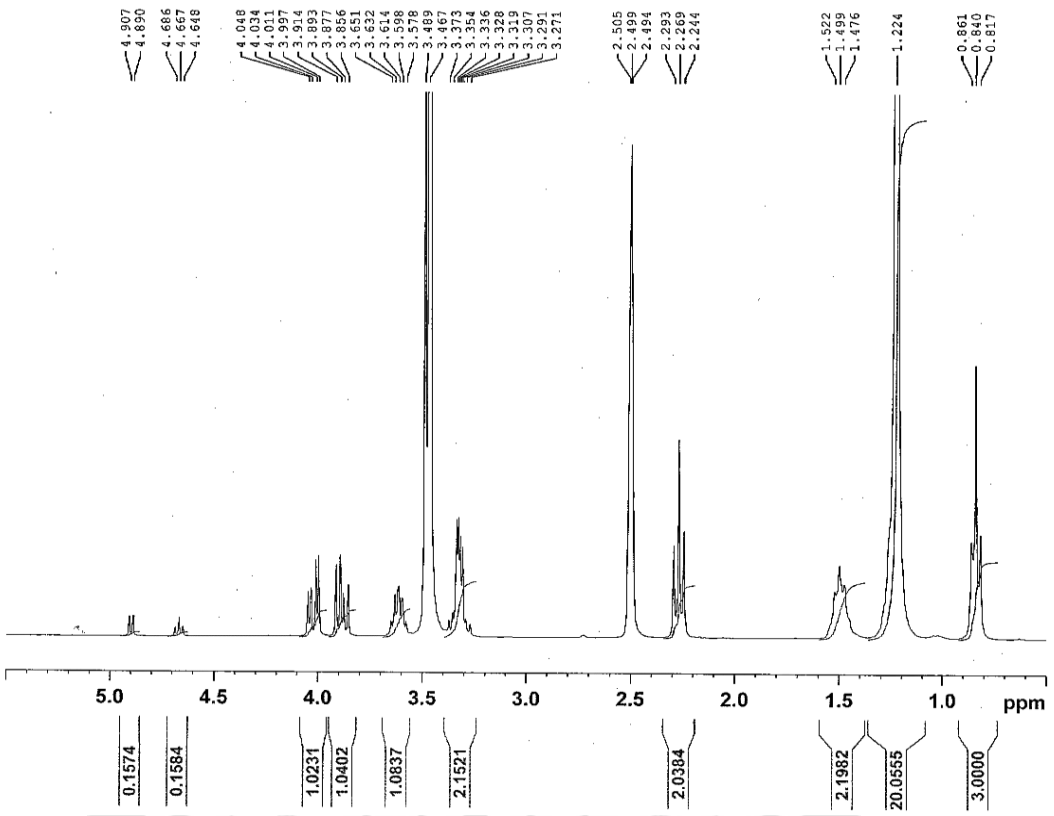

Figure 33 ^{1}H NMR spectrum of MM before sonication (P5)

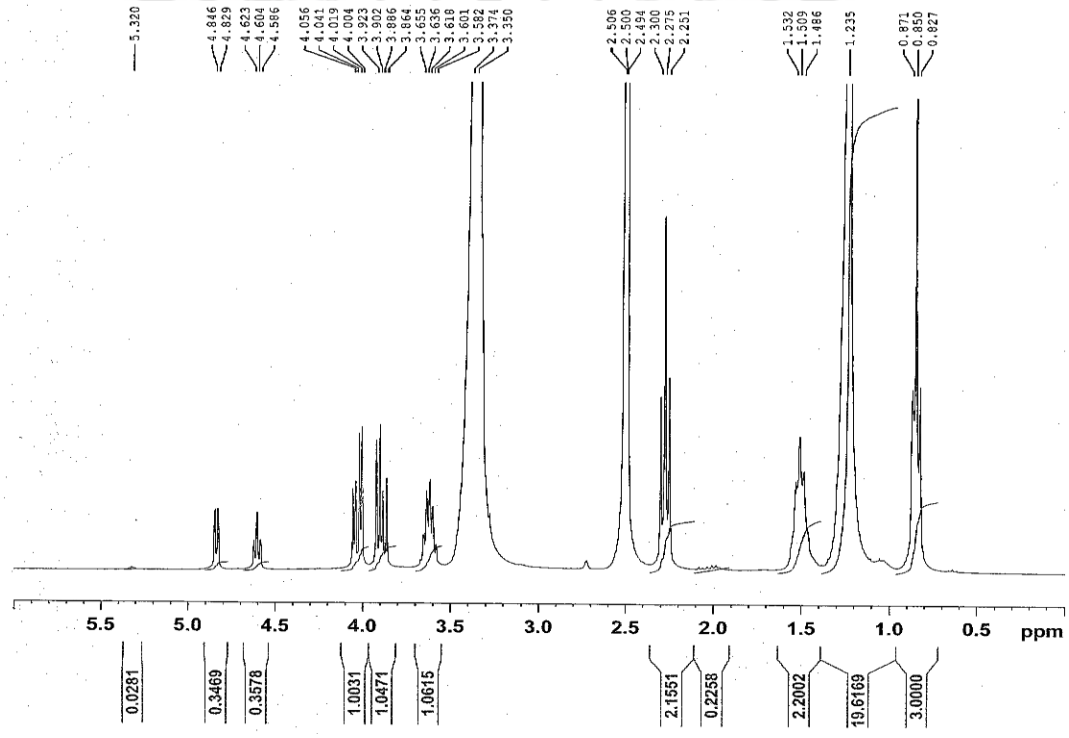

Figure 34 ^{1}H NMR spectrum of MM after sonication (P5)

II. Stability of FITC after ultrasonication

Figure 35 to figure 36 showed ^{1}H NMR spectra of FITC before and after sonication at P5. After sonication process at P5, the peaks corresponding to structural components of FITC approximately at 6.56-6.859, 7.2, 7.8, 8.2, and 10 ppm were found (DMSO at 2.5 ppm; D_2O at 3.4 ppm) (Figure 36). These appeared peaks were not significantly different from the peaks before sonication (Figure 35), indicated that FITC can be used in the synthesize process of FITC-loaded nanoparticles.

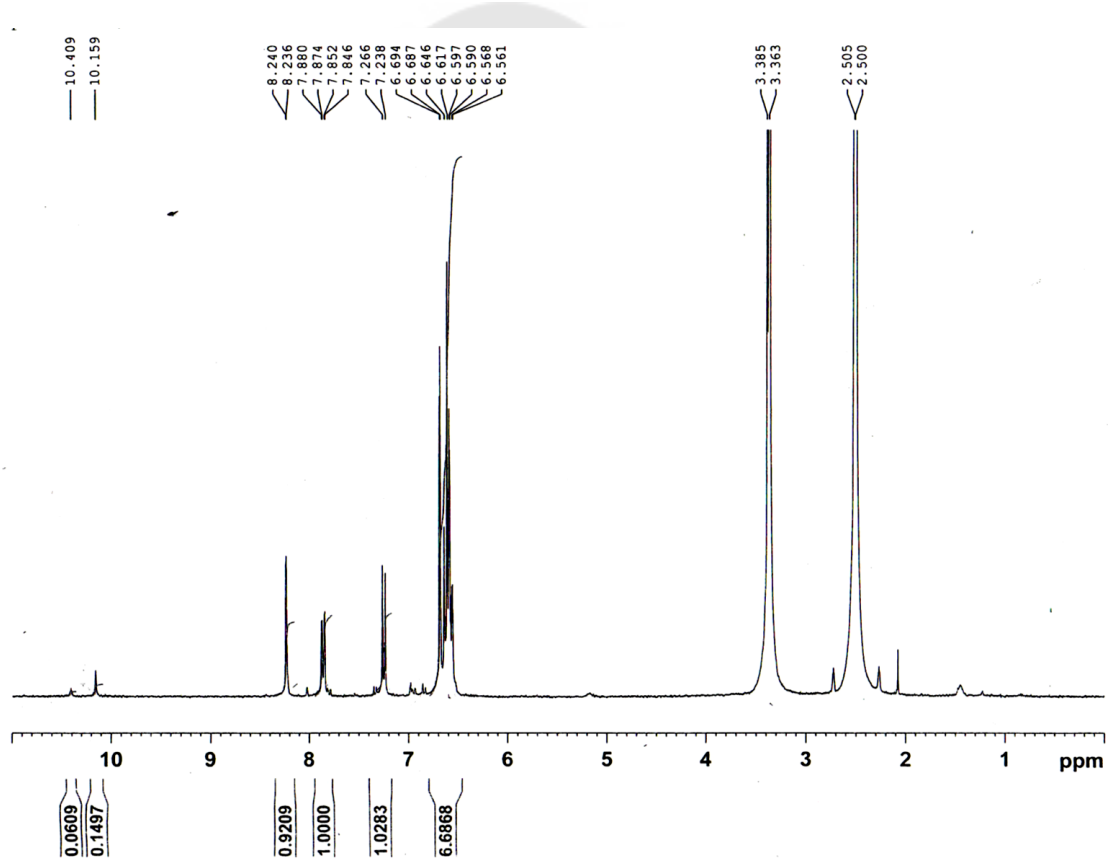

Figure 35 ^{1}H NMR spectrum of FITC before sonication (P5)

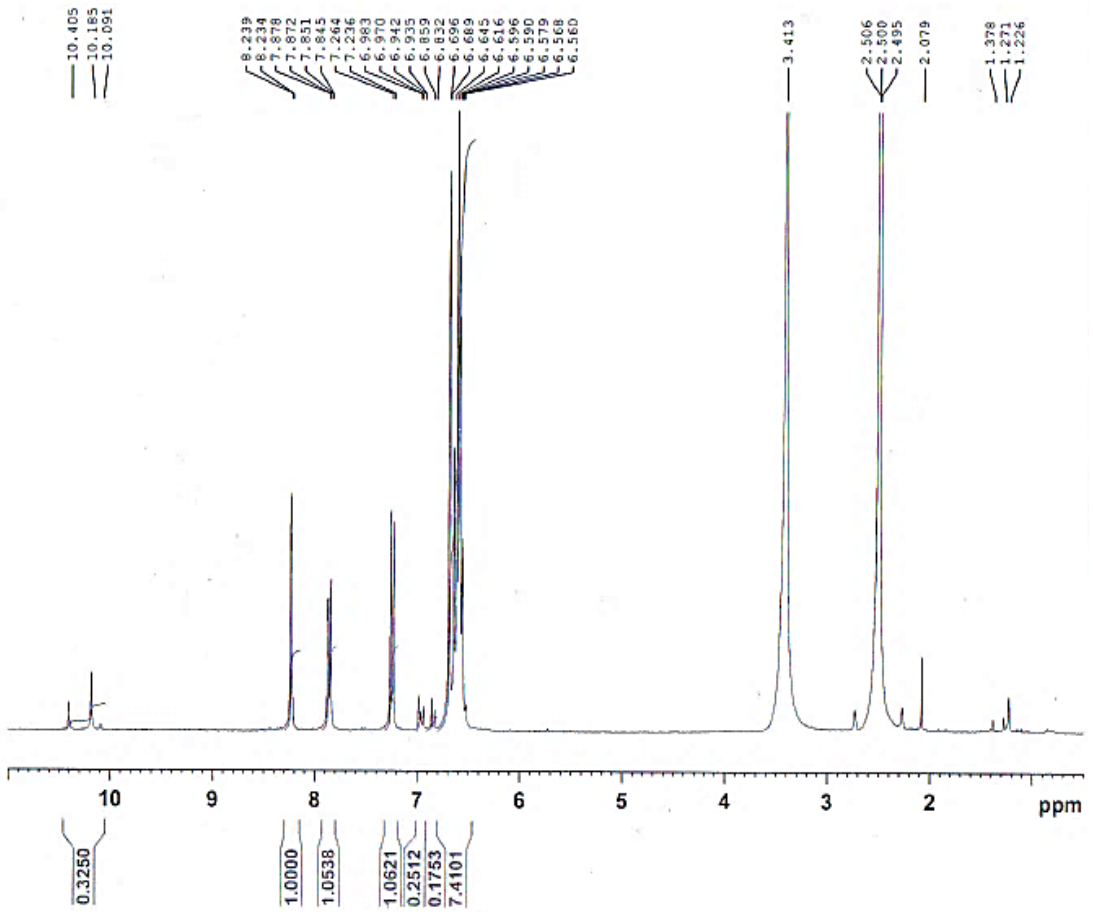

Figure 36 ^{1}H NMR spectrum of FITC after sonication (P5)

4.5.1.2 Solubility of MM and FITC in D_2O

I. Solubility of MM in D_2O

In development of NPs, the nature solubility of MM and FITC in D_2O was checked with the compositions of the transparent part of solution after sediment separation by using ^{1}H NMR analysis. The obtained result from MM study was shown in Figure 37. The peak at 4.789 ppm was of D_2O and peaks at 6.9 to 7.3 ppm were of phenol, a reference. By comparing to ^{1}H NMR spectrum of MM (Figure 67, Appendix C), There were small peaks at 1.24 and 3.3-3.8 ppm that might corresponded to MM and any impurities. This probably showed that very small amount of MM might dissolve in water (D_2O).

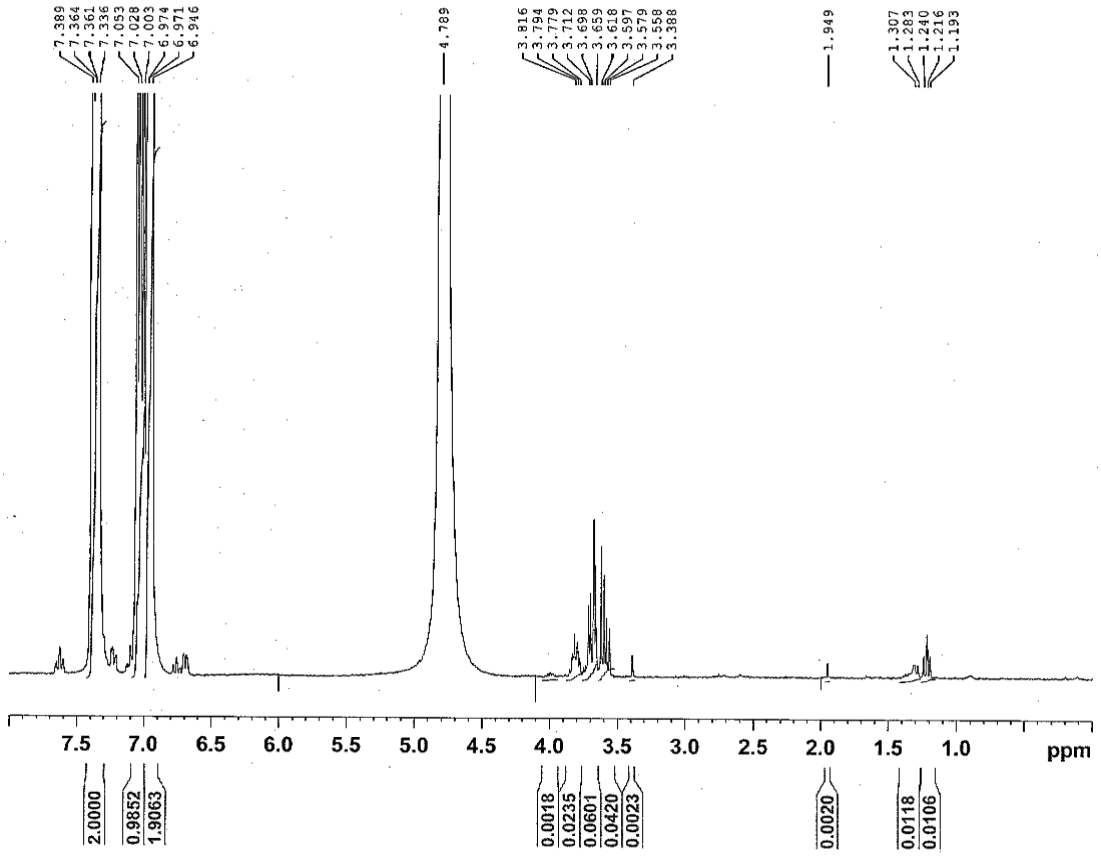

Figure 37 ^{1}H NMR spectrum of MM in D_2O, using phenol as a reference

II. Solubility of FITC in D_2O

In study of FITC solubility, the obtained result was shown in Figure 38. ^{1}H NMR spectrum did not show the peak of FITC as compared to NMR spectrum of FITC (Figure 69, Appendix C). Only the peaks of D_2O at 4.79 ppm and butanol-2 at 0.9, 1.2, 1.5, 3.7 ppm were found, indicating that FITC was not dissolve in D_2O.

Accordingly, it was inferred that MM was rarely soluble while FITC was insoluble in water even if water is used in the emulsion-solvent evaporation process of nanoparticle synthesis.

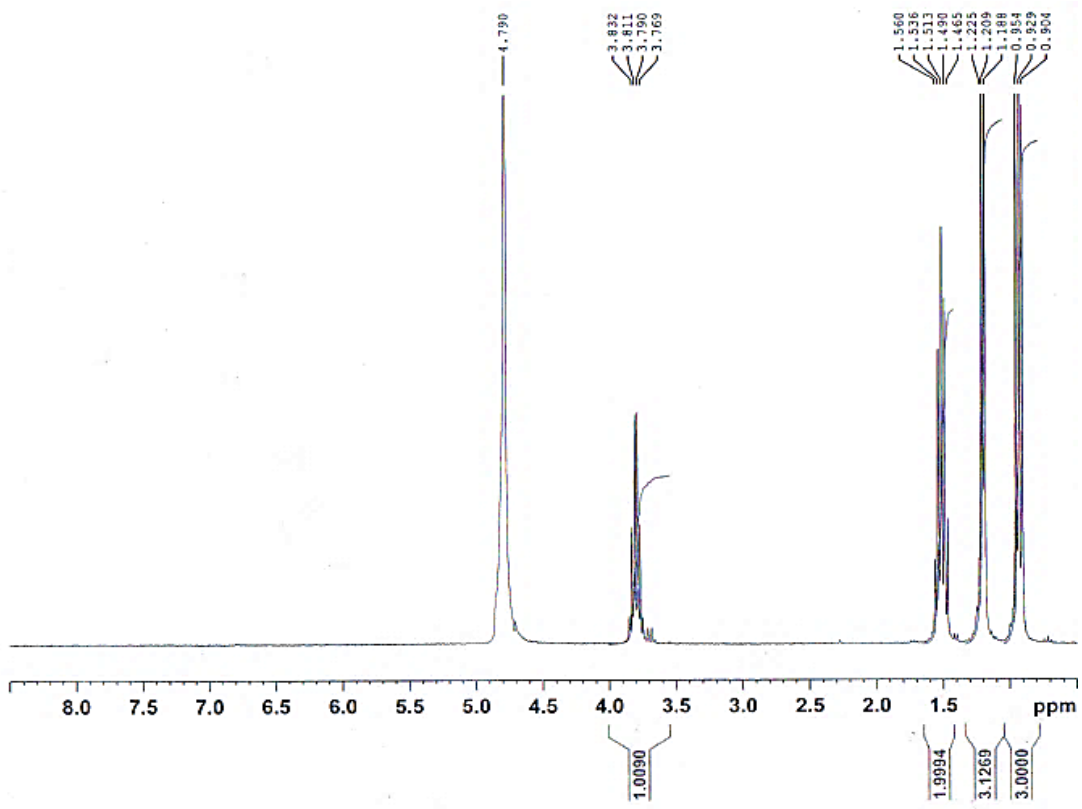

Figure 38 ^{1}H NMR spectrum of FITC in D_2O, using butanol-2 as a reference

4.5.1.3 Miscibility of MM and FITC with PLA

I. Miscibility of MM and PLA

The ratios (5: 5, 7: 3, 8: 2, 9: 1, 9.5: 5) of PLA/MM mixture were studied for miscibility using DSC technique. Figure 39 and Figure 40 showed DSC thermogram of 100 wt% PLA and 100 wt% MM, respectively. The experimental glass transition temperature of PLA was 51.9 ^{o}C, while melting transition temperature [150] of MM were 27.3 ^{o}C and 53.6 ^{o}C. Figure 41 to Figure 45 showed DSC traces obtained during continuous heating of PLA/MM mixture at various ratios. It was found that when amount of MM was gradually reduced, PLA and MM were more miscible. The results clearly showed that very good miscibility of PLA and MM was at 9:1 (10 wt% MM/PLA mixed) and 9.5:0.5 (5 wt% MM/PLA mixed) ratios, of which the transition temperatures of the two compounds were blended and reduced to 30.7 ^{o}C and 41.2 ^{o}C, respectively (Figure 44 and Figure 45), as compared to T_g of pure PLA (51.9 ^{o}C) and T_m of pure MM (53.6 ^{o}C).

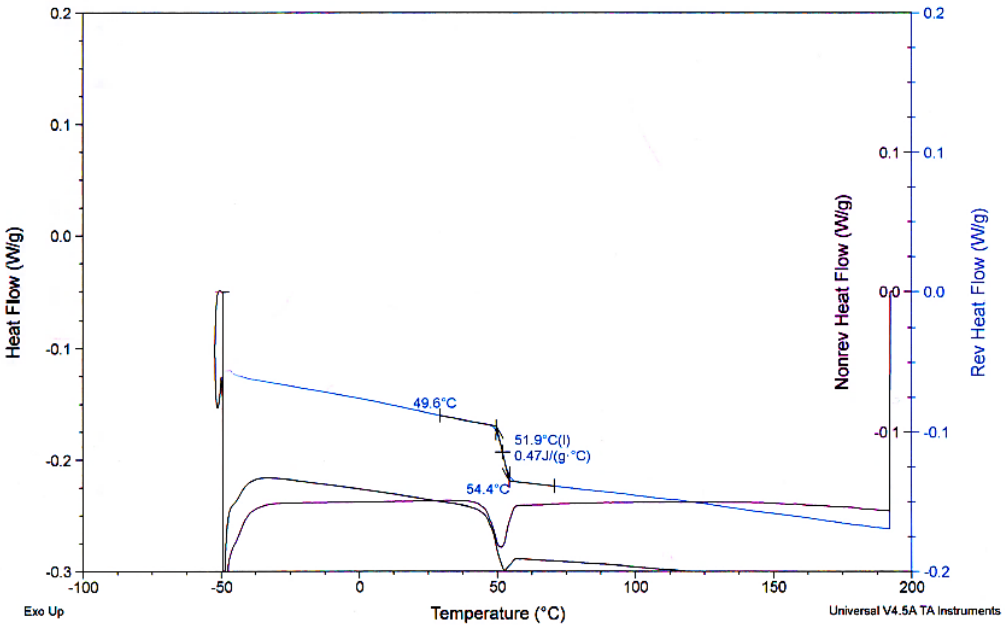

Figure 39 The DSC thermogram of 100 wt% PLA

A glass transition temperature of PLA was 51.9 °C.

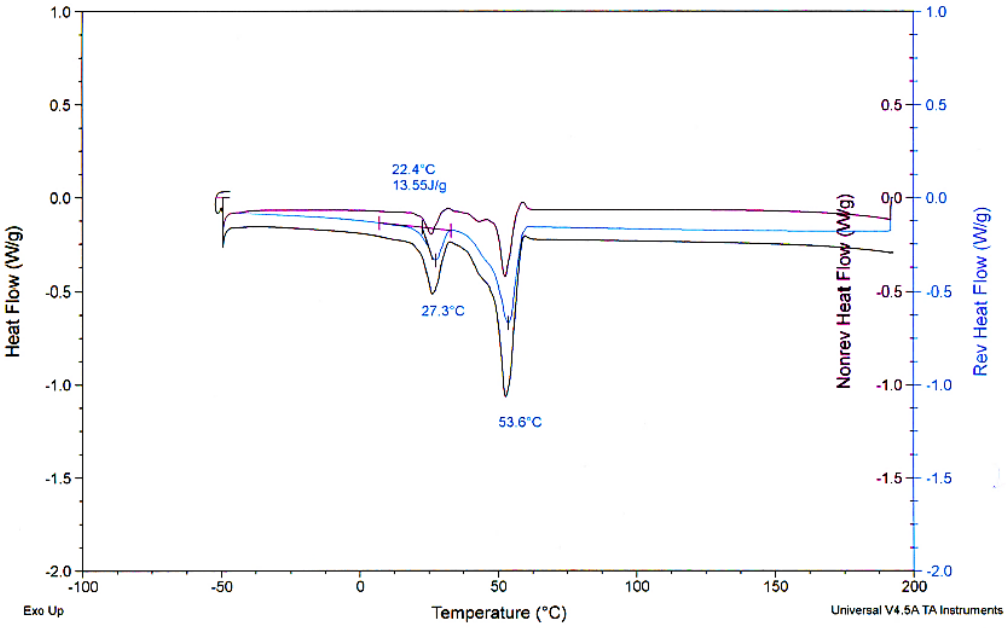

Figure 40 The DSC thermogram of 100 wt% MM

The melting transition temperatures [150] of MM were **27.3 °C and 53.6 °C.**

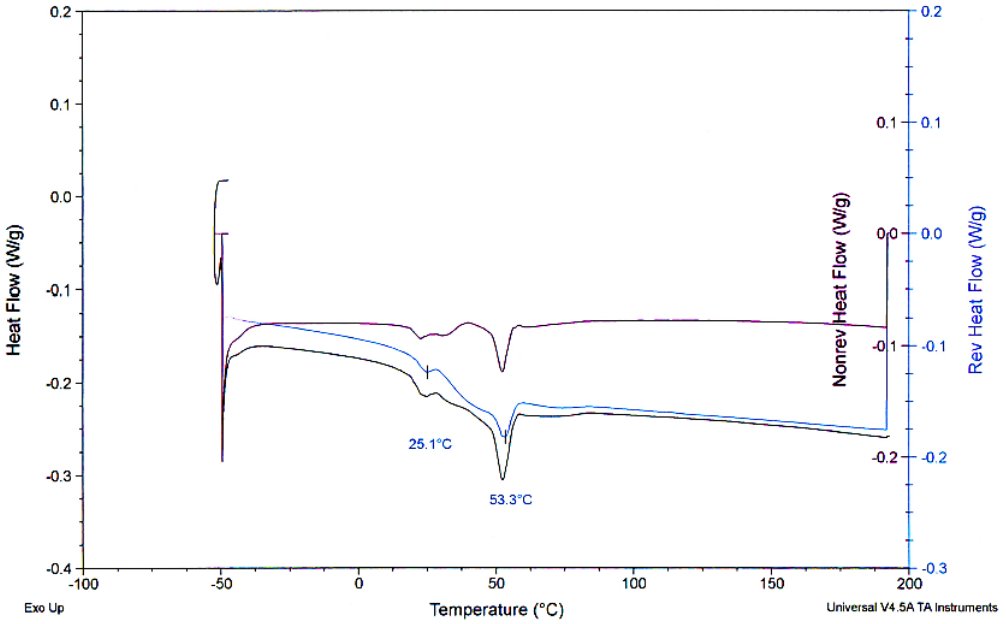

Figure 41 The DSC thermogram of 50 wt% MM/PLA blend (PLA/MM ratio 5:5)

The transition temperatures of the mixture were 25.1 °C and 53.3 °C.

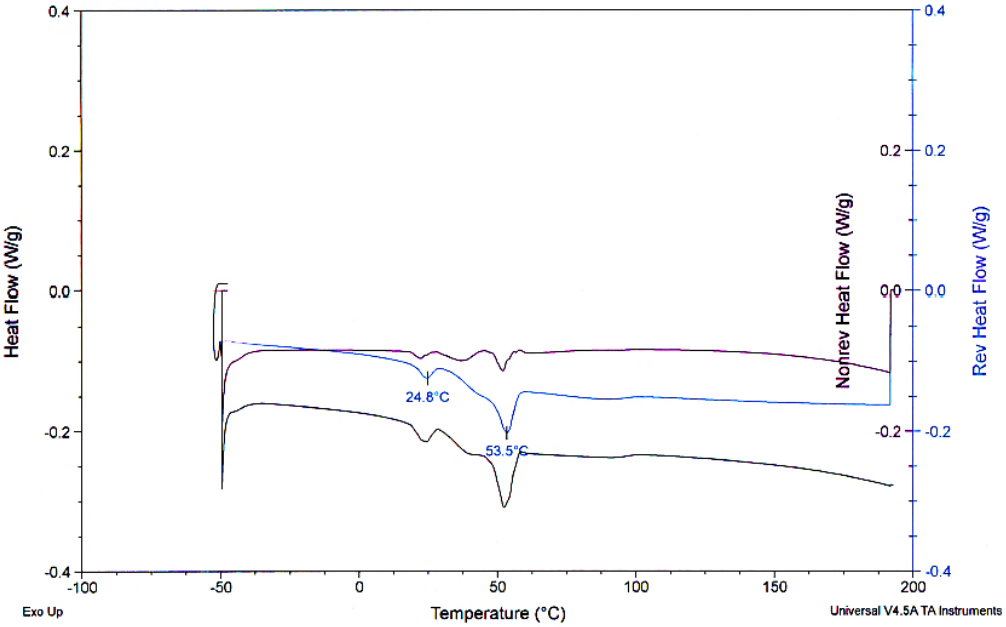

Figure 42 The DSC thermogram of 30 wt% MM/PLA blend (PLA/MM ratio 7:3)

The transition temperatures of the mixture were 24.8 °C and 53.5 °C.

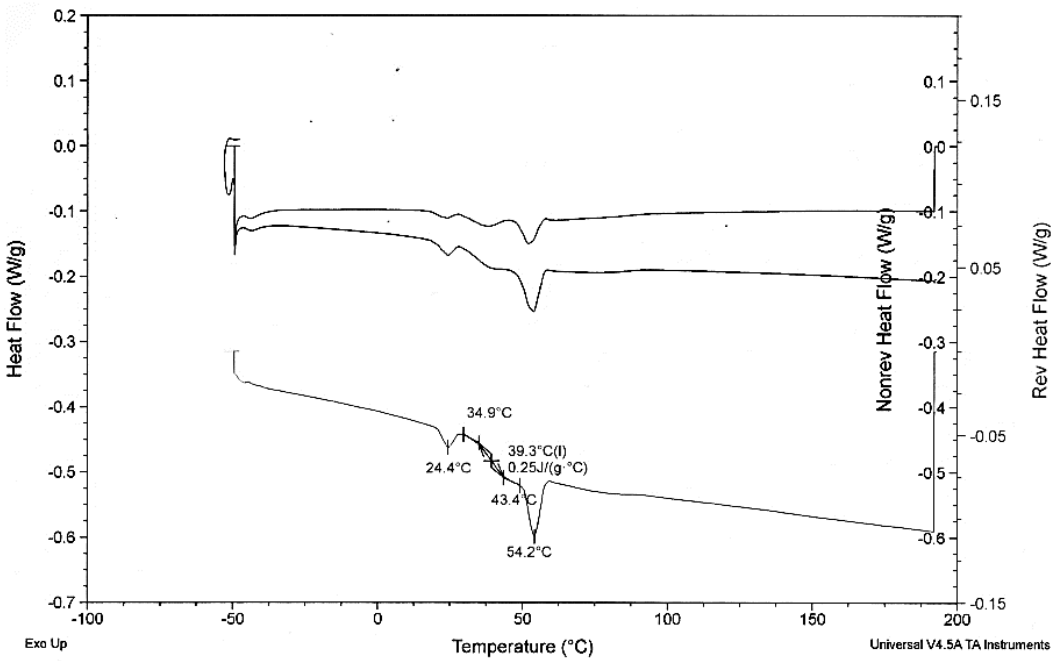

Figure 43 The DSC thermogram of 20 wt% MM/PLA blend (PLA/MM ratio 8:2)

The transition temperatures of the mixture were 24.4 °C, 39.3 °C, and 54.2 °C.

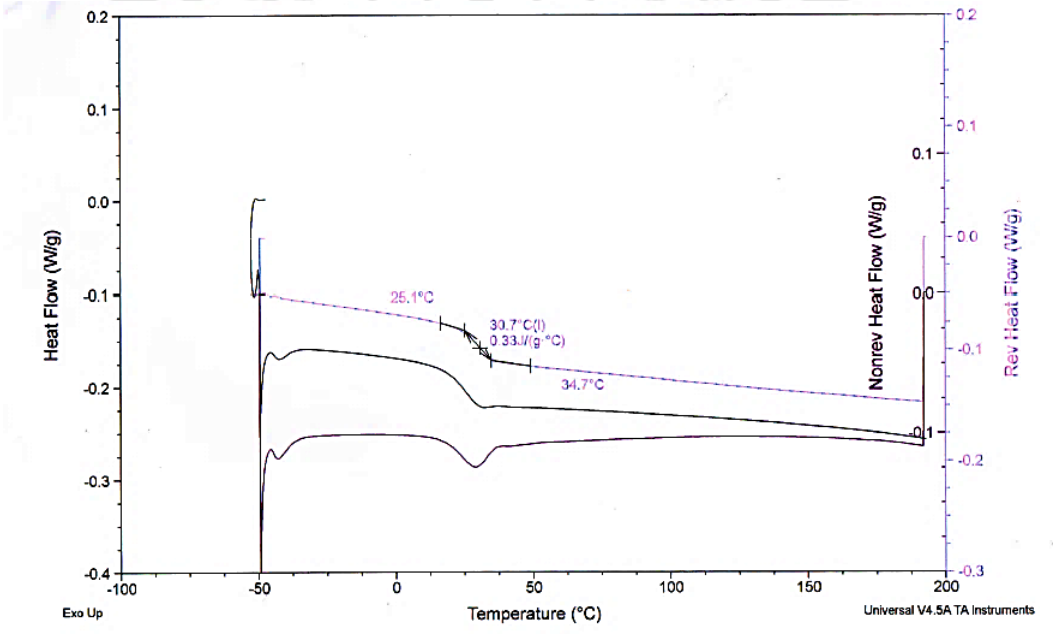

Figure 44 The DSC thermogram of 10 wt% MM/PLA blend (PLA/MM ratio 9:1)

The transition temperature of the mixture was 30.7 °C.

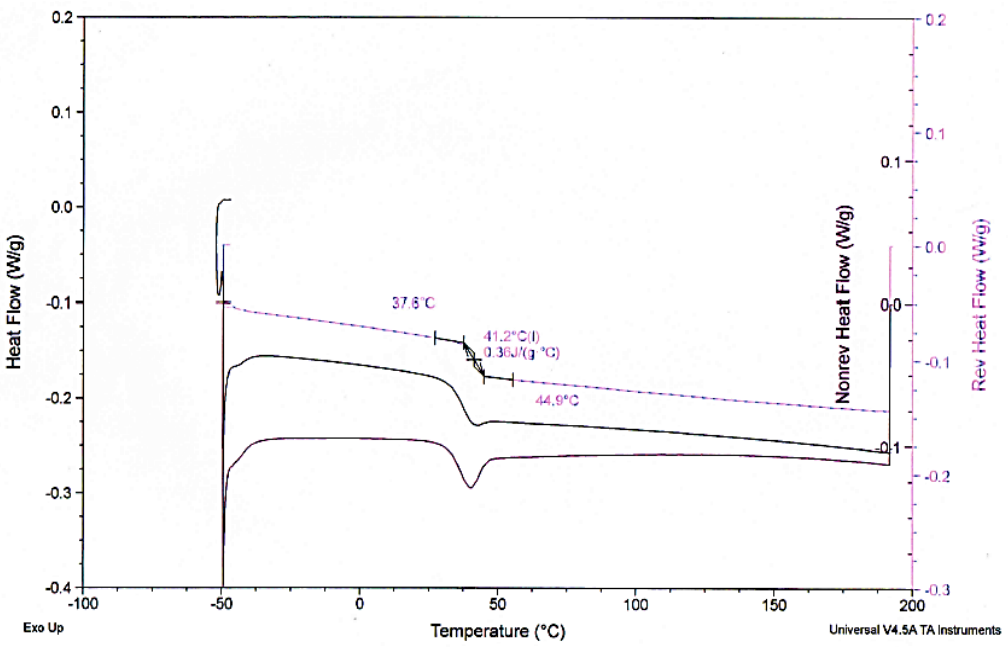

Figure 45 The DSC thermogram of 5 wt% MM/PLA blend (PLA/MM ratio 9.5:0.5)

The transition temperature of the mixture was 41.2 °C.

II. Miscibility of FITC and PLA

Miscibility of PLA and FITC was studied at a ratio of 9:1. It was found that the two compounds were highly miscible since the blended transition temperature of the mixture was presented at 55.9 °C (Figure 46).

Though the complete mixture of PLA and MM was prepared from at 9:1 and 9.5:0.5 ratios, a ratio of 9:1 is preferable for the encapsulation synthesis of MM-loaded nanoparticles, in order to encapsulate the maximum amount of MM. Accordingly, a ratio of both PLA: MM and PLA: FITC at 9:1 will be used in the preparation of drug-loaded nanoparticles.

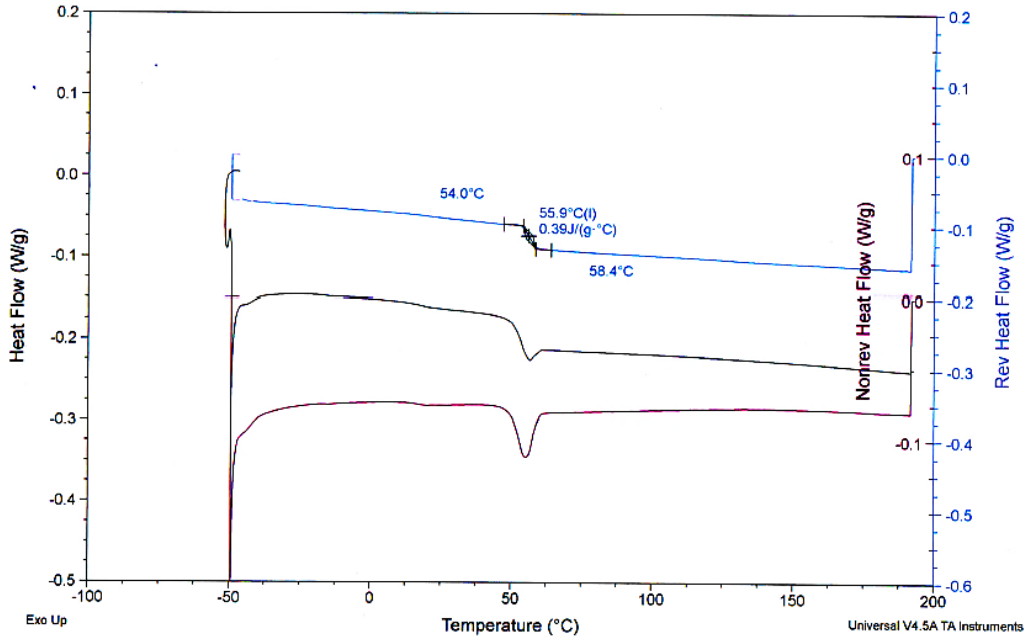

Figure 46 The DSC thermogram of 10 wt% MM/PLA blend (FITC/MM ratio 9:1)

The transition temperature of the mixture was found at 55.9 °C.

4.5.2 Characterizations of MM-NPs and FITC-NPs

4.5.2.1 Size measurement

A ratio of PLA/MM and PLA/FITC at 9:1 was used to prepare drug-loaded NPs via emulsion-solvent evaporation method with P5 sonication. The size measurements of the encapsulated NPs after wash confirmed the colloidal stability: MM-NPs showed low aggregations (Figure 47B), while FITC-NPs showed no aggregation (Figure 47C), compared to the result of PLA NPs which shows no aggregation (previously described in 4.4.1), with $DexP_{26}$ as a stabilizer and P5 sonication (Figure 47A). The average particle sizes were 126, 113, 198 nm of PLA NPs, MM-NPs, and FITC-NPs, respectively.

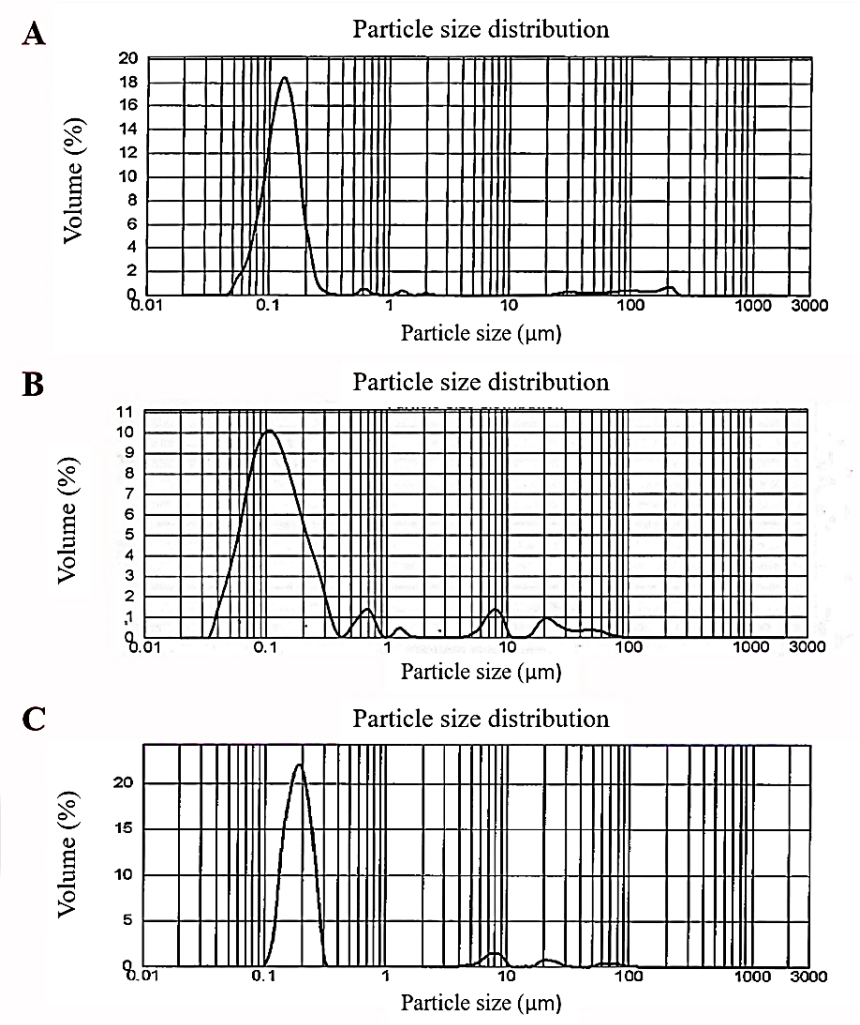

Figure 47 Size distribution of $DexP_{26}$-grafted PLA NPs (A), $DexP_{26}$-grafted MM-NPs (B), and $DexP_{26}$-grafted FITC-NPs (C) after wash

4.5.2.2 ^{1}H NMR analysis

I. NMR analysis of MM

Figure 48 showed ^{1}H-NMR spectrum of $DexP_{26}$-grafted MM-NPs in DMSO and D_2O. The peaks at: 6.91-7.27 and 4.673 ppm attributed to $5H_{phenoxy}$ and $H_{anomeric}$ respectively, corresponded to dextran-phenoxy; 1.448 (CH_3) and 5.165 (CH) ppm attributed to PLA protons (H^+); 0.823 (CH_3), 1.23 (20H), and 2.275 (2H) ppm attributed to MM protons (H^+). Therefore, the NMR spectrum clearly showed the presence of all NPs components—i.e. $DexP_{26}$, PLA, MM, of the developed $DexP_{26}$-grafted MM-NPs.

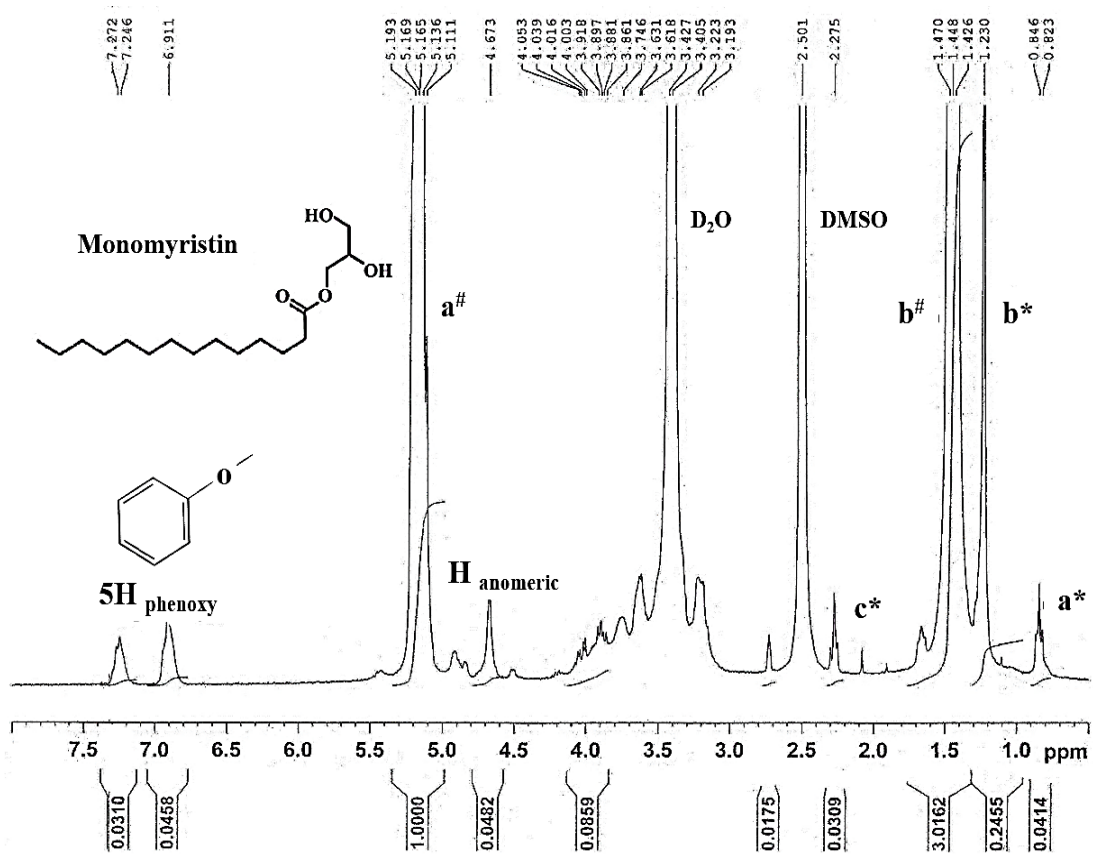

Figure 48 ^{1}H-NMR spectra of $DexP_{26}$-grafted MM-NPs, dissolved in DMSO and D_2O

A ratio of core materials, PLA/MM, at 9:1 was used. The peaks of MM ($C_{17}H_{34}O_4$): a*, b*, c*, and PLA: $a^{\#}$, $b^{\#}$, are displayed. The spectra of $5H_{phenoxy}$ and $H_{anomeric}$ correspond to $DexP_{26}$.

II. Calculation of loaded MM amount in MM-NPs

The areas under ^{1}H NMR peaks were used to calculate the molar ratios of $DexP_{26}$/PLA, MM/PLA and the amount of loaded MM, according to equations (3)-(5):

$$DexP_{26}/PLA = A_{Hanomeric} \times MW_{DexP26} / A_{CHPLA} \times MW_{PLA} \quad (3)$$

$$= [0.0482 \times 201] / [1 \times 72]$$

$$= 0.135 \text{ g}$$

$$MM/PLA = A_{MM} \times MW_{MM} / A_{CHPLA} \times MW_{PLA} \quad (4)$$

$$= [0.0414/3 \times 302.46] / [1 \times 72]$$

$$= 0.058 \text{ g}$$

$$MM/NP = [MM/PLA] / [1 + DexP_{26}/PLA + MM/PLA] \quad (5)$$

$$= [0.058 / [1 + 0.135 + 0.058]$$

$$= 0.049 \text{ g}$$

(MW_{DexP26} = 201 g/mol, MW_{PLA} = 72 g/mol, MW_{MM} = 302.46 g/mol)

From areas under peaks: $A_{Hanomeric}$ at 4.673 ppm was 0.0482; A_{CHPLA} at 5.165 ppm was 1.000; A_{MM} at 0.823 ppm was 0.0414. The calculated amount was 0.135 g$DexP_{26}$/gPLA and 0.058 gMM / gPLA. Therefore, amount of the encapsulated MM was 0.049 g per gram NPs.

III. NMR analysis of FITC

Figure 49 showed ^{1}H-NMR spectrum of $DexP_{26}$-grafted FITC-NPs in DMSO and D_2O. The peaks approximately at: 6.913-6.934 and 7.238-7.266 ppm attributed to $5H_{phenoxy}$; 4.674 attributed to $H_{anomeric}$; 1.451 (CH_3) and 5.164 (CH) ppm attributed to PLA protons (H^+); 6.561-6.695, 7.238-7.266, 7.8, 8.2, 10 ppm attributed to FITC protons (H^+). To note that a peak at 7.238-7.266 ppm is from the merging peaks of $2H_{phenoxy}$ and FITC. The solvents DMSO and D_2O were peaks at 2.5 and 3.372, respectively. Therefore, the NMR spectrum clearly showed the presence of all NPs components—i.e. $DexP_{26}$, PLA, FITC, of the developed $DexP_{26}$-grafted FITC-NPs.

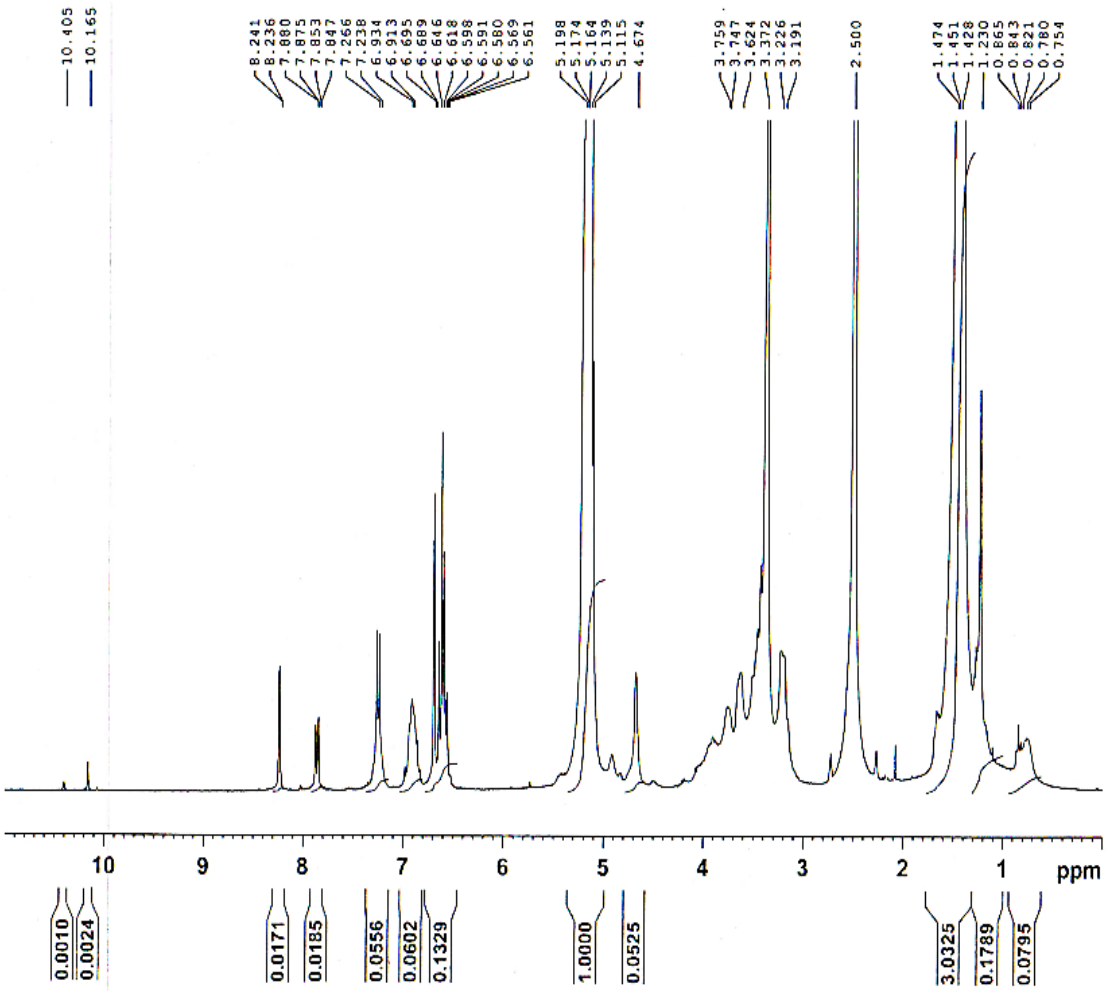

Figure 49 ^{1}H-NMR spectra of DexP_{26}-grafted FITC-NPs, dissolved in DMSO and D_2O

A ratio of core materials, PLA/FITC, at 9:1 was used. The peaks of FITC ($C_{21}H_{11}NO_5S$): 6.561-6.695, 7.238-7.266, 7.8, 8.2, 10 ppm; $5H_{phenoxy}$: 6.913-6.934 and 7.238-7.266 ppm; $H_{anomeric}$: 4.674 ppm; PLA: 1.451 and 5.164 ppm.

IV. Calculation of loaded FITC amount in FITC-NPs

The areas under ^{1}H NMR peaks were used to calculate the molar ratios of DexP_{26}/PLA, FITC/PLA and the amount of loaded FITC similar as loaded MM, according to equations (6)-(8).

$DexP_{26}/PLA = A_{Hanomeric} \times MWDexP26 / A_{CHPLA} \times MW_{PLA}$ (6)

$= 0.0525 \times 201 / 1 \times 72$

$= 0.147$ g

$FITC/PLA = A_{FITC} \times MW_{FITC} / A_{CHPLA} \times MW_{PLA}$ (7)

$= (0.1329/6) \times 389.4 / 1 \times 72$

$= 0.120$ g

$FITC/NP = [FITC/PLA] / [1 + DexP_{26}/PLA + FITC/PLA]$ (8)

$= [0.1198] / [1 + 0.1466 + 0.1198]$

$= 0.095$ g

($MW_{DexP26} = 201$ g/mol, $MW_{PLA} = 72$ g/mol, $MW_{FITC} = 389.4$ g/mol)

From areas under peaks: $A_{Hanomeric}$ at 4.674 ppm was 0.0525; A_{CHPLA} at 5.164 ppm was 1.000; A_{FITC} at 6.646 ppm (6H) was 0.1339. The calculated amount was 0.1466 g$DexP_{26}$/gPLA and 0.1198 gFITC/gPLA. Therefore, the amount of encapsulated FITC was 0.095 0.08 g per gram NPs.

4.5.3 MM and FITC release study

In the synthesis of $DexP_{26}$-grafted MM-NPs and $DexP_{26}$-grafted FITC-NPs, nanoparticle suspensions were subjected to drug release study in water. The areas from NMR peaks of remaining drugs within NPs were used to estimate the released amounts of MM and FITC at 5, 16, 24, 48, and 72 h. These amounts were used to create the releasing curves versus time of dialysis. Figure 50 showed the releasing curve of $DexP_{26}$-grafted drug-loaded NPs. The curves showed that low amount of MM and FITC were gradually released from NPs within 72 h of dialysis.

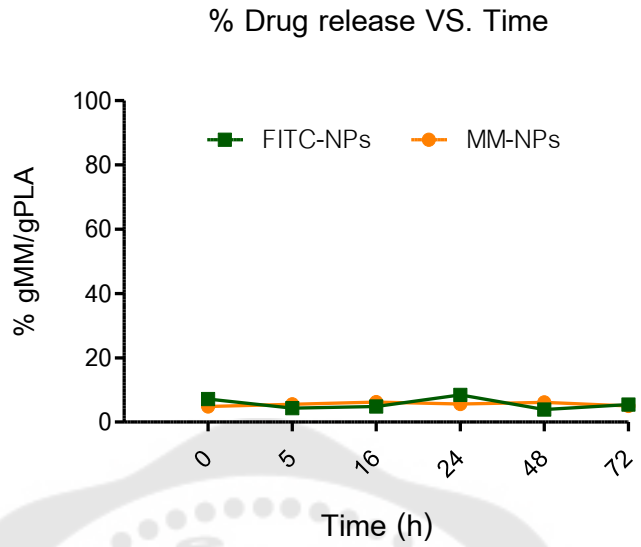

Figure 50 The releasing curve of $DexP_{26}$-grafted drug-loaded NPs.

4.6 Preparation and characterizations of Tf-conjugated drug-loaded NPs

4.6.1 Synthesis of carboxylated dextran-phenoxy$_{26}$ ($DexP_{26}$-COOH)

$DexP_{26}$ was modified by the addition of COOH to obtain carboxylated dextran-phenoxy$_{26}$ ($DexP_{26}$-COOH) that was titrated with NaOH to determine the % of COOH grafted on $DexP_{26}$. Figure 51 showed the graph of increasing pH with the volume of NaCl used in titration. By calculation, it was found that 8.76 % of COOH was grafted on 1 g dextran.

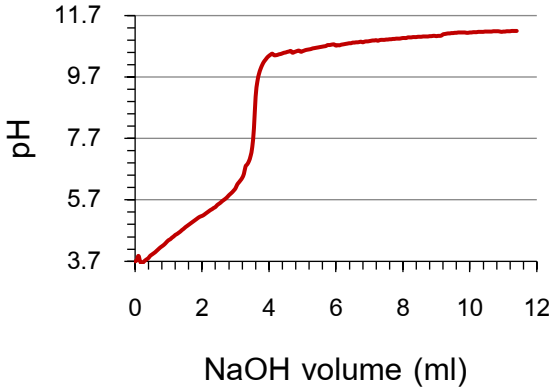

Figure 51 Increased volume of NaOH in determination of % COOH grafted on $DexP_{26}$ The graph showed the increasing pH vs. NaOH volume (ml) used in titration.

4.6.2 Synthesis and characterizations of drug-loaded NPs

4.6.2.1 Size measurement

I. $DexP_{26}$-COOH-grafted MM-NPs

Figure 52 showed the compared size distributions of PLA NPs (52A and 52C) and MM-NPs (52B and 52D) before (52A and 52B) and after (52C and 52D) Tf conjugation. Both PLA NPs and MM-NPs showed very low aggregations before Tf conjugation (Figure 52.A and 52B). However, after conjugation the Tf-PLA NPs increased in a big aggregate but reduced in several small aggregates, while Tf-MM-NPs slightly increased in several aggregates (Figure 52C and 52D). The average sizes, D[3,2], of PLA NPs before Tf conjugation was 120 nm and did not change after Tf conjugation, while of MM-NPs before Tf conjugation was 133 nm and then changed to 187 nm after conjugation (Figure 85 to Figure 88, Appendix D).

Before Tf conjugation, the specific surface area (A_p) of $DexP_{26}$-COOH on PLA (A_p $DexP_{26}$-COOH/gPLA) was reduced from 40.1 m^2/g (PLA NPs) to 36.2 m^2/g (MM-NPs), as shown in Figure 85 and Figure 87, Appendix D, indicating that MM encapsulation resulted in reduction of A_p which related to NPs size and aggregation as that the larger size resulted in smaller specific surface area. Therefore, MM encapsulation into PLA NPs resulted in little increase in NPs size, that resulted to the lowered surface area and the increased particle aggregation.

After Tf conjugation, though specific surface area of $DexP_{26}$ /gPLA of Tf-PLA NPs was not changed, but found to decrease in Tf-MM-NPs to 25.7 m^2/g (Figure 85 and 88, Appendix D). Therefore, the calculated surface coverage of $DexP_{26}$ on PLA of MM-NPs was 0.001321 g/m2PLA.

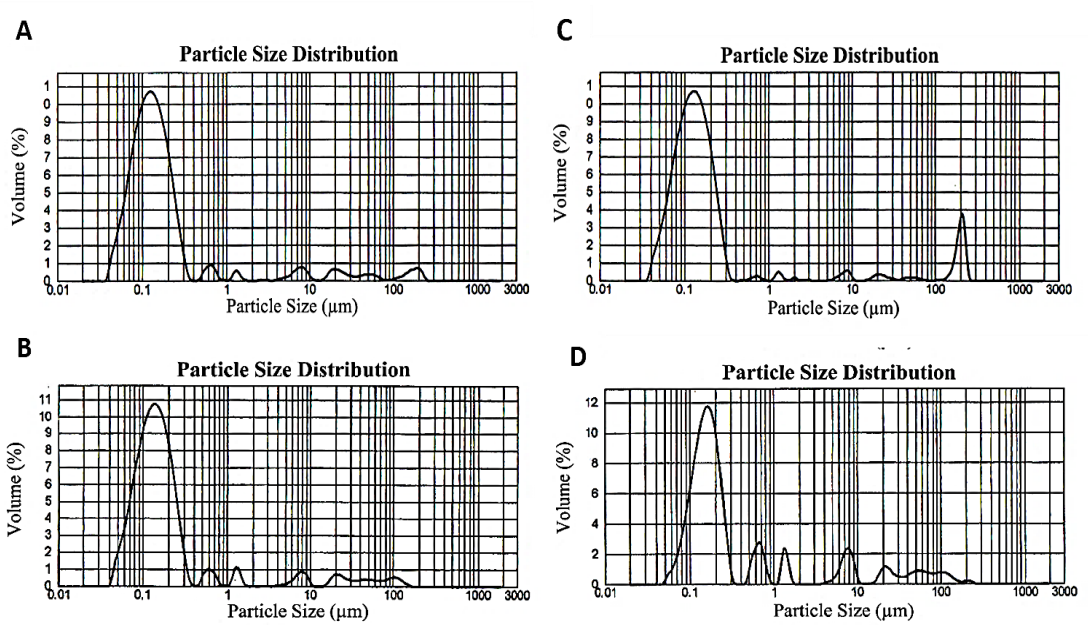

Figure 52 Size distributions of PLA NPs (A, C) and MM-loaded NPs (B, D) before (A, B) and after (C, D) Tf conjugation.

i) Calculation of Tf moles and molecules absorbed on $DexP_{26}$-COOH-grafted NPs

Specific surface area of $DexP_{26}$/gPLA, i.e., 40.1 m^2/g of PLA NPs and 36.2 m^2/g of MM-NPs, were used to estimate the number of moles and Tf molecules fully absorbed on 1 g of $DexP_{26}$-COOH-grafted NPs according to equation (9).

$$Tf_{max} / m^2\ NP = MW_{Tf} / \P r^2 N_A \qquad (9)$$

According to equation (9), Tf_{max} refers to maximum Tf on 1 m^2 NP, MW_{Tf} refers to molar mass of a Tf molecule equal to 80,000 g/mol, $\P r^2$ is area of a Tf with a radius r = 4.5 nm, and N_A is Avogadro's number of particles / mole (6.02×10^{23}). Estimated maximum Tf adsorbed on 1 m^2 NP is 2.09×10^{-3} g/mol.m^2. By specific surface area (40.1 and 36.2 m^2) per gram NPs, thus Tf amount was about 1.048×10^{-6} moles (6.307×10^{17} molecules) and 9.457×10^{-7} moles (5.693×10^{17} molecules) on $DexP_{26}$-

COOH-grafted PLA NPs and $DexP_{26}$-COOH-grafted MM-NPs, respectively. In cytotoxicity test, number of Tf molecules at IC_{50} was used for weight subtraction to calculate the amount of loaded MM in Tf-MM-NPs.

4.6.2.2 ^{1}H NMR analysis

I. $DexP_{26}$-COOH-grafted PLA NPs

^{1}H-NMR spectrum of $DexP_{26}$-COOH-grafted PLA NPs was shown in Figure 53 NMR peaks at: 1.45 (CH_3) and 5.164 (CH) ppm attributed to PLA protons (H^+); 6.912-7.271 attributed to $5H_{phenoxy}$; 4.673 ppm attributed to $H_{anomeric}$. The areas under these peaks were used to estimate the amount of loaded MM as explained below:

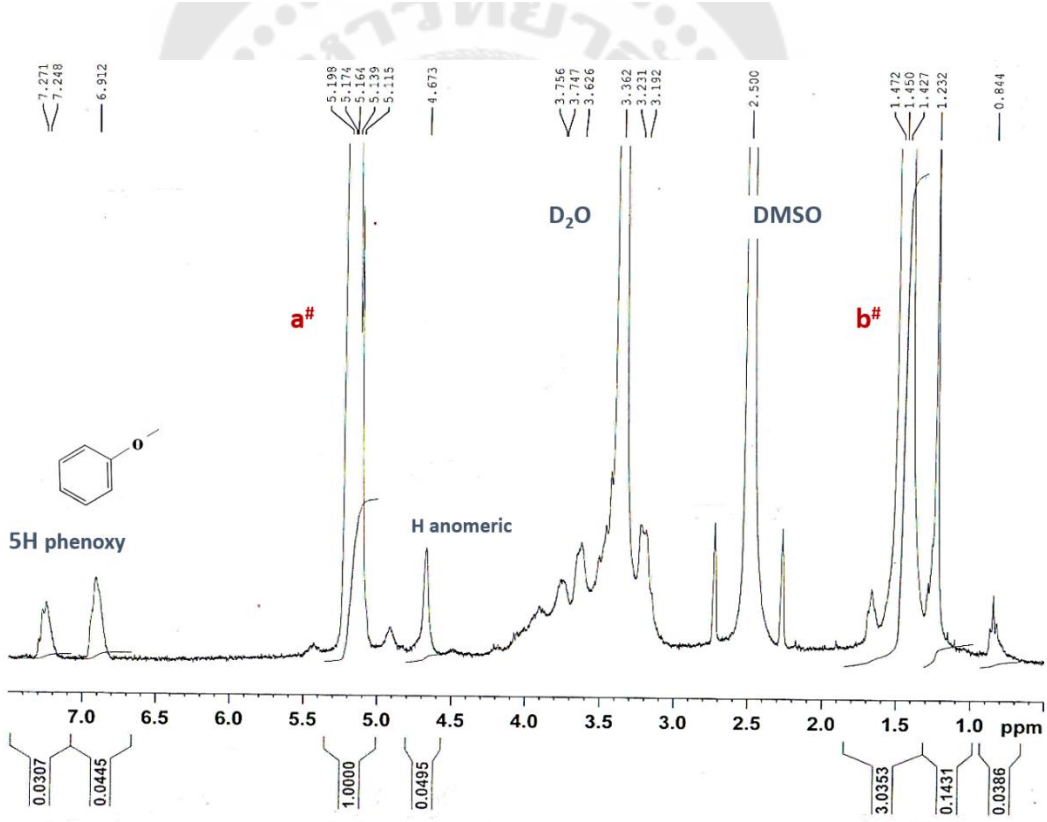

Figure 53 ^{1}H-NMR spectra of $DexP_{26}$-COOH-grafted PLA NPs, in DMSO and D_2O

The peaks ($a^{\#}$) and ($b^{\#}$) were designated as PLA. The peaks $5H_{phenoxy}$ and $H_{anomeric}$ corresponded to dextran-phenoxy$_{26}$ ($DexP_{26}$).

II $DexP_{26}$-COOH-grafted MM-NPs

^{1}H-NMR spectrum of DexP_{26}-COOH-grafted MM-NPs was shown in Figure 54 NMR peaks at: 0.85 (CH_3), 1.234 (20H), and 2.277 (2H) ppm attributed to MM protons (H^+); 1.451 (CH_3) and 5.165 (CH) ppm attributed to PLA protons (H^+); 6 . 91-7 . 27 attributed to $5H_{phenoxy}$; 4 . 6 71 ppm attributed to $H_{anomeric}$. The areas under these peaks were used to estimate the amount of loaded MM as explained below:

The molar ratios of DexP/PLA, MM/PLA, and MM/NP were calculated according to equations (3)-(5), section 4.5.2.2 $A_{Hanomeric}$ was the area under a peak of dextran anomeric protons at 4.671 ppm. A_{CHPLA} corresponded to the areas of PLA methine proton peak centered at 5.165 ppm, while A_{MM} corresponded to the areas of MM protons peak centered at 0.85 ppm.

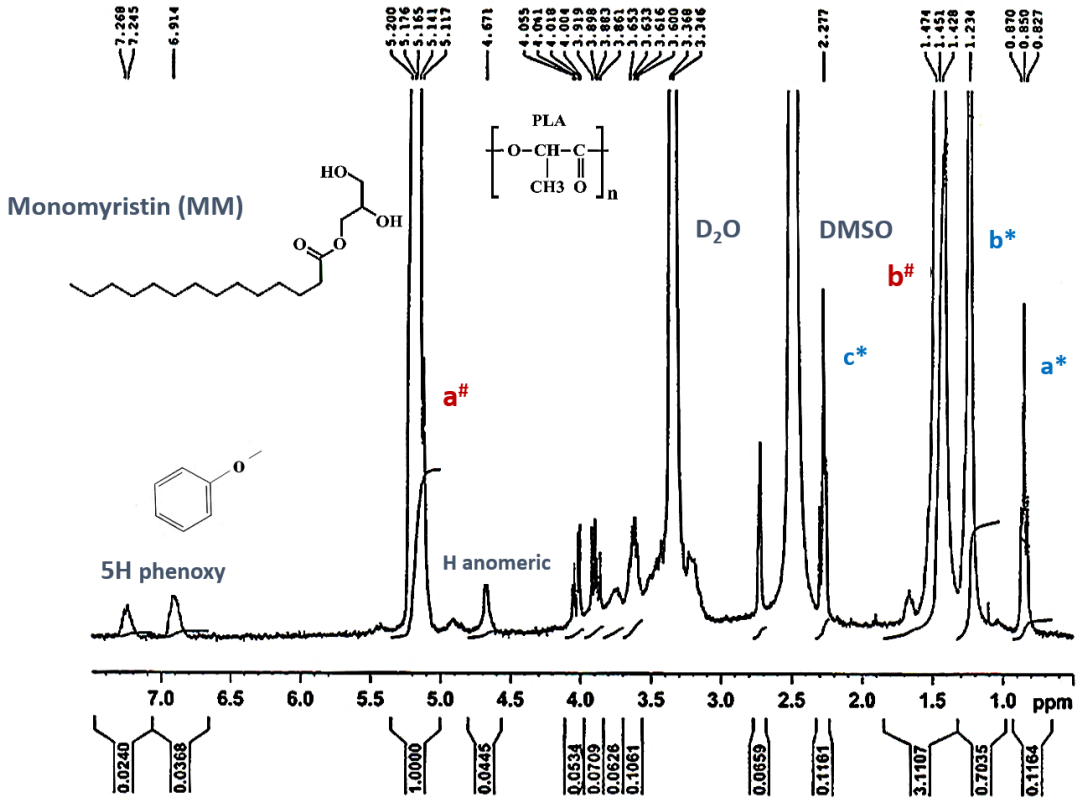

Figure 54 ^{1}H-NMR spectra of DexP_{26}-COOH-grafted MM-NPs, in DMSO and D_2O

The peaks (a*), (b*), and (c*) were designated as MM ($C_{17}H_{34}O_4$). The peaks ($a^{\#}$) and ($b^{\#}$) were designated as PLA. The peaks $5H_{phenoxy}$ and $H_{anomeric}$ corresponded to dextran-$phenoxy_{26}$ (DexP_{26}).

i) Calculation of loaded MM amount in MM-NPs

The areas under ^{1}H NMR peaks were used to calculate the molar ratios of $DexP_{26}$/PLA, MM/PLA and the amount of loaded MM (according to equations (3)-(5)).

$$\text{DexP}_{26} / \text{PLA} = A_{Hanomeric} \times \text{MW}_{\text{DexP26}} / A_{CHPLA} \times \text{MW}_{\text{PLA}}$$
$$= 0.0445 \times 201 / 1 \times 72$$
$$= 0.124 \text{ g}$$
$$\text{MM /PLA} = A_{MM} \times \text{MW}_{\text{MM}} / A_{CHPLA} \times \text{MW}_{\text{PLA}}$$
$$= [0.1164/3 \times 302.46] / [1 \times 72]$$
$$= 0.163 \text{ g}$$
$$\text{MM / NP} = [\text{MM/PLA}] / [1 + \text{DexP}_{26}/\text{PLA} + \text{MM/PLA}]$$
$$= [0.163] / [1 + 0.124 + 0.163]$$
$$= 0.127 \text{ g}$$

(MW_{DexP26} = 201 g/mol, MW_{PLA} = 72 g/mol, MW_{MM} = 302.46 g/mol)

Therefore, the calculated g$DexP_{26}$/gPLA was 0.124, gMM/gPLA was 0.163, and gMM/gNPs was 0.127.

III. $DexP_{26}$-COOH-grafted FITC-NPs

^{1}H-NMR spectrum of $DexP_{26}$-COOH-grafted FITC-NPs was shown in Figure 55. NMR peaks approximately at: 6.91-to 7.35 ppm attributed to $5H_{phenoxy}$; 4.674 attributed to $H_{anomeric}$; 1.45 (CH_3) and 5.17 (CH) ppm attributed to PLA protons (H^+); 6.533 to 10 ppm attributed to FITC protons (H^+). Note that peaks approximately at 7.247-7.351 ppm are the merging peaks of $2H_{phenoxy}$ and FITC. The solvents DMSO and D_2O were peaks at 2.5 and 3.366 ppm, respectively. Therefore, the NMR spectrum clearly showed the presence of all NPs components—i.e. $DexP_{26}$, PLA, FITC, of the developed $DexP_{26}$-grafted FITC-NPs.

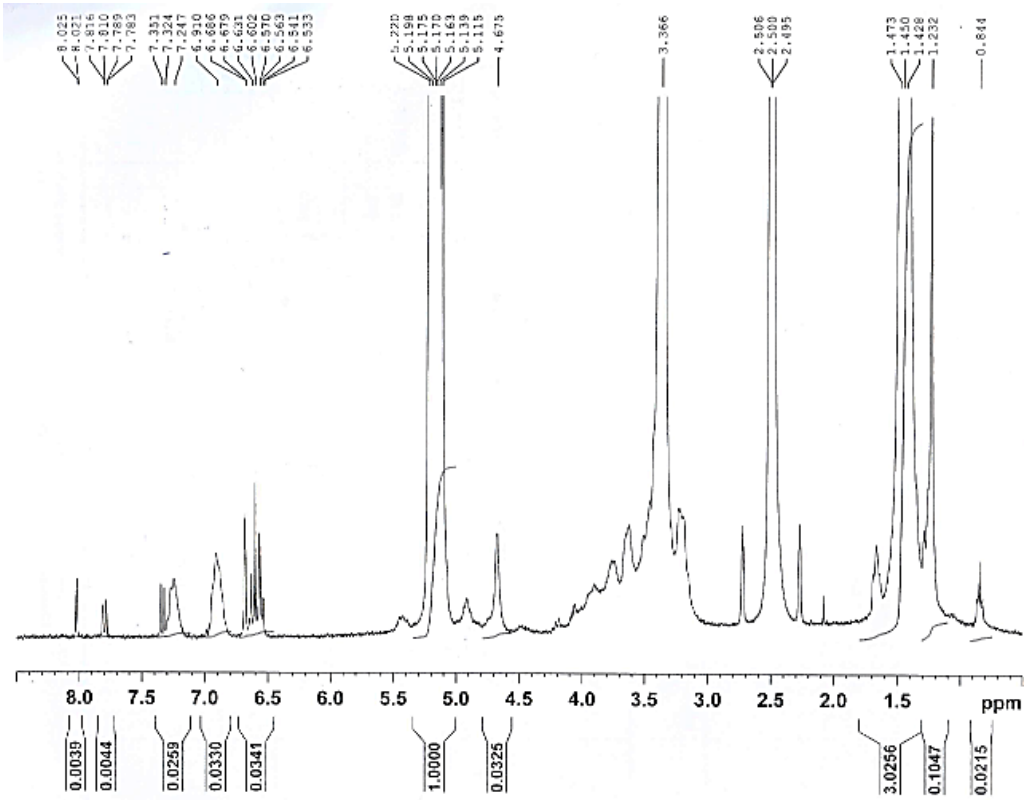

Figure 55 ^{1}H-NMR spectra of $DexP_{26}$-COOH-grafted FITC-NPs, in DMSO and D_2O

i) Calculation of loaded FITC amount in FITC-NPs

The areas under ^{1}H NMR peaks were used to calculate the molar ratios of $DexP_{26}$/PLA, FITC/PLA and the amount of loaded FITC, according to equations (6)-(8).

$DexP_{26}/PLA = A_{Hanomeric} \times MW_{DexP26} / A_{CHPLA} \times MW_{PLA}$

$= 0.0325 \times 201 / 1 \times 72$

$= 0.091$ g

$FITC/PLA = A_{FITC} \times MW_{FITC} / A_{CHPLA} \times MW_{PLA}$

$= (0.0341/6) \times 389.4 / 1 \times 72$

$= 0.031$ g

$FITC/NP = [FITC/PLA] / [1 + DexP_{26}/PLA + FITC/PLA]$

$= [0.0307] / [1 + 0.0907 + 0.0307]$

$= 0.027$ g

(MWDexP26 = 201 g/mol, MWPLA = 72 g/mol, MWFITC = 389.4 g/mol)

From areas under peaks: $A_{Hanomeric}$ at 4.675 ppm was 0.0325; A_{CHPLA} at 5.17 ppm was 1.000; A_{FITC} at 6.57 ppm (6H) was 0.0341. The calculated amount was 0.0907 g$DexP_{26}$/gPLA and 0.0307 gFITC/gPLA. Therefore, amount of the encapsulated FITC was 0.027 g per gram NPs.

4.6.2.3 Colloidal stability of synthesized Tf-NPs in presence of NaCl

Figure 56 showed the colloidal stability of $DexP_{26}$-COOH-grafted NPs. $DexP_{26}$-COOH-grafted PLA NPs were stable in NaCl up to 1M, while $DexP_{26}$-COOH-grafted MM-NPs were stable in a salt condition up to 4 M. The normal sodium (Na^+) concentration in blood is 0.136-0.145 M, and Na^+ concentration of culture media is 0.137-0.164 M [160, 204]. Therefore, these results imply that the developed PLA NPs and MM-NPs grafted with $DexP_{26}$-COOH were stable in the salt condition as in blood circulation as well as culture media and thus can be used for further step of Tf conjugation with MM-loaded NPs, section 3.10.3.

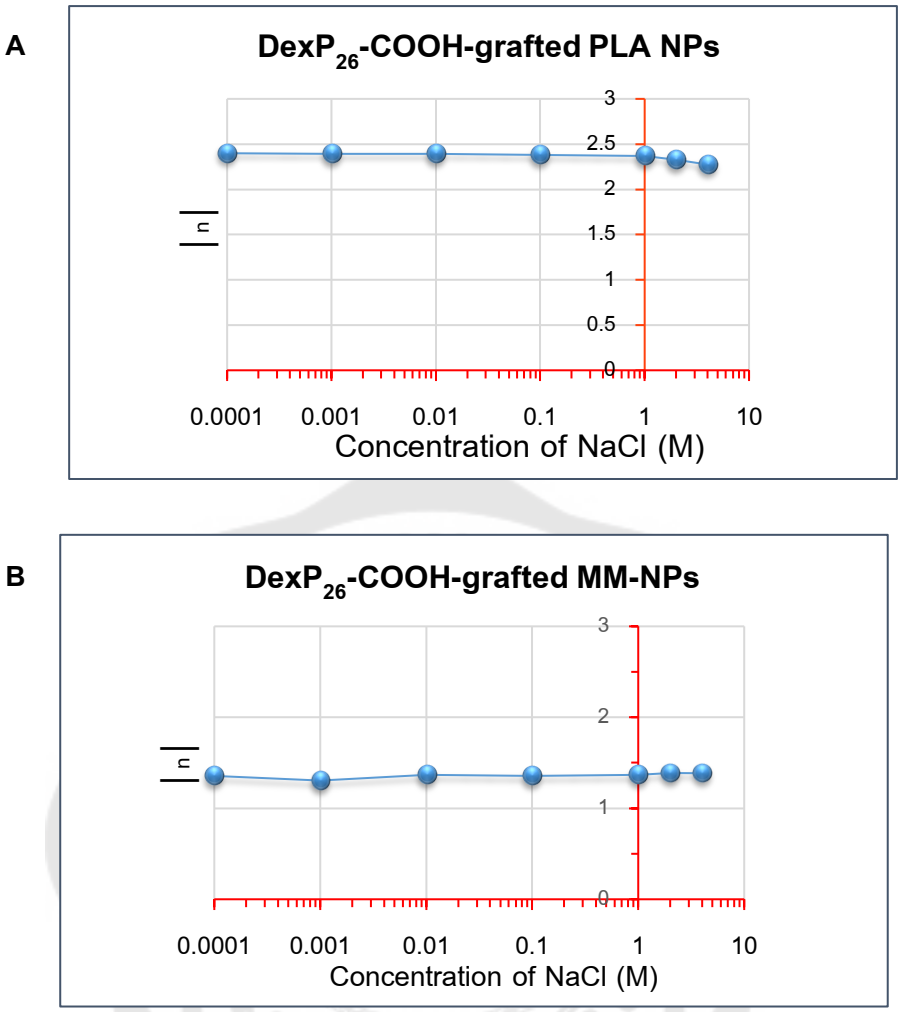

Figure 56 The colloidal stability of $DexP_{26}$-COOH-grafted PLA NPs (A) and $DexP_{26}$-COOH-grafted MM-NPs (B)

Graphs were represented by mean of $|n|$ versus concentration of NaCl (M). The results demonstrated that both PLA and MM-NPs grafted with $DexP_{26}$-COOH were stable suspended in NaCl up to and higher than 1M.

4.7 Cytotoxicity of MM-loaded NPs against HeLa, Vero and endometrial cells

Figure 57 showed the % cell viability of HeLa (A), Vero (B) and uterine endometrial (C) cells after 24-h incubation with MM and various forms of NPs (1.95-1,000 µg/ml). From the results, MM in solution (prepared in section 3.5) and all NP forms showed the cytotoxicity against HeLa cells in dose dependent manner (Figure 57A). While all treatments showed cytotoxicity against Vero and endometrial cells at high

concentrations, except MM-NPs for Vero cells (Figure 57B and Figure 57C). The % cell viability of HeLa cells treated with MM showed a sharp decrease after 15.63 µg/ml, with a significant difference from the control (*p*-value <0.001) (Figure 57A). MM resulted in a sharp decrease of cell viability at the concentrations from 62.5 µg/ml for Vero cells (Figure 57B), while MM showed lower toxicity to uterine endometrial cells.

For NPs treatment, the results showed that the cytotoxicity at lower than 31.25 µg/ml of MM-NPs against HeLa cells was higher than MM solution; while that of Tf-MM-NPs was higher than both MM-NPs and MM solution especially at low doses of <62.5 µg/ml (*p*-value <0.001). These result were probably enhanced due to the encapsulation and the molecular targeting of the attached Tf on NPs surface, thus led NPs to accumulate on HeLa cells surface. To evaluate the effect of NPs vehicle controls, PLA NPs and Tf-PLA NPs were tested. The results of PLA NPs showed very low cytotoxic effects against all three cell types especially in endometrial cells; while Tf-PLA NPs showed low cytotoxic effects on HeLa cells and no effects on Vero and endometrial cells. Thus indicated that PLA NP vehicle was not toxic to both cell lines and thus implied that cytotoxic effects of MM-loaded NPs were actually from the loaded MM in NPs Meanwhile, MM-loaded NPs—i.e. MM-NPs and Tf-MM-NPs, significantly inhibited HeLa cells growth more than NPs vehicles control—i.e. PLA NPs and Tf-PLA NPs, with *p*-value <0.05 and < 0.01, respectively.

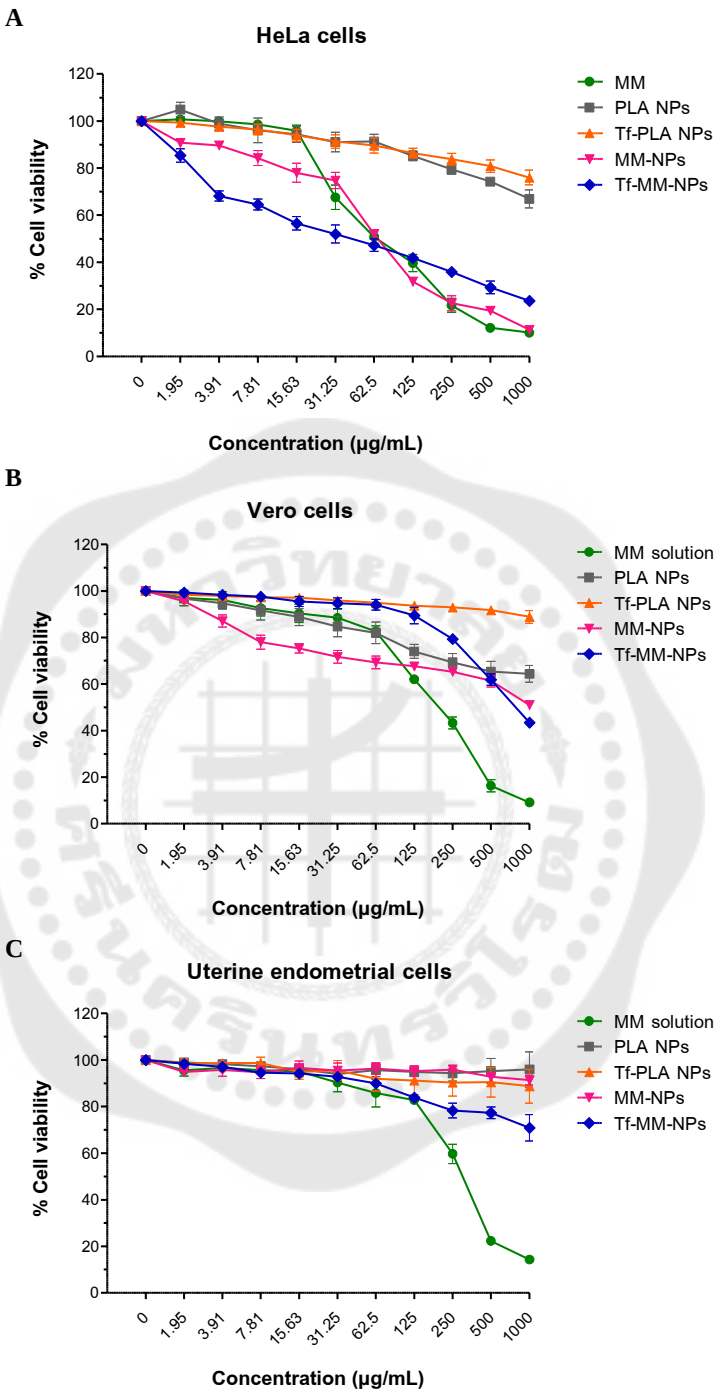

Figure 57 The % cell viability of HeLa (A), Vero (B) and uterine endometrial cells after 24-h incubation of MM and NPs (1.95-1,000 µg/ml)

The results are shown as mean ± SEM. Abbreviations: MM, monomyristin; Tf-PLA NPs, transferrin-conjugated PLA nanoparticles; Tf-MM-NPs, transferrin-conjugated MM-encapsulated nanoparticles.

Table 10 showed the IC_{50} of all treatments against HeLa and Vero cells after 24 h of incubation. The IC_{50} of MM solution, MM-NPs, Tf-MM-NPs, PLA NPs and Tf-PLA NPs against HeLa cells were 78.58±1.069, 69.51±1.07, 50.56±1.148, 3,299±1.364, and 15,655±1.615 µg/ml, respectively. The results showed that IC_{50} of Tf-MM-NPs (~50.56 µg/ml) on HeLa was ~1.37-fold lower than MM-NPs (~69.51 µg/ml). The MM amount was calculated to be 0.049 g per g MM-NPs and 0.127 g per g Tf-MM-NPs. Thus, the actual IC_{50} of MM against HeLa cells was only 3.37±0.05 µg/ml and 5.92±0.13 µg/ml in MM-NPs and Tf-MM-NPs, respectively. This shows the good cytotoxic efficacy of both MM-NPs and Tf-MM-NPs against HeLa cells by the encapsulation and targeting. The IC_{50} of MM solution, MM-NPs, Tf-MM-NPs, PLA NPs against Vero cells were 180.8±1.058, 1,248±1.333, 798.1±1.052, 2,747±1.395 µg/ml, respectively, which showed very low toxicity. The IC_{50} of MM solution and Tf-MM-NPs against endometrial cells were 284.4±1.061 and 6,490±1.368 µg/ml, respectively. This shows that all NP forms including NP vehicles did not have the effect against endometrial cells.

Table 10 IC_{50} of MM solution and developed NPs against HeLa, Vero and uterine endometrial cells at 24-h incubation

Cell types	IC_{50} of MM solution, MM in NP forms, and plain NPs (µg/ml)				
	MM solution	MM-NPs	TF-MM-NPs	PLA NPs	Tf-PLA NPs
HeLa	78.58±1.069	69.51±1.07 [a] (MM=3.37.05)	50.56±1.148 [a, b] (MM=5.92±0.13)	3,299±1.364	15,655±1.615
Vero	180.8±1.058	1,248±1.333 (MM=60.65±0.06)	798.1±1.052 (MM=100.91±0.15)	2,747±1.395	ND
Endometrial	284.4±1.061	ND	6,490±1.368	ND	ND

Data were expressed as mean ± SEM. The values in the brackets were MM amount in NPs; a means statistically significant difference compared to MM solution at $p<0.001$; b means statistically significant difference compared to MM-NPs at $p<0.001$. ND means higher than $1x10^4$. 10000

4.8 Specificity of Tf-MM-NPs with HeLa cervical cancer cells

In order to confirm the specificity of Tf-MM-NPs and Tf receptor on the surface of HeLa cells, the competitive inhibition assay was performed by using the free Tf as a competitive binding molecule versus Tf-MM-NP and then evaluated cell viability with the MTT assay. The results were compared to that obtained from Tf-MM-NPs treatment without Tf preincubation. Figure 58 showed the % cell viability of HeLa cells pre-incubated with Tf (100 µg/mL and 500 µg/ml), and followed by Tf-MM-NPs (1.95-1,000 µg/ml) treatment for 24 h.

The IC_{50} of Tf-MM-NPs alone was 50.56 µg/ml, while IC_{50} of Tf-MM-NPs with 100 µg/ml and 500 µg/ml of Tf were increased to 536.8 and 1,676 respectively. Therefore, HeLa cells treated with Tf-MM-NPs in the presence of Tf (100 µg/mL and 500 µg/ml) showed the reduction of Tf-MM-NPs efficacy against HeLa cells. This study implied that Tf has the competitive ability to bind on HeLa cell surface and inhibit binding of Tf-MM-NPs and thus confirmed the specificity of the attached Tf molecules on NPs surface with HeLa cells.

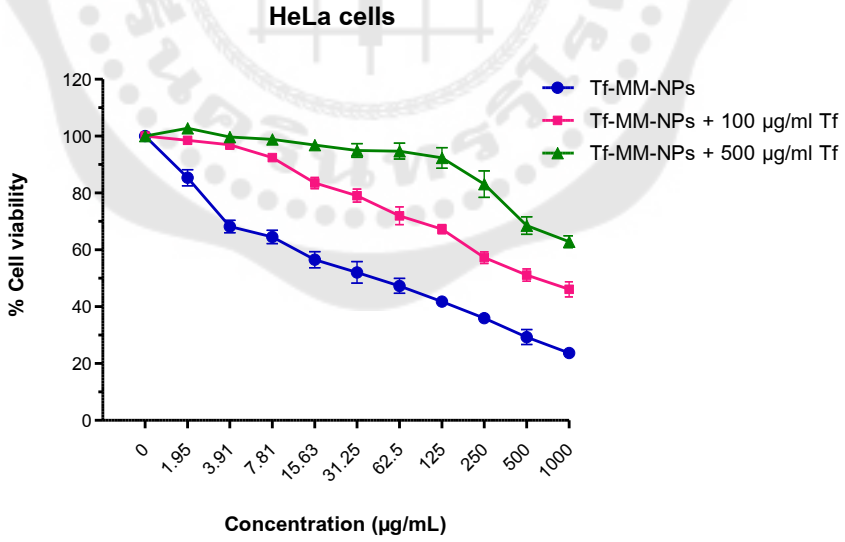

Figure 58 The % cell viability of HeLa cells after 24-h incubation of Tf-MM-NPs (1.95-1,000 µg/ml) with Tf

The results are shown as mean ± SEM. Abbreviations: Tf-MM-NPs, transferrin-conjugated monomyristin-encapsulated nanoparticles; Tf, transferrin.

4.9 Internalization of FITC-loaded NPs in HeLa cells

Internalization of FITC-loaded NPs was examined by using FITC as a model drug for tracing NPs. Internalization in HeLa cells was measured by using the Amnis FlowSight® Imaging Flow Cytometer and analyzed with the IDEAS® 6.2 image analysis software. The intracellular distribution of FITC in HeLa cells was observed.

4.9.1 Internalization analysis of Tf-FITC-NPs in HeLa cells

Figure 59 showed the analysis of 10,000 cells after treatment with Tf-FITC-NPs (50 μg/mL) for 4 h by using the imaging flow cytometry. Out of total, 8,203 cells were gated as a focused cell population (top left), of which 8,194 cells was gated as a single cell population (top right). The 69.8% of a single cell population was gated as the FITC-positive population (bottom left), of which 88.6% was found the internalization of Tf-FITC-NPs (bottom right).

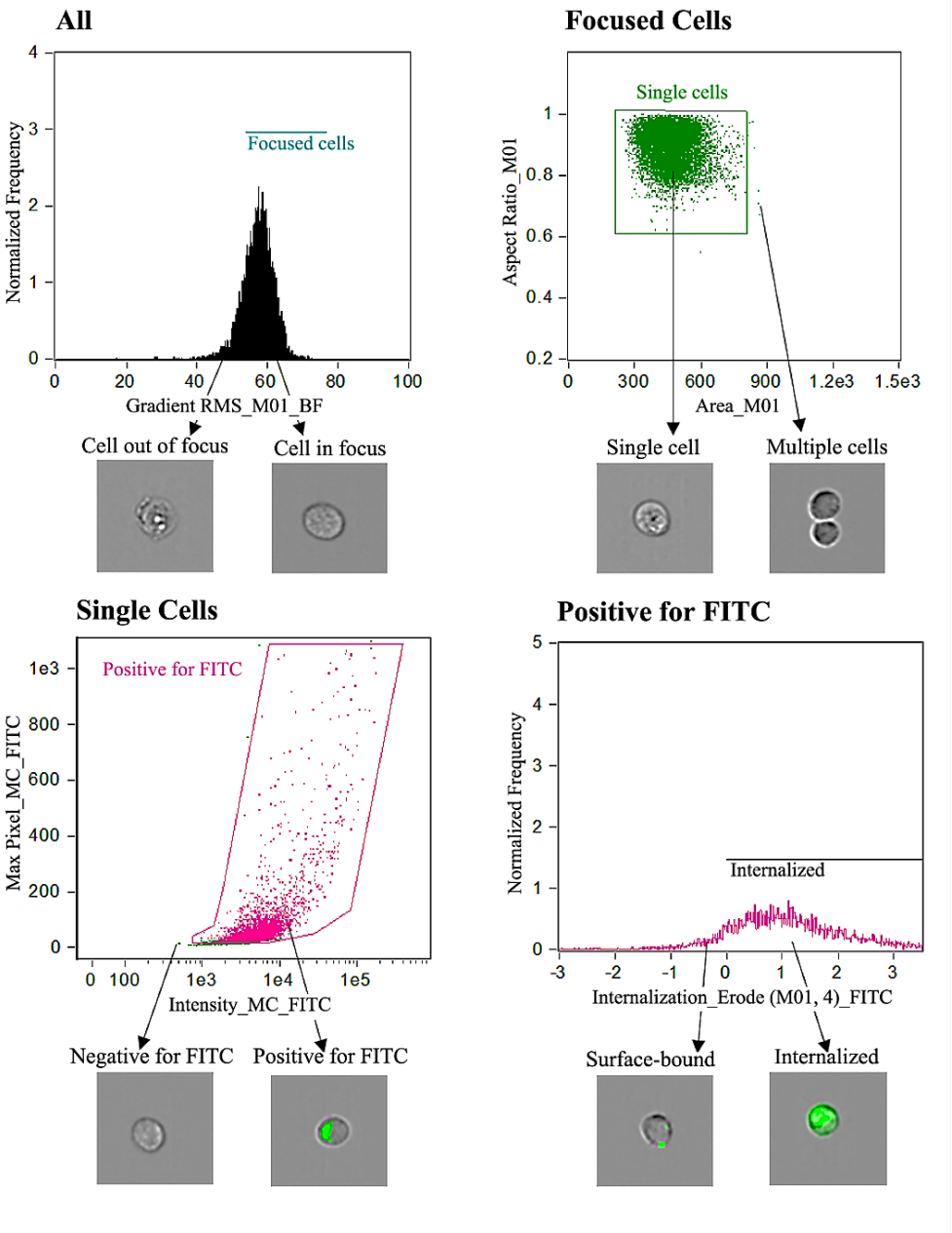

Figure 59 Internalization analysis of the representative HeLa cells using the Amnis FlowSight® Imaging Flow Cytometer

After HeLa cells were incubated with Tf-FITC-NPs (50 μg/mL) for 4 h, cells were measured and analyzed with the IDEAS® 6.2 Image Analysis Software. Top left, focused cells gating; top right, single cells gating; bottom left, FITC-positive population; bottom right, the FITC-internalized population. The results revealed that internalization of Tf-FITC-NPs occurred in 88.6% of FITC-positive HeLa cells after 4 h.

4.9.2 The internalization of Tf-FITC-NPs in HeLa cells

Figure 60 showed internalization results from analysis of the representative HeLa cells treated with Tf-FITC-NPs (50 µg/mL) for 4 h. HeLa cells with bright field (BF), FITC (NPs), and merged photos are shown. The increasing degrees of internalization are from row 2 to row 6. The increasing degrees of intracellular distribution of FITC within representative HeLa cells were seen after membrane-bound and internalization of Tf-FITC-NPs—as a mist-like FITC fluorescence (green color) clearly shown from row 4 to row 6. These results demonstrated the uptake of Tf-FITC-NPs (50 µg/mL) and intracellular distribution of FITC in HeLa cells after 4 h of NPs incubation.

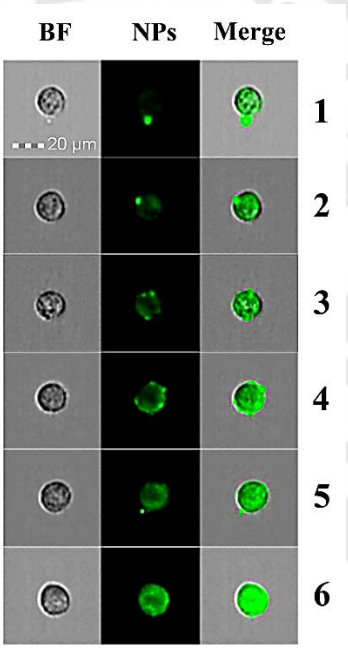

Figure 60 Internalization study of the representative HeLa cells treated with Tf-FITC-NPs (50 µg/mL) for 4 h

HeLa cells were analyzed with the IDEAS® 6.2 Image Analysis Software. Column: BF, HeLa cells taken by bright field channel; NPs, HeLa cells taken by FITC channel; Merge, overlay of BF and NPs. The series of cellular uptake and internalization occurred at: row 1-5, Tf-FITC-NPs were membrane-bound; row 2-6, internalized and distributed.

4.9.3 Time-response internalization of FITC-loaded NPs in HeLa cells

FITC was used as a model drug to study the internalization of FITC-NPs and Tf-FITC NPs. The result (Figure 61) shows the results from analysis of HeLa cells treated with FITC-loaded NPs (FITC amount ~1.29 µg/mL). It has been shown that both NPs forms were internalized into HeLa cells in time-dependent manner: FITC-NPs, 24.603±0.133, 25.945±0.103%, 27.095±0.002, 27.265± 0.021; Tf-FITC-NPs were 31.864±0.763, 50.269±8.121 and 65.689±5.082, 94.166±2.214 % for 0.5, 1, 4 and 16 h respectively. These results revealed that Tf-FITC-NPs were internalized into HeLa cells much rapid than FITC-NPs which infer higher efficiency of NPs with Tf targeting that could bring the loaded-FITC into HeLa cells.

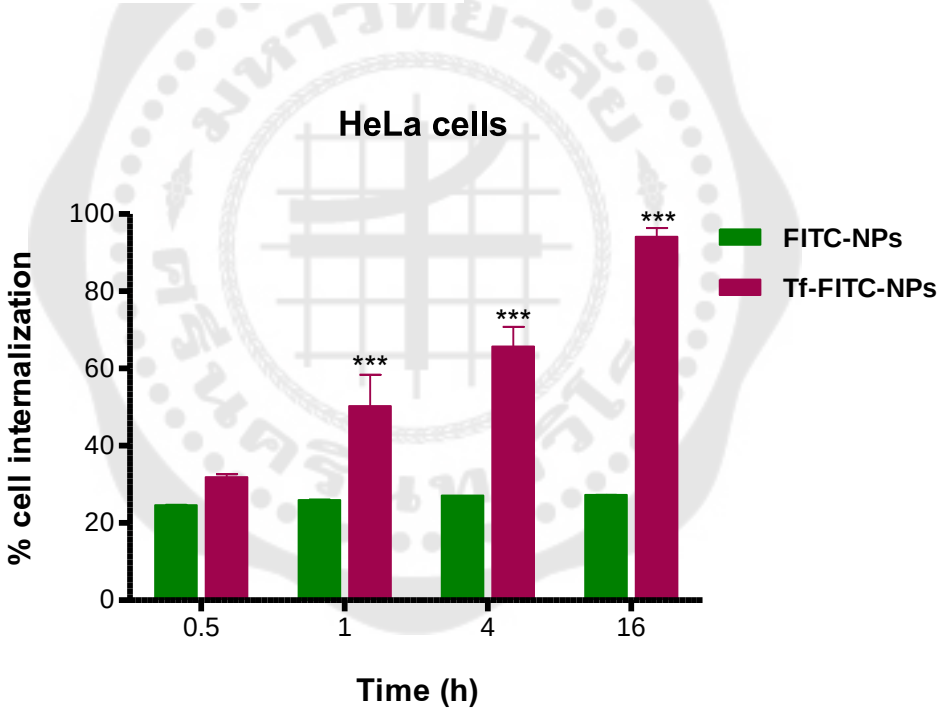

Figure 61 The % cell internalization (HeLa cells) treated with FITC-NPs and Tf-FITC-NPs (~1.29 µg/mL FITC) for 0.5, 1, 4 and 16 h

The results are shown as mean ± SEM. Abbreviations: FITC-NPs, FITC-loaded nanoparticles; Tf-FITC-NPs, transferrin-conjugated FITC-loaded nanoparticles. *** means statistically significant difference compared to FITC-NPs at $p<0.001$.

CHAPTER V
DISCUSSION

This study demonstrated that MM significantly inhibited Hela cells growth in a dose-dependent manner. The apoptosis of HeLa cells induced by MM was then examined. Apoptosis is a programmed cell death that plays the critical roles in life homeostatic mechanisms, the normal tissue development, as well as to execute the cancerous cells. By performing the Annexin Red Assay, a recombinant phosphatidylserine (PS)-binding protein, Annexin V, could strongly and specifically interact with PS residues [207]. The HeLa cells undergoing apoptosis by the effect of MM with the feature of membrane phospholipid PS translocated to the outer leaflet and exposed to extracellular surface are thus detected by Annexin V-CF647/7-AAD double stain, to identify early and late apoptotic cells. The results from the Annexin Red Assay demonstrated that HeLa cells treated with MM (70-150 µg/mL) increased in the number of apoptotic cells in a dose-dependent manner. Apoptosis via the intrinsic pathway is one of the main pathways in apoptosis, as well, the inner mitochondrial membrane is a key indicator of cell health. Thus, the inner mitochondrial membrane potential change is the major characteristic that lead to the downstream apoptotic mechanisms which include the release of pro-apoptotic proteins to activate caspase-9 and subsequent caspase-3 that can lead to downstream apoptotic cascades [208]. Therefore, monitoring the changes of mitochondrial membrane potential is crucial for the early apoptosis. By using cationic fluorescent red dye, MitoSense Red, that accumulated in healthy mitochondria or dropped in red fluorescence signal in mitochondrial-damaged cells could thus signify the collapse of mitochondria and assessed the mitochondrial toxicity in apoptotic cells. Using two dyes simultaneously, i.e., MitoSense Red and 7-AAD, could identify the healthy and apoptotic cells. The results clearly revealed that apoptotic HeLa cells induced by MM were involved with the activation of mitochondrial pathway, which could probably lead to the cytochrome c release from the mitochondria as well as the

activation of downstream apoptotic proteins such as caspases. Although, previous study revealed that MM induced HeLa cell apoptosis via triggering the caspase-3 activation which finally led to the DNA fragmentation [209]. Nevertheless, we report here the first time the toxicity in cultured Hela cells induced by MM was found to be due to the intrinsic (mitochondrial) pathway.

Although, this study demonstrated the inhibition of MM on the Hela cell growth, the poor water-soluble property limits MM a bioactive agent against cancer. Therefore, we developed the MM-loaded polymeric NPs with the targeting ligand, Tf, for delivery MM towards HeLa cells. The stability of NPs is relied on a stabilizer of the synthesized NPs. It has been shown that using the dextran grafted onto the polymeric NPs provides good colloidal stability [164, 165, 210] and prevent protein adsorption [10]. In the previous work, a low degree of modified dextran, i.e., $DexP_{20,}$ was synthesized and successfully used to encapsulate [10]. In this work, by using the similar protocol with modification [211], different low degrees of modified dextran, i.e., $DexP_{15.5}$, $DexP_{21}$, $DexP_{26}$ were obtained. Using the $DexP_{26}$ in combination with PLA is a useful polar hydrophobic polymer to encapsulate low water-soluble drugs [10], MM and FITC. In the development of PLA NPs and MM-NPs from $DexP_{26}$ and PLA, the NMR spectra showed the presence of PLA, $DexP_{26}$ and MM. Size distribution results showed that PLA NPs were stable as there were no aggregations after wash while MM-NPs had negligible aggregation. In the previous study of Chiewpattanakul et al., 2010 [10] to synthesize the MM-NPs by using $DexP_{20}$ as a stabilizer, it was noted about the presence of macroscopic aggregates of MM-NPs particularly when emulsion-solvent evaporation process was used. The cause was considered that might be due to chemical structure of MM that combines hydrocarbon tail and hydrogen bonding groups at the surface which might limit the adsorption of stabilizer, thus led to particle aggregation [10]. In the development of Tf-targeted NPs, the NMR spectrum indicated the presence of NPs components i.e. $DexP_{26}$-COOH and PLA. The results from size measurement of MM-NPs indicated the reduction in specific surface area of $DexP_{26}$ on PLA but revealed the insignificant increase of NPs size and particle aggregations. However, after Tf conjugation the Tf-PLA

NPs increased in a big aggregate while Tf-MM-NPs slightly increased in aggregations. Incidentally, it seemed that there were some heterogeneous dissolutions of Tf-conjugated NPs samples, i.e., Tf-MM-NPs and Tf-FITC-NPs which may be considered as aggregations that thus lead to little diminishing of cytotoxicity and internalization results of the Tf-conjugated NPs. Furthermore, the polymeric NPs were determined the colloidal stability in a salt (Na^+) condition as in blood electrolyte, i.e., 0.136-0.145 M. The results indicated that all developed NPs, i.e., $DexP_{26}$-grafted PLA NPs, $DexP_{26}$-COOH-grafted PLA NPs, $DexP_{26}$-COOH-grafted MM-NP, were stably suspended in salt conditions as in blood electrolyte.

In cytotoxicity study, it was clearly shown that even low amount of the loaded MM in MM-NPs and Tf-MM-NPs much inhibited HeLa cells growth, indicating the delivery efficiency and enhanced toxicity due to encapsulation and targeting ability of Tf conjugated to the MM-loaded NPs. Meanwhile, MM-loaded NPs, either MM-NPs or Tf-MM-NPs, could secure the normal cells, i.e., Vero and uterine endometrial cells, from the inhibitory effect of MM. This suggested the medicinal capability of the developed nanocarriers toward HeLa cells only. Moreover, the specificity of the conjugated Tf on MM-NP was already verified as that HeLa cells growth is elevated in the presence of the competitive free Tf molecules. In addition, the internalization characteristics of Tf-MM-NP showed the time dependent effect. The improved delivery of encapsulated MM and the subsequent cellular uptake of the Tf-MM-NPs by HeLa cells was shown. This shows the good cytotoxic efficacy of both MM-NPs and Tf-MM-NPs against HeLa cells by the encapsulation and targeting. The IC_{50} of MM solution, MM-NPs, Tf-MM-NPs, PLA NPs against Vero cells were 180.8±1.058, 1,248±1.333, 798.1±1.052, 2,747±1.395 μg/ml, respectively, which showed very low toxicity. The IC_{50} of MM solution and Tf-MM-NPs against endometrial cells were 284.4±1.061 and 6,490±1.368 μg/ml, respectively. This shows that all NP forms including NP vehicles did not have the effect against endometrial cells.

REFERENCES

1. Bray F, Ferlay J, Soerjomataram I, Siegel RL, Torre LA, Jemal A. Global Cancer Statistics 2018: GLOBOCAN Estimates of Incidence and Mortality Worldwide for 36 Cancers in 185 Countries. CA Cancer J Clin. 2018.

2. Organization WH. Cancer fact sheets: All cancers: International Agency for Research on Cancer (IARC); 2018 [cited 20/09/2018. Available from: http://gco.iarc.fr/today/data/factsheets/cancers/39-All-cancers-fact-sheet.pdf.

3. Kalyanaraman B, Joseph J, Kalivendi S, Wang S, Konorev E, Kotamraju S. Doxorubicin-induced apoptosis: implications in cardiotoxicity. Mol Cell Biochem. 2002;234-235(1-2):119-24.

4. Day TW, Wu CH, Safa AR. Etoposide induces protein kinase Cdelta- and caspase-3-dependent apoptosis in neuroblastoma cancer cells. Mol Pharmacol. 2009;76(3):632-40.

5. Park SJ, Wu CH, Gordon JD, Zhong X, Emami A, Safa AR. Taxol induces caspase-10-dependent apoptosis. J Biol Chem. 2004;279(49):51057-67.

6. Wang S, Konorev EA, Kotamraju S, Joseph J, Kalivendi S, Kalyanaraman B. Doxorubicin induces apoptosis in normal and tumor cells via distinctly different mechanisms. intermediacy of H(2)O(2)- and p53-dependent pathways. J Biol Chem. 2004;279(24):25535-43.

7. Burd EM. Human papillomavirus and cervical cancer. Clin Microbiol Rev. 2003;16(1):1-17.

8. Naumov GN, Townson JL, MacDonald IC, Wilson SM, Bramwell VH, Groom AC, et al. Ineffectiveness of doxorubicin treatment on solitary dormant mammary carcinoma cells or late-developing metastases. Breast Cancer Res Treat. 2003;82(3):199-206.

9. Sarikapan W. Epidemiologic report of gynecologic cancer in Thailand. J Gynecol Oncol. 2009;20(2):81-3.

10. Chiewpattanakul P, Covis R, Vanderesse R, Thanomsub B, Marie E, Durand A. Design of polymeric nanoparticles for the encapsulation of monoacylglycerol. Colloid and Polymer Science. 2010;288(9):959-67.

11. Philippoussis F, Arguin C, Mateo V. Monoglycerides induce apoptosis in human leukemic cells while sparing normal peripheral blood mononuclear cells. Blood. 2003;101(1):292-4.

12. Phonnok S, Uthaisang-Tanechpongtamb W, Wongsatayanon Thanomsub B. Anticancer and apoptosis-inducing activities of microbial metabolites. Electron J Biotechn. 2010;13(5).

13. Qian ZM, Li H, Sun H, Ho K. Targeted drug delivery via the transferrin receptor-mediated endocytosis pathway. Pharmacol Rev. 2002;54(4):561-87.

14. Sakaguchi N, Kojima C, Harada A, Koiwai K, Emi N, Kono K. Effect of transferrin as a ligand of pH-sensitive fusogenic liposome-lipoplex hybrid complexes. Bioconjug Chem. 2008;19(8):1588-95.

15. Hanahan D, Weinberg RA. The hallmarks of cancer. Cell. 2000;100(1):57-70.

16. Kleinsmith LJ. Principles of cancer biology. Pearson international ed: Benjamin Cummings; 2005.

17. Organization WH. Global Health Observatory. Geneva: World Health Organization; 2018.

18. Parkin DM, Bray F, Ferlay J, Pisani P. Global cancer statistics, 2002. CA Cancer J Clin. 2005;55(2):74-108.

19. Jemal A, Bray F, Center MM, Ferlay J, Ward E, Forman D. Global cancer statistics. CA Cancer J Clin. 2011;61(2):69-90.

20. Torre LA, Bray F, Siegel RL, Ferlay J, Lortet-Tieulent J, Jemal A. Global cancer statistics, 2012. CA Cancer J Clin. 2015;65(2):87-108.

21. Ferlay J, Colombet M, Soerjomataram I. Global and Regional Estimates of the Incidence and Mortality for 38 Cancers: GLOBOCAN 2018. Lyon: International Agency for Research on Cancer/World Health Organization; 2018.

22. Ferlay J, Soerjomataram I, Ervik M, Dikshit R, Eser S, Mathers C, et al. GLOBOCAN 2012 v1.0, Cancer Incidence and Mortality Worldwide. Lyon, France: International Agency for Research on Cancer 2013.

23. Bray F, Jemal A, Grey N, Ferlay J, Forman D. Global cancer transitions according

to the Human Development Index (2008-2030): a population-based study. Lancet Oncol. 2012;13(8):790-801.

24. Cancer in Thailand Volume VII, 2007-2009. Khuhaprema T, Attasara P, Sriplung H, Wiangnon S, Sangrajrang S, editors. Bangkok: Ministry of Public Health; 2013.

25. Wilailak S. Epidemiologic report of gynecologic cancer in Thailand. Journal of Gynecologic Oncology. 2009;20(2):81-3.

26. Vatanasapt V, Sriamporn S, Vatanasapt P. Cancer control in Thailand. Jpn J Clin Oncol 2002(supplement 1) S82-S91.

27. Cancer in Thailand Vol I, 1988–1991. Vatanasapt V, Martin N, Sriplung H, Chindavijak K, Sontipong S, Sriamporn S, et al., editors. Lyon: IARC 1993. 88-9 p.

28. Cancer in Thailand. Vol. II, 1992-1994. Deerasamee S, Martin N, Sontipong S, Sriamporn S, Sriplung H, et al., editors. Lyon, France: National Cancer Institute, International Agency for Research on Cancer [IARC]; 1999.

29. Khuhaprema T, Attasara P, Sriplung H, et al. Cancer in Thailand Volume VI, 2004–2006. . Bangkok

NCIB; 2012.

30. Cancer in Thailand Vol. V, 2001–2003. Khuhaprema T, Srivatanakul P, Attasara P, Sriplung H, Wiangnon S, Sumitsawan Y, editors: Bangkok Medical Publisher; 2010.

31. Cancer in Thailand. Vol IV, 1998-2000. Khuhaprema T, Srivatanakul P, Sriplung H, Wiangnon S, Sumitsawan Y, Attasara P, et al., editors. Bangkok2007.

32. Cancer in Thailand. Vol III,1995-1997. Sriplung H, Sontipong S, Martin N, Wiangnon S, Vootiprux V, Cheirsilpa A, et al., editors. Bangkok2003.

33. Khuhaprema T. Current Cancer Situation in Thailand. Thai J Toxicol. 2008;23(2):60-1.

34. Foulds L. Tumor progression. Cancer research. 1957;17(5):355-6.

35. Foulds L. The development of tumors. Proc Natl Cancer Conf. 1960;4:85-9.

36. Ukraintseva SV, Yashina AI. Cancer as "rejuvenescence". Annals of the New York Academy of Sciences. 2004;1019:200-5.

37. Rak J, Filmus J, Finkenzeller G, Grugel S, Marme D, Kerbel RS. Oncogenes as

inducers of tumor angiogenesis. Cancer metastasis reviews. 1995;14(4):263-77.

38. Yokota J. Tumor progression and metastasis. Carcinogenesis. 2000;21(3):497-503.

39. Hanahan D, Weinberg RA. Hallmarks of cancer: the next generation. Cell. 2011;144(5):646-74.

40. Ringshausen I, Peschel C, Decker T. Cell cycle inhibition in malignant lymphoma: disease control by attacking the cellular proliferation machinery. Curr Drug Targets. 2006;7(10):1349-59.

41. Caldon CE, Sutherland RL, Musgrove E. Cell cycle proteins in epithelial cell differentiation: implications for breast cancer. Cell Cycle. 2010;9(10):1918-28.

42. Ghobrial IM, Witzig TE, Adjei AA. Targeting apoptosis pathways in cancer therapy. CA Cancer J Clin. 2005;55(3):178-94.

43. Adams JM, Cory S. The Bcl-2 apoptotic switch in cancer development and therapy. Oncogene. 2007;26(9):1324-37.

44. Willis SN, Adams JM. Life in the balance: how BH3-only proteins induce apoptosis. Current opinion in cell biology. 2005;17(6):617-25.

45. Ashkenazi A. Targeting death and decoy receptors of the tumour-necrosis factor superfamily. Nature reviews Cancer. 2002;2(6):420-30.

46. White E, DiPaola RS. The double-edged sword of autophagy modulation in cancer. Clin Cancer Res. 2009;15(17):5308-16.

47. Baeriswyl V, Christofori G. The angiogenic switch in carcinogenesis. Seminars in cancer biology. 2009;19(5):329-37.

48. Bergers G, Benjamin LE. Tumorigenesis and the angiogenic switch. Nature reviews Cancer. 2003;3(6):401-10.

49. Hicklin DJ, Ellis LM. Role of the vascular endothelial growth factor pathway in tumor growth and angiogenesis. J Clin Oncol. 2005;23(5):1011-27.

50. Chui CH, Gambari R, Lau FY, Cheng GY, Wong RS, Kok SH, et al. In vitro anti-cancer activity of a novel microbial fermentation product on human carcinomas. Int J Mol Med. 2006;17(4):675-9.

51. Talmadge JE, Fidler IJ. AACR centennial series: the biology of cancer metastasis:

historical perspective. Cancer research. 2010;70(14):5649-69.

52. Fidler IJ. The pathogenesis of cancer metastasis: the 'seed and soil' hypothesis revisited. Nature reviews Cancer. 2003;3(6):453-8.

53. Schlesinger M. Role of platelets and platelet receptors in cancer metastasis. Journal of hematology & oncology. 2018;11(1):125-.

54. Lou X-L, Sun J, Gong S-Q, Yu X-F, Gong R, Deng H. Interaction between circulating cancer cells and platelets: clinical implication. Chinese journal of cancer research = Chung-kuo yen cheng yen chiu. 2015;27(5):450-60.

55. Joyce JA, Pollard JW. Microenvironmental regulation of metastasis. Nature reviews Cancer. 2009;9(4):239-52.

56. Parkin DM, Laara E, Muir CS. Estimates of the worldwide frequency of sixteen major cancers in 1980. Int J Cancer. 1988;41(2):184-97.

57. Jordan MA, Wilson L. Microtubules as a target for anticancer drugs. Nature reviews Cancer. 2004;4(4):253-65.

58. Grem JL, Takimoto CH, Multani P, Chu E, Ryan D, Chabner BA, et al. Antimetabolites. Cancer Chemother Biol Response Modif. 1999;18:1-38.

59. Gaynon PS, Carrel AL. Glucocorticosteroid therapy in childhood acute lymphoblastic leukemia. Adv Exp Med Biol. 1999;457:593-605.

60. Barker S. Anti-estrogens in the treatment of breast cancer: current status and future directions. Curr Opin Investig Drugs. 2003;4(6):652-7.

61. Anderson J. The role of antiandrogen monotherapy in the treatment of prostate cancer. BJU Int. 2003;91(5):455-61.

62. Ross JS, Schenkein DP, Pietrusko R, Rolfe M, Linette GP, Stec J, et al. Targeted therapies for cancer 2004. Am J Clin Pathol. 2004;122(4):598-609.

63. Hidalgo M, Pierson AS, Holden SN, Bergen M, Eckhardt SG. Therapeutic angiogenesis inhibitors in the treatment of cancer. Adv Intern Med. 2001;47:159-90.

64. Ramnath N, Creaven PJ. Matrix metalloproteinase inhibitors. Curr Oncol Rep. 2004;6(2):96-102.

65. Druker BJ. Imatinib as a paradigm of targeted therapies. Advances in cancer

research. 2004;91:1-30.

66. Emens LA, Jaffee EM. Cancer vaccines: an old idea comes of age. Cancer Biol Ther. 2003;2(4 Suppl 1):S161-8.

67. Fojo T, Bates S. Strategies for reversing drug resistance. Oncogene. 2003;22(47):7512-23.

68. Gottesman MM. Mechanisms of cancer drug resistance. Annu Rev Med. 2002;53:615-27.

69. Pommier Y, Sordet O, Antony S, Hayward RL, Kohn KW. Apoptosis defects and chemotherapy resistance: molecular interaction maps and networks. Oncogene. 2004;23(16):2934-49.

70. Grossman D, Altieri DC. Drug resistance in melanoma: mechanisms, apoptosis, and new potential therapeutic targets. Cancer metastasis reviews. 2001;20(1-2):3-11.

71. Fraser M, Leung B, Jahani-Asl A, Yan X, Thompson WE, Tsang BK. Chemoresistance in human ovarian cancer: the role of apoptotic regulators. Reprod Biol Endocrinol. 2003;1:66.

72. Agarwal R, Kaye SB. Ovarian cancer: strategies for overcoming resistance to chemotherapy. Nature reviews Cancer. 2003;3(7):502-16.

73. Human papillomavirus (HPV) and cervical cancer: World Health Organization (WHO); 2018 [updated February 2018. Available from: http://www.who.int/mediacentre/factsheets/fs380/en/.

74. Fang CY, Ma GX, Tan Y. Overcoming Barriers to Cervical Cancer Screening Among Asian American Women. North American journal of medicine & science. 2011;4(2):77-83.

75. Ferlay J, Shin HR, Bray F, et al. GLOBOCAN 2008. Lyon, France: International agency for research on cancer (IARC); [Available from: http://www.globocan.iarc.fr.

76. Guo F, Liu Y, Li Y, Li G. Inhibition of ADP-ribosylation factor-like 6 interacting protein 1 suppresses proliferation and reduces tumor cell invasion in CaSki human cervical cancer cells. Mol Biol Rep. 2010;37(8):3819-25.

77. Ellerbroek SM, Stack MS. Membrane associated matrix metalloproteinases in

metastasis. Bioessays. 1999;21(11):940-9.

78. Wojtowicz-Praga SM, Dickson RB, Hawkins MJ. Matrix metalloproteinase inhibitors. Invest New Drugs. 1997;15(1):61-75.

79. Raistrick H, Smith G. Studies in the biochemistry of micro-organisms: The metabolic products of Aspergillus terreus Thom. A new mould metabolic product-terrein. Biochem J. 1935;29(3):606-11.

80. Demasi M, Felicio AL, Pacheco AO, al. e. Studies on terrein as a new class of proteasome inhibitors. J Braz Chem Soc 2010;21:299-305.

81. Cervical Cancer Treatment-Patient Version: General Information About Cervical Cancer: National Cancer Institute; 2018 [Available from: http://www.cancer.gov/cancertopics/pdq/treatment/cervical/Patient/page1.

82. Pengpanich S. The inhibitory effect of terrein on cervical carcinoma Cell line migration. Bangkok: Srinakharinwirot University; May 2012.

83. Understanding cervical cancer: A guide for women with cancer, their families and friends Sydney, NSW: Cancer Council Australia; September 2017 [Available from: https://www.cancercouncil.com.au/wp-content/uploads/2017/09/Cervical_web.pdf.

84. Burd EM. Human papillomavirus and cervical cancer. Clinical microbiology reviews. 2003;16(1):1-17.

85. Lacey JV, Jr., Swanson CA, Brinton LA, Altekruse SF, Barnes WA, Gravitt PE, et al. Obesity as a potential risk factor for adenocarcinomas and squamous cell carcinomas of the uterine cervix. Cancer. 2003;98(4):814-21.

86. Cubie HA. Diseases associated with human papillomavirus infection. Virology. 2013;445(1):21-34.

87. Taking time-lapse genomic snapshots of cervical cancer Bethesday, MD: National Cancer Institute, National Institutes of Health; 2008.

88. Cervical Cancer: Physiopedia; [Available from: http://www.physio-pedia.com/Cervical_Cancer.

89. Cervical cancer FAQs: HPV and cervical cancer [Available from: https://goo.gl/images/nsuhZz.

90. Cervical cancer: Stages, types and grades London, UK: Cancer Research UK; [updated 31 May 2017. Available from: https://www.cancerresearchuk.org/about-cancer/cervical-cancer/stages-types-grades/stage-4.

91. Salani R, Backes FJ, Fung MF, Holschneider CH, Parker LP, Bristow RE, et al. Posttreatment surveillance and diagnosis of recurrence in women with gynecologic malignancies: Society of Gynecologic Oncologists recommendations. Am J Obstet Gynecol. 2011;204(6):466-78.

92. Monie A, Hung C-F, Roden R, Wu TC. Cervarix: a vaccine for the prevention of HPV 16, 18-associated cervical cancer. Biologics : targets & therapy. 2008;2(1):97-105.

93. Mohanty KC, Rand RJ, Berry B. Cryotherapy in the management of cervical ectopy. Genitourinary medicine. 1985;61(5):335-7.

94. Surgery to Treat Cancer: National Institutes of Health, National Cancer Institute; [updated April 29, 2015. Available from: https://www.cancer.gov/about-cancer/treatment/types/surgery.

95. Radiation Therapy to Treat Cancer: National Institutes of Health, National Cancer Institute; [updated July 19, 2017. Available from: https://www.cancer.gov/about-cancer/treatment/types/radiation-therapy.

96. Mercade ME, Monleon L, Andres C, et al. Screening and selection of surfactant producing bacteria from waste lubricating oil. Appl Bacyeriol. 2003;81:161-6.

97. Rahman P, Edward G. Production, Characterisation and Applications of Biosurfactants-Review2008.

98. Edwards JR, Hayashi JA. Structure of a rhamnolipid from Pseudomonas aeruginosa. Archives of Biochemistry and Biophysics. 1965;111(2):415-21.

99. Phonnok S. Thesis on Cytotoxicity test of microbial extracts against cancer cell lines in vitro Bangkok, Thailand: Srinakharinwirot University; 2008.

100. Infante MR, Perez L, Moran C, Pons R, A P. Synthesis, aggregation properties, and applications of biosurfactants derived from arginine. AOCS Press, Champaign ed. Hayes DG, Kitamoto D, Solaiman DKY, Ashby RD, editors. IL, USA2009.

101. Kitamoto D, Morita T, Fukuoka T, Konishi M-a, Imura T. Self-assembling properties

of glycolipid biosurfactants and their potential applications. Current Opinion in Colloid & Interface Science. 2009;14(5):315-28.

102. Samuel Fortin S-LC, inventor; Centre de Recherche sur les Biotechnologies Marines, Rimouski (CA), assignee. Polyunsaturated fatty acid monoglycerides, derivatives, and uses thereof USA patent US 8,198,324 B2 Jun. 12, 2012

103. Otomo NB. Biobased Surfactants and Detergents: Synthesis, Properties, and Applications. Hayes DG, Kitamoto D, Solaiman DKY, Ashby RD, editors. Champaign, IL: AOCS Press; 2009.

104. Kabara J, et al. Antimicrobials in Food. Davidson P, et al., editors. Boca Raton, USA CRC Press, ; 2005.

105. Vltavska P, Kasparková V, Janis R, Bunková L. Antifungal and antibacterial effects of 1-monocaprylin on textile materials. Eur J Lipid Sci Technol 2012;114:849.

106. Bergsson G, Arnfinnsson J, Steingrimsson O, Thormar H. Killing of Gram-positive cocci by fatty acids and monoglycerides. APMIS : acta pathologica, microbiologica, et immunologica Scandinavica. 2001;109(10):670-8.

107. Bergsson G, Arnfinnsson J, Steingrimsson O, Thormar H. In vitro killing of Candida albicans by fatty acids and monoglycerides. Antimicrobial agents and chemotherapy. 2001;45(11):3209-12.

108. Thormar H, Isaacs CE, Brown HR, Barshatzky MR, Pessolano T. Inactivation of enveloped viruses and killing of cells by fatty acids and monoglycerides. Antimicrobial agents and chemotherapy. 1987;31(1):27-31.

109. Kabara JJ, Vrable R. Antimicrobial lipids: natural and synthetic fatty acids and monoglycerides. Lipids. 1977;12(9):753-9.

110. Philippoussis F, Przybytkowski E, Fortin M, Arguin C, Pande SV, Steff AM, et al. Derivatives of monoglycerides as apoptotic agents in T-cells. Cell death and differentiation. 2001;8(11):1103-12.

111. Philippoussis F, Arguin C, Mateo V, Steff AM, Hugo P. Monoglycerides induce apoptosis in human leukemic cells while sparing normal peripheral blood mononuclear cells. Blood. 2003;101(1):292-4.

112. Goetzl EJ, An S. Diversity of cellular receptors and functions for the lysophospholipid growth factors lysophosphatidic acid and sphingosine 1-phosphate. FASEB journal : official publication of the Federation of American Societies for Experimental Biology. 1998;12(15):1589-98.

113. Chan GC, Hinds TR, Impey S, Storm DR. Hippocampal neurotoxicity of Delta9-tetrahydrocannabinol. The Journal of neuroscience : the official journal of the Society for Neuroscience. 1998;18(14):5322-32.

114. Batovska DI, Todorova IT, Tsvetkova IV, Najdenski HM. Antibacterial study of the medium chain fatty acids and their 1-monoglycerides: individual effects and synergistic relationships. Polish journal of microbiology. 2009;58(1):43-7.

115. Tsuchido T, Ahn YH, Takano M. Lysis of Bacillus subtilis Cells by Glycerol and Sucrose Esters of Fatty Acids. Applied and environmental microbiology. 1987;53(3):505-8.

116. Chaibi A, Ababouch IH, Busta F. Inhibition of Bacterial Spores and Vegetative Cells by Glycerides. Journal of Food Protection. 1996;59:716-22.

117. Sun CQ, O'Connor CJ, Roberton AM. Antibacterial actions of fatty acids and monoglycerides against Helicobacter pylori. FEMS immunology and medical microbiology. 2003;36(1-2):9-17.

118. Cordova-Albores LC, Zapotitla ES, Rios MY, Barrera-Necha LL, Hernandez-Lopez M, Bautista-Banos S. Microscopic study of the morphology and metabolic activity of Fusarium oxysporum f. sp. gladioli treated with Jatropha curcas oil and derivatives. Journal of microscopy and ultrastructure. 2016;4(1):28-35.

119. Shimada H, Tyler VE, McLaughlin JL. Biologically active acylglycerides from the berries of saw-palmetto (Serenoa repens). Journal of natural products. 1997;60(4):417-8.

120. Jefferies WA, Brandon MR, Hunt SV, Williams AF, Gatter KC, Mason DY. Transferrin receptor on endothelium of brain capillaries. Nature. 1984;312(5990):162-3.

121. Couvreur P. Polyalkylcyanoacrylates as colloidal drug carriers. Critical reviews in therapeutic drug carrier systems. 1988;5(1):1-20.

122. Hamidi M, Azadi A, Rafiei P. Hydrogel nanoparticles in drug delivery. Advanced drug delivery reviews. 2008;60(15):1638-49.

123. Heydari A, Namazi H, F. F. The delivery of nanoparticles. Hashim AA, editor. 51000 Rijeka, Croatia: InTech Janeza Trdine 9.

124. Suganeswari M, Shering A, Bharathi P, JayaSutha J. Nano Particles: A Novel System In Current Century. International Journal of Pharmaceutical & Biological Archives2011. p. 847-54.

125. Kreter JK. Nanoparticles. In colloidal drug delivery systems,. Dekker M, editor. New York1994.

126. Reverchon E, Adami R. Nanomaterials and supercritical fluids. The Journal of Supercritical Fluids. 2006;37(1):1-22.

127. Rolland JP, Maynor BW, Euliss LE, Exner AE, Denison GM, DeSimone JM. Direct fabrication and harvesting of monodisperse, shape-specific nanobiomaterials. Journal of the American Chemical Society. 2005;127(28):10096-100.

128. Kompella U, Bandi N, Ayalasomayajula S. Poly (lactic acid) nanoparticles for sustained release of budesonide. Drug Deliv Technol. 2001:1-7.

129. Niwa T, Takeuchi H, Hino T, Kuno N, Kawashima Y. Preparations of biodegradable nanospheres of water-soluble and insoluble drugs with D,L-lactide/glycolide copolymer by a novel spontaneous emulsification solvent diffusion method, and the drug release behavior. J Control Release. 1993;25 89 -98.

130. Calvo P, Remuñán-López C, L. Vila-Jato J, Alonso M. Novel hydrophilic chitosan-polyethylene oxide nanopraticles as protein carrier. Journal of Applied Polymer Science. 1998;63:125 - 32.

131. Calvo P, Remunan-Lopez C, Vila-Jato JL, Alonso MJ. Chitosan and chitosan/ethylene oxide-propylene oxide block copolymer nanoparticles as novel carriers for proteins and vaccines. Pharmaceutical research. 1997;14(10):1431-6.

132. Jung J, Perrut M. Particle design using supercritical fluids: Literature and patent survey. The Journal of Supercritical Fluids. 2001;20(3):179-219.

133. Anto S, Bharathi P. Nano Particles: A Novel System In Current Century. Review article International Journal of Pharmaceutical and Biological Archives. 2011;2(2):847-54.

134. Desai MP, Labhasetwar V, Amidon GL, Levy RJ. Gastrointestinal uptake of

biodegradable microparticles: effect of particle size. Pharmaceutical research. 1996;13(12):1838-45.

135. Fang J, Nakamura H, Maeda H. The EPR effect: Unique features of tumor blood vessels for drug delivery, factors involved, and limitations and augmentation of the effect. Advanced drug delivery reviews. 2011;63(3):136-51.

136. Torchilin V. Tumor delivery of macromolecular drugs based on the EPR effect. Advanced drug delivery reviews. 2011;63(3):131-5.

137. Bertrand N, Wu J, Xu X, Kamaly N, Farokhzad OC. Cancer nanotechnology: the impact of passive and active targeting in the era of modern cancer biology. Advanced drug delivery reviews. 2014;66:2-25.

138. Maeda H, Nakamura H, Fang J. The EPR effect for macromolecular drug delivery to solid tumors: Improvement of tumor uptake, lowering of systemic toxicity, and distinct tumor imaging in vivo. Advanced drug delivery reviews. 2013;65(1):71-9.

139. Xu X, Ho W, Zhang X, Bertrand N, Farokhzad O. Cancer nanomedicine: from targeted delivery to combination therapy. Trends in molecular medicine. 2015;21(4):223-32.

140. Danquah MK, Zhang XA, Mahato RI. Extravasation of polymeric nanomedicines across tumor vasculature. Advanced drug delivery reviews. 2011;63(8):623-39.

141. Danhier F, Preat V. Strategies to improve the EPR effect for the delivery of anti-cancer nanomedicines2015. e808 p.

142. Zhang B, Hu Y, Pang Z. Modulating the Tumor Microenvironment to Enhance Tumor Nanomedicine Delivery. Frontiers in pharmacology. 2017;8:952-.

143. Chiewpattanakul P, Covis R, Vanderesse R, Thanomsub B, Marie E, Durand A. Design of polymeric nanoparticles for the encapsulation of monoacylglycerol. Colloid Polym Sci. 2010;288:959–67.

144. Albanese A, Tang PS, Chan WC. The effect of nanoparticle size, shape, and surface chemistry on biological systems. Annu Rev Biomed Eng. 2012;14:1-16.

145. Han-Chung W, Chang D-K, Chia-Ting H. Targeted Therapy for Cancer2006.

146. Sapra P, Allen TM. Improved outcome when B-cell lymphoma is treated with

combinations of immunoliposomal anticancer drugs targeted to both the CD19 and CD20 epitopes. Clin Cancer Res. 2004;10(7):2530-7.

147. Gabizon A, Shmeeda H, Horowitz AT, Zalipsky S. Tumor cell targeting of liposome-entrapped drugs with phospholipid-anchored folic acid-PEG conjugates. Advanced drug delivery reviews. 2004;56(8):1177-92.

148. Medina OP, Zhu Y, Kairemo K. Targeted liposomal drug delivery in cancer. Curr Pharm Des. 2004;10(24):2981-9.

149. Noble CO, Kirpotin DB, Hayes ME, Mamot C, Hong K, Park JW, et al. Development of ligand-targeted liposomes for cancer therapy. Expert opinion on therapeutic targets. 2004;8(4):335-53.

150. Kircheis R, Wightman L, Kursa M, Ostermann E, Wagner E. Tumor-targeted gene delivery: an attractive strategy to use highly active effector molecules in cancer treatment. Gene therapy. 2002;9(11):731-5.

151. Kratz F, Beyer U. Serum proteins as drug carriers of anticancer agents: a review. Drug delivery. 1998;5(4):281-99.

152. Singh M. Transferrin As A targeting ligand for liposomes and anticancer drugs. Curr Pharm Des. 1999;5(6):443-51.

153. Vyas SP, Sihorkar V. Endogenous carriers and ligands in non-immunogenic site-specific drug delivery. Advanced drug delivery reviews. 2000;43(2-3):101-64.

154. Kawamoto M, Horibe T, Kohno M, Kawakami K. A novel transferrin receptor-targeted hybrid peptide disintegrates cancer cell membrane to induce rapid killing of cancer cells. BMC Cancer. 2011;11:359.

155. Lee JH, Engler JA, Collawn JF, Moore BA. Receptor mediated uptake of peptides that bind the human transferrin receptor. European journal of biochemistry. 2001;268(7):2004-12.

156. Wangler C, Nada D, Hofner G, Maschauer S, Wangler B, Schneider S, et al. In vitro and initial in vivo evaluation of (68)Ga-labeled transferrin receptor (TfR) binding peptides as potential carriers for enhanced drug transport into TfR expressing cells. Molecular imaging and biology : MIB : the official publication of the Academy of Molecular Imaging.

2011;13(2):332-41.

157. Zheng Q, Xiong YL, Su ZJ, Zhang QH, Dai XY, Li LY, et al. Expression of curcin-transferrin receptor binding peptide fusion protein and its anti-tumor activity. Protein expression and purification. 2013;89(2):181-8.

158. Li H, Qian ZM. Transferrin/transferrin receptor-mediated drug delivery. Med Res Rev. 2002;22(3):225-50.

159. Bezkorovainy A. Biochemistry of nonheme iron. New York: Springer US; 1980. 436 p.

160. Metz-Boutigue MH, Jolles J, Mazurier J, Schoentgen F, Legrand D, Spik G, et al. Human lactotransferrin: amino acid sequence and structural comparisons with other transferrins. European journal of biochemistry. 1984;145(3):659-76.

161. Baggiolini M, De Duve C, Masson PL, Heremans JF. Association of lactoferrin with specific granules in rabbit heterophil leukocytes. The Journal of experimental medicine. 1970;131(3):559-70.

162. Qian ZM, Wang Q. Expression of iron transport proteins and excessive iron accumulation in the brain in neurodegenerative disorders. Brain Res Brain Res Rev. 1998;27(3):257-67.

163. Leibman A, Aisen P. Distribution of iron between the binding sites of transferrin in serum: methods and results in normal human subjects. Blood. 1979;53(6):1058-65.

164. Sun H, Li H, Sadler PJ. Transferrin as a metal ion mediator. Chemical reviews. 1999;99(9):2817-42.

165. Dewan JC, Mikami B, Hirose M, Sacchettini JC. Structural evidence for a pH-sensitive dilysine trigger in the hen ovotransferrin N-lobe: implications for transferrin iron release. Biochemistry. 1993;32(45):11963-8.

166. Grossmann JG, Mason AB, Woodworth RC, Neu M, Lindley PF, Hasnain SS. Asp ligand provides the trigger for closure of transferrin molecules. Direct evidence from X-ray scattering studies of site-specific mutants of the N-terminal half-molecule of human transferrin. Journal of molecular biology. 1993;231(3):554-8.

167. Tortorella S, Karagiannis TC. Transferrin receptor-mediated endocytosis: a useful

target for cancer therapy. J Membr Biol. 2014;247(4):291-307.

168. Aisen P, Leibman A, Zweier J. Stoichiometric and site characteristics of the binding of iron to human transferrin. J Biol Chem. 1978;253(6):1930-7.

169. Richardson DR, Ponka P. The molecular mechanisms of the metabolism and transport of iron in normal and neoplastic cells. Biochim Biophys Acta. 1997;1331(1):1-40.

170. Schneider C, Sutherland R, Newman R, Greaves M. Structural features of the cell surface receptor for transferrin that is recognized by the monoclonal antibody OKT9. J Biol Chem. 1982;257(14):8516-22.

171. Huebers HA, Finch CA. The physiology of transferrin and transferrin receptors. Physiol Rev. 1987;67(2):520-82.

172. Schneider C, Owen MJ, Banville D, Williams JG. Primary structure of human transferrin receptor deduced from the mRNA sequence. Nature. 1984;311(5987):675-8.

173. Neckers LM, Trepel JB. Transferrin receptor expression and the control of cell growth. Cancer Invest. 1986;4(5):461-70.

174. McClelland A, Kuhn LC, Ruddle FH. The human transferrin receptor gene: genomic organization, and the complete primary structure of the receptor deduced from a cDNA sequence. Cell. 1984;39(2 Pt 1):267-74.

175. Daniels TR, Delgado T, Rodriguez JA, Helguera G, Penichet ML. The transferrin receptor part I: Biology and targeting with cytotoxic antibodies for the treatment of cancer. Clin Immunol. 2006;121(2):144-58.

176. Zerial M, Melancon P, Schneider C, Garoff H. The transmembrane segment of the human transferrin receptor functions as a signal peptide. The EMBO journal. 1986;5(7):1543-50.

177. Calzolari A, Larocca LM, Deaglio S, Finisguerra V, Boe A, Raggi C, et al. Transferrin receptor 2 is frequently and highly expressed in glioblastomas. Translational oncology. 2010;3(2):123-34.

178. Trinder D, Baker E. Transferrin receptor 2: a new molecule in iron metabolism. Int J Biochem Cell Biol. 2003;35(3):292-6.

179. Kawabata H, Germain RS, Vuong PT, Nakamaki T, Said JW, Koeffler HP.

Transferrin receptor 2-alpha supports cell growth both in iron-chelated cultured cells and in vivo. J Biol Chem. 2000;275(22):16618-25.

180. Deaglio S, Capobianco A, Cali A, Bellora F, Alberti F, Righi L, et al. Structural, functional, and tissue distribution analysis of human transferrin receptor-2 by murine monoclonal antibodies and a polyclonal antiserum. Blood. 2002;100(10):3782-9.

181. Dubljevic V, Sali A, Goding JW. A conserved RGD (Arg-Gly-Asp) motif in the transferrin receptor is required for binding to transferrin. Biochem J. 1999;341 (Pt 1):11-4.

182. Ryschich E, Huszty G, Knaebel HP, Hartel M, Buchler MW, Schmidt J. Transferrin receptor is a marker of malignant phenotype in human pancreatic cancer and in neuroendocrine carcinoma of the pancreas. European journal of cancer (Oxford, England : 1990). 2004;40(9):1418-22.

183. Tsuji T, Yoshitomi H, Usukura J. Endocytic mechanism of transferrin-conjugated nanoparticles and the effects of their size and ligand number on the efficiency of drug delivery. Microscopy (Oxford, England). 2013;62(3):341-52.

184. Prades R, Guerrero S, Araya E, Molina C, Salas E, Zurita E, et al. Delivery of gold nanoparticles to the brain by conjugation with a peptide that recognizes the transferrin receptor. Biomaterials. 2012;33(29):7194-205.

185. Ponka P, Lok CN. The transferrin receptor: role in health and disease. Int J Biochem Cell Biol. 1999;31(10):1111-37.

186. Moos T, Morgan EH. Transferrin and transferrin receptor function in brain barrier systems. Cell Mol Neurobiol. 2000;20(1):77-95.

187. Kawamoto M, Kohno M, Horibe T, Kawakami K. Immunogenicity and toxicity of transferrin receptor-targeted hybrid peptide as a potent anticancer agent. Cancer chemotherapy and pharmacology. 2013;71(3):799-807.

188. Habeshaw JA, Lister TA, Stansfeld AG, Greaves MF. Correlation of transferrin receptor expression with histological class and outcome in non-Hodgkin lymphoma. Lancet. 1983;1(8323):498-501.

189. Kondo K, Noguchi M, Mukai K, Matsuno Y, Sato Y, Shimosato Y, et al. Transferrin receptor expression in adenocarcinoma of the lung as a histopathologic indicator of

prognosis. Chest. 1990;97(6):1367-71.

190. Walker RA, Day SJ. Transferrin receptor expression in non-malignant and malignant human breast tissue. The Journal of pathology. 1986;148(3):217-24.

191. Yang DC, Wang F, Elliott RL, Head JF. Expression of transferrin receptor and ferritin H-chain mRNA are associated with clinical and histopathological prognostic indicators in breast cancer. Anticancer research. 2001;21(1b):541-9.

192. Prior R, Reifenberger G, Wechsler W. Transferrin receptor expression in tumours of the human nervous system: relation to tumour type, grading and tumour growth fraction. Virchows Arch A Pathol Anat Histopathol. 1990;416(6):491-6.

193. Das Gupta A, Shah VI. Correlation of transferrin receptor expression with histologic grade and immunophenotype in chronic lymphocytic leukemia and non-Hodgkin's lymphoma. Hematologic pathology. 1990;4(1):37-41.

194. Calzolari A, Oliviero I, Deaglio S, Mariani G, Biffoni M, Sposi NM, et al. Transferrin receptor 2 is frequently expressed in human cancer cell lines. Blood cells, molecules & diseases. 2007;39(1):82-91.

195. Prutki M, Poljak-Blazi M, Jakopovic M, Tomas D, Stipancic I, Zarkovic N. Altered iron metabolism, transferrin receptor 1 and ferritin in patients with colon cancer. Cancer Lett. 2006;238(2):188-96.

196. Seymour GJ, Walsh MD, Lavin MF, Strutton G, Gardiner RA. Transferrin receptor expression by human bladder transitional cell carcinomas. Urological research. 1987;15(6):341-4.

197. Win KY, Feng SS. Effects of particle size and surface coating on cellular uptake of polymeric nanoparticles for oral delivery of anticancer drugs. Biomaterials. 2005;26(15):2713-22.

198. Phelan MC. Basic Techniques for Mammalian Cell Tissue Culture. Current Protocols in Cell Biology. Greenwood, South Carolina: John Wiley & Sons, Inc.; 1998.

199. Watanabe I, Okada S. Stationary phase of cultured mammalian cells (L5178Y). The Journal of cell biology. 1967;35(2):285-94.

200. Guidelines for Maintaining Cultured Cells.: ThermoFisher Scientific; 2018 [Available

from: http://www.lifetechnologies.com/th/en/home/references/gibco-cell-culture-basics/cell-culture-protocols/maintaining-cultured-cells.html.

201. Arima K, Kakinuma A, Tamura G. Surfactin, a crystalline peptidelipid surfactant produced by Bacillus subtilis: isolation, characterization and its inhibition of fibrin clot formation. Biochemical and biophysical research communications. 1968;31(3):488-94.

202. Mosmann T. Rapid colorimetric assay for cellular growth and survival: application to proliferation and cytotoxicity assays. Journal of immunological methods. 1983;65(1-2):55-63.

203. McKee TJ, Komarova SV. Is it time to reinvent basic cell culture medium? American journal of physiology Cell physiology. 2017;312(5):C624-C6.

204. Chauvierre C1, Vauthier C, Labarre D, Couvreur P, Marden MC, L. L. A new generation of polymer nanoparticles for drug delivery. Cell Mol Biol (Noisy-le-grand). 2004, May;50(3):233-9.

APPENDIX

APPENDIX A
REAGENT

1. Phosphate buffered saline (1XPBS)

For preparation of solution, all compounds in the following order are dissolved in distilled water.

NaCl	8	g
KCl	0.2	g
Na_2HPO_4	1.44	g
KH_2PO_4	0.24	g
H_2O (distilled water)	800	ml
H_2O (distilled water) adjust volume to	1000	ml
adjust pH 7.4 with HCl		

The solution was sterilized by 0.2 μm filter membrane and stored at room temperature.

2. MTT solution (0.5 mg/ml)

MTT	5	mg
DMEM or M199 medium	10	ml

APPENDIX B
CULTURE MEDIUM

1. DMEM medium

DMEM medium (Gibco RRL, NY, USA)		
(with L-glutamine and 25 mM HEPES buffer)	10.43	g
$NaHCO_3$	3.7	g
100 µg/ml Streptomycin-100 units/ml penicillin G	10	ml
sterile distilled water to make	1000	ml

adjusted pH 7.2 with HCl or NaOH before adjusted volume with water and sterilize by cellulose acetate filter (pore size 0.22 µm)

2. M199 medium

M199 medium (Gibco RRL, NY, USA)		
(with L-glutamine and 25 mM HEPES buffer)	10.43	g
$NaHCO_3$	2	g
100 µg/ml Streptomycin-100 units/ml penicillin G	10	ml
sterile distilled water to make	1000	ml

adjusted pH 7.2 with HCl or NaOH before adjusted volume with water and sterilize by cellulose acetate filter (pore size 0.22 µm)

3. Freezing medium

M199 or DMEM medium	50%
Fetal calf serum	40%
Dimethysulfoxide (DMSO)	10%

APPENDIX C

REACTION AND MATERIALS IN NANOPARTICLE PREPARATION

1. Chemical reaction to obtain DexP

The synthesis of Dextran-phenoxy, DexP, was done by the attachment of aromatic (epoxy) groups on dextran backbone. Figure 67 showed the chemical reaction of Dextran T40 with 1, 2-epoxy-3-phenoxypropane to obtain the low degree of hydrophobic modified dextran, DexP.

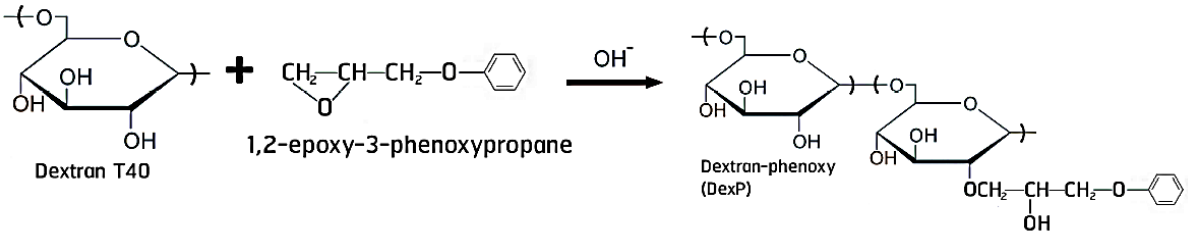

Figure 62 Chemical reaction between Dextran T40 and 1, 2-epoxy-3-phenoxypropane to obtain the DexP

2. Materials used in nanoparticle preparation

2.1 DexP$_\tau$

Structure of dextran bearing with phenoxy group (DexP$_\tau$) was shown in Figure 68, of which the percentages of modified to non-modified molecules [102] were 15.5% or 21% or 26%.

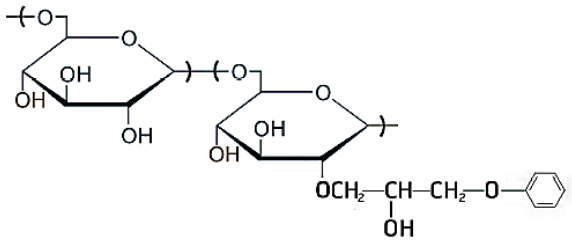

Figure 63 Chemical structure of DexP$_\tau$ (Phenoxy-bearing dextran)

2.2 Poly(D,L-lactide) (PLA)

Chemical structure and ^{1}H NMR spectrum of PLA in DMSO were shown in Figure 69 and Figure 70, respectively.

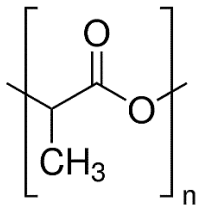

Figure 64 Chemical structure of Poly(D,L-lactide) (PLA)

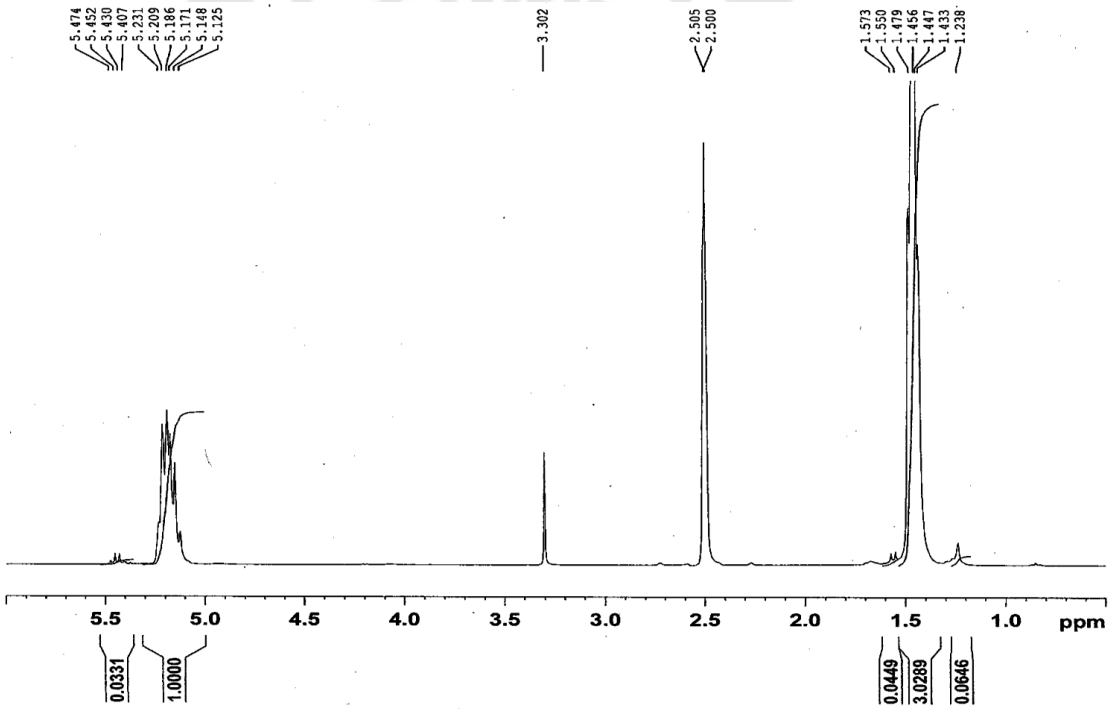

Figure 65 ^{1}H NMR spectrum of PLA in DMSO, 300MHz

2.3 Monomyristin (MM)

Chemical structure and ^{1}H NMR spectrum of monomyristin (MM) in DMSO and D_2O were shown in Figure 71 and Figure 72, respectively.

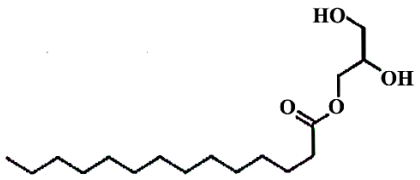

Figure 66 Chemical structure of monomyristin (MM)

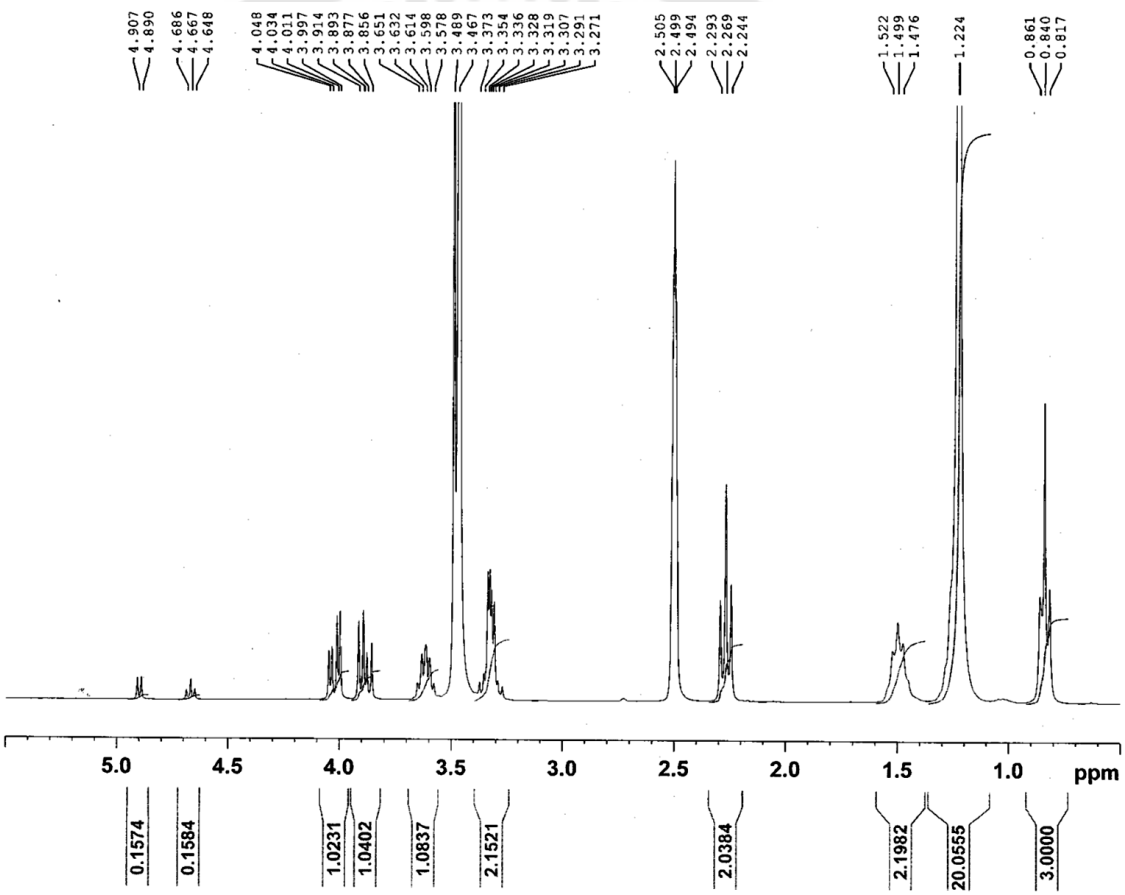

Figure 67 ^{1}H NMR spectrum of MM in DMSO and D_2O, 300 MHz

2.4 Fluorescein isothiocyanate (FITC)

Chemical structure and ^{1}H NMR spectrum of Fluorescein isothiocyanate (FITC) ($C_{21}H_{11}NO_5S$, 389.381 Da) in DMSO and D_2O were shown in Figure 73 and Figure 74, respectively.

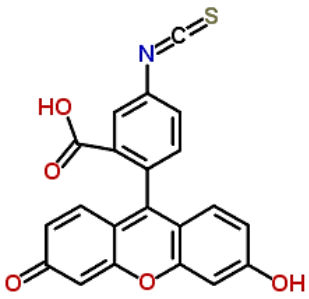

Figure 68 Chemical structure of Fluorescein isothiocyanate (FITC)

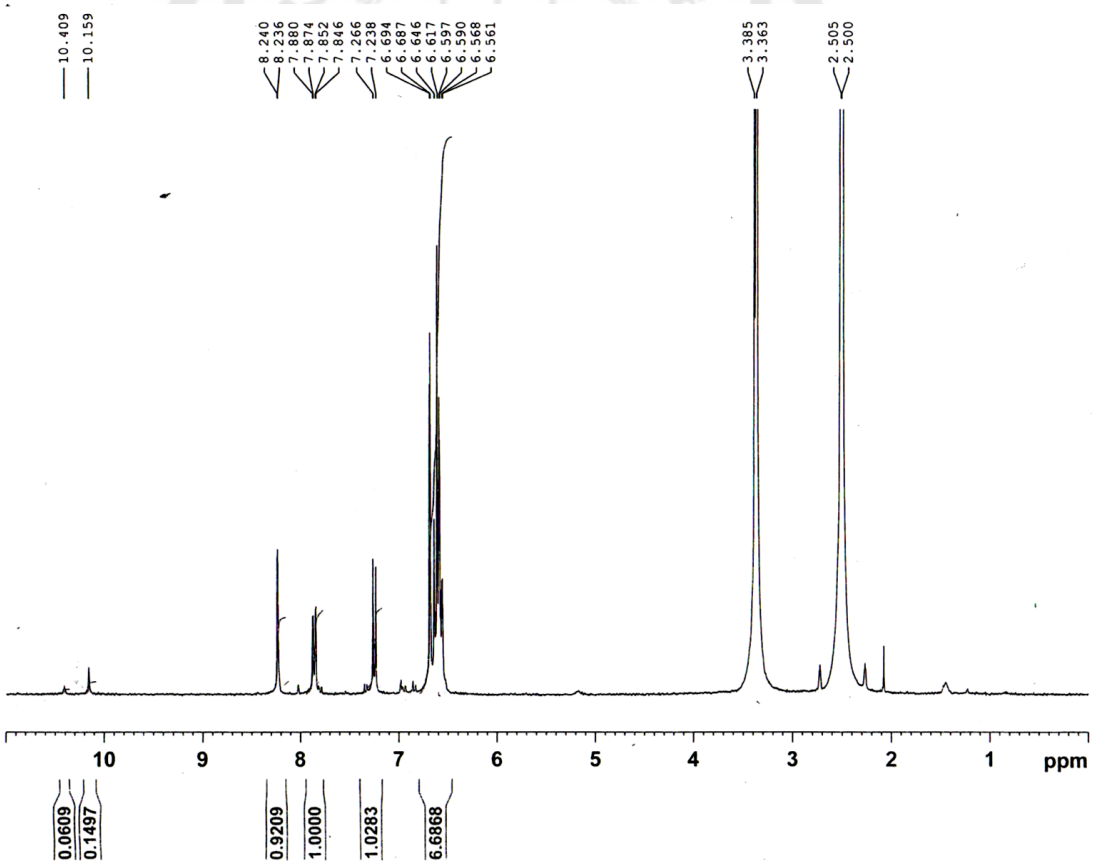

Figure 69 ^{1}H NMR spectrum of FITC in DMSO and D_2O, 300 MHz

APPENDIX D

NANOPARTICLE CHARACTERIZATIONS

1. DexP$_{\tau}$-grafted PLA NPs

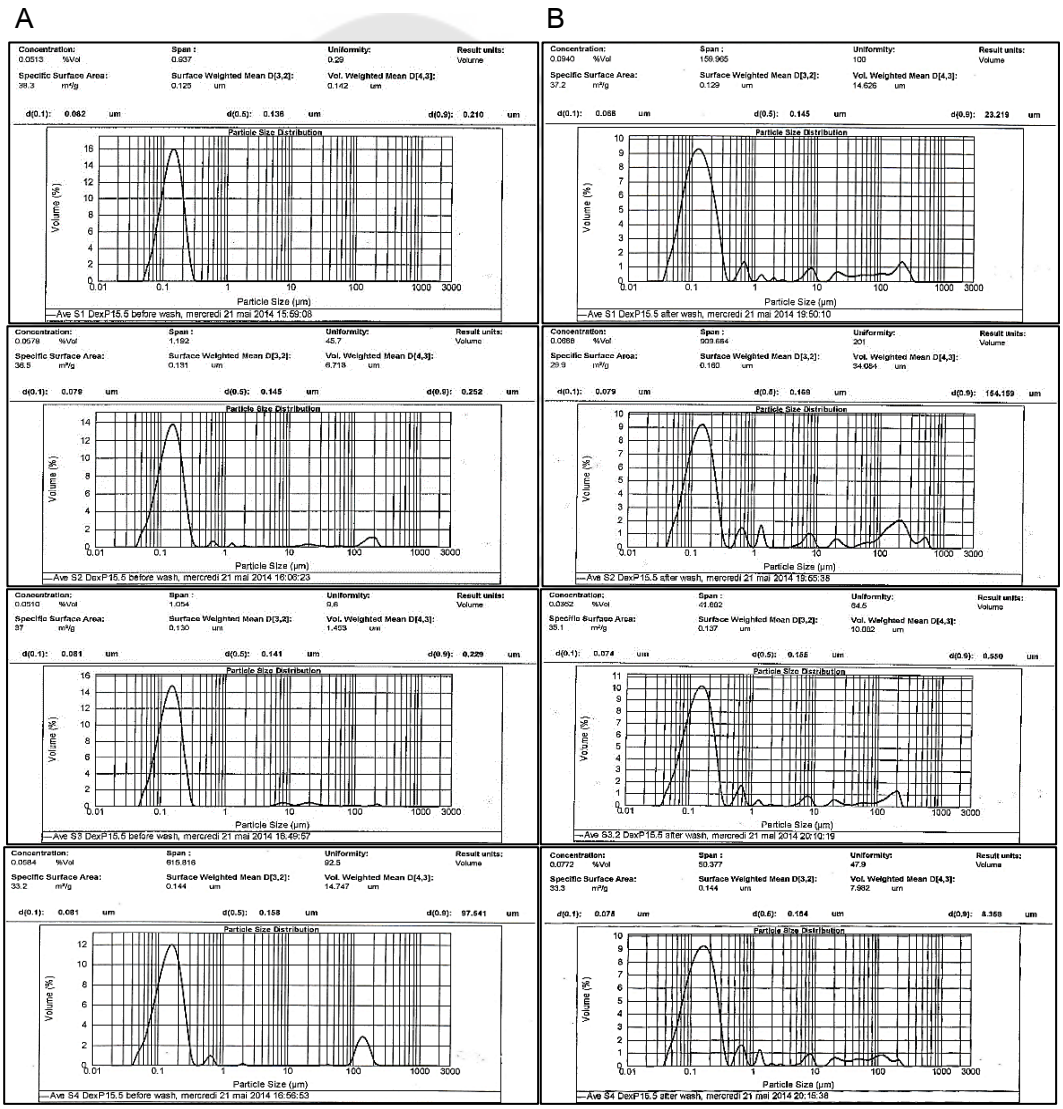

Figure 70 Size distributions of DexP$_{15.5}$-grafted PLA NPs (A) before and (B) after wash, with sonication power (P) 5 to 8

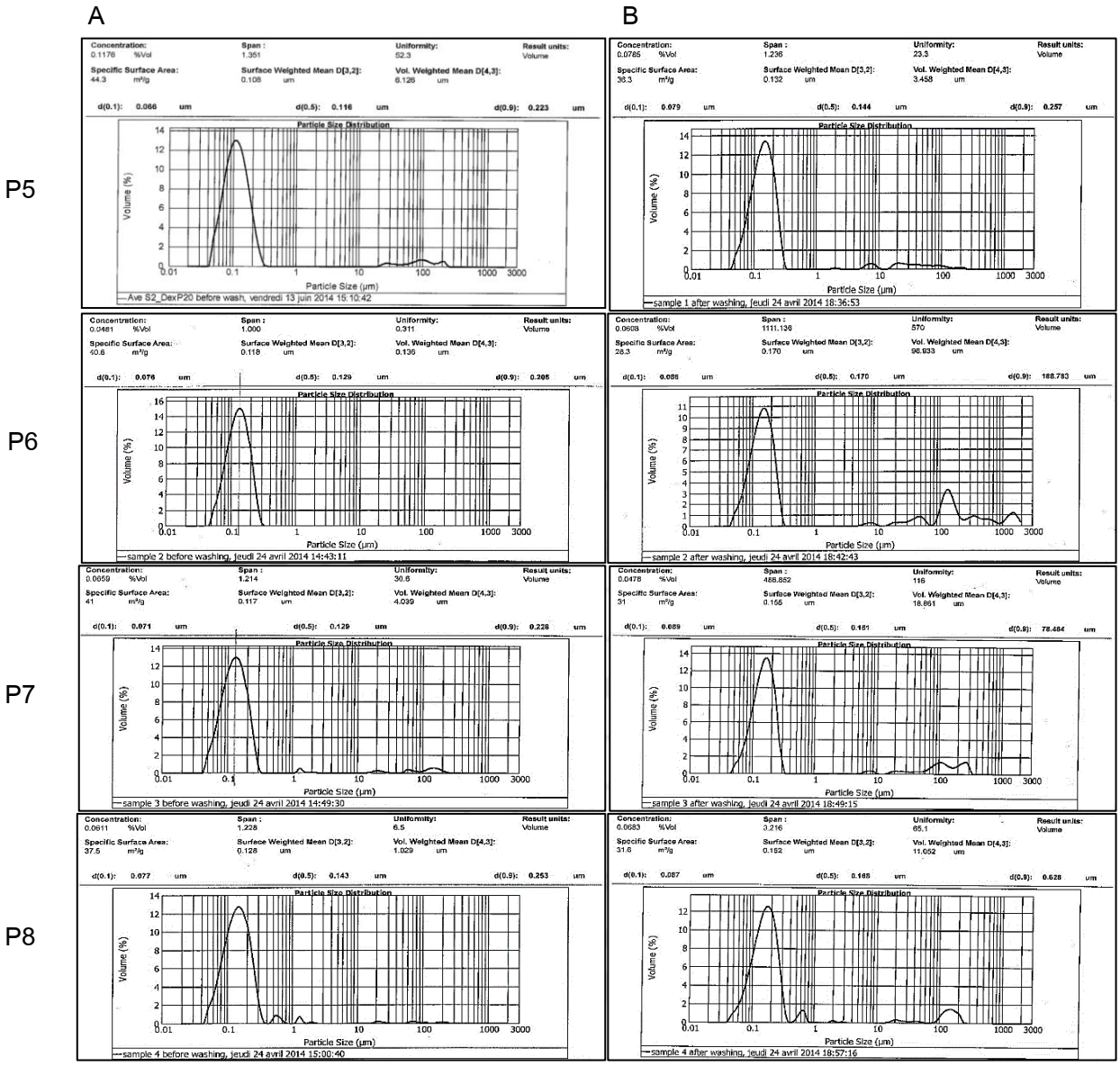

Figure 71 Size distributions of $DexP_{21}$-grafted PLA NPs (A) before and (B) after wash, with sonication power (P) 5 to 8

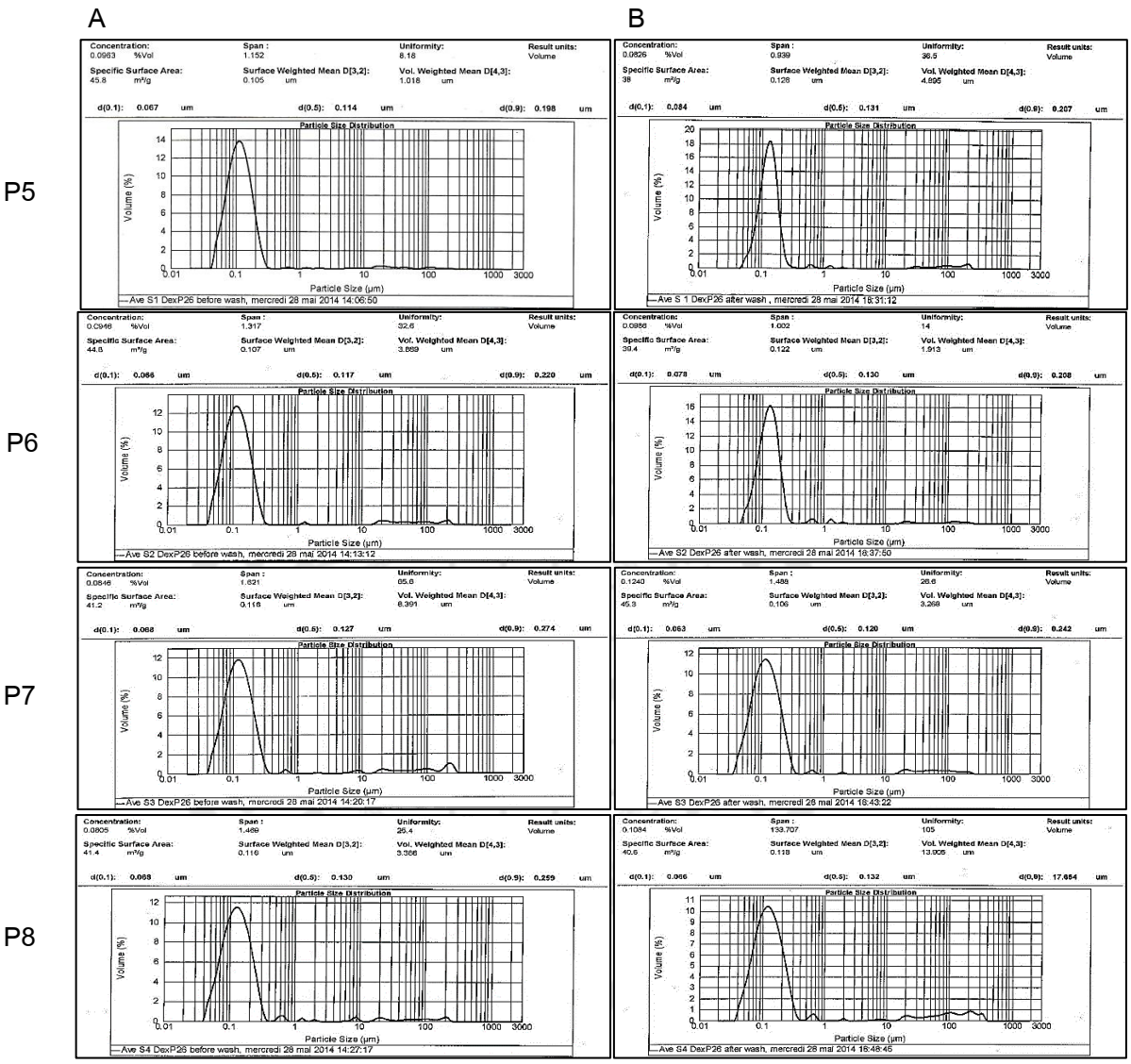

Figure 72 Size distributions of $DexP_{26}$-grafted PLA NPs (A) before and (B) after wash, with sonication power (P) 5 to 8

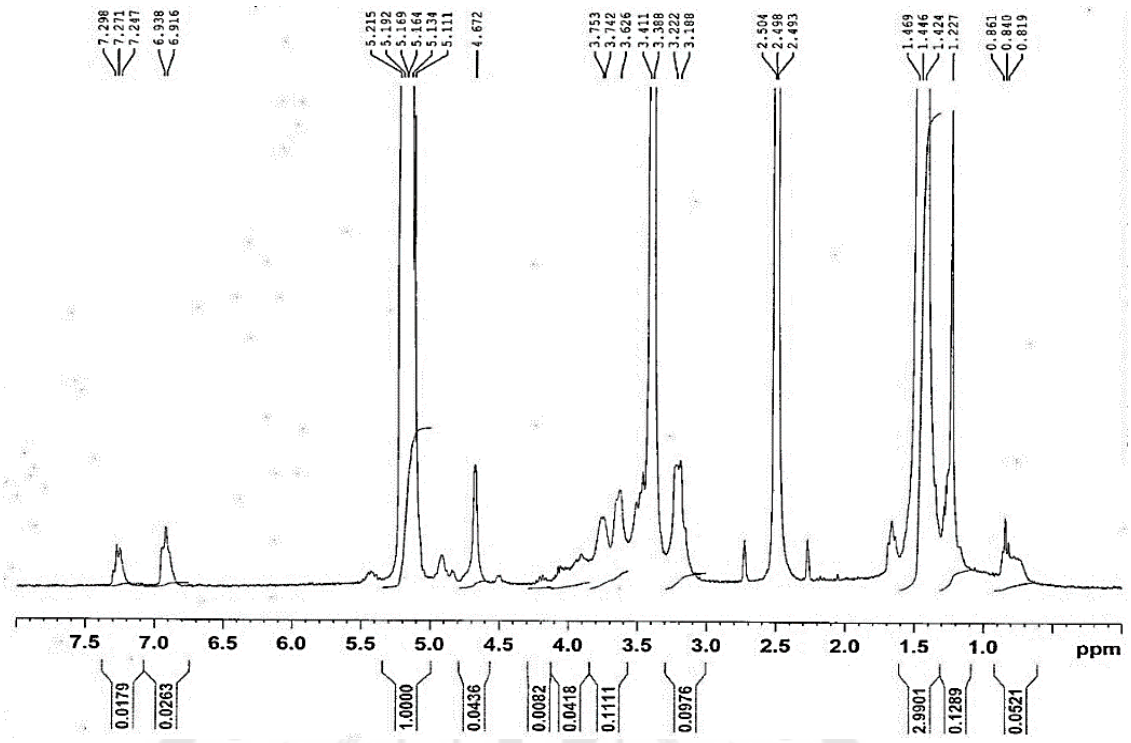

Figure 73 ^{1}H NMR spectra of Dex$P_{15.5}$-grafted PLA NPs synthesized by using P5.

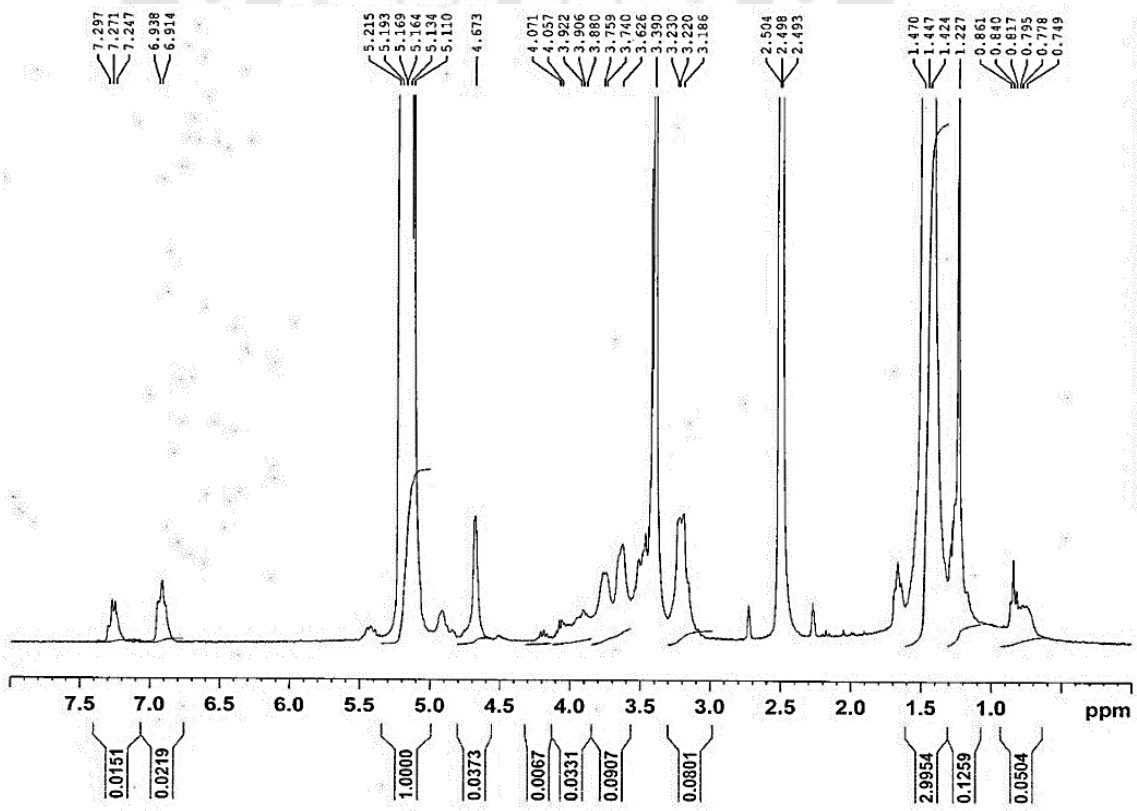

Figure 74 ^{1}H NMR spectra of Dex$P_{15.5}$-grafted PLA NPs synthesized by using P6.

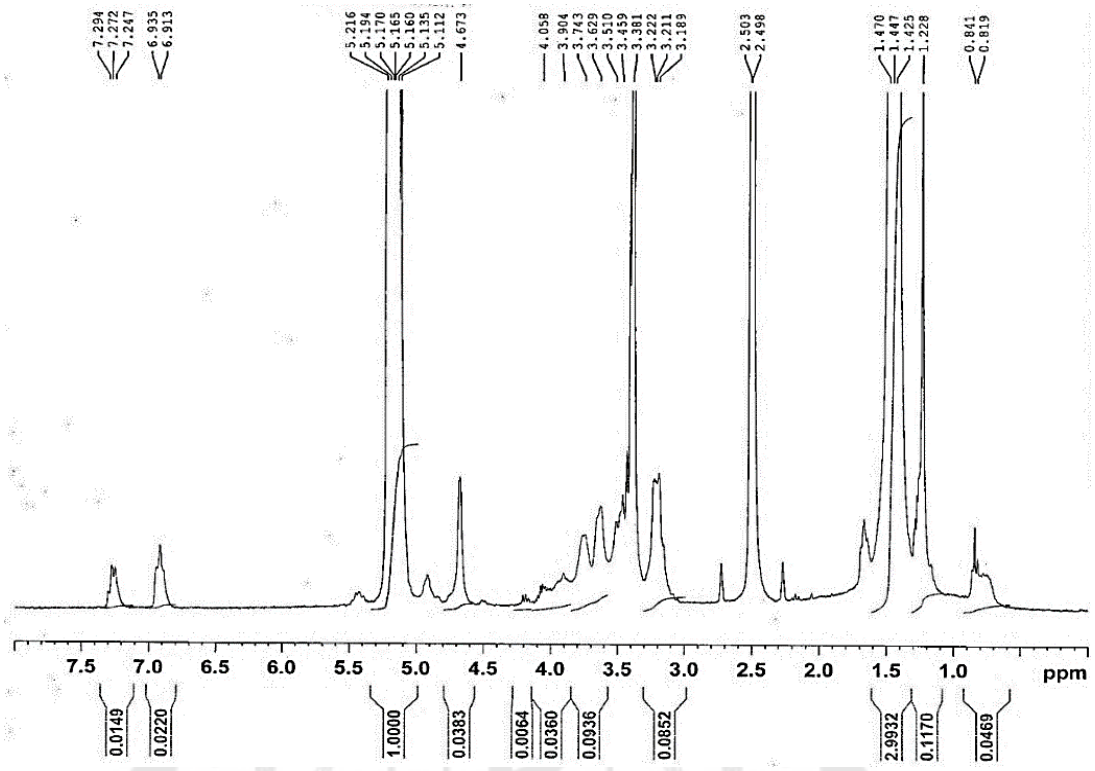

Figure 75 ^{1}H NMR spectra of Dex$P_{15.5}$-grafted PLA NPs synthesized by using P7.

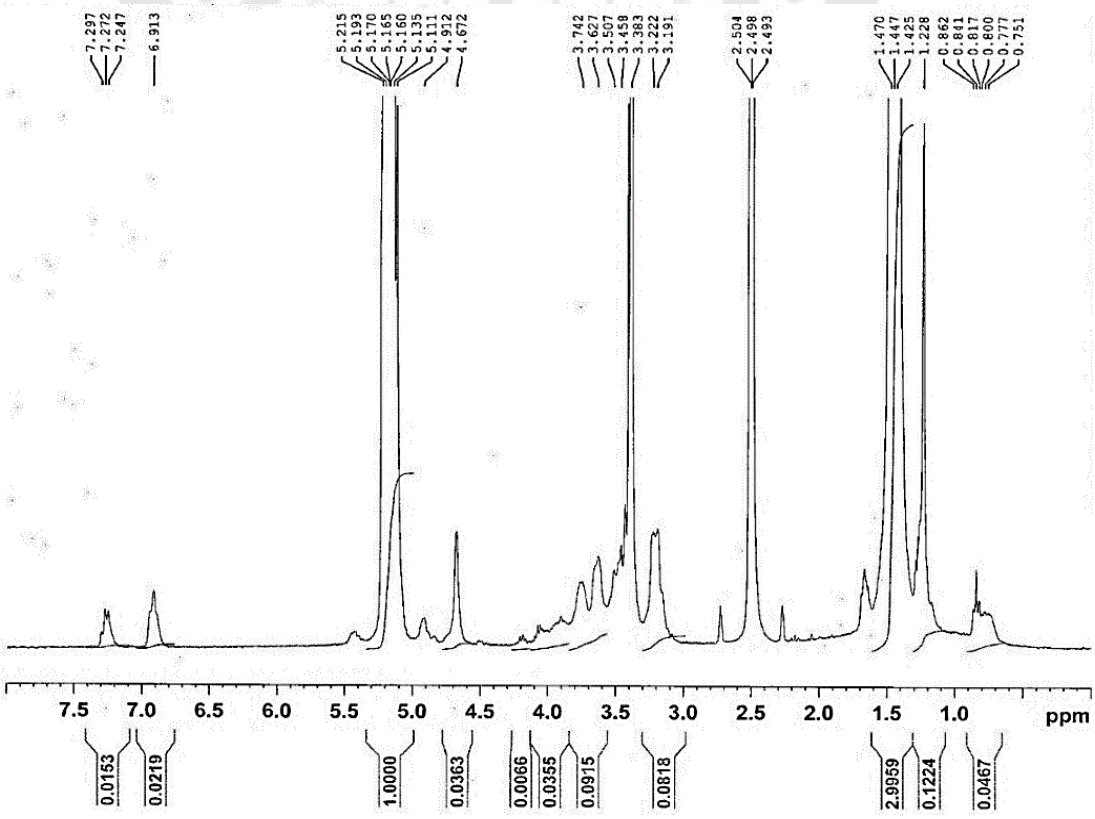

Figure 76 ^{1}H NMR spectra of Dex$P_{15.5}$-grafted PLA NPs synthesized by using P8.

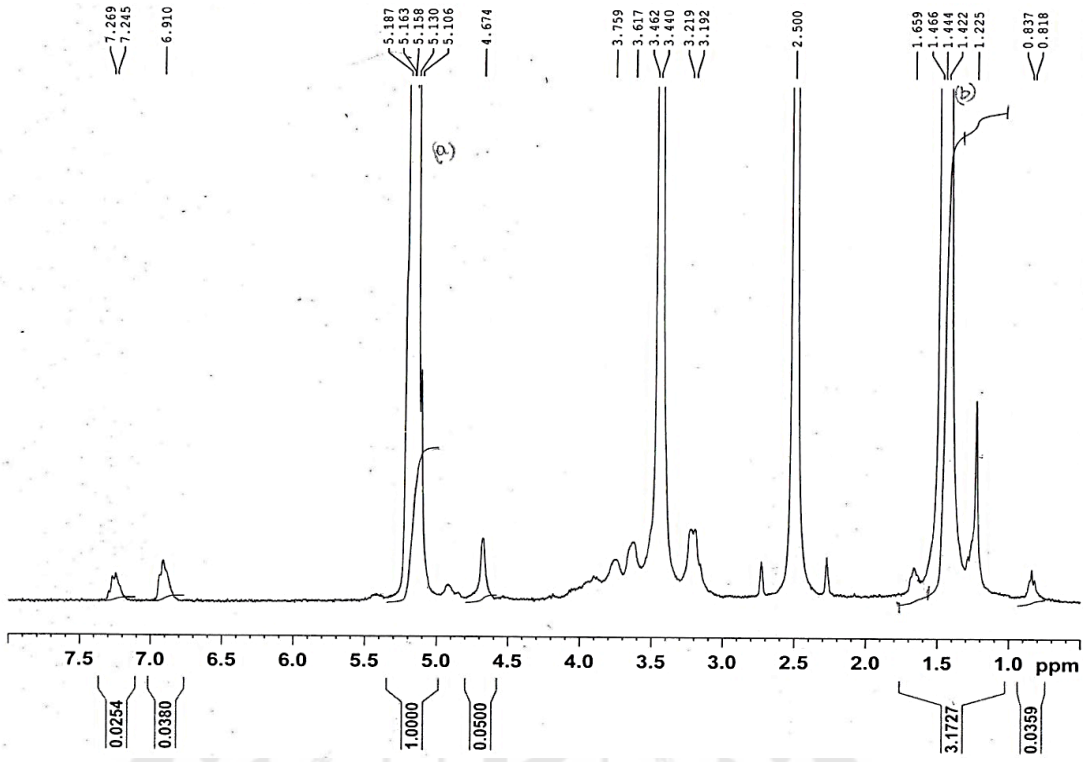

Figure 77 ^{1}H NMR spectra of DexP_{21}-grafted PLA NPs synthesized by using P5.

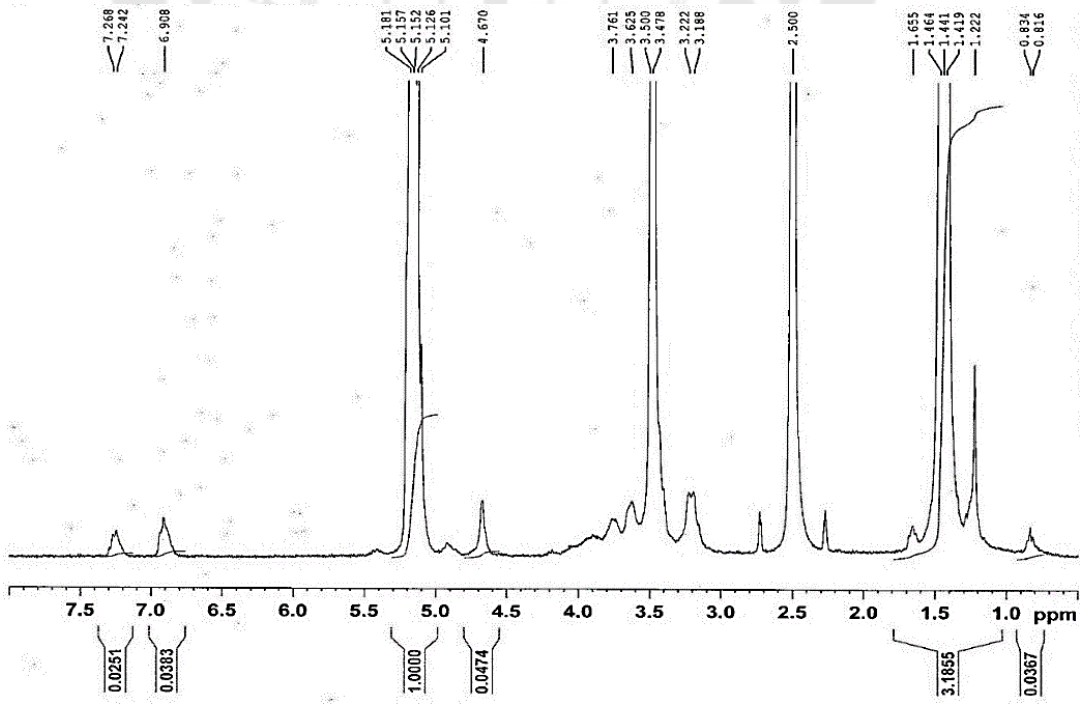

Figure 78 ^{1}H NMR spectra of DexP_{21}-grafted PLA NPs synthesized by using P6.

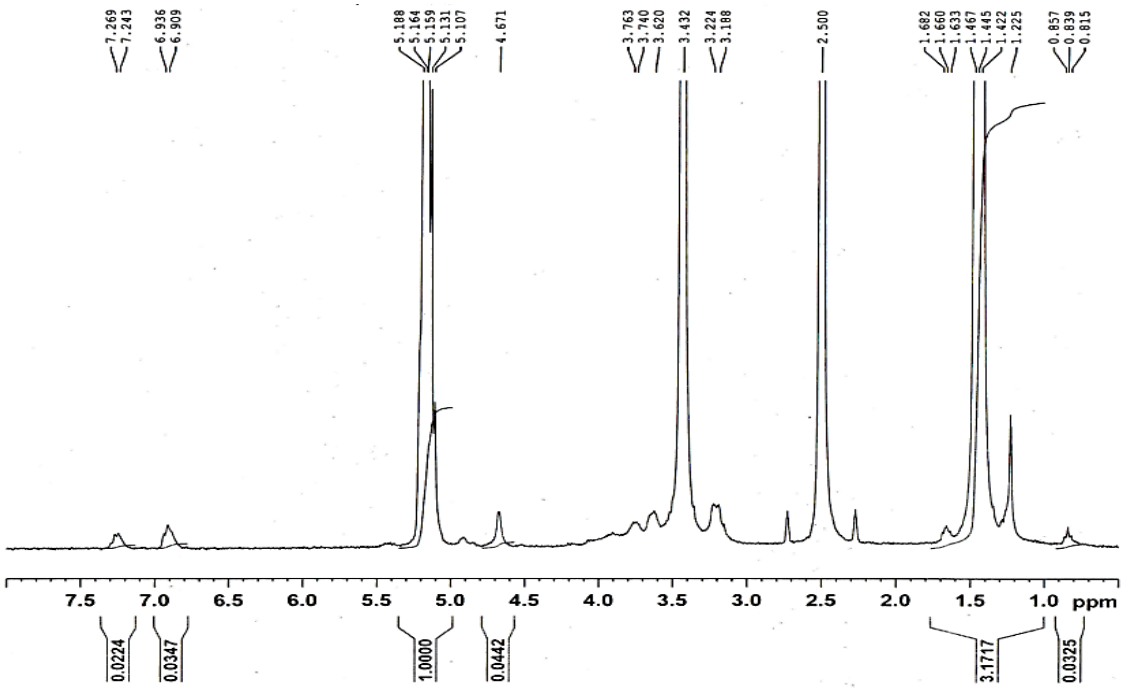

Figure 79 ^{1}H NMR spectra of DexP_{21}-grafted NPs PLA NPs synthesized by using P7.

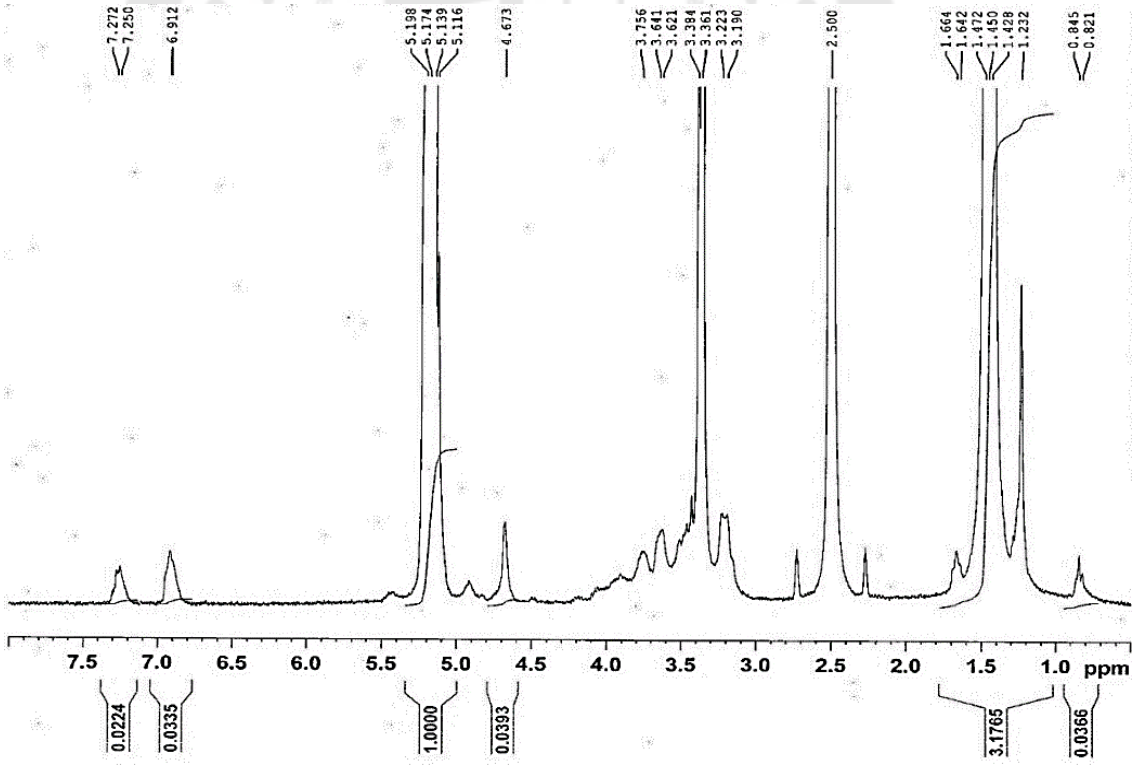

Figure 80 ^{1}H NMR spectra of DexP_{21}-grafted PLA NPs synthesized by using P8.

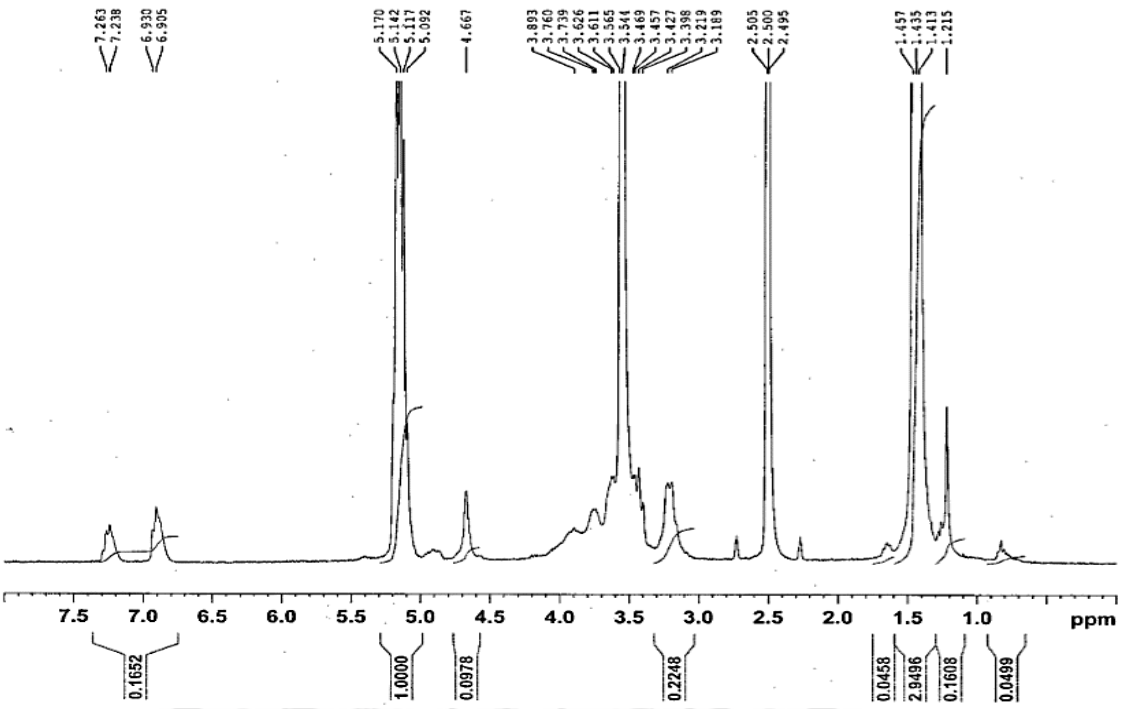

Figure 81 ^{1}H NMR spectra of DexP_{26}-grafted PLA NPs synthesized by using P5.

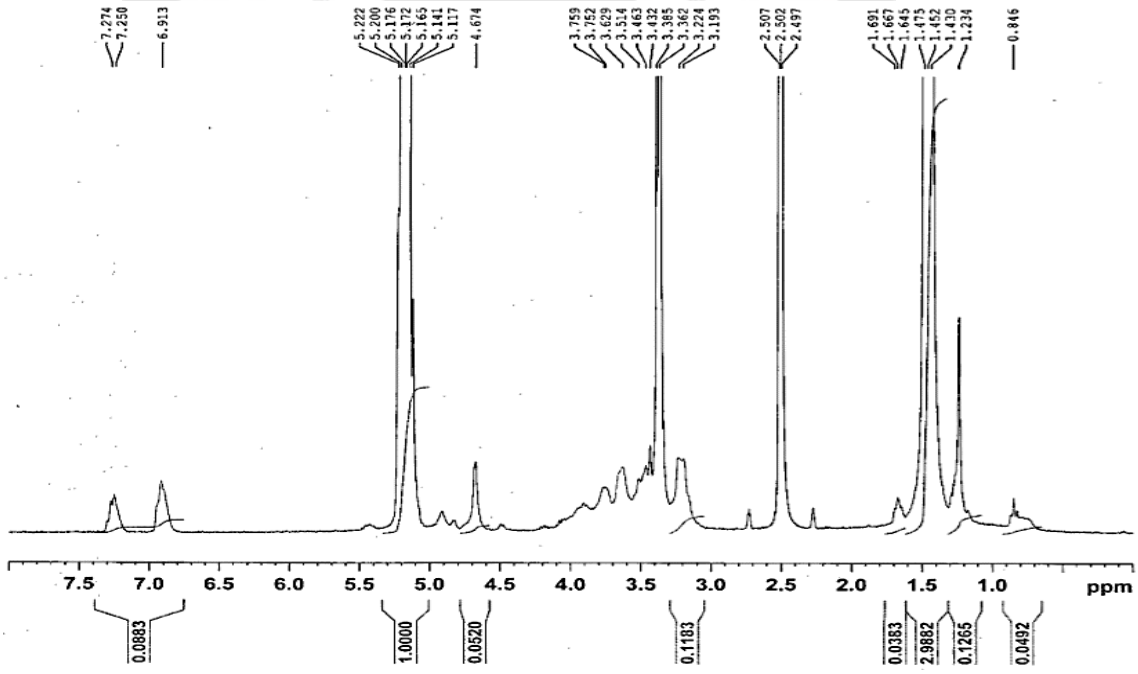

Figure 82 ^{1}H NMR spectra of DexP_{26}-grafted PLA NPs synthesized by using P6.

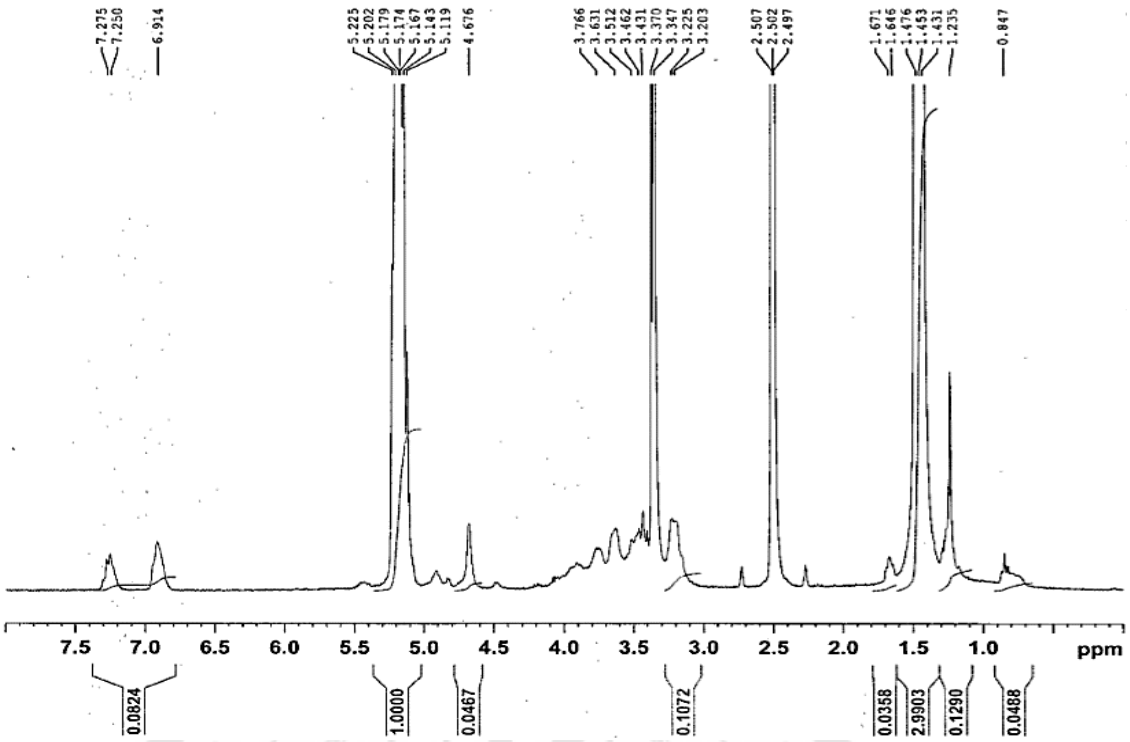

Figure 83 ^{1}H NMR spectra of DexP_{26}-grafted PLA NPs synthesized by using P7.

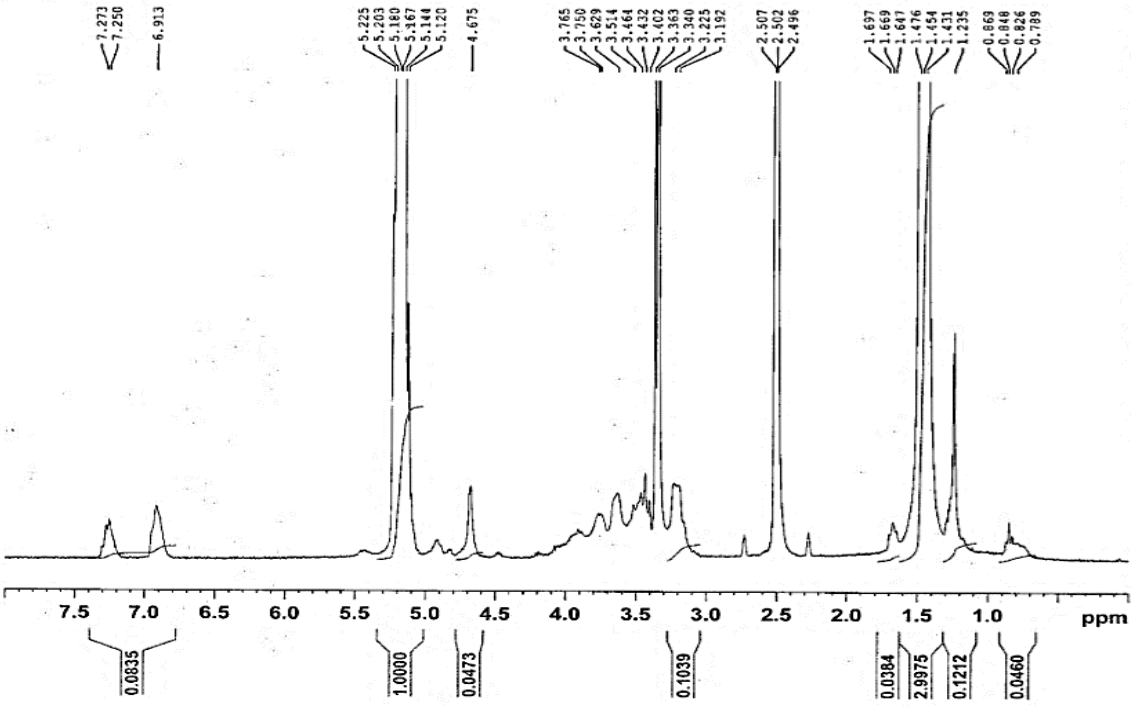

Figure 84 ^{1}H NMR spectra of DexP_{26}-grafted PLA NPs synthesized by using P8.

2. DexP_{26}-COOH-grafted NPs

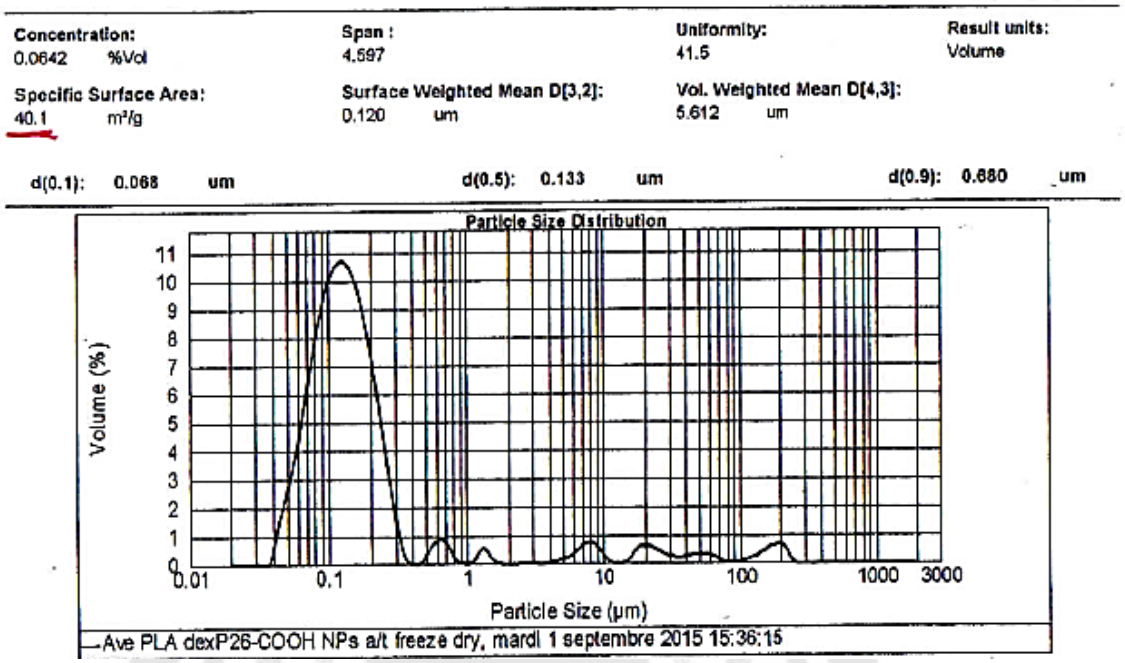

Figure 85 DexP_{26}-COOH PLA NPs before Tf conjugation.

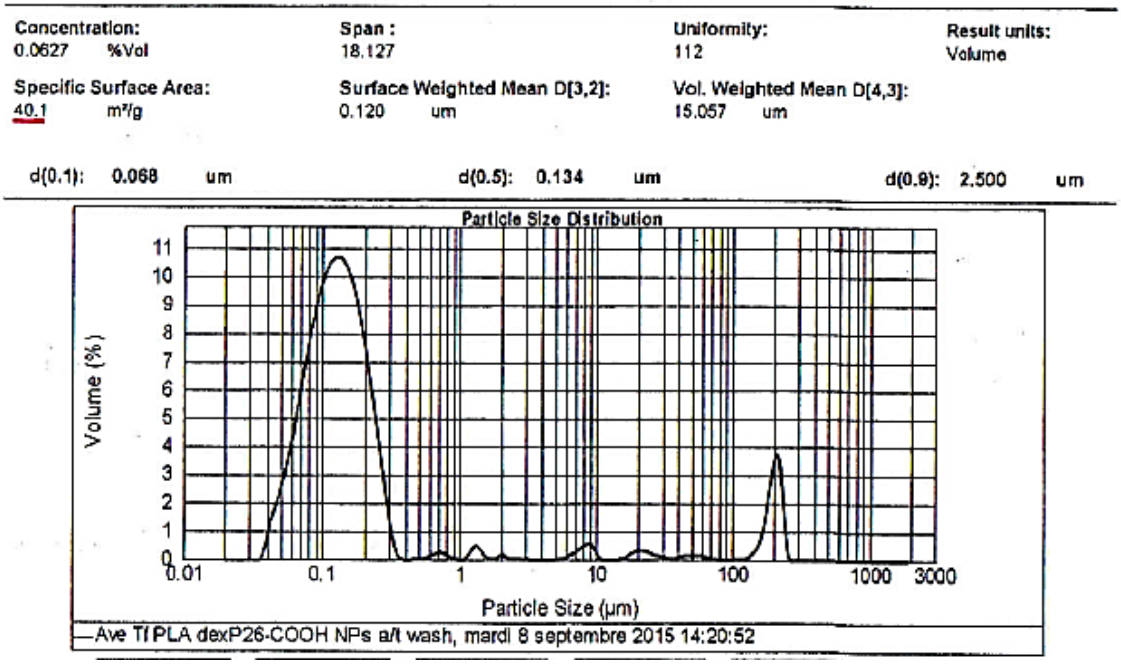

Figure 86 DexP_{26}-COOH PLA NPs after Tf conjugation.

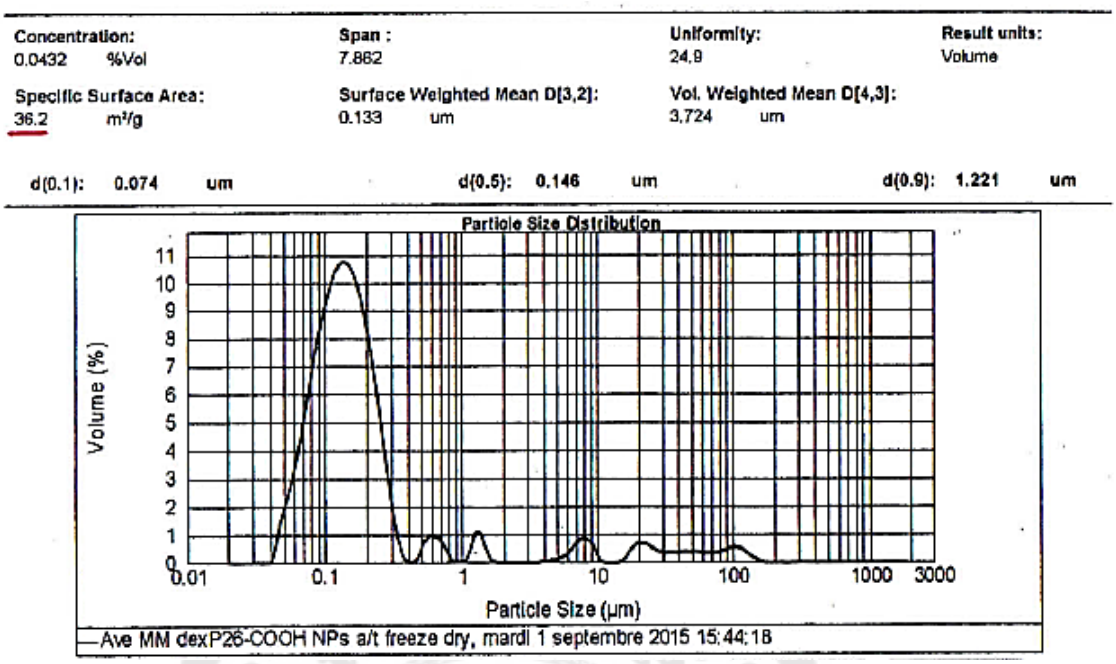

Figure 87 DexP_{26}-COOH MM-NPs before Tf conjugation.

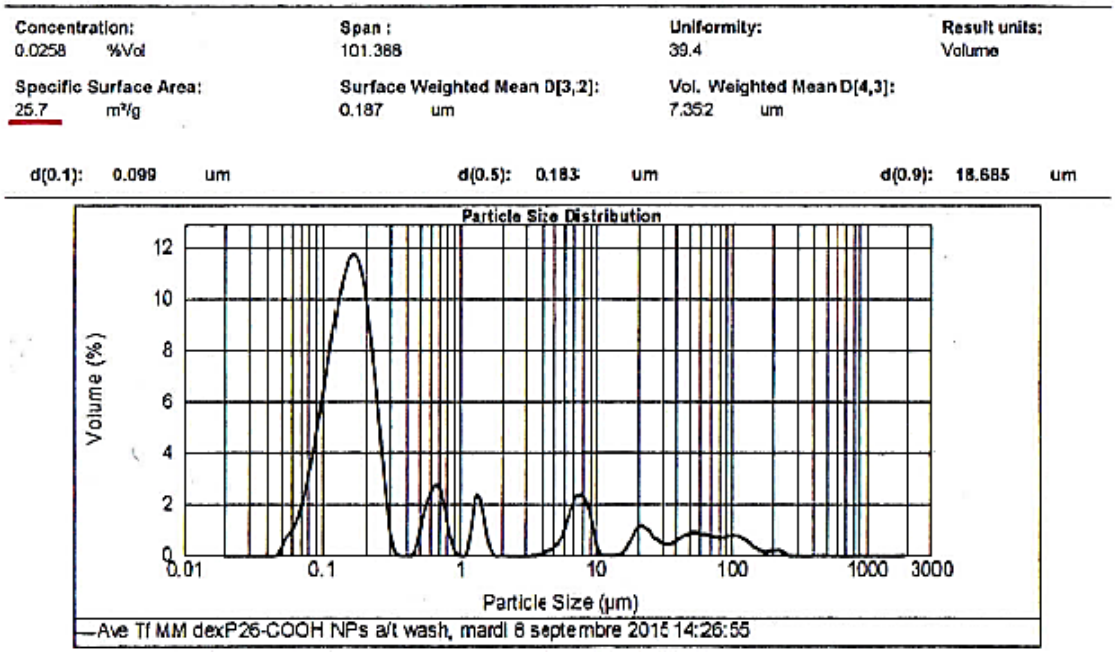

Figure 88 DexP_{26}-COOH MM-NPs after Tf conjugation.

VITA

NAME	Sirirat Boondireke
DATE OF BIRTH	6 November 1983
PLACE OF BIRTH	Hatyai, Songkhla, Thailand
INSTITUTIONS ATTENDED	1999 - 2002, High School: Windsor House Academy and Edenglen High school, Johannesburg, The Republic of South Africa. 2003 - 2007, Bachelor of Science (BSc) Degree in Biotechnology, Ramkhamhaeng University, Bangkok, Thailand 2007 - 2010, Master of Science (MSc) Degree in Microbiology (International Program), Mahidol University, Bangkok, Thailand. 2012 - 2018, Doctor of Philosophy (Ph.D.) Degree in Biomedical Science, Srinakharinwirot University, Bangkok, Thailand.
HOME ADDRESS	30/28 Ivy Ratchada Condominium, Ratchadapisek 20, Ratchadapisek Rd., Samsen Nok, Huai Khwang, Bangkok 10310, Thailand.
AWARD RECEIVED	2012-2018, The Royal Golden Jubilee Ph.D. (RGJ-Ph.D.) scholarship, The Thailand Research Fund (TRF).